Universidade Nova de Lisboa

Instituto de Higiene e Medicina Tropical

Generation and characterisation of monoclonal antibodies against cell cycle and cytokinesis regulators in *Trypanosoma brucei*

Cristina Isabel Correia de Almeida Costa

DISSERTAÇÃO PARA A OBTENÇÃO DO GRAU DE DOUTOR EM CIÊNCIAS BIOMÉDICAS, ESPECIALIDADE DE PARASITOLOGIA

(MARÇO, 2013)

Universidade Nova de Lisboa

Instituto de Higiene e Medicina Tropical

Thesis: Generation and characterisation of monoclonal antibodies against cell cycle and cytokinesis regulators in *Trypanosoma brucei*

Author: Cristina Isabel Correia de Almeida Costa

Supervisor: Doctor Carlos Novo, IHMT, UNL

Co-supervisor: Professor Tansy C. Hammarton (University of Glasgow)

Tutorial Committee:
Doctor Carlos Novo (IHMT, UNL)
Doctor Luís Távora Tavira (IHMT, UNL)
Professor Virgílio Estólio do Rosário (IHMT, UNL)

Dissertation presented to obtain a PhD degree in Biomedical Sciences, speciality of Parasitology, under the supervision of Doctor Carlos Novo, Professor Tansy C. Hammarton and Professor Virgílio Estólio do Rosário. Financial support was provided by Fundação para a Ciência e Tecnologia (FCT) with a PhD fellowship Grant (SFRH / BD / 40223 / 2007).

Universidade Nova de Lisboa

Instituto de Higiene e Medicina Tropical

Título da tese: Produção e caracterização de anticorpos monoclonais contra reguladores do ciclo celular e da citocinese em *Trypanosoma brucei*

Autor: Cristina Isabel Correia de Almeida Costa

Orientador: Investigador Doutor Carlos Novo, IHMT, UNL

Co-orientador: Professora Doutora Tansy C. Hammarton (University of Glasgow)

Comissão Tutorial:
Investigador Doutor Carlos Novo (IHMT, UNL)
Investigador Doutor Luís Távora Tavira (IHMT, UNL)
Professor Doutor Virgílio Estólio do Rosário (IHMT, UNL)

Dissertação apresentada para cumprimento dos requisitos necessários à obtenção do grau de Doutor em Ciências Biomédicas, especialidade de Parasitologia, realizada sob a orientação científica do Investigador Doutor Carlos Novo, da Professora Doutora Tansy C. Hammarton Professor e do Professor Doutor Virgílio Estólio do Rosário. Apoio financeiro da FCT com a bolsa de doutoramento SFRH / BD / 40223 / 2007 no âmbito do III Quadro Comunitário de Apoio.

Dedico esta tese,

À minha irmã Ana Isabel que comigo construiu um castelo
À minha mãe, minha estrela-guia, que me tornou na mulher que sou hoje
Ao meu querido avô, que tanta saudade deixa, que me ensinou a ser "Guerreira"

"...Ser feliz é reconhecer que vale a pena viver
Apesar de todos os desafios, incompreensões e períodos de crise.
Ser feliz é deixar de ser vítima dos problemas e
Se tornar um autor da própria história.
É atravessar desertos fora de si, mas ser capaz de encontrar
Um oásis no recôndito da sua alma...
É agradecer a Deus a cada manhã pelo milagre da vida.
Ser feliz é não ter medo dos próprios sentimentos.
É saber falar de si mesmo.
É ter coragem para ouvir um 'não'.
É ter segurança para receber uma crítica, mesmo que injusta.

Pedras no caminho?
Guardo todas, um dia vou construir um castelo..."
(Fernando Pessoa)

ACKNOWLEDGEMENTS

A lot of people have been by my side on this amazing adventure.

First of all, I would like to thank my supervisor, Dr Carlos Novo, for all the trust he put on me, for the guidance and support, and especially for always having my back and helping me when I was in need.

I would also like to thank my co-supervisor Prof. Tansy Hammarton, who allowed me to work in her lab and taught me so many things I would not know where to start. Thank you for the support, the confidance and for helping me "grow" in the lab.

This project allowed me to meet amazing people, whether in former UTPAM: Tiago, Bé, Ângela, Maria, Carla, Sofia, Ana Armada, Ana Domingos and Fernando; and recently in IHMT: Pimpolho, Cátia, Isabel, Pedro, Ana, Idalécia and so many other people. To all of you, thanks for the support and for accompanying me on this journey.

During my PhD I travelled regularly to Glasgow and a part of me will always stay there. First of all I would like to thank my "brother" Dave (one of my Musketeers). He turned Glasgow into a second home, his friendship helped me through the bad moments, but most important: he always had a HUG and a SMILE to share. To my two other Musketeers: Will and Nath, our adventures shall be immortal. To my sweet Craig, for caring and giving me love; to Elaine, for the fun and friendship; to Cat, for being my shoulder on the last year; to Jimbo, for the fun and the boozy lunches. To the brasilian gang: Herbert (my dear friend Safado), Tatiana, Dani, thank you for the the crazy times. To the Hammarton group: Corinna, Sophie, Glynn, Elizabeth, thanks for the help around the lab and for making work days such a blast. To everyone else (Jeremy, Elmarie, Esther, Amy, Ben, Fiona, Kirsty, Eileen…), it has been a pleasure to share such great moments and unforgettable experiences. I hope to see you all one day again, on a Friday afternoon at 4 p.m. in the usual place: Tennents!!

Although everyone was important for this journey, two special people have walked alongside me, suffered my drawbacks and enjoyed my victories: my Marias. To Maria Sandra: thanks for always being there for me and for always caring. You are an amazing person with a giant heart, and I am blessed to call you a friend. Having you, Carqueijo and Mini-Spartacus in my life has lightened it up. To my other Maria, Maria

Raquel, this would not have been possible without you. You became my “sister”, and I shall never forget that you always saw the best in me. Thank you for always being there, for supporting me through the Westerns of Doom, for the crazy adventures, and for letting me be a part of your life outside the lab where I met Zé and Mini-Tarzan. Still today, when I am sad, I grab a glass of wine, start cooking and a voice starts singing…”You are the dancing queen….”.

To my family: thank you for believing in me. To my mother and father: without your faith in me I would not have successfully finished this project. To my guiding-star, my mum, for teaching me how to be loyal to myself and helping me become who I am today. Life has given me a lot of lessons, but it was you who helped me to interpret them and gave me the strength and values to stand up for myself. To my sister, we have been through a lot together… But we are two strong branches of the same tree, and we stay united and true. My admiration for you has no end, and no matter what life brings you, you will always have me to lean on. To my brother-in-law, for being so unique and special. To my second mum, Neia, for giving me the greatest gift of all: unconditional love. To my “little sister” Dani, for showing me the poem that will accompany me for the rest of my life and for guiding me so many times. To my family in Lisbon, thank you for giving me so many reasons to smile, especially my small princesses that bring me so much joy.

E porque a amizade é o maior ingrediente na receita da vida, finalmente um agradecimento a todos os meus amigos. Ao pessoal de Viseu, em especial à Suzy, Joaninha, Rafa, Mafaldinha e Vitinho, obrigada pela força. Um agradecimento especial à Marta e à Xanó, que ao longo dos últimos 13 anos têm sido as minhas “soul sisters”. Ao pessoal de Lisboa, entre muitos: o Afilhado, o Zica, a Marta e Fáfá (a dupla que tanto me aguentou…), o Duarte e Inês, foi um prazer partilhar estes anos com vocês e receber tanto.

E por último, a um amigo especial, que me convenceu que a vida dá mesmo muitas voltas. Ao Filipe, que trouxe de volta o brilho nos meus olhos e o meu lado de criança: Obrigado por seres exatamente como és, porque o que muitos não vêm é exatamente o teu tesouro. Que saibamos sempre apreciar a união da tempestade com a calmaria.

ABSTRACT

Generation and characterisation of monoclonal antibodies against cell cycle and cytokinesis regulators in *Trypanosoma brucei*

Cristina Isabel Correia de Almeida Costa

Keywords: *Trypanosoma brucei*, cell cycle regulation, CRK12:CYC9, endocytosis, cytokinesis, synchronization, monoclonal antibodies, cytoskeleton

Trypanosoma brucei is the causative agent of African Trypanosomiasis, being transmitted by the bite of a blood-feeding invertebrate vector into the mammalian host. It affects 36 sub-Saharan African countries and the lack of efficient diagnostic methods and safe and effective drugs has led to the need for new control measures and novel treatment strategies.

Cell cycle progression in *T. brucei* is quite unique. Being so distinct from the mammalian cell cycle, regulatory proteins are believed to constitute good drug targets. However, many of these proteins remain to be identified, and their roles in specific pathways are still unknown. The cdc-2 related kinases (CRKs) and their cyclin partners are among the different cell cycle regulators that are vital for an accurate progression through the cell cycle. In *T. brucei*, several CRKs (CRK1-4 and CRK6-12) and cyclins (CYC2-11) have been identified, although a role in cell cycle regulation has not been established for all of them and only two active CRK:cyclin complexes have been identified *in vivo*. During this project, CRK12 and CYC9 have been proved to constitute a novel CRK:cyclin complex *in vivo*, in both the bloodstream (BSF) and the procyclic (PCF) stages. Interestingly, each protein regulates different biological processes in BSF trypanosomes. In fact, while CYC9 is involved in cell cycle regulation, blocking cytokinesis once depleted, CRK12 has a critical role in the endocytic pathway. It is the first time a CRK is connected with regulation of endocytosis, causing enlargement of the flagellar pocket if depleted. The interaction of CRK12 and CYC9 with additional proteins and the presence of functional redundancy between kinases/cyclins might explain the different functions.

The use of monoclonal antibodies (MAbs) and immunisation strategies as therapeutic techniques has been the subject of several studies. With that aim, α-CRK12 MAbs were efficiently generated, recognising the protein specifically in different *T. brucei* cell extracts. However, this MAb might not be suitable for immunolocalisation studies. Time constraints did not allow neutralization/protection studies.

A parallel approach was taken to identify new proteins as cell cycle regulators. BSF cultures were synchronized in S-phase by addition of hydroxyurea, and cytoskeleton extracts of populations enriched for cells in mitosis and cytokinesis were used for MAb generation. After different screening techniques, a total of 28 MAbs were selected and the proteins they recognised, their cell cycle specificity and immunolocalisation of the recognised antigens analysed. Although a specific antigen was not identified as a possible mitosis/cytokinesis regulator, interesting MAbs were generated with respect to to their localisation in the *T. brucei* cytoskeleton. Additionally, these MAbs could become valuable tools to understand cellular biology and different biological pathways in *T. brucei*.

RESUMO

Produção e caracterização de anticorpos monoclonais contra reguladores do ciclo celular e da citocinese em *Trypanosoma brucei*

Cristina Isabel Correia de Almeida Costa

Palavras-chave: *Trypanosoma brucei*, regulação ciclo celular, CRK12:CYC9, endocitose, citocinese, sincronização, anticorpos monoclonais, citoesqueleto

Trypanosoma brucei é o parasita que causa Trypanossomose Africana, sendo transmitido pela picada de um inseto vetor para a corrente sanguínea do hospedeiro mamífero. Afeta atualmente 36 países sub-saharianos e a falta de métodos de diagnóstico eficazes e de tratamentos seguros e eficazes, levou à necessidade de se desenvolverem novas medidas de controlo e novas estratégias terapêuticas.
O ciclo celular do parasita *T. brucei* é invulgar. Uma vez que é tão distinto do ciclo celular dos mamíferos, as proteínas que o regulam têm sido consideradas como possíveis alvos terapêuticos. No entanto, muitas proteínas reguladoras ainda não foram identificadas e a função específica de algumas proteínas envolvidas na progressão do ciclo celular é desconhecida. De entre os diversos reguladores do ciclo celular, estão as CRKs e as ciclinas que as ativam. Em *T. brucei*, foram identificadas 11 CRKs (CRK1-4 and CRK6-12) e 10 ciclinas. No entanto, ainda nem todas têm uma função conhecida e apenas dois complexos CRK:ciclina foram identificados *in vivo*. Durante este projeto, provou-se a existência de um novo complexo: CRK12:CYC9, que interage *in vivo* tanto na forma sanguínea como na forma procíclica. Um resultado interessante é que, apesar de interagirem, cada proteína regula diferentes processos biológicos na forma sanguínea do parasita. Na realidade, enquanto a CYC9 está envolvida na regulação do ciclo celular, levando a um bloqueio da citocinese em células em que não é expressa, a cinase CRK12 assume um papel essencial na regulação da endocitose. Esta consiste na primeira vez que uma CRK foi relacionada com o processo de endocitose de *T. brucei*, levando na sua ausência a um alargamento da bolsa flagelar. De forma a garantir estas diferentes funções, tanto a cinase CRK12 como a ciclina 9 podem interagir com outras proteínas, ou ser substituídas funcionalmente por outras cinases/ciclinas.
O uso de anticorpos monoclonais e ensaios de proteção têm sido estudados frequentemente como alternativas terapêuticas. Com esse objetivo, anticorpos monoclonais foram produzidos contra CRK12. Apesar de se ter produzido um anticorpo que reconhece especificamente esta cinase em diferentes extratos celulares de *T. brucei*, não foi possível usar o mesmo em estudos de localisação por fluorescência e os ensaios de neutralização/proteção não foram feitos devido a limitações de tempo.
Um projeto alternativo desenvolvido tinha como objetivo identificar possíveis proteínas reguladoras. Como tal, extratos de citoesqueleto foram obtidos em células sincronizadas em mitose e citocinese, e usados para geração de anticorpos monoclonais. Um total de 28 anticorpos foram selecionados. Apesar de não mostrarem especificidade contra uma fase específica do ciclo celular, produziram-se anticorpos com imunolocalisações muito interessantes. Além disso, estes anticorpos poderiam num futuro ser usados como ferramentas valiosas para estudar diferentes processos biológicas em *T. brucei*.

ABREVIATIONS

4-NPP	4-nitrophenyl phosphate
AE	attached epimastigote
AP	alkaline phosphatase
ApoAI	apolipoprotein AI
ApoLI	apolipoprotein L-I
AUK	aurora kinase
BB	basal body
BiP	binding protein
bp	basepair
BSA	bovine serum albumin
BSD	blasticidin
BSF	bloodstream form *Trypanosoma brucei*
CBP	calmodulin binding protein
CDK	cyclin-dependent kinase
CIP	calf intestinal alkaline phosphatase
CLH	clathrin
CRK	cdc-2 related kinase
CYC	cyclin
DABCO	4-diazabicyclo[2.2.2]octane
DAPI	4,6-diamidino-2-phenylindole
DE	asymmetrically dividing epimastigote
DMEM	Dulbecco modified Eagle's medium
DNA	deoxyribonucleic acid
dNTP	deoxyribonucleotide triphosphate
DTT	dithiothreitol
EDTA	ethylene diamine tetra acetic acid
EGTA	ethylene glycol tetraacetic acid
ELISA	enzyme linked immunosorbent assay
EM	electron microscopy

ER	endoplasmic reticulum
ES	expression site
ESAG	expression site associated gene
FAZ	flagellar attachment zone
FBS	foetal bovine serum
FITC	fluorescein isothiocyanate
FP	flagellar pocket
FPC	flagellar pocket collar
FTZ	flagellum transition zone
FTZC	flagellum transition zone component
GFP	green fluorescent protein
GPI	glycosylphosphatidylinositol
Hb	haemoglobin
HDL	high-density lipoprotein
HGPRT	hypoxanthine guanine phosphoribosyltransferase
HMW	high molecular weight (protein ladder)
Hpr	haptoglobin related protein
HRP	horse radish peroxidase
HSLS	high salt lysis solution
HU	hydroxyurea
HYG	hygromycin
IFA	immunofluorescence
IFT	intraflagellar transport
IP	immunoprecipitation
IPTG	isopropyl β-D-1-thiogalactopyranoside
kDNA	kinetoplast DNA
LB	Luria bertani medium
LE	long epimastigote
LMW	low molecular weight (protein ladder)
LSG	lysis solution with glycerol
LSGI	lysis solution with glycerol and inhibitors
MAbs	monoclonal antibodies

MAPs	microtubule associated proteins
MBP	myelin basic protein
MOPS	3-(N-morpholino)propanesulfonic acid
MS	mesocyclic trypomastigote
MT	metacyclic epimastigote
MTOC	microtubule-organizing center
MtQ	microtubule quartet
M-VATs	metacyclic variable antigen types
N/K	nucleus/kinetoplast
NEO	neomycin
NHS	normal human serum
NLS	nuclear localisation signal
NP40	octylphenyl-polyethylene glycol
NSR	normal rabbit serum
OD	optical density
ORF	open reading frame
PAP	peroxidase anti-peroxidase
PBS	phosphate buffered saline
PCF	procyclic form *Trypanosoma brucei*
PDEB	phosphodiesterase
PEG-DMSO	polyethylene glycol–dimethyl sulfoxide
PFA	paraformaldehyde
PFR	paraflagellar rod
PLK	polo-like kinase
PMSF	phenylmethanesulfonylfluoride
PNPP	p-nitrophenyl phosphate
proBB	pro-basal body
RAB	ras-related proteins in brain
RNA	ribonucleic acid
RNAi	ribonucleic acid interference
SAXO	stop axonemal protein
SDS-PAGE	sodium dodecyl sulphate polyacrylamide gel electrophoresis

SE	short epimastigote
SL	slender trypomastigote
SRA	serum-resistance associated
ST	stumpy trypomastigote
TAC	tripartite attachment complex
TAP	tandem affinity purification
TAX	trypanosome axonemal protein
TbHPHbR	haptoglobin-Hemoglobin receptor
TBS	tris buffered saline
TDB	trypanosome dilution buffer
TEM	transmission electron microscopy
Tet	tetracycline
Tf	transferrin
TfR	transferrin receptor
TLF	trypanosome lytic factor
TOR	target of rapamycin
UTR	untranslated region
v/v	volume to volume
vPBS	Voorheis's modified PBS
VSG	variant surface glycoprotein
w/v	weight to volume
WB	western blotting
WT	wildtype
X-gal	5-bromo-4-chloro-3 indolyl-β-D galactopyranoside

TABLE OF CONTENTS

INDEX OF FIGURES

INDEX OF TABLES

1. INTRODUCTION

1.1. AFRICAN TRYPANOSOMIASIS

Trypanosomiasis is an infectious disease caused by unicellular parasites from the Protozoa kingdom and genus *Trypanosoma*. *Trypanosoma* species infect a variety of hosts, and the genus includes two human-infective species: *T. cruzi* which causes Chagas' disease in South America and accounts for 13,000 deaths per year (Barrett *et al.*, 2003) (also known as American Trypanosomiasis); and *T. brucei* that causes Human African Trypanosomiasis (HAT, also known as Sleeping Sickness) in sub-Saharan Africa. These species differ considerably in terms of their biology and host-parasite interactions, causing diverse symptoms and there is a need for several approaches in terms of control and treatment (Barrett *et al.*, 2003). Besides human infective hosts, several *Trypanosoma* species can affect animals: *T. vivax* infects ruminants, horses and camels; *T. equiperdum* causes venereal equine disease and can be spread through coitus; *T. congolense* causes acute fever, anaemia and neurological signs in dogs and cats; *T. simiae* leads to pyrexia in pigs; while *T. evansi* affects all domestic mammals. Recent studies (Lai *et al.*, 2008) have shown that *T. equiperdum* and *T. evansi* are actually strains of *T. brucei* that have lost part or all of their kinetoplastid DNA (kDNA), and in 2005 it was confirmed the first report of human infection due to *T. evansi*, transmitted probably by the blood of an infected animal (Joshi *et al.*, 2005).

African Trypanosomiasis is caused by *Trypanosoma brucei*, which affects both people (HAT) and animals (Animal African Trypanosomiasis [AAT] or Nagana). Two human infective subspecies can cause HAT: *Trypanosoma brucei gambiense* (*T.b.g.*) and *Trypanosoma brucei rhodesiense* (*T.b.r.*); while *T. brucei brucei* causes Nagana in cattle and other livestock and also affects domestic animals. The parasite is transmitted by the bite of a blood-feeding invertebrate vector – the tsetse flies (genus *Glossina*), and is able to undergo several metabolic changes in order to survive in both hosts. The transmitted parasites proliferate in the blood, lymph and later on the Central Nervous System (CNS), leading to progressive neurological dysfunction then death. Current treatments are inadequate, as drugs discovered so far are highly toxic and there are no prospects for disease preventing medicines, such as vaccines.

Human sleeping sickness occurs in 36 sub-Saharan African countries and takes two forms according to the subspecies of parasite causing the infection: *T. b. gambiense* causes a chronic infection and is found in west and central Africa; while an acute disease arises from infection with *T. b. rhodesiense*, which mainly affects both eastern and southern Africa. *T. b. gambiense* causes more than 95% of all cases reported. Both species are fatal if left untreated, although recent data have shown that infection with *T. b. gambiense* is not 100% fatal and can naturally progress to an asymptomatic infection or to a spontaneous resolution (Jamonneau *et al.*, 2012). Epidemiological history and actual data are reported mainly by the World Health Organization (WHO – www.who.int), which has described a decrease of the total number of HAT cases in 2009 to below 10,000, for the first time in 50 years. However, an approximate estimate suggests that 10% of cases are left unreported, and for those reported, the commencement of treatment is delayed due to time taken to visit the health centres, inappropriate diagnosis and lack of diagnostic facilities. According to WHO, elimination of HAT is feasible if new diagnosis and staging methods are created, if safe and effective drugs are generated for both stages of the disease, if mobile teams are used to find new active cases and vector control is employed.

1.1.1. **Epidemiology**

African Trypanosomiasis has been identified and characterised in several reservoirs in the African continent since the 14th century (Cox, 2004). By 1903, Scottish pathologist and microbiologist David Bruce had identified the causative agent and the vector, and concluded that the bite of the tsetse fly would transmit the disease (Cox, 2004, Fevre *et al.*, 2006). In 1910, the differentiation between subspecies of the protozoa was achieved, a time at which the first treatment was introduced, an arsenic-based drug which caused blindness as a side effect. *T. b. gambiense* was described by Forde in 1902 (Forde, 1902), while *T. b. rhodesiense* was only identified in 1910 in Zambia (Stephens and Fantham, 1910).

The evolution of trypanosomatids has been extensively studied by several groups, and it was in the early 1990s that it became obvious that the control of HAT

was dependent on understanding the life cycle and adaptive changes undergone by the parasite, involving activation or repression of metabolic pathways and ultrastructural changes (Vickerman, 1985, Vickerman, 1994). Phylogenetic trees were created using the gene encoding for the nuclear small subunit (SSU) rRNA, which underwent an evolutionary change in history and as such allowed an estimation of the relationship between kinetoplastids. The Kinetoplastida taxon was created 40 years ago, consisting of protozoan flagellates with a disk-shaped mass of mitochondrial DNA (kDNA), condensed in a structure termed the kinetoplast, located at the base of the flagellum and associated with the basal body (BB). Molecular phylogenetic studies soon included other informative markers, such as heat-shock proteins, which meant that our understanding of the evolutionary relationship between different protozoans evolved over the years (Cavalier-Smith, 1993, Fernandes *et al.*, 1993, Stevens *et al.*, 2001, Simpson *et al.*, 2006). In the first studies, *T. brucei* appeared on a long deep branch of the phylogenetic trees, considered then to be the most ancient divergent within the trypanosomatids and having a distant relationship with the *Leishmania* genera. In 2001 (Stevens *et al.*, 2001) with the study of the molecular evolution of trypanosomatids, the idea of *T. brucei* and *T. cruzi* clades appeared, having a close relationship between themselves and with *Leishmania*. Later on (Simpson *et al.*, 2006), the phylogenetic trees showed that *Leishmania* and *Trypanosoma* were two of the branches inside the Trypanosomatida group, the second one further divided into the *T. brucei* and *T. cruzi* clades.

Although HAT was identified early, its prevalence has changed considerably over the past 100 years, influenced by the political and economic situation of the countries affected, and due to control and intervention programmes (Cox, 2004, Barrett, 2006, Simarro *et al.*, 2008, Brun *et al.*, 2010). In the early 20th century the number of cases reported was higher than 60,000, and the disease was almost eradicated in the early 1960s due to systematic screening and treatment (Simarro *et al.*, 2008). A lack of surveillance and an abandonment of control programmes lead to major outbreaks and a dramatic reappearance of HAT in the 1990s, caused mainly by three devastating epidemics around 1906, 1920 and 1970 (Smith *et al.*, 1998, Brun *et al.*, 2010). In 1995, when 60 million people were at risk and approximately 300,000 cases were reported per year, the Programme Against African Trypanosomiasis (PAAT) was created to identify

a solution to this problem, involving the collaboration of several agencies, organizations and research institutes. Between 1995 and 2006, the total number of cases showed a 68% decrease, stimulated mainly by an increase of awareness and surveillance, and from the effort of public institutions and private pharmaceutical companies, such as Aventis, that in 2001 agreed to supply eflornithine to WHO for free (Barrett, 2006).

Currently, the number of cases reported to the WHO has decreased to <10,000, although it is believed that a lot of cases are left unreported or undiagnosed, and care should be taken as negligence could lead to resurgence of HAT. However, the prevalence of the disease differs from one country to another, and the numbers differ between the two different species. The reduction in cases observed until 2006 was mostly visible for *T. b. gambiense*, while *T. b. rhodesiense* cases did not show a similar decrease due to lack of control measures. A 69% decrease in new cases was observed for infections due to *T. b. gambiense*, responding to the implementation of control activities and active surveillance. On the contrary, for *T. b. rhodesiense* (causing 3% of the total number of cases) the containment measures were insufficient, probably due to the part played by the animals as reservoirs for transmission (MacLeod *et al.*, 2001b, MacLeod *et al.*, 2001a, Welburn *et al.*, 2001, Hide and Tait, 2009). In the years between 1997 and 2006, 24 of the 36 endemic countries for HAT suffered from *T. b. gambiense* transmission, while in 2006, 11 out of these 24 reported no cases (Simarro *et al.*, 2008). In that same period, 13 countries endemic for *T. b. rhodesiense* showed a 21% reduction in the number of new cases reported, even though only 4 countries implemented control measures (Simarro *et al.*, 2008).

T. b. gambiense is rarely observed in short term tourists (Brun *et al.*, 2010), although its long incubation period leads to the necessity of a close follow-up since the last stay in endemic countries (Chappuis *et al.*, 2005). The contrary can be observed for *T. b. rhodesiense*, where tourists travelling to east African game reserves might become infected (Chappuis *et al.*, 2005) (see Figure 1. 1). Infected cases within the local population and tourists in 2010 are shown in Figure 1. 1, demonstrating also the spatially discrete distribution of the disease, and the distinct geographical locations of both human-infective species.

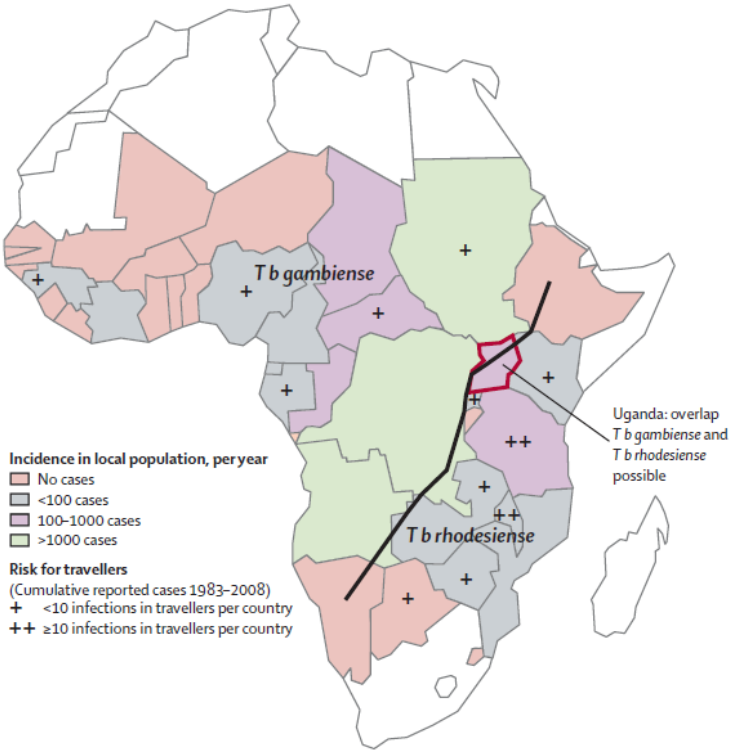

Figure 1. 1 - Distribution of Human African trypanosomiasis and prevalence of each human-infective species. The black line divides the area between the distribution of each species. (Brun *et al.*, 2010)

1.1.2. **Origin of human infectivity**

Despite the widespread distribution of tsetse vectors and animal trypanosomiasis, the human disease is only found in discrete foci, which periodically give rise to epidemics followed by periods of endemicity. Nearly 300 separate active foci are recognised. Over the years, several biochemical and molecular tools have been designed and used to better understand parasite genetic diversity, increasing our knowledge on the role of reservoir hosts and population structure in the epidemic events (MacLeod *et al.*, 2001b, MacLeod *et al.*, 2001a, Hide and Tait, 2009).

Early analyses of *T. brucei* isolates from game and cattle showed that some were infective for humans whereas others were not, and that 2-3% mixed infections were reported in mammals. Taking into account the prevalence of the parasite in the fly (0.1%-1%), and considering that infections were independent, the estimated frequency for mixed infections in the vector was extremely low: 0.01%-0.0001% (MacLeod *et al.*,

2001a). Considering that mixed infections occur at a significant frequency, and a significant proportion of tsetse flies carry more than one genotype, the possibility of genetic exchange occurring in the field arises.

The extent of genomic exchange in *T. brucei* spp. is unclear, and has been debated over the years using different molecular epidemiological tools (Sternberg and Tait, 1990, Tait and Turner, 1990, Gibson and Stevens, 1999). Enzyme-based and DNA-based methods (Hide and Tait, 2009) have shown that the presence of significant genetic exchange could explain the emergence of new epidemics. Using these tools and considering the major epidemics observed during the years, Hide and Tait (Hide and Tait, 2009) concluded that new outbreaks could be generated by the importation of reservoir species with a human strain into an area previously occupied only by animal strains (Welburn *et al.*, 2001). The emergent human strain spreads quickly into the naive population, establishing a new site of human-infective species, masking the occurrence of genetic exchange.

Human infectivity had multiple origins (MacLeod *et al.*, 2001a, Barrett *et al.*, 2003) and generated independently in different geographical regions. Using different marker systems, researchers have concluded that evolution of *T. brucei* seemed to have occurred in four separate occasions, giving rise to *T. b. rhodesiense* Uganda; *T. b. rhodesiense* Zambia; *T. b. gambiense* Type 1 and *T. b. gambiense* type 2 (MacLeod *et al.*, 2001a). Type 1 gambiense trypanosomiasis is genetically highly homogeneous and distinguishable from the other human-infective strain and *T. b. brucei*, while Type 2 is closely related to West African *T. b brucei* (Barrett *et al.*, 2003). *T. b. rhodesiense* expresses a serum-resistance associated (SRA) gene (section 1.3), as opposed to the animal-infective species and to *T. b. gambiense*, a gene that has been extensively used in epidemiological studies (MacLeod *et al.*, 2001a, Barrett *et al.*, 2003, Hide and Tait, 2009). These studies have shown that human-infective trypanosomes are present in animal populations, and analysis of *T. b. rhodesiense* isolates lead to the conclusion that these strains are host-range variants of local *T. b. brucei* populations, that have become genetically isolated.

In 2005, the *T. b. brucei* genome was sequenced (Berriman *et al.*, 2005), the 11 megabase-sized chromosomes were analysed, and the results allowed the identification

of new drug targets and pathways, and provided a starting point for functional studies. Being a model for the human-infective species, the animal-infective parasite has been used for a long time in research to increase the understanding of parasite development and biological characteristics.

1.1.3. **AAT**

Trypanosomiasis affects human health, both directly through sleeping sickness but also indirectly by the destruction of livestock. Parasite diseases that affect livestock cause serious economical problems, leading to food shortages in the communities and making impossible the use of animals for transport and traction. AAT can be caused by several species, the most important being: *T. congolense*, *T. vivax* and *T. b. brucei*, but concurrent infection can be observed with more than one species. AAT caused by the species *T. b. brucei* affects a large range of animals, from cattle and sheep, to dogs and cats. However, the major obstacle to economic development of affected rural areas comes from the presence of the disease in cattle (Nagana) which causes an acute or chronic disease characterised by fever, anaemia, diarrhoea, and often resulting in animal death.

Trypanosomes are transmitted by blood-feeding flies of the genus *Glossina*, of which around 30 species and subspecies of tsetse flies (Brun *et al.*, 2010) exist. In terms of habitats, tsetse flies can be separated into three groups, as they have highly focal distributions, determined mainly by environmental requirements. The parasite develops for one to a few weeks in the tsetse fly, where it undergoes several differentiation steps, and once the developmental cycle is complete the infected fly can transmit the disease by biting an animal and transmitting the parasite in its saliva (Figure 1. 2). The incubation period ranges from 4 days to 8 weeks, as described by the Center for Food Security and Public Health (CFSPH - http://www.cfsph.iastate.edu/), but the severity of the disease varies with the species and the age of the animal infected, with cattle with poor nutrition normally suffering from a chronic course and high mortality. The first clinical signs include intermittent fever, anaemia and weight loss, accompanied by neurological signs, cardiac lesions, appetite loss and reproductive problems. Besides

acting indirectly in human health, animals can also host human pathogen parasites, and act as an important reservoir for human infection (Welburn *et al.*, 2001).

1.1.4. **HAT**

As mentioned previously, inside the Trypanosomatidae, two different species can lead to HAT, having different rates of progression and clinical features, but being both spread by the bite of tsetse flies (Figure 1. 2). The parasite can be found in the peripheral circulation in the first stage, in what is known as a haemolymphatic phase (Barrett *et al.*, 2003, Brun *et al.*, 2010). The leading signs of the first stage are chronic and intermittent fever, headache, general malaise, anaemia, and parasites can be found in the blood or lymph, although usually they are below detection levels. The intermittent fever is related to the mounting of an immune system response by the host (Brun *et al.*, 2010), which the parasite can evade by antigenic variation.

In the second stage, the so-called neurological phase, the nervous system is disturbed and the more obvious signs appear: changes in behaviour, confusion, sensory disturbance, and disruption of the sleep cycle (Barrett *et al.*, 2003, Brun *et al.*, 2010). Brains function deteriorates, culminating in coma and then death. Such disorders are rarely seen during the first stage, and their frequency increases with the duration of the infection.

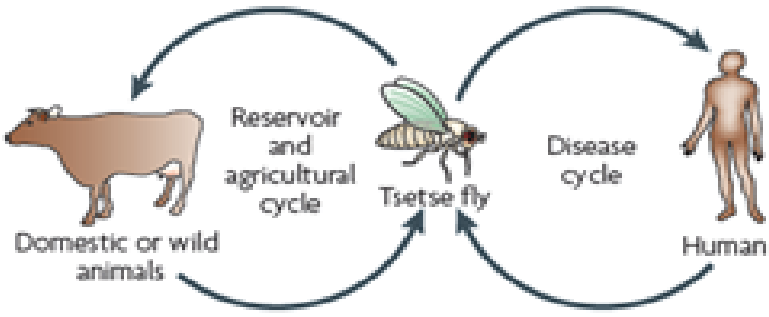

Figure 1. 2 - Life cycle of Trypanosomes, showing the role of the insect vector and the human and animal reservoirs in the *T. brucei* cycle. (Field and Carrington, 2009)

Over the years, the clinical signs have been followed to increase our knowledge of disease progression and distribution (Smith *et al.*, 1998, Fevre *et al.*, 2006). Patient follow-up has proved that the symptoms of HAT differ between African patients and travellers, with normally the latter presenting greater abnormalities (Brun *et al.*, 2010). The presence of a chancre at the site of the bite is more common, patients suffer from acute fevers whatever the causative agent, and other severe symptoms like loss of kidney function have been described in travellers.

The clinical presentations of disease caused by the human-infective species – *T. b. gambiense* and *T. b. rhodesiense* – are remarkably different. The former causes a chronic illness that lasts for years, while the latter usually appears as an acute febrile illness that leads to patient death in weeks/months if left untreated.

T. b. gambiense affects populations in west and central Africa, being transmitted by flies of the *G. palpalis* or *G. fuscipes* groups (Chappuis *et al.*, 2005). Infection occurs mainly in forested rivers, shores or near plantations, causing a chronic infection in which people can be infected for several months with an asymptomatic disease (Barrett *et al.*, 2003, Brun *et al.*, 2010). When symptoms appear, the patients are normally in an advanced stage, where the CNS is affected. The disease progresses slowly, starting with mild symptoms such as intermittent fever, headaches, muscle and joint aches, and possible itching, swollen lymph nodes and weight loss. Normally, after 1-2 years, neurological signs appear due to CNS invasion, such as personality changes, daytime sleepiness and progressive confusion, together with hormonal imbalances and balance or walking problems. If untreated, the infection often kills in 3 years and rarely lasts longer than 6-7 years (Brun *et al.*, 2010), and patients suffer from dysfunction of the immune system, enter a deep coma and often show parallel bacterial infections (Chappuis *et al.*, 2005).

T. b. rhodesiense can be found in east and southern Africa and causes an acute infection that develops rapidly. Transmission occurs by the bite of an infected fly (*G. morsitans* or *G. fuscipes* groups), usually around savannas. 19% of patients infected with *T. b. rhodesiense* develop a chancre at the site of the tsetse bite (Brun *et al.*, 2010). 46% of European patients coming from Eastern countries develop a chancre, much higher than for locals and for those coming from Western and Central Africa (23%)

(Chappuis *et al.*, 2005). The first symptoms appear within 1-2 weeks of the infective bite, being indistinguishable from other tropical fevers. As opposed to *T. b. gambiense* infection, even at the early stage, the patient can show severe symptoms, such as heart failure or pulmonary oedema (Barrett *et al.*, 2003), which can cause patient death even before the CNS is invaded by the parasite (Chappuis *et al.*, 2005). Staging of infection for this specie is not easy, although normally the second stage of the disease starts a few weeks after infection and most deaths (80%) occur within months (Chappuis *et al.*, 2005, Brun *et al.*, 2010).

1.1.5. **Diagnosis**

Although clinical symptoms can point to HAT, they cannot be taken into consideration alone, as other diseases such as malaria, enteric fever and HIV can mimic the signs and lead to misdiagnosis (Chappuis *et al.*, 2005). Laboratory methods are needed to confirm infection with trypanosomes, and complete the insufficient data given by the clinical features. Diagnosis is performed in three steps: screening for a potential infection; diagnostic confirmation by examination of blood, lymph node or Cerebral Spinal Fluid (CSF) aspirates; and finally staging to determine disease progression and course of treatment, by examining the CSF. It is necessary to take into account that material resources and human investment are scarce in Africa, and consequently many infected individuals might perish before being diagnosed.

An early diagnosis should be obtained to prevent the appearance of neurological signs and the need to perform risky procedures. Because infection with *T. b. gambiense* is relatively asymptomatic, an exhaustive and active screening programme is required. The card agglutination test for trypanosomiasis (CATT) was developed in the 1970s (Magnus *et al.*, 1978), and consists of a fast and practical test that can detect specific antibodies against a variable antigen type (VAT) of *T. b. gambiense*, LiTat 1.3, and can be performed on blood, plasma or serum. Reports show that this method is the most efficient in screening, with high sensitivity (87%-98%) and specificity (95%) (Jamonneau *et al.*, 2000, Truc *et al.*, 2002, Chappuis *et al.*, 2005, Brun *et al.*, 2010). False-negatives can occur with CATT, when variants do not express the test antigen,

and as such an alternative test was created: LATEX/*T. b. gambiense* (Büscher *et al.*, 1999), which is similar to CATT but uses a combination of three VATs (LiTat 1.3, 1.5 and 1.6). When compared to CATT, this assay has a higher specificity (96%-99%) but a lower or similar sensitivity (Chappuis *et al.*, 2005).

Some serological tests such as immunofluorescence (IFA), enzyme-linked immunosorbent assays (ELISA) (Olaho-Mukani *et al.*, 1994, Lejon *et al.*, 1998) and PCR (Kanmogne *et al.*, 1996, Truc *et al.*, 1999, Kabiri *et al.*, 1999, Kyambadde *et al.*, 2000) can be performed, although their use is limited in remote areas and conditions need to be standardized (Barrett *et al.*, 2003, Fevre *et al.*, 2006). Some assays use antibody levels as infection markers, as IgG and IgM antibodies are present in high concentrations during infection, although this technique greatly depends on the antigen used (Barrett *et al.*, 2003, Chappuis *et al.*, 2005, Fevre *et al.*, 2006). New technologies have also been reviewed, such as detection of trypanosome specific antibodies in the saliva (Lejon *et al.*, 2003), or the use of proteomic signatures and mass spectrometry analysis (Papadopoulos *et al.*, 2004), although these assays would be impossible to perform in the field.

Parasitological confirmation is made by microscopic examination of lymph node aspirates, blood, or CSF (Cattand *et al.*, 1988, Barrett *et al.*, 2003, Chappuis *et al.*, 2005, Fevre *et al.*, 2006, Brun *et al.*, 2010), which gives a definite diagnosis. This method of direct detection is only accurate at parasite concentrations above $10^4.ml^{-1}$ (Fevre *et al.*, 2006), which makes it easier to detect *T. b. rhodesiense* infections, due to the higher density of circulating parasites. Because there is no serological test for *T. b. rhodesiense*, detection of infection due to this agent relies primarily on clinical symptoms and signs, which can be quite non-specific, followed by molecular methods such as PCR analysis for the SRA gene (Welburn *et al.*, 2001) and microscopic confirmation (Chappuis *et al.*, 2005, Brun *et al.*, 2010).

Stage determination of HAT to determine the course of treatment is similar for both infective species, relying on CSF examination by lumbar puncture (Cattand *et al.*, 1988). Although trypanosomes might not be frequently seen in the CSF, the host's inflammatory response can be a diagnostic indicator. According to WHO (www.who.int), second stage disease is determined by the presence in CSF of one or

more of the following: trypanosomes; raised white blood cells (more than 5 cells.μl^{-1}); increased protein content (370 $mg.l^{-1}$). As the second stage causes sleeping disorders, sleep-wake recordings can be used to access the CNS involvement (Buguet *et al.*, 2005, Simarro *et al.*, 2008).

Over the years, advances have been made in diagnostic tools for HAT. However, care should be taken that these are suitable for African rural centres, which need the most basic and cost-effective techniques.

1.1.6. **Treatment and control**

There are no vaccines against sleeping sickness, and preventive measures consist of minimizing contact with tsetse flies. The principles of control consist of treating the infected individuals, finding and treating new cases promptly, and controlling the vector. In terms of treatment, few drugs are available for treatment of HAT and selection is dependent on the parasite species involved and on the stage of the disease. Drugs need to be of low toxicity and easy to administer, which is not the case for current first stage and second stage drugs; while drugs for the late stage need to be able to cross the blood-brain barrier in order to clear trypanosomes in the CSF. Along with the toxicity of the drugs used, other difficulties arise from lack of supply and the development of parasite resistance (Matovu *et al.*, 2001b, Geerts *et al.*, 2001).

A small number of drugs have been developed, but their low efficacy for late stage disease (Burchmore *et al.*, 2002, Brun *et al.*, 2010), their toxicity (Burchmore *et al.*, 2002, Fevre *et al.*, 2006, Brun *et al.*, 2010) and emergence of parasite resistance (Matovu *et al.*, 2001b, Geerts *et al.*, 2001, Barrett *et al.*, 2003), mean there is a need to develop new treatment courses. Treatment of HAT caused by *T. b. rhodesiense* is based mainly on the use of suramin or melarsoprol, for early and late stages, respectively (Van Nieuwenhove, 1999). Such drugs can also be used for *T. b. gambiense* infections, although suramin is mainly used when resistance to pentamidine leads to drug failure; and use of melarsoprol in the late stage is not as efficient for this strain and is only used in countries were eflornithine is not available. As such, *T. b. gambiense* infection is preferably treated with pentamidine for early-stage disease, while eflornithine can be

used at both stages of the disease although being preferably used for late stage infection (Van Nieuwenhove, 1999).

Suramin, indicated for early-stage treatment, consists of a highly charged molecule that is believed to be taken up by the trypanosomes by receptor-mediated endocytosis, when bound to serum proteins (Burchmore *et al.*, 2002). It was discovered in 1921, is administered intravenously, but along with its high toxicity has been reported to fail in 25%-35% of the cases (Burchmore *et al.*, 2002). Its dosage begins with 5 $mg.kg^{-1}$ weight on day 1 and treatment continues for 30 days using 20 $mg.kg^{-1}$ (Burchmore *et al.*, 2002, Barrett *et al.*, 2003), provoking, however, certain undesirable side effects in the urinary tract and allergic reactions (May and Allolio, 1991).

The second drug used only for early stage disease is pentamidine, which is generally well tolerated by patients as it is not as toxic as other HAT drugs (Fevre *et al.*, 2006, Brun *et al.*, 2010), although it is less effective against early stage *T. b. rhodesiense* (Apted, 1980). Pentamidine has been used for over 50 years for sleeping sickness treatment (Pépin and Milord, 1994), and appears to work directly on the parasite, although the way it induces parasite clearance has not been established yet (Burchmore *et al.*, 2002). It is given intramuscularly daily, for a total of 7 to 10 injections of 4 $mg.kg^{-1}$ weight (Burchmore *et al.*, 2002, Barrett *et al.*, 2003).

Second-stage treatments add in major problems, as a result of the difficulty in administration and the lower efficacy of treatment. As mentioned above, the main drugs consist of melarsoprol (Pépin *et al.*, 1994) and eflornithine (Burri and Brun, 2003), the latter used only for *T. b. gambiense* infections (Iten *et al.*, 1995). Melarsoprol is an organic arsenical drug, leading to a rapid trypanosome cell lysis following its accumulation in the parasite due to an amino-purine transporter present (Burchmore *et al.*, 2002). Treatment induces many undesirable side effects, the most severe of which is an encephalopathic syndrome (Haller *et al.*, 1986, Pépin *et al.*, 1995), which occurs in approximately 4.7% and 8%, for patients with infections caused by *T. b. gambiense* and *T. b. rhodesiense*, respectively, with an average fatality ratio of 44% and 57%, respectively (Barrett *et al.*, 2003, Brun *et al.*, 2010). Besides having the worst side effects, melarsoprol resistant cases have been heightened over the years (Burri and

Keiser, 2001, Matovu *et al.*, 2001a), with increasing reports of drug failures concentrated mainly in central Africa, reaching averages of 30% in some foci.

In the case of HAT caused by *T. b. gambiense*, when patients reach the second stage of the disease, their other possible treatment relies on eflornithine injections (Burri and Brun, 2003), given for a total of 14 days with several daily infusions due to the short half-life of the drug (Burchmore *et al.*, 2002, Simarro *et al.*, 2008, Brun *et al.*, 2010). This anti-trypanocidal drug was first developed as an anti-cancer agent, being uptaken from the plasma membrane in a passive mode and acting as an inhibitor to a decarboxylase enzyme. Its high efficiency, low mortality rate and reduced adverse reactions make eflornithine the first line treatment for sleeping sickness caused by this specie. As side effects, patients can suffer from anaemia, diarrhoea and vomiting, amongst others; but the major drawback of this treatment is its high price. A drug used for treatment of Chagas disease – Nifurtimox – has been recently introduced as a combined treatment with eflornithine (Priotto *et al.*, 2009), although being effective only for infections with *T. b. gambiense*.

To overcome the adverse effects of trypanocidal drugs, combination treatments have been studied, which would lessen the dose-related side effects (Priotto *et al.*, 2006, Priotto *et al.*, 2007, Priotto *et al.*, 2009). On the other hand, a new orally available drug – DB289 - is at the final clinical trial phase but seems to be effective only in first stage disease (Barrett *et al.*, 2003, Simarro *et al.*, 2008).

Drug discovery and availability are reported by several programmes, including the Drugs for Neglected Diseases Initiative (DNDI - http://www.dndi.org/), which for example has started the First Human Phase I trial in 2011 of a new drug (SCYX-7158). Major challenges hold back the development of new drugs, as the treatment should be safe, affordable and easy to administer. On the other hand, the increasing use of trypanocides has lead to the emergence of drug-resistant parasites (Matovu *et al.*, 2001b, Geerts *et al.*, 2001), where there is a temporary or permanent loss of sensitivity against the active substance. Many factors can induce drug resistance (Matovu *et al.*, 2001b), related mainly to the host, as its immune system can strongly influence the course of treatment, but also the vector, which enables genetic exchange to occur inducing evolution of resistance, the drug and the parasite. Results show that cross-

resistance occurs more often when drugs target related metabolic pathways (Matovu *et al.*, 2001b), raising the possibility that by affecting different metabolic processes in combination, one can increase the efficiency of treatment.

The development of new drugs should focus on pathways that are present in the parasite but absent from their hosts (Barrett *et al.*, 1999), using technologies such as comparative biochemistry and comparative genomics to identify ideal targets. The trypanosome genome project (Berriman *et al.*, 2005) was essential to detect new potential drug targets and establish them as new treatment pathways. Target validation has been based widely on gene knockout and ribonucleic acid interference (RNAi) approaches (Ngô *et al.*, 1998, Wirtz *et al.*, 1999, Barrett *et al.*, 1999, Alsford and Horn, 2008, Monnerat *et al.*, 2009), although lately, high-throughput screening approaches have emerged (Alsford *et al.*, 2011, Alsford *et al.*, 2012). By stipulating that a gene is essential for parasite viability, one cannot assume that it consists of a good target; and caution should be taken when using gene knockout experiments as the sole criterion. Several metabolic pathways and signalling pathways have been studied over the years as credible targets (Burchmore *et al.*, 2002, Barrett *et al.*, 2003); and key cell cycle regulators have been established as good drug targets (Hammarton *et al.*, 2003b).

As treatment of HAT has considerable risks and due to the neglected status of the disease, measures are being directed more and more to prevention and control. While in the colonial times the authorities did not recognise the essential differences between the diseases causes by the two human infective *T. brucei* species and their influence in terms of controlling sleeping sickness, nowadays science and technology aim at controlling trypanosomiasis by reducing parasite transmission from host to vector and on to further hosts. The optimal control strategy rests on reducing the disease reservoir and controlling the tsetse fly vector (Barrett *et al.*, 2003, Fevre *et al.*, 2006, Brun *et al.*, 2010). Vector control includes the use of traps or insecticides, particularly the use of certain colours (blue) and chemicals (cow urine) to attract the insects. In terms of reducing the disease reservoir, and this is most important for infections with *T. b. gambiense*, where people remain asymptomatic for long periods (section 1.1.3), the major control technique is active case-finding and treatment. For *T. b. rhodesiense*,

decrease in reservoir infection is more difficult due to the variety of animal hosts (section 1.1.3). As such, vector control is the primary strategy used.

1.2. LIFE CYCLE

Elucidation of the life cycle of African trypanosomes started in 1894, when British Officer Bruce went to South Africa to investigate the outbreak of a disease in cattle. Although expecting to find a bacterial source for the disease, he discovered trypanosomes in the blood of the infected animals, and demonstrated that transfer of parasites could be achieved from one animal to the other (Cox, 2004). The role of the tsetse flies as carriers of the disease was also identified by Bruce, allowing later on the establishment of the overall life cycle of *T. brucei* (Figure 1. 2).

Over the years, the life cycle of *T. brucei* has been the subject of several studies (Vickerman, 1985, Matthews, 1999, Matthews *et al.*, 2004, Van Den Abbeele *et al.*, 2010, Peacock *et al.*, 2011), with significant advances in our knowledge of the different morphologies, gene expression rates and proliferation statuses at the different stages, and allowing the identification of the regulatory machinery. Being transmitted by the bite of the tsetse fly, *T. brucei* has a biphasic life cycle, linked strongly with the cell cycle as the parasite passes through replicative and cell cycle-arrested forms (Matthews and Gull, 1994, Hammarton *et al.*, 2003b), and undergoes several pre-adaptive morphological changes (Matthews, 1999, Matthews *et al.*, 2004, Matthews, 2005, Macgregor *et al.*, 2012).

1.2.1. *T. brucei* development in the mammalian host

Metacyclic trypanosomes are transmitted to the mammalian host by the bite of a tsetse fly, where they live within the bloodstream (Bloodstream form trypanosomes – BSF) and quickly differentiate into proliferating long slender trypomastigotes (Table 1. 1). A heterogeneous population exists in this host, comprising proliferative slender forms and transmissible stumpy forms, the latter being cycle arrested and appearing at

the peak of parasitaemia (Matthews, 1999, Matthews *et al.*, 2004, Matthews, 2005, Macgregor *et al.*, 2012). Infections can be sustained due to the capacity of trypanosomes for antigenic variation (Ziegelbauer and Overath, 1990), allowing them to periodically change their variant surface glycoproteins (VSG) which constitute their surface coat (McCulloch, 2004, Pays *et al.*, 2004), outpace the immune system and maintain an infection. Together with antigenic variation, immune evasion is enabled by endocytic recycling of membrane bound antibodies (Overath and Engstler, 2004, Vanhollebeke *et al.*, 2010).

Trypanosome infections exhibit a characteristic undulating parasitaemia profile (Figure 1. 3) (Matthews, 1999, Matthews *et al.*, 2004, Macgregor *et al.*, 2012), created by the transition between slender (SL) and stumpy (ST) forms, which is induced by release of the stumpy induction factor (SIF). SIF accumulates during parasitaemia (Figure 1. 3), stimulating transition into intermediate forms and then ST forms, and as ST forms are more resistant to complement-mediated killing, these dominate infection. ST forms do not revert to SL forms, and the majority of the population that is not taken up in the blood meal of a tsetse fly is removed by the host immune system, generating a decrease in parasitaemia, which is later on reversed by the growth of a new population of SL forms (Figure 1. 3). This new population has undergone antigen switching, and as such antigenic variation also contributes to the undulating profile (Ziegelbauer and Overath, 1990). This infection profile carefully balances the extension of the infection, by prolonging host survival, with an increase in the potential for transmission. Trypanosomes that are less reactive to SIF would possess a growth advantage and result in uncontrolled parasitaemia, but on the other hand are unable to ensure the existence of transmission stages (Matthews *et al.*, 2004, Macgregor *et al.*, 2012). Such is the example of the monomorphic cell lines used in laboratory, which are incapable of generating ST forms by failing to produce or respond to SIF, being able however to proliferate incessantly.

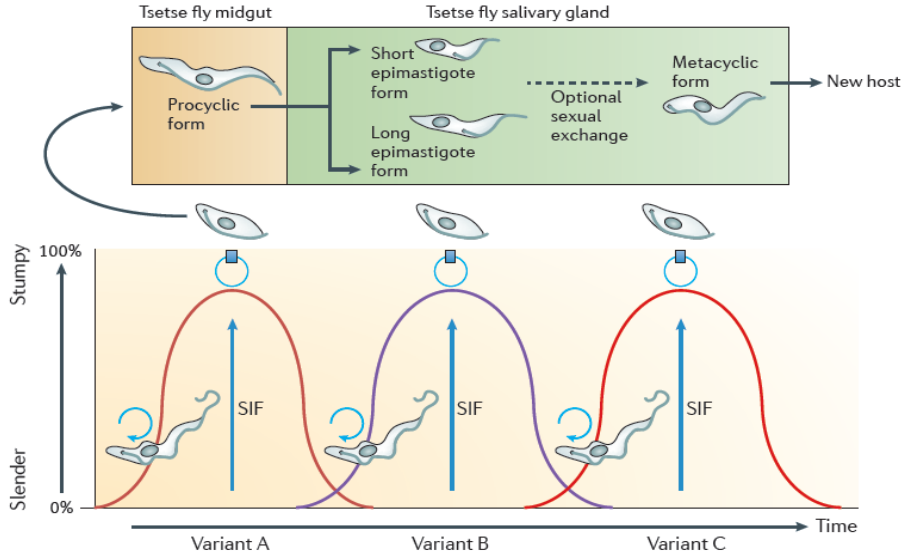

Figure 1. 3 – The life cycle and parasiteamia profile of *T. brucei* in the mammalian host. An undulating parasiteamia profile is maintained by the transition between the two BSF: proliferative slender and cell cycle arrested stumpy forms; the first being responsible for the increase in parasite numbers. Transformation into ST forms is induced by the release of SIF, leading to developmental changes in order to generated transmissible *T. brucei* forms, adapted for uptake by a tsetse fly during a blood meal. Once in the vector host, they differentiate to midgut procyclic forms, after which they proliferate and migrate to the salivary glands, where they attach and develop to metacyclic forms, which are infective to mammals. (Macgregor *et al.*, 2012)

SL form parasites are able to take advantage of the nutrients present in the bloodstream, degrading them in spherical glycosomes, and components of the Krebs cycle and oxidative phosphorylation are mainly absent. The replacement of proliferative with non-proliferative forms ensures the morphological changes needed for survival in the invertebrate host. A few days after the infection, the parasite population consists uniformly of proliferative SL form trypanosomes. After 4 days of infection, differentiation into ST forms begins and cells become arrested in G_1 phase (Macgregor *et al.*, 2012) (Figure 1. 4), which also translates at the molecular level with different gene expression profiles appearing (Figure 1. 4). Continuation of the cell cycle only occurs once the parasite enters the midgut of the tsetse fly (section 1.2.2). Loss of BSF specific VSG occurs 4 to 5 hours post-initiation of differentiation into ST forms, while presentation of EP procyclin is detectable after 2 hours (Matthews *et al.*, 2004, Matthews, 2005). Besides these events, morphological transformations allow progression into ST forms after 6-7 days of infection (Figure 1. 4), by expansion of the flagellar pocket (FP), reduction of flagellar length, repositioning of lysosome,

modification of the kinetoplast position by growth of the posterior end of the cell. An essential change upon differentiation into ST form is the mitochondrial elaboration, which is estimated to occur after 15 minutes of the start of differentiation (Bakker *et al.*, 1995). SL form parasites are adapted to the rich glucose environment of the blood, and as ST forms quickly need to adapt to loss of glucose when in the tsetse fly, a fully active mitochondrial respiratory chain is essential. All these changes are essential as they pre-adapt the parasites to the fly midgut (Tetley and Vickerman, 1985). Additionally, transition from SL to ST form is accompanied by changes in the endocytic machinery, as this pathway is mainly absent from procyclic forms (PCF) (Vanhollebeke *et al.*, 2010). Among these changes, a relocalisation of the lysosome is observed, with it acquiring an anterior position to the nucleus (Vanhollebeke *et al.*, 2010), and internalisation of several ligands is reduced. In fact, in ST form trypanosomes, the haptoglobin-hemoglobin receptor (TbHpHbR) is downregulated (Vanhollebeke *et al.*, 2010), causing a block in uptake of the complex, making this form more resistant to the trypanolytic particles in human serum.

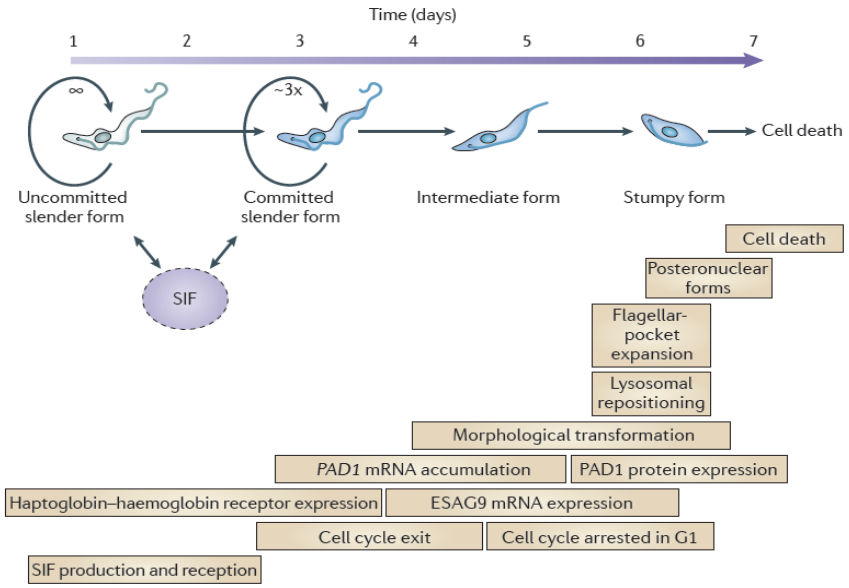

Figure 1. 4 – Transition from slender to stumpy forms in the mammalian host. Release of SIF stimulates slender forms to begin the transition to stumpy forms. Before cell cycle arrest in G_1 phase, a committed slender form can still undergo 3 rounds of cell division, after which SIF production is lost. By this time, intermediate forms no longer express the TbHpHbR, but express PAD1 and ESAG9 (expression site associated gene-9) proteins. Several morphological changes then occur upon transformation into stumpy forms, and cells that are not uptaken by the tsetse fly are eventually removed from the bloodstream. (Macgregor *et al.*, 2012)

Initiation and coordination of differentiation is controlled by different signalling pathways (Hammarton *et al.*, 2003b, Matthews *et al.*, 2004), which consequently ensure a correct organelle positioning and establish metabolic pathways that are characteristic of a PCF form.

1.2.2. *T. brucei* development in the tsetse fly host

When the tsetse fly feeds on an infected mammal the resulting bloodmeal contains both SL and ST parasites. The latter are arrested in the G_0/G_1 position of the cell cycle and possess a pre-adapted metabolism, making them ideal candidates to start the differentiation process and colonize the tsetse fly midgut. Once within the tsetse fly, parasites undergoes several complex cycles of differentiation and multiplication in distinct compartments of the tsetse fly (Figure 1. 5 and Table 1. 1). In the first two to three days after feeding, approximately 99% of the ingested parasites and cleared by the tsetse fly, and the remaining are fully differentiated into PCF cells (Van Den Abbeele *et al.*, 1999). One of the first detailed studies focusing on the life cycle in the invertebrate host was published in 1913 (Robertson, 1913), and subsequently added to by various labs (Lewis and Langridge, 1947, Tetley and Vickerman, 1985, Vickerman *et al.*, 1988, Van Den Abbeele *et al.*, 1999, Van Den Abbeele *et al.*, 2010, Gibson and Bailey, 2003, Macleod *et al.*, 2007).

Midgut colonization occurs from the posterior to the anterior end, and PCF parasites establish a robust stable population. There is a physical elongation of the parasites and long mesocyclic trypomastigotes (MS) are found close to the proventriculus after 6 days of infection (Van Den Abbeele *et al.*, 1999). These cells migrate into the tsetse foregut and proboscis, where they undergo further differentiation, replicating their DNA and repositioning the kinetoplast and BB to a location anterior of nucleus, thus becoming long epimastigote forms (LE) (Figure 1. 5 and Table 1. 1). Following mitosis conclusion, cells divide asymmetrically producing long and short daughter cells (SE), which migrate to the salivary gland using the flagellar beat of the long epimastigote (Van Den Abbeele *et al.*, 1999). Once in the salivary gland, short

epimastigotes attach to the wall and can proliferate even while attached (Vickerman *et al.*, 1988), can undergo meiosis and engage in sexual changes (Gibson and Bailey, 1994, Gibson *et al.*, 2008, Peacock *et al.*, 2011), expressing meiosis-specific proteins in the nucleus. Short epimastigotes further develop into metacyclic epimastigotes (MT), a cell cycle arrested form ready for retransmission into a mammalian host (Van Den Abbeele *et al.*, 1999) and expressing metacyclic-specific VSG (Tetley *et al.*, 1987).

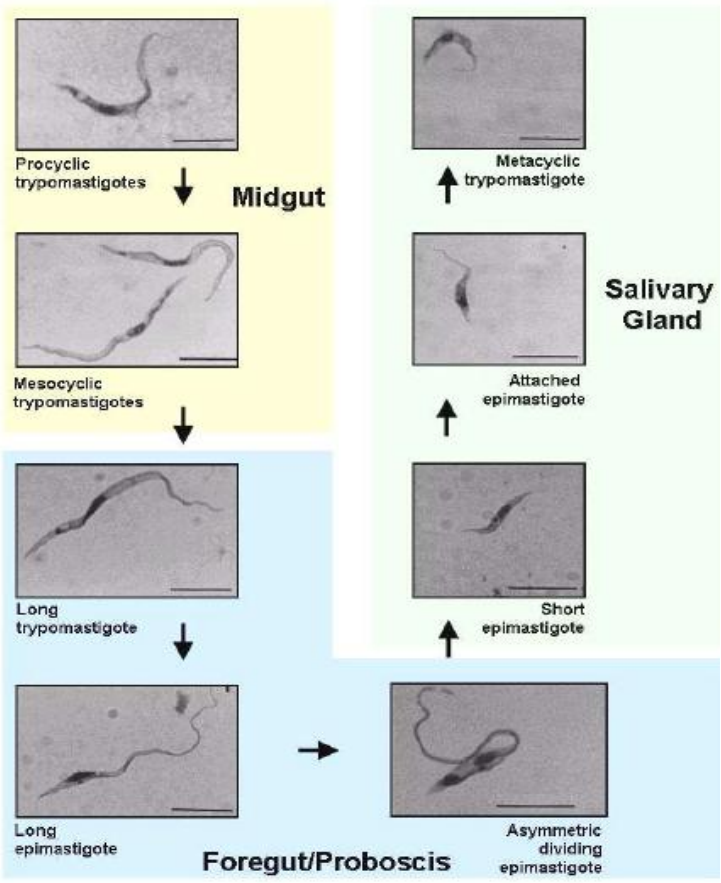

Figure 1. 5 – Development of *T. brucei* in the tsetse fly. Light microscopy images showing different morphological stages of *T. brucei* in the different compartments of the tsetse fly. Scale bar – 10 µm. (Van Den Abbeele *et al.*, 1999)

Inside the invertebrate host, we can divide the life cycle into two main events: establishment, as it has to establish as a PCF population in the midgut; and maturation, as the human infective trypanosomes need to leave the midgut and migrate into the salivary glands, where epimastigotes will multiply. A complete cycle needs a minimum

of 2 weeks, and in the end, the fly has the ability to produce metacyclics incessantly. In nature, there are a high amount of refractory tsetse flies (Welburn and Maudlin, 1999), which means that the high prevalence of mixed infections is concentrated in a small proportion of flies.

Analysis of the differentiation of the ST form into the PCF *in vitro* is possible by stimulating the cells with citrate and *cis*-aconitate and by reducing the temperature from 37ºC to 27ºC (Ziegelbauer *et al.*, 1990). *Cis*-aconitate addition to the medium is able to induce the differentiation events, even when the incubation temperature is not lowered.

Table 1. 1 - Localisation of each stage during the parasite life cycle. * - indicates proliferative stages. SL – slender trypomastigote; ST – stumpy trypomastigote; PC – PCF trypomastigote; MS – mesocyclic trypomastigote; DE – asymmetrically dividing epimastigote; LE – long epimastigote; SE – short epimastigote; AE – attached epimastigote; MT – metacyclic epimastigote. (Rotureau *et al.*, 2011)

		→ Parasite cycle →			
Morphotype	**Stage**	**Mammalian host**	**Tsetse fly vector**		
		Blood	Midgut	Proventriculus and foregut	Salivary glands
Trypomastigote	Slender *	**SL**			
	Stumpy	**ST**	**ST**		
	Procyclic *		**PC**		
	Mesocyclic		**MS**	**MS**	
Epimastigote	Dividing *			**DE**	
	Long			**LE**	
	Short			**SE**	**SE**
	Attached *				**AE**
Trypomastigote	Metacyclic				**MT**

During the development of the PCF in the tsetse fly midgut, a series of events take place including surface antigen changes (Overath *et al.*, 1983, Roditi *et al.*, 1989), changes in cell morphology (Matthews *et al.*, 1995, Rotureau *et al.*, 2011), and development of proliferative cells from the cell cycle arrested ST forms (Matthews and Gull, 1994). A striking transformation is seen, for example, at the level of the cytoskeleton components (Rotureau *et al.*, 2011), which translates as an increase in cell volume and elongation by microtubule extension at the posterior end, resulting in a remodelling of the entire sub-pellicular microtubule cytoskeleton. The increase in cell

length is accompanied by kinetoplast migration and metabolic changes, mainly related to the fact that the PCF displays a relatively conventional Krebs cycle, linked to electron transport chain-mediated ATP generation, and as such, expression of mitochondrial enzymes and proteins increases. A huge difference between BSF and PCF trypanosomes is the reduced endocytic activity in the latter, and one of the most characterised events in PCF differentiation is the gain of the insect stage-specific procyclin coat and loss of the BSF VSG coat.

1.3. HUMAN NATURAL IMMUNITY AND TRYPANOSOME IMMUNE EVASION

1.3.1. The trypanosome lytic factor

Humans have generated a particular innate immunity system against African trypanosomes, which is the reason why *T .b. brucei* is non-infective to humans. In fact, only *T. b. gambiense* and *T. b. rhodesiense* can resist trypanolysis caused by this defense and cause sleeping sickness. The host proteins involved in this process and the resistance mechanisms created by the parasites have been reviewed by several authors (Raper *et al.*, 2001, Vanhamme, 2010, Vanhollebeke and Pays, 2010).

The first reported cases of human natural immunity to African Trypanosomiasis date to more than 100 years ago (Laveran, 1902), but it was only in 1978 that the human component responsible for this resistance was identified (Rifkin, 1978). The resistance-specific transcript was first identified using serum-resistant and serum-sensitive *T. b rhodesiense* forms, revealing by Northern-blot analyses a differential expression of this gene in each form (De Greef *et al.*, 1989). Southern-blot results showed that both the resistant and the sensitive *T. b rhodesiense* forms have the gene coding for this transcript, but that it is absent from *T. b gambiense*, indicating resistance to trypanolysis by different mechanisms (De Greef *et al.*, 1989). This resistance-specific transcript was later on termed serum resistance associated gene (*SRA)* (Xong *et al.*, 1998).

Later in 1989, Hadjuk and colleagues demonstrated that resistance to lysis is due to resistance to a component present in normal human serum (NHS), a specific subclass of a high-density lipoprotein (HDL) (Hajduk *et al.*, 1989). The components responsible for lysis of the trypanosomes are called trypanosome lytic factor (TLF), and several authors reported the presence of two independent trypanolytic particles (Smith *et al.*, 1995, Tomlinson *et al.*, 1995, Hager and Hajduk, 1997, Raper *et al.*, 1999) (Figure 1. 6): TLF1 contains apolipoprotein AI (ApoAI), apolipoprotein AII, paraoxonase and haptoglobin related protein (Hpr); while TLF2 consists of a complex made of ApoAI, IgM and Hpr (Tomlinson *et al.*, 1995, Raper *et al.*, 1999).

Characteristics of TLF1 and TLF2.

Characteristic	TLF1	TLF2
Lipid	40%	<1%
Apolipoprotein A-I	+	+
Haptoglobin-related protein	+	+
IgM	–	+
Apolipoprotein A-II	Trace	–
Paraoxonase	Trace	–
Inhibited by haptoglobin	Yes	No
Density (g/ml)	1.20–1.26	1.28
Molecular mass (kDa)	550	1000
*[Plasma] (µg/ml)	10	12
*ng/LU	‡10–†375	‡625
*[Trypanolytic] minimum	0.15–3.75 nM	3 nM

*Calculated from TLF purification tables [10•,34]. LU (lytic unit) refers to 50% lysis of †3×10^6 trypanosomes in 300 µl/120 min/37°C [9] or ‡2×10^6 trypanosomes in 200 µl/120 min/37°C [10•].

Figure 1. 6 – Characteristics of the two trypanolytic particles, TLF1 and TLF2. (Raper *et al.*, 2001)

The animal-infective specie *T. b. brucei* does not infect humans due to killing by the TLF. Mice infected with *T. b. brucei* and treated with TLF1 show a decrease in parasite numbers, and pre-treatment with the same factor results in protection against *T. b. brucei* (Barker *et al.*, 2001).

In order to establish an infection, both human-infective *Trypanosoma* species need to resist TLF. However, the way the different species resist trypanolysis is quite distinct and also distinguishes the two groups inside *T. b. gambiense* species. While *T.*

b. gambiense group 1 resists lysis in a constitutive way, *T. b. gambiense* group 2 shows variable resistance (Mehlitz *et al.*, 1982, Tait *et al.*, 1984, Zillmann *et al.*, 1984, Agbo *et al.*, 2001, Capewell *et al.*, 2011). As *T. b. gambiense* does not have the *SRA* gene, which is responsible for serum resistance in *T. b. rhodesiense*, they are thought to have evolved an independent mechanism to avoid killing by trypanolytic human serum factors (Kieft *et al.*, 2010, Capewell *et al.*, 2011, Symula *et al.*, 2012, Bullard *et al.*, 2012). Initial studies on this subject indicate that *T. b. gambiense* group 1 parasites evade human innate immunity by decreasing expression of the TbHpHbR (section 1.3.3) and by presenting sequence changes to this receptor (Kieft *et al.*, 2010, Symula *et al.*, 2012). On the contrary, *T. b. gambiense* group 2 serum resistance seems to be independent of TbHpHbR (Capewell *et al.*, 2011, Symula *et al.*, 2012), suggesting differences in the mechanism of serum resistance between the two groups.

These results have also elucidated the role of the TbHpHbR in serum resistance. In fact, early analyses proved that this receptor's function in humans changed in order to elicit innate host immunity against the parasite (Vanhollebeke *et al.*, 2008). Although entry of TLF1 and TLF2 can be performed via this receptor, parasites have also evolved alternative pathways for uptake of these factors, either by the use of other receptors or by fluid-phase uptake (Bullard *et al.*, 2012).

As opposed to *T. b. gambiense*, *T. b. rhodesiense* resistance is found to depend on expression of the *SRA* gene, which is not always expressed as it is associated with antigenic variation and expressed as a VSG-expression site (ES) (Xong *et al.*, 1998). Later studies showed the homology between *SRA* and *VSG*, and confirmed that resistance to TLF is related to high level of expression of SRA in *T. b. rhodesiense* resistant forms (Milner and Hajduk, 1999). In TLF-resistant parasites, *SRA* mRNA is present in 1000-fold higher amounts than in *T. b. rhodesiense* sensitive trypanosomes.

The presence of NHS was found necessary to trigger the selection of the unique *SRA* containing ES, leading to transcription of this gene under these conditions only (Xong *et al.*, 1998). SRA expression is not only necessary but sufficient to guarantee trypanolysis resistance (Xong *et al.*, 1998). At first considered as a surface molecule, SRA was later on demonstrated to localise to the endocytic pathway (Vanhamme *et al.*, 2003, Oli *et al.*, 2006). The protein is present in the endosomes (Stephens and Hajduk,

2011), being trafficked to the FP transiently, and its mode of action is highly dependent on its N-terminal α-helix (Vanhamme *et al.*, 2003).

By affinity chromatography and using immobilized SRA and soluble NHS, SRA was shown to bind strongly apolipoprotein L-I (ApoL1). The fact that recombinant ApoL1 displays trypanolytic activity (Vanhamme *et al.*, 2003), its presence in both TLF1 and TLF2 (Molina-Portela *et al.*, 2005), and the fact that confocal microscopy proves it to be uptaken through the endocytic pathway to the lysosome (Vanhamme *et al.*, 2003), has led to the conclusion that toxicity of TLF is due to this component. ApoL1 is thus considered the key component of the TLF (Vanhamme *et al.*, 2003). Inactivation of ApoL1 results from direct interaction between the N-terminal α-helix of SRA protein with the C-terminal α-helix of ApoL1 (Oli *et al.*, 2006, Molina-Portela *et al.*, 2008), as opposed to initial data that suggested SRA mediated resistance by decreasing TLF endocytosis (Hager and Hajduk, 1997).

Besides its importance as a trypanolytic factor, *in vitro* studies showed that mutations in ApoL1 induce lysis of a deadly subspecies of *Trypanosoma* that is normally completely resistant to ApoLI lytic activity (Genovese *et al.*, 2010). In fact, specific deletions in *ApoL1* gene in a group of African-Americans prevent the interaction between SRA and ApoL1, and as such the host becomes resistant to trypanosomiasis caused by *T. b. rhodesiense*, while none of the variant forms lyse *T. b. gambiense*. This study shows also that, although these variants of ApoL1 are capable of lysing *T. b. rhodesiense*, the host develops instead a kidney disease. In fact, ApoL1 variants contribute to the increased risk of renal disease in African-Americans, such that 30% of African-American chromosomes contain the APOL1 risk alleles for renal disease (Genovese *et al.*, 2010).

Recent work with infected patients has proved that ApoL1 expression is induced in patients infected with *T. b. gambiense* although it is not associated with susceptibility to sleeping sickness (Ilboudo *et al.*, 2012). ApoL1 resembles pro- and anti-apoptotic members of the Bcl2 family and a model for its mode of action was created in 2006 (Pays *et al.*, 2006). Figure 1. 7 depicts the mode of action of ApoL1 and how the SRA protein prevents trypanolysis.

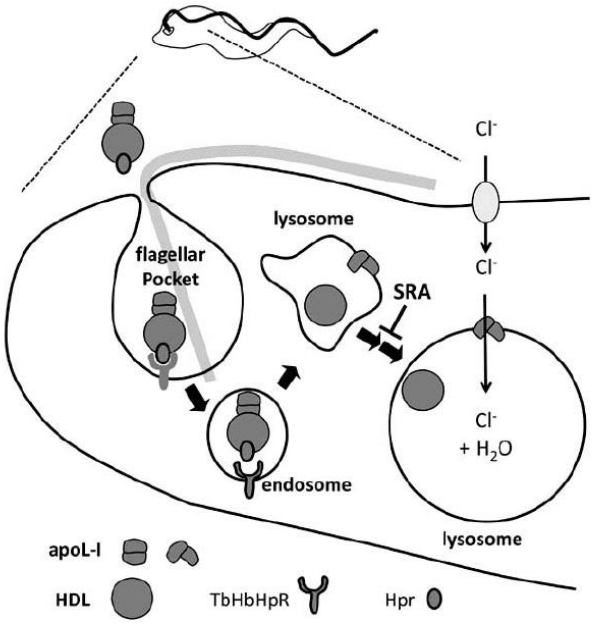

Figure 1. 7 – Model of the lytic mechanism. The representation depicts the internalisation of components from the TLF complex by the trypanosome's FP and its progression through the endocytic pathway until promotion of cell lysis. Entry of TLF is performed by interaction of the Hpr protein with the haptoglobin-hemoglobin receptor present in the FP, after which the complex follows the endocytic pathway until the lysosome. Once in this organelle, ApoL1 is freed and promotes entry of chloride ions into the lysosome, leading to an increase of water import and lysosome inflation. In parallel, this leads to an increase in uptake of chloride ions from the extracellular medium. Both these phenomena eventually lead to cell death. (Vanhamme, 2010)

HDL-bound ApoL1 enters the cell by endocytosis via the FP (section 1.3.2). Entry of TLF1 is proven to be dependent on a specific receptor, the TbHpHbR (section 1.3.3), which forms a complex not with Hpr alone but rather with haemoglobin (Hb) complexed with Hp or Hpr (Vanhollebeke *et al.*, 2008). This receptor is present on the trypanosome's FP and is responsible for the uptake of Hb-charged TLF1 complexes, while TLF2 uptake seems to be independent of this receptor (Vanhollebeke *et al.*, 2008). Although not having trypanolytic activity, Hpr is involved in binding and uptake of TLF by the parasite.

After being taken up by the parasite, the complex follows the endocytic pathway (Figure 1. 7), where progressive acidification occurs (Pérez-Morga *et al.*, 2005). Once in the lysosome, the decrease in pH causes the toxin to dissociate from the HDL carrier and to be inserted into the endosomal membrane where it promotes the import of chloride ions into the lysosome. Consequently, besides triggering import of water into

the lysosome and lysosomal inflation, it also activates entry of chloride ions from the extracellular medium through plasma membrane channels (Pérez-Morga *et al.*, 2005, Pays *et al.*, 2006). These two phenomena create an irreversible circle, ultimately leading to cell death.

The innate immunity mechanism present in the human host, where ApoL1 plays a pivotal role, allows the host to resist most African trypanosome species that otherwise cause fatal disease in livestock.

1.3.2. The endocytic apparatus and immune evasion

The endocytic system of *T. brucei* is highly polarized, and apart from the endoplasmic reticulum (ER), which is distributed throughout the cytoplasm, the secretory and endocytic organelles are all located between the nucleus and kinetoplast (Morgan *et al.*, 2002a, Morgan *et al.*, 2002b, Bonhivers *et al.*, 2008b). A complex machinery guarantees that, at the same time as external molecules are being imported, cell surface components and secreted material reach the plasma membrane by exocytosis.

The endo-exocytic apparatus starts in the FP (section 1.4.7), which maintains specific receptors protected from the host immune system, but is also responsible for sorting protective parasite glycoproteins and removing host antibodies from the cell surface (Barry, 1979, Overath and Engstler, 2004, Engstler *et al.*, 2007, McKean and Gull, 2010, Natesan *et al.*, 2011). This creates a direct connection between the endocytic pathway and evasion of the mammalian host immune system (section 1.3.1).

The endocytic machinery and its mechanisms of action have been the subject of several studies over the years (Webster and Russell, 1993, Landfear and Ignatushchenko, 2001, Morgan *et al.*, 2002a, Morgan *et al.*, 2002b, Overath and Engstler, 2004). Recent advances in understanding the endosomal compartments have been made possible due to EM visualisation (Souza *et al.*, 2009) and MAb generation (Field *et al.*, 1998, Jeffries *et al.*, 2001, Pal *et al.*, 2002).

In Trypanosomatids, endocytosis is clathrin-dependent (Morgan *et al.*, 2001, Allen *et al.*, 2003, Adung'a *et al.*, 2013). Clathrin-coated vesicles were detected in BSF trypanosomes, distributed through numerous structures on the posterior end of the cell (Morgan *et al.*, 2001). In PCF trypanosomes, clathrin (CLH) expression is 10 times lower, and restricted to structures close to the FP. In general, clathrin-coated vesicles bud off from the FP, carrying ingested materials that are delivered to early endosomes (Field and Carrington, 2009). The separation of the ligands from the receptors is made, allowing recycling of the different proteins to their initial locations and targeting of endocytosed material to lysosomes. The endocytic pathway is represented in Figure 1. 8.

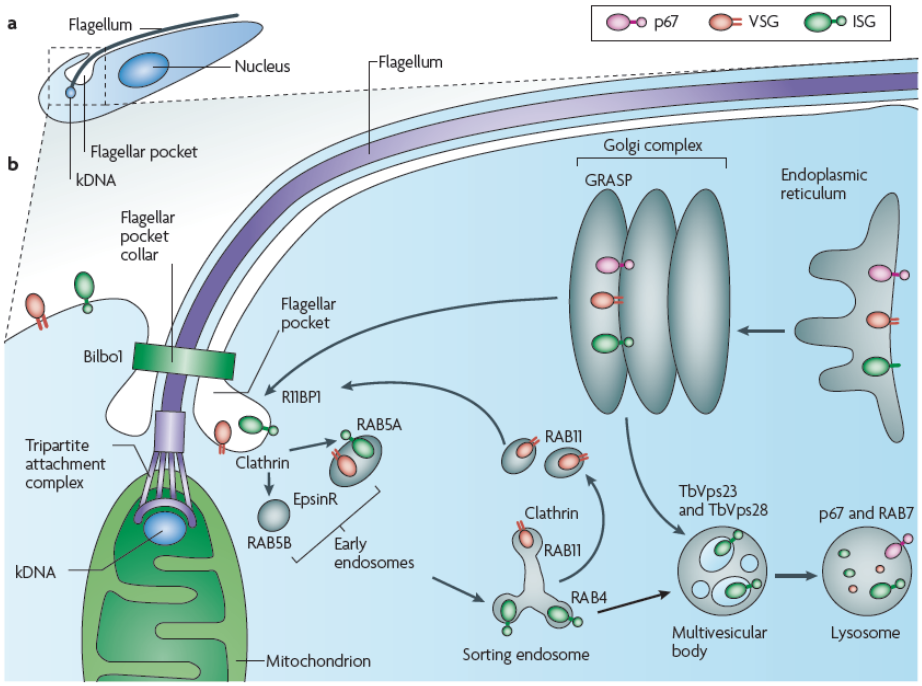

Figure 1. 8 – Schematic representation of the *T. brucei* endocytic system. (a) representation of a T. *brucei* cell. (b) Endocytic and recycling pathways, showing compartments and proteins involved in each process (Field and Carrington, 2009).

Tracking of the progress of imported material is possible with co-localisation with antibodies raised against endosomal specific markers. One of the first identified markers was TbBiP (Binding protein), which allows ER staining (Bangs *et al.*, 1993), and later on components of the clathrin-dependent pathway were also described

(Morgan *et al.*, 2001). In parallel, several TbRAB (Ras-related proteins in brain) proteins have also been identified (Field *et al.*, 1998, Field *et al.*, 2000, Jeffries *et al.*, 2001, Pal *et al.*, 2002), allowing visualisation of the different stages in the endosomal pathway. These proteins are great markers for subcellular compartments, and a total of five TbRABs have been localised within the pathway: TbRAB7 is associated with the lysosome (Field *et al.*, 2000, Silverman *et al.*, 2011), whereas TbRAB4, 5A, 5B and 11 are components of the endosomal system (Field *et al.*, 1998, Jeffries *et al.*, 2001, Pal *et al.*, 2002). For example, early endosomes are RAB5-positive compartments, although the two isoforms have been demonstrated to have different localisation in BSF trypanosomes (Field *et al.*, 1998, Pal *et al.*, 2002). The co-localisation of these markers with some of the endocytosed material but not all suggest the presence of several endosomal pathways, allowing basal endocytosis of certain proteins like VSG to occur without interfering with the recycling of other molecules.

Clathrin-mediated endocytosis is essential for cellular viability (Allen *et al.*, 2003) and depletion of CLH is lethal and causes severe swelling of the FP, a phenotype commonly referred to as the "Big-Eye" phenotype. TbCLH ablation in the mammalian form prevents uptake of nutrients from the external medium which remain concentrated in the FP, while the exocytic process remains unaffected, resulting in an enlargement of this structure (Allen *et al.*, 2003). The equilibrium maintained in normal cells between endocytosis and exocytosis is lost in TbCLH depleted cells. On the contrary, in PCF trypanosomes, an accumulation of vesicles in the cytoplasm is observed; suggesting a functional variation of TbCLH for the different life cycle stages. Developmental regulation is also seen for example in the uptake of several ligands. This is the case of the downregulation of uptake of the HprHb complex observed in ST forms when compared to SL forms (Vanhollebeke *et al.*, 2010).

Besides CLH, there are several distinct *T. brucei* proteins which, when depleted, cause a decrease in endocytic activity (García-Salcedo *et al.*, 2004, Price *et al.*, 2010, Spitznagel *et al.*, 2010). Among them is the enzyme myristoyl-CoA:protein N-myristoyltransferase (Price *et al.*, 2010), which after 72 hours post-induction of the RNAi cell line causes 50% of cells to display defects in endocytic uptake. Although not presenting enlargement of the FP, vesicle accumulation around the FP is observed, and

the cell line is unable to establish an infection in a mouse model (Price *et al.*, 2010). Endocytic uptake and recycling is of significant importance for trypanosome survival in the mouse model (Natesan *et al.*, 2011). Recent studies show that trypanosomes are severely affected by defects in the recycling pathway but tolerate defects in CLH expression and in the early endosomal components (Natesan *et al.*, 2011).

The importance of endocytosis in survival in the mammalian host is firstly related to its role in surface-protein trafficking (Overath and Engstler, 2004). Although antigenic variation is the primary response mechanism to an increase in anti-VSG antibody concentration, recycling of the major surface protein of BSF trypanosomes, the VSG, is essential to maintain parasitaemia. The VSG polypeptide itself is highly immunogenic and its recycling process is constitutive. VSG uptake is representative of membrane uptake, sharing some endocytic steps with fluid-phase endocytosis (Figure 1. 9).

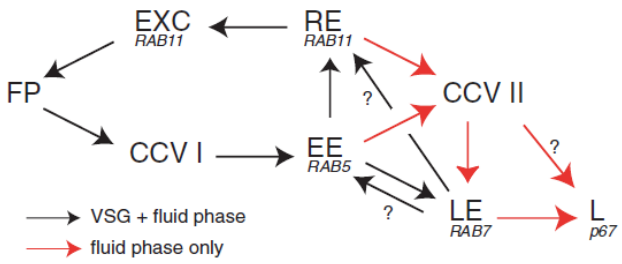

Figure 1. 9 – Flow diagram of fluid-phase and VSG through the endocytic apparatus. The red arrows refer to steps only seen for fluid-phase cargo, while the remaining are common (black arrows). FP – FP; CCV I and CCV II– class I and class II clathrin-coated vesicles, respectively; EE – early endosomes; LE – Late endosomes; L – lysosome; RE – recycling endosomes; EXC – exocytic carrier. (Overath and Engstler, 2004)

The VSG rapidly cycles through the FP and different endosomal structures. This rapid recycling of VSG has an important role on host immune evasion. Upon exposure to host antibodies, the VSG-Ig complex is rapidly formed, capped and endocytosed in the FP, moving then towards the nuclear area. From early RAB5-positive endosomes it moves directly to RAB11-positive recycling endosomes while the remainder goes to late endosomes (Figure 1. 9). A second and slower transfer to recycling endosomes occurs at this point. Disruption of the VSG-Ig connection allows internal degradation of the antibodies, while the intact VSG passes through multiple endocytic compartments

until is returned to the cell surface. The mechanisms by which the parasites destroy the antibodies are unknown, although they are essential for maintaining the infection. In terms of fluid-phase cargo, after leaving early endosomes the cargo fills the late endosomal compartment and by additional slow transfer ends up accumulating in the lysosome (Figure 1. 9). The complexity and organization of this system allows it to recycle membrane and VSG from late endosomes, while transferring fluid-phase material to the lysosome. The specific mechanisms on how this occurs remain to be found.

1.3.3. Surface receptors

Two receptors with significant importance for the BSF and with roles in endocytosis are located within the FP: the transferrin receptor (TfR) and the TbHpHbR.

BSF trypanosomes need host-derived growth factors for their survival and multiplication, and early studies demonstrated that transferrin (Tf) is essential for growth in the mammalian stage (Schell *et al.*, 1991). Its uptake requires a specific receptor (Steverding *et al.*, 1995) and the interaction between receptor and ligand has been analysed by several groups over the years (Bitter *et al.*, 1998, Mehlert *et al.*, 2012, Steverding *et al.*, 2012). The TfR from *T. brucei* is quite distinct from the mammalian one (Steverding, 2000), in terms of structure, properties and function.

The TfR is located in the FP and consists of a heterodimeric protein encoded by two homologous *ESAG*s - *ESAG6* and *ESAG7* – which are located upstream of the *VSG* ESs (Ligtenberg *et al.*, 1994, Steverding *et al.*, 1994). As in *T. brucei* several ES genes are present, different tranferrin receptors are expressed. The small differences among the different receptors affect severely the binding affinity for Tf of different mammals and consequently the survival on different hosts (Bitter *et al.*, 1998). Such results suggest that the ability to switch between different TfR genes allows the parasites to cope with the sequence diversity in the Tf of the host (Bitter *et al.*, 1998). This might explain how *T. brucei* is able to colonize different mammals and take up Tf from the blood of the host, without interference from the anti-TfR antibodies raised by the latter.

The connection between the receptor and the membrane is made by a glycosylphosphatidylinositol (GPI) anchor at the C-terminus of ESAG6 (Bitter *et al.*, 1998). While VSG is maintained by two GPI anchors, the single anchor in the TfR leads to a relatively weak interaction with the FP membrane, which might allow the receptor to leave the membrane and relocate to the fluid phase of the FP (Mehlert and Ferguson, 2007, Mehlert *et al.*, 2012). This would allow the TfR to find space within the VSG coat to capture Tf, without exposing the underlying plasma membrane.

After internalisation through the FP, the Tf-TfR complexes are taken to early endosomes where the acidic pH triggers the release of iron from Tf (Dautry-Varsat *et al.*, 1983, Maier and Steverding, 1996). Within the endosomal system, apotransferrin is delivered into lysosomes where it is proteolytically degraded (Grab *et al.*, 1992). Large peptide fragments are released from the trypanosomes, which can be recovered from the medium, while iron remains in the cell (Steverding *et al.*, 1995). The GPI-anchored receptor is recycled to the FP via recycling endosomes. Figure 1. 10 shows the overall steps on Tf uptake and receptor recycling.

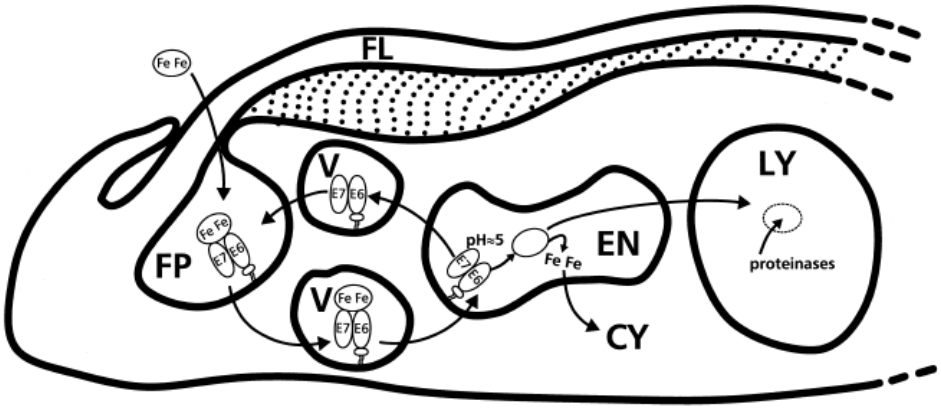

Figure 1. 10 – Schematic representation on Tf uptake in BSF trypanosomes. E6/E7 – heterodimeric transferrin receptor; FP – FP; FL – flagellum; V – vesicles from the endo- and exocytic pathway; EN – endosome; LY – lysosome; CY . cytosol. Tf-TfR complexes are internalised via the FP and taken to arely endosomes. The acidic pH in these structures leads to the releas of iron from Tf. Apotransferrin is then delivered to the lysosomes where degradation occurs. The GPI-anchored receptor is recycled back to the FP, while iron remains in the cell. (Steverding, 2000)

Another receptor characterised in *T. brucei* is the HpHbR, also located to the FP. The crystal structure of *T. congolense* HpHbR has been recently solved and investigation on the dimensions of *T. brucei* HpHbR and VSG have revealed that the receptor is more elongated than VSG and thus the presence of a VSG coat does not prevent immunoglobulin binding (Higgins *et al.*, 2013). The main role for this receptor is to provide haem to the trypanosomes, coming from the host Hb.

In parallel, this receptor facilitates internalisation of TLF1 (Vanhollebeke *et al.*, 2008) present in the human serum and associated with the HpHb complex, triggering trypanosome lysis (section 1.3.1). The rate of uptake through this receptor is dependent on the relative amounts of TLF1-Hpr-Hb and Hp-Hb (Barker *et al.*, 2001, Vanhollebeke and Pays, 2010). *In vivo*, the competing Hp-Hb is maintained at extremely low levels by the host (Fagoonee *et al.*, 2005), leading to uptake of TLF1-Hpr-Hb complex instead. The amount of this complex is as such controlled by the rate of Hb release and also by the turnover rate of the TLF protein.

Mutations in this receptor have been hypothesized to lead to reduced uptake of TLF1 and confer resistance to human serum for susceptible *T. b. gambiense* groups (Symula *et al.*, 2012). The trypanolysis mechanisms and proteins have been reviewed in section 1.3.

1.4. CELL BIOLOGY

The trypanosome cell is vermiform, around 15-30 µm long, contains a highly polarized microtubule cytoskeleton and constantly moves with the help of a flagellum. Independent of the life cycle stage, the trypanosome's vermiform shape is maintained by a set of subpellicular microtubules (section 1.4.2) that run along the axis of the cell beneath the plasma membrane (Sherwin and Gull, 1989a). The cytoskeleton and its major components will be described in detail in sections 1.4.1 to 1.4.8.

The cellular organelles are similar to other eukaryotic cells (Figure 1. 11), such as nucleus, ER, Golgi apparatus, amongst others. Distinct features include the presence of the kinetoplast and its close association with the BB and the flagellum.

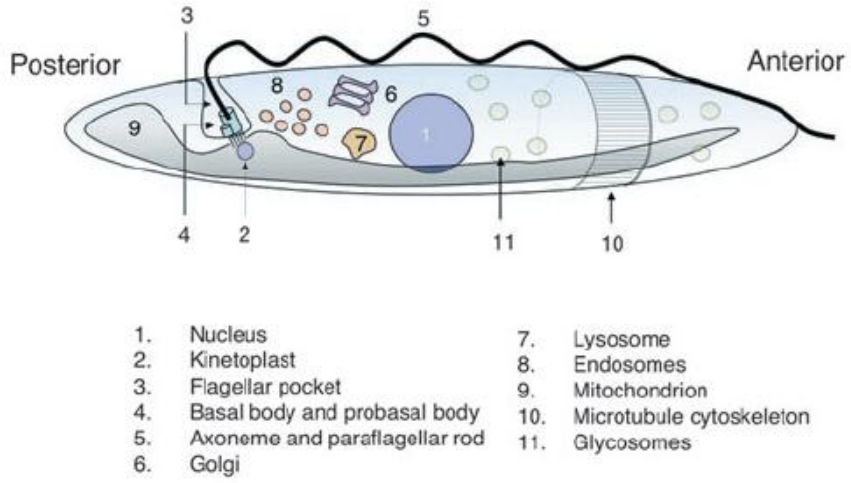

Figure 1. 11 – Schematic representation of a *T. brucei* BSF cell. Major cellular structures are indicated. (Matthews, 2005)

The nuclear genome of *T. brucei* contains 11 megabase chromosomes and around 100 minichromosomes of 50 to 500 kb (Gottesdiener *et al.*, 1990, Melville *et al.*, 1998). The large chromosomes contain most genes, while the minichromosomes harbour genes involved in antigenic variation, including the *VSG* genes. The genome has been sequenced (Berriman *et al.*, 2005).

Besides the nuclear DNA, trypanosomes have a single mitochondrial genome, the kDNA, whose replication is coordinated with that of the nucleus. The kDNA is composed of two classes of circular DNA: maxicircles and minicircles (Klingbeil and Englund, 2004), which encode for mitochondrial proteins and short guide RNAs, respectively. The latter are necessary for post-transcriptional changes of the maxicircles (RNA editing), which occur at the editosome (Madison-Antenucci *et al.*, 2002), and are required for cellular viability of both life cycle stages (Schnaufer *et al.*, 2001).

The mitochondrion itself is an elongated structure that runs from the posterior to the anterior end of the cell. PCF trypanosomes have a highly active mitochondrion, to

compensate for the lack of glucose as an energy source (Bochud-Allemann and Schneider, 2002, van Weelden *et al.*, 2003). On the contrary, the mitochondrion of BSF trypanosomes consists of only a tubular structure without cristae, reflecting the lack of mitochondrial respiration in the mammalian host. During this stage, energy generation is obtained by glycolysis in specialized organelles: the glycosomes (Parsons, 2004). Mitochondrion activity is developmentally regulated, as upon uptake by a tsetse fly, energy generation changes from being exclusively dependent on glycolysis to a mitochondrion-based system (Matthews, 2005).

The endocytosis process in *T. brucei* is developmentally regulated and membrane trafficking is highly polarized, with all endocytosis and exocytosis occurring at the FP. The endocytic apparatus and mechanisms are described in detail in section 1.3.2.

The need for the parasites to adjust to two distinct hosts has led to the development of several unusual organelles and features of cell biology. The transition between the different life cycle forms is accompanied by a set of morphological changes in cell size, shape and positioning of organelles (Rotureau *et al.*, 2011). One of the most obvious difference between BSF and PCF parasites concerns the position of the kinetoplast (Matthews, 2005). While PCF trypanosomes have a kinetoplast located midway between the nucleus and the posterior end of the cell, in BSF cells, this structure localises close to the posterior end of the cell.

Additionally, while PCF parasites have a surface glycoprotein coat comprised of procyclins (Acosta-Serrano *et al.*, 1999), the BSF, found living freely in the blood of the mammalian host, is covered in a dense coat comprised of VSG (Johnson and Cross, 1977). Trypanosomes have a repertoire of approximately 1500 *VSG* genes and pseudogenes (Berriman *et al.*, 2005). To be expressed, the VSG gene has to be located at one of around 20 ES, and only one ES is active at a time and therefore only one VSG is expressed (Navarro and Gull, 2001). The VSG ESs contain numerous expression site associated genes (ESAG), all co-transcribed with the same promoter.

1.4.1. Cytoskeleton

Figure 1. 12 depicts the basic organization of the trypanosome cytoskeleton. Besides the clear presence of the subpellicular corset along the cell body, a single flagellum exits from the FP and is attached to the cell body by a microtubule system called the flagellar attachment zone (FAZ). The flagellum comprises the axoneme and the paraflagellar rod (PFR).

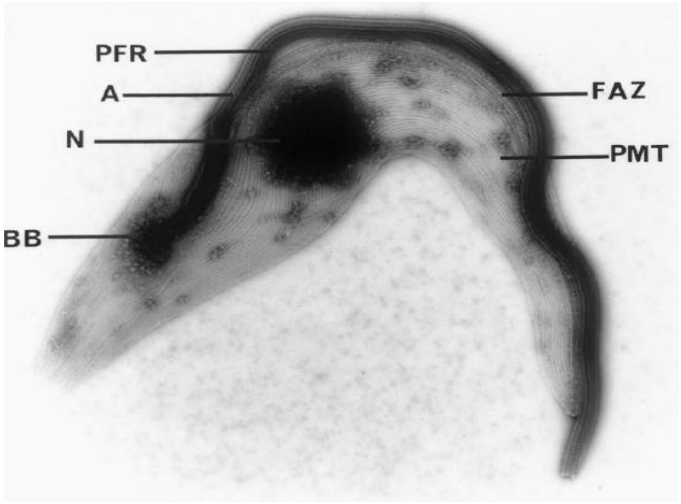

Figure 1. 12 – Negatively stained PCF *T. brucei* cytoskeleton after detergent extraction. A – axoneme; BB – basal body; FAZ – flagellar attachment zone; N – nucleus; PFR – paraflagellar rod; PMT – subpellicular microtubules. (Gull, 1999)

Besides being responsible for maintaining the cell shape during differentiation, the trypanosome cytoskeleton is involved in motility and attachment to host cell surfaces. Genome analysis (Berriman *et al.*, 2005), together with studies using specific MAbs (Woods *et al.*, 1989), has allowed the identification of cytoskeleton components (Figure 1. 12). At the same time, different microtubule associated proteins (MAPs) have been characterised (Kohl and Gull, 1998). Detergent extraction techniques allow purification of cytoskeleton structures from other cellular components, permitting further analyses of the different components.

1.4.2. Subpellicular microtubules

In Trypanosomatids, parallel rows of microtubules lie under a pellicle, and thus are known as subpellicular microtubules, and constitute the basic scaffold that maintains cell shape. The major proteins comprising microtubules are αβ-tubulins, that associate with each other in order to form a polymeric structure, remaining intact throughout the entire cell cycle (Sherwin and Gull, 1989a). Improvement in transmission electron microscopy (TEM) techniques has allowed the visualisation and study of these structures.

The subpellicular corset is formed from more than 100 microtubules made from repeated αβ-tubulin heterodimers of 24 nm diameter and variable length, cross-linked to each other and to the plasma membrane (Sherwin and Gull, 1989a). During cell division, there is an increase in the number of microtubules, although the distance between them is kept constant (Sherwin and Gull, 1989a). This suggests the existence of a mechanism that controls the assembly of new microtubules while regulating the increase in cell diameter, in response to the insertion of new plasma membrane components. It is said that cytoskeletal inheritance is semiconservative, as rather than breaking down during cell division, the daughter cytoskeleton microtubules are assembled between the existing ones (Sherwin and Gull, 1989b).

Subpellicular microtubules are present throughout the cell body of the trypanosomes, except at the FP region, where the microtubule corset is replaced by the FAZ. The microtubules have a uniform polarity which contributes directly to the cell asymmetry: minus ends are anterior and plus ends are posterior (Robinson *et al.*, 1995). This cytoskeletal corset also influences the position of single-copy organelles, which remain concentrated between the posterior end and the centre of the cell. This polarization is opposed to that observed in the flagellar axoneme, where the positive end is at the distal tip of the flagellum (anterior end) (Robinson *et al.*, 1995). These cortical microtubules are highly stable upon detergent extraction, allowing separation from remaining organelles upon fractionation and revealing the detailed substructure of the cytoskeletal filaments (Sherwin and Gull, 1989a).

The assembly of microtubules has been mainly assessed by analyses of their sensitivity to disrupting agents, for example low temperatures, high pressure and several drugs. The success in purifying and assembling *in vitro T. brucei* tubulin into microtubules (MacRae and Gull, 1990) allows the direct screening of inhibitors and analyses of their effectiveness. For instance, drugs that depolymerize microtubules in mammalian cells do not affect the subpellicular microtubules of trypanosomatids. Such is the case for colchicines and the benzimidazoles (Filho *et al.*, 1978). On the contrary, vinblastine and maytansine remain good inhibitors of microtubule polymerization *in vitro* (MacRae and Gull, 1990).

Coumpounds as triflurin and other herbicides (Chan and Fong, 1994) have shown to be strong disruptors of the trypanosomatid cytoskeleton. On the other hand, drugs such as Taxol stabilize microtubules and induce significant morphological changes, producing profound effects on cytokinesis (Baum *et al.*, 1981). Phenotypes obtained with another antimicrotubule inhibitor – rhizoxin - are quite distinct, as mitosis is inhibited but segregation of other organelles as BB and flagellum still take place (Robinson *et al.*, 1995).

All these data, together with the fact that microtubules remain stable throughout the cell cycle, point to unique control of their assembly; and indicate the presence of different cell cycle checkpoints to regulate organelle segregation as well as cytokinesis events.

1.4.3. Core cytoskeleton components: actin and tubulin

In most eukaryotic cells, actin plays an essential role in structure and dynamics. So far, no actin-based motility has been described in trypanosomatids, although its involvement in endocytosis and intracellular transport has been analysed (McPherson, 2002, Stamnes, 2002, García-Salcedo *et al.*, 2004). Actin is essential for BSF trypanosomes and seems to be required for the first step in the endocytic pathway – the formation of vesicles from the FP (García-Salcedo *et al.*, 2004). Such a functional role is not visible in PCF cells, where the FP is not affected by actin knockdown but rather

the Golgi becomes distorted and vesicles accumulate. As to its localisation, actin co-localises with the highly polarized endocytic pathway in BSF trypanosomes, whereas in the insect stage it is distributed throughout the cell (García-Salcedo *et al.*, 2004).

Because proteins associated with actin functions in other cells are present and expressed in trypanosomatids, an unknown role for the actomyosin microfilament system is suggested (García-Salcedo *et al.*, 2004).

On the contrary, six members of the tubulin superfamily have been identified in *T. brucei* (Berriman *et al.*, 2005): α-, β-, γ-, ζ-, δ-, and ε-, the final two *characteristic* of flagellated organisms with BB. Tubulin genes are arranged in a cluster of tandemly repeated α/β pairs, with a maximum of 19 repeats (Seebeck *et al.*, 1983). Data suggest that all of the genes in the tubulin loci encode the same α- or β-tubulin, and thus presence of different tubulin isotypes is due to post-translational modifications – glutamylation, acetylation and detyrosination (Gallo and Precigout, 1988). Acetylation of α-tubulin occurs at lysine 40 and this isoform is evenly distributed through the subpellicular MTs, being also present in the flagellar axoneme and the mitotic spindles (Sasse and Gull, 1988). The acetylated isoform (α3) originates from α1-tubulin and is modified just before or just after the assembly of the microtubules (Sasse and Gull, 1988). The unmodified isotype (α1) is almost absent from axonemal microtubules, yet is the main component of the cytoplasmic pool. Distribution of acetylated α-tubulin is essentially the same at all cell cycle stages (Sasse and Gull, 1988).

The tyrosine present at the C-terminus of the primary translation product can be removed – detyrosination – after the tubulin has been inserted into a microtubule. In old and stable microtubules, most of the α-tubulin present is detyrosinated, and therefore, tyrosinated α-tubulin can function as a marker for newly formed microtubules (Sherwin *et al.*, 1987). Use of an anti-tyrosinated α-tubulin antibody (YL1/2) (Kilmartin *et al.*, 1982), revealed the cell cycle modulation of microtubule assembly, showing the dynamic localisation of tyrosinated α-tubulin (Sherwin *et al.*, 1987). Recently, β-tubulin has been shown to also occur as a detyrosinated isotype, although the enzymes involved in this process have not yet been identified.

The third modification consists of polyglutamylation, involving addition of glutamate residues to the carboxy terminus of both α- and β-tubulin (Schneider *et al.*, 1997), which might be related to the binding of kinesins.

Acetylation and detyrosination are two independently regulated post-translational modifications. In general, stable microtubules consist of detyrosinated and acetylated tubulin. So while antibodies directed against total α-tubulin and acetylated α-tubulin stain the whole cell body together with the flagellar axoneme (Woods *et al.*, 1989), anti-tyrosinated α-tubulin antibodies stain the posterior third of the cell body and the BB, and localisation is modulated during the cell cycle (Sherwin *et al.*, 1987). β-tubulin localisation studies show co-staining of the mitotic spindles, as has been proved by the use of monoclonal antibodies (MAbs) against it (KMX, (Birkett *et al.*, 1985)).

Another member of the tubulin super family identified in *T. brucei* was γ-tubulin, which comprises a molecular indicator of microtubule-organizing centres (MTOCs), and is associated with different structures (Scott *et al.*, 1997). Immunolocalisation studies reveal that γ-tubulin has a specific distribution, with a dynamic localisation pattern throughout the cell cycle, being mainly associated with BBs, but also present in the anterior tip of the cell body, the subpellicular microtubules and a discrete dot within the nucleus (Scott *et al.*, 1997).

Recent studies have shown that immunisation of mice with *T. brucei* tubulin confers protection against infection from both animal and human trypanosomiasis (Lubega *et al.*, 2002), suggesting an important role for these proteins as possible drug targets.

1.4.4. FAZ

The trypanosome flagellum is attached to the cell body along most of its length and is maintained by a complex system of filaments, membrane connections and specialized microtubules, which define the FAZ. This involves a series of 25 nm diameter structures present at the site where the flagellum and the cell body membranes

are in close contact (Sherwin and Gull, 1989a). The most obvious feature is the cytoplasmic, electron-dense filament, which in a longitudinal view of the FAZ is represented as a row of punctate structures intercalated in the subpellicular corset (Figure 1. 13 A). A second structure is seen to the left of these filaments: a group of four specific microtubules, closely associated with the ER, which comprise a very stable structure. The membrane region associated with the FAZ is connected with the PFR by several filamentous structures (Figure 1. 16 C).

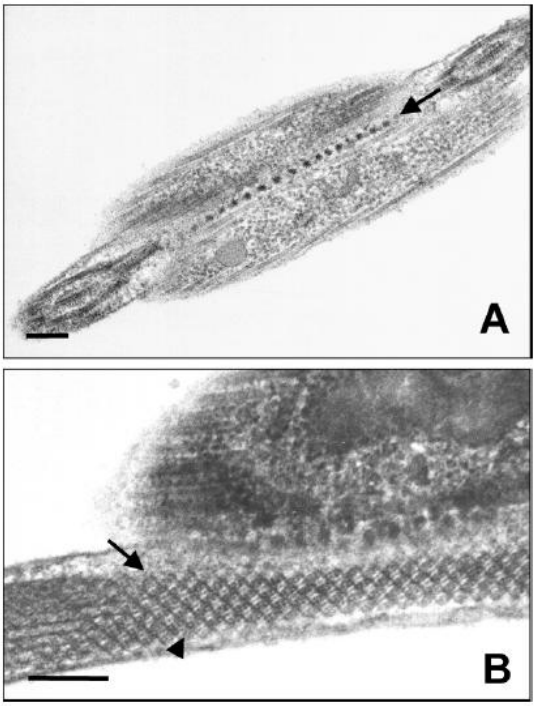

Figure 1. 13 – Longitudinal section of the FAZ (A) and the PFR (B). The arrow points to the punctate structure which constitutes the FAZ; the arrowhead indicates the thick filaments of the PFR. Scale bar – 200 nm. (Bastin *et al.*, 2000)

The FAZ filament has an important role in the life cycle transitions and divides in a very controlled way during cell cycle progression (Sherwin and Gull, 1989a). This structure is present in all stages and its length follows that of the flagellum (Rotureau *et al.*, 2011). During the cell cycle, the FAZ and PFR growth initiate at different time points, and their elongation rates are quite distinct (Kohl *et al.*, 1999). PFR growth is only initiated after the axoneme exits the FP, before which the pro-basal bodies

(proBBs) have already matured and growth of the new FAZ has commenced. The axoneme and the PFR extend at the same rate, as opposed to the FAZ which extends at a slower rate, thus suggesting the need for a complete flagellar structure before cross-linking to the external FAZ.

FAZ location is invariant; the site is duplicated before cytokinesis and it has been suggested that it provides positional cues for cleavage during cell division (LaCount *et al.*, 2002). Such conclusions arose from studies involving a *T. cruzi* homologue of a surface glycoprotein involved in flagellum adhesion – GP72 (Nozaki *et al.*, 1996). When *GP72* is deleted, cells exhibit a free flagellum and although the mutant cell lines grow normally and show an overall unmodified morphology, their motility is decreased and parasites tend to accumulate at the bottom of the flask (Cooper *et al.*, 1993). This protein, denominated FLA1 in *T. brucei*, is essential for both PCF and BSF cell growth and seems to localise to the flagellum and to the FP of the trypanosomes (Nozaki *et al.*, 1996). Knockdown analyses prove that FLA1 is required for a stable FAZ, and consequently for flagellum attachment, causing in parallel cytokinesis defects but not affecting mitotic events. Cytokinesis blocks caused by loss of FLA1 were explained by the authors as being due to the improperly formed FAZ filament, setting the connection between this structure and a correct cell division. In parallel, studies showed that in BSF parasites, *FLA1* knockdown is accompanied by knockdown of a novel *FLA1*-related gene, named *FLA2* by the authors (Nozaki *et al.*, 1996).

Another major protein essential for the correct formation of the FAZ filament was identified in 2007 – FAZ1 - by the use of a library of MAbs (Vaughan *et al.*, 2008). Although not being essential for flagellum growth, FAZ1 inducible knockdown led to cells with partially or completely detached flagella, resulting in formation of a compromised FAZ (Figure 1. 14).

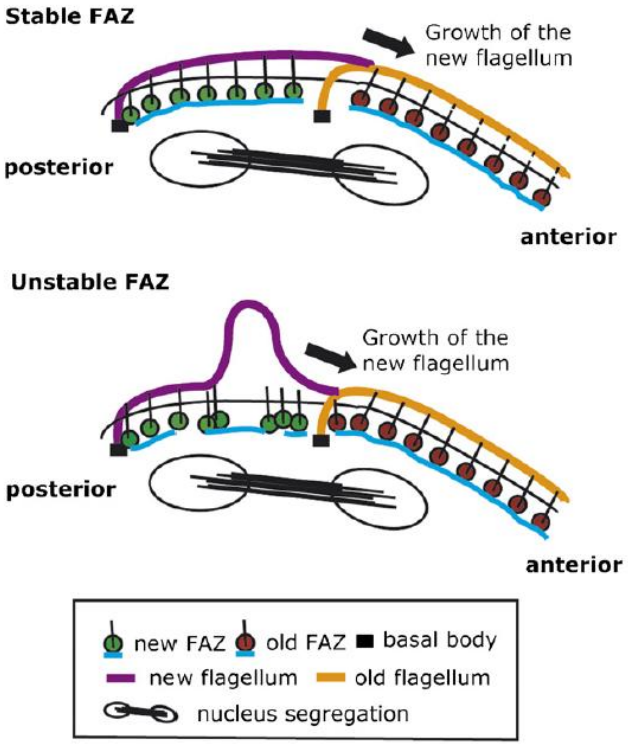

Figure 1. 14 – Schematic representation of a stable vs unstable FAZ in *T. brucei* cells following knockdown of FAZ1. In the presence of an unstable FAZ, the assembly of the new FAZ is defective, causing an intermittent FAZ assembly and detached flagellum. (Vaughan *et al.*, 2008)

Additionally, FAZ1 depletion causes defects in cytokinesis, in accordance with the idea that an attached flagellum is important for cellular morphogenesis. Other studies have also proved that there is a direct relationship between the assembly of a correct FAZ and cytokinesis (Kohl *et al.*, 2003).

1.4.5. PFR

The PFR is a structure unique to the Kinetoplastida and Euglenida (Bastin *et al.*, 1996b, Berriman *et al.*, 2005), and although the defining components appear conserved, its ultrastructure is variable in size between species. It consists of a tri-laminar lattice-like structure that runs alongside the axoneme from its exit site at the FP to the distal tip of the flagellum (Figure 1. 15 A), having a crescent shape with a 150 nm diameter.

Together with the axoneme, it constitutes the major component of the trypanosome's flagellum.

Several techniques have been used to study the structure and function of the PFR. Results obtained by cryoelectron tomography suggest that the bihelical motion of the flagellum involves the PFR, the axoneme and the proteins connecting the PFR to the axoneme (Koyfman *et al.*, 2011). In fact, the beating axoneme causes compression of the PFR lattice by the connecting proteins, resulting in trypanosome propulsion (Koyfman *et al.*, 2011).

Recently, visualisation of the 3D architecture of the flagellum has also been achieved (Hughes *et al.*, 2012). Data obtained over the years has allowed the discrimination of three domains in the PFR structure, defined by their relative position to the axoneme: a short proximal domain, an intermediate and a more developed distal domain (Figure 1. 16 C). The proximal and distal domains have a very similar structure, consisting of several "plates" stacked parallel to each other, while the intermediate domain is made of filaments linking the other two. The PFR relative position to the axoneme remains constant, linked to the axonemal doublets 4-7 (Figure 1. 15 B) by the proximal domain, which in turn is linked to the inner face of the flagellar membrane and the FAZ guaranteeing the presence of an attached flagellum (Figure 1. 16 C). The attachment between the axoneme and the PFR is resistant to detergent and salt extractions, but susceptible to treatment with trypsin (Russell *et al.*, 1983).

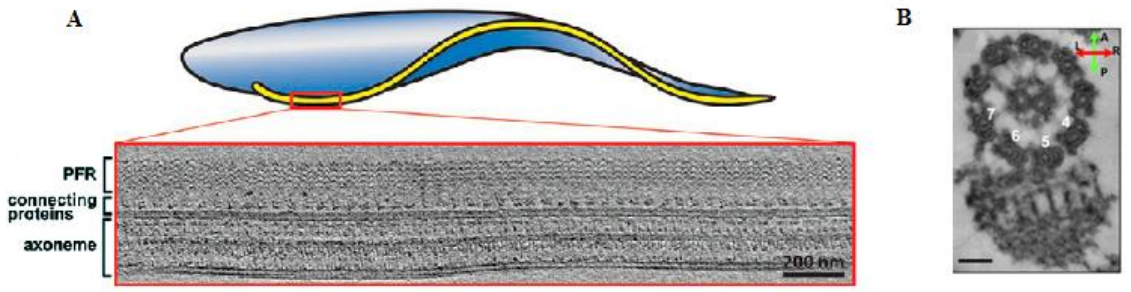

Figure 1. 15 – The *T. brucei* flagellum and the PFR. A - Cryoelectron tomography reconstruction of an isolated straight flagellum, depicting the axoneme, the PFR and connecting proteins (Koyfman *et al.*, 2011). B – Cross section of the connecting doublets 4-7 between the axonemal proteins and the proximal domains of the PFR. Scale bar – 50 nm (Hughes *et al.*, 2012).

More than 40 proteins have been associated with the PFR (Portman and Gull, 2010), and analyses of these proteins has allowed a clearer definition of the PFR role in trypanosomatids. At the same time, immunisation of mice with the major PFR proteins conferred protection against *T. cruzi* infection (Miller *et al.*, 1996, Luhrs *et al.*, 2003), revealing the importance of this structure.

Early studies on several species allowed the identification of two major components of the PFR – PFR1 (70 – 80 kDa) and PFR2 (65-72 kDa) – after separation of flagellar preparations in sodium dodecyl sulphate polyacrylamide gel electrophoresis (SDS-PAGE) gels (Russell *et al.*, 1983). The characterisation of these proteins in *T. brucei* showed that they are encoded by tandemly linked genes of identical nucleotide sequence (Schlaeppi *et al.*, 1989, Berriman *et al.*, 2005), producing stable mRNAs of similar length.

Deletion of both clusters of the *PFR2* gene proved it to encode an essential protein, as in 1997 authors were unable to produce a PFR2 double-knockout cell line (Hunger-Glaser and Seebeck, 1997). Similarly, knockdown experiments were performed to analyse the role of this protein in PFR assembly and to infer the function of the PFR structure in PCF parasites (Bastin *et al.*, 1998). Despite growing normally, induced cells concentrate at the bottom of the flasks and appear paralyzed (Bastin *et al.*, 1999b), meaning that an abnormal PFR structure is associated with decrease in flagellar wave frequency and amplitude for PCF trypanosomes. Cytoskeleton fractionation proved that in the absence of PFR2, the PFR1 protein remains in the soluble fraction and does not associate with the cytoskeleton. In terms of structure, TEM data shows that the intermediate and distal domains of the PFR are missing and the proximal one is highly reduced (Figure 1. 16 A and B). However, this structure is still properly connected to the axoneme and the FAZ (Bastin *et al.*, 1998).

Although in PCF *PFR2* RNAi induced cells remain paralysed but grow at normal rates, in BSF trypanosomes this mutant causes a rapid and lethal phenotype, with appearance of monstrous cells (Broadhead *et al.*, 2006). Defective cell motility leads to cytokinesis failure, resulting in cells with multiple nuclei, kinetoplasts and flagella. Importantly, defects in motility occur before cytokinesis is impaired. PFR2 depleted cells become multiflagellated, with many cells containing two axonemes and

some having an attached flagellum inside the enlarged but active FP (Broadhead *et al.*, 2006). Thus, while ablation of PFR2 results in a reduction in flagellar beating and consequently cellular sedimentation in PCF cells, the lethal phenotype observed in BSF cells proves that the PFR structure is essential for cellular viability. Knockdown of PFR2 in BSF cells has been proven to also be lethal *in vivo* (Griffiths *et al.*, 2007). Data suggests a general requirement for normal flagellar function in the BSF trypanosomes, making the PFR a valuable target for therapeutic interventions.

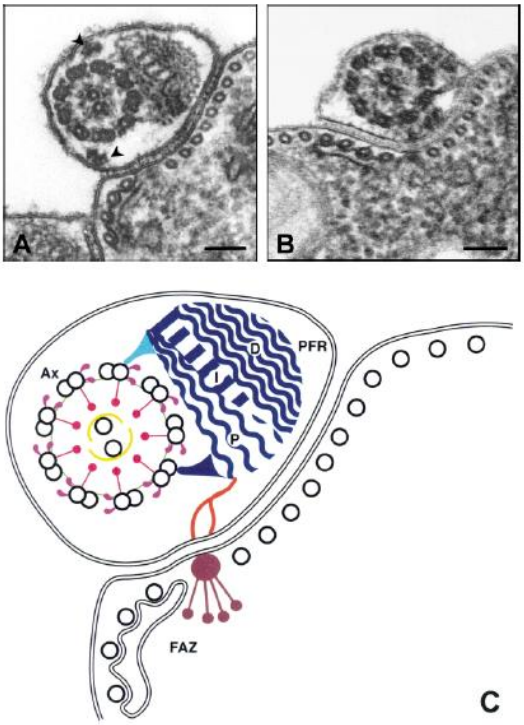

Figure 1. 16 – Transverse sections of uninduced and induced *PFR2* RNAi cells. A complete PFR is present in the uninduced cells (A), while induced cells only present part of the proximal domain of the PFR (B). In (C), the basic components of the flagellum are represented. Ax – axoneme; PFR – paraflagellar rod with its three domains; P – proximal domains; I – intermediate domain; D – distal domain; FAZ – flagellar attachment zone. Arrowheads in (A) point to intraflagellar particles. Scale bar – 100 nm. (Bastin *et al.*, 2000)

Over the years, the number of PFR proteins identified has increased using a series of different techniques. For example, monoclonal antibody (MAb) techniques have provided ROD1 antibody (Woods *et al.*, 1989), which labels the PFR and recognises by WB a doublet of 180 and 200 kDa. One major drawback of this technique

is that PFR proteins are highly immunogenic, leading to high cross-reactivity. Alternatively, phage expression libraries were also used for screening of minor cytoskeleton proteins. One antigen discovered by this technique, named λ5.20, locates along the PFR by immunogold labeling and appears to migrate in polyacrylamide gels as a protein doublet of 180 and 200 kDa (Woodward *et al.*, 1994). Whether this is the antigen identified by ROD 1 remains unknown, although their labeling patterns are very similar.

More candidate PFR proteins were identified in 1995, named I2 and I17, which strongly recognise the flagellum of *T. brucei* although labeling different areas (Imboden *et al.*, 1995). These proteins were discovered using infected bovine serum against cell/cytoskeleton extracts and further confirmed by screening of a cDNA expression library. Recent combination of RNAi techniques with comparative proteomics (Portman *et al.*, 2009) and genome analysis (Berriman *et al.*, 2005) have allowed an increasing characterisation of PFR proteins, identifying also structural dependency relations among them.

In terms of function, the PFR structure has been linked to the attachment to epithelia via the flagellum in the insect host. Additionally, as mentioned above, the PFR has been associated with flagellar motility.

As mentioned in section 1.4.4, the PFR assembly during the cell cycle occurs once the axoneme exits the FP, after growth of a new FAZ and maturation of the proBBs (Kohl *et al.*, 1999). RNAi and inducible tagged cell lines have allowed further analyses of the cell cycle regulation of the PFR structure (Bastin *et al.*, 1999a). Data show that upon development of the new flagellum, two sites of PFR2 incorporation are observed: the distal tip of the flagellum and a minor site along its length. Simultaneously, analyses of PFR2 mutant proteins allowed identification of amino-acid sequences that drive PFR2 localisation upon cell division (Bastin *et al.*, 1999a).

Overall, the PFR serves as a scaffold for assembly of regulatory proteins that contribute to the flagellum function.

1.4.6. Basal body

The BB is comprised of 9 triplet microtubules, forming a barrel-shaped structure. It is a complex structure positioned between the base of the FP and the kinetoplast (Figure 1. 17), made of a mature BB subtending the axoneme and a shorter adjacent proBB found in a perpendicular position. The BB is located at the posterior end of the cell and remains closely associated with the kinetoplast throughout the cell cycle (Figure 1. 11). It is responsible for the assembly of the flagellar axoneme and the microtubule quartet (MtQ), being as such considered as the MTOC in *T. brucei*.

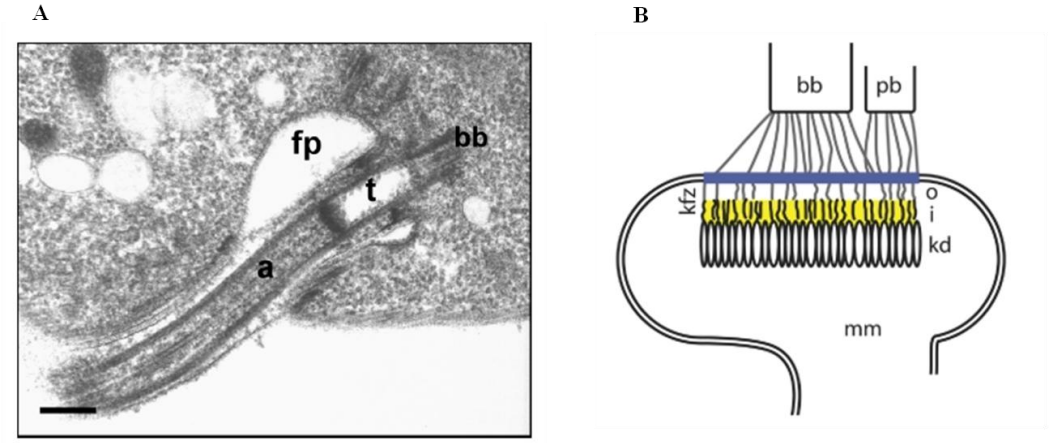

Figure 1. 17 – BB architecture. (A) Longitudinal section of the BB/FP region of *T. brucei* showing the emergence of the flagellum from the cell body. bb – basal body; a – axoneme; fp – FP. Scale bar – 200nm. (B) – Drawing of a longitudinal section of the tripartite attachment complex (TAC), showing the kinetoplast of *T. brucei* (kd) and the filaments (i and o) linking it to the pro-basal body (pbb) and the basal body (bb). (adapted from (Bastin *et al.*, 2000)

Several proteins have been identified which localise to the BB, including γ-tubulin (section 1.4.3) and centrin (Woodward *et al.*, 1995, Scott *et al.*, 1997, Dilbeck *et al.*, 1999, Selvapandiyan *et al.*, 2007). In 1996, the *T. brucei* basal body component (TBBC) protein was shown to localise to the BB, as well as at the posterior end of the cell, to the nucleus and over the flagellum (Dilbeck *et al.*, 1999). This protein is found to localise close to other BB components, such as γ-tubulin and BBA4 (Woods *et al.*, 1989), although TBBC assumes a more distal position than these ones with respect to

kDNA. Additionally, several proteins have been shown in *T. brucei* to function in BB duplication (Pradel *et al.*, 2006, Hammarton *et al.*, 2007a).

The assembly and the rotational movements of the BB are directly connected to correct kinetoplast segregation (Gluenz *et al.*, 2011), as inhibition of BB migration results in a block in kDNA segregation (Robinson and Gull, 1991). This is due to a complex net of filaments that connect the kDNA to the proximal side of the BB, known as the tripartite attachment complex (TAC) (Figure 1. 17 B). This complex is maintained during cell division, coupling the duplication of both organelles. A 3D reconstruction of kinetoplast division (Figure 1. 18) shows the rotational movement of the BBs and its importance for correct kinetoplast segregation. Segregation of the replicated kinetoplast is thus microtubule-mediated and is dependent on the correct separation of the BB complexes (Gluenz *et al.*, 2011).

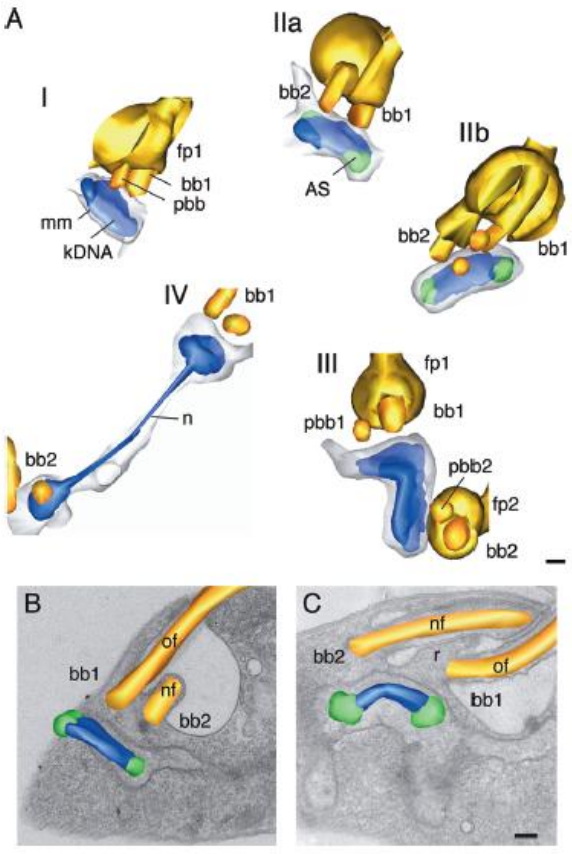

Figure 1. 18 – Model of the kinetoplast duplication cycle. (A) – 3D reconstructions of the duplication cycle of the kinetoplast. (B) – TEM image where the bb2 is anterior to bb1. (C) – TEM image after bb undergoes rotational movement. nf – new flagellum; og – old flagellum; r – ridge between old and new FP; pbb – pro-basal body; bb1 – basal body of old flagellum; bb2 – basal body of new flagellum. Scale bar – 200 nm. (Gluenz *et al.*, 2011)

BB separation is a physical marker or checkpoint in the trypanosome's cell cycle (Ploubidou *et al.*, 1999), and its duplication is one of the earliest events in the cell division cycle (Sherwin and Gull, 1989a). The order and timing of BB maturation, proBB genesis and flagellum formation has been the subject of several studies (Sherwin and Gull, 1989a, Woodward and Gull, 1990, Bastin *et al.*, 1999a, Kohl *et al.*, 1999).

Different techniques have been used to analyse the duplication of the BB, including a combination of electron microscopy (EM) and tomography that gave a 3D view of this process and also allowed analyses on the influence of BB division in other organelles (Lacomble *et al.*, 2010). At the start of the cell cycle, cells contain one BB and a proBB, the latter being anterior to the BB of the single flagellum (Figure 1. 19). During the G_1-S transition, the proBB matures, elongates and invades the pre-existing FP to form the new flagellar axoneme, while a new proBB forms next to each BB (Sherwin and Gull, 1989a). The new BB adopts an anterior location in relation to the old BB. The new BB complex undergoes a rotational movement around the BB of the old flagellum (Figure 1. 19), which results in the new BB being located posterior to the old BB. This rotation and subsequent posterior movements are essential for a correct positioning of the organelles, defining a correct morphogenesis for the daughter cells.

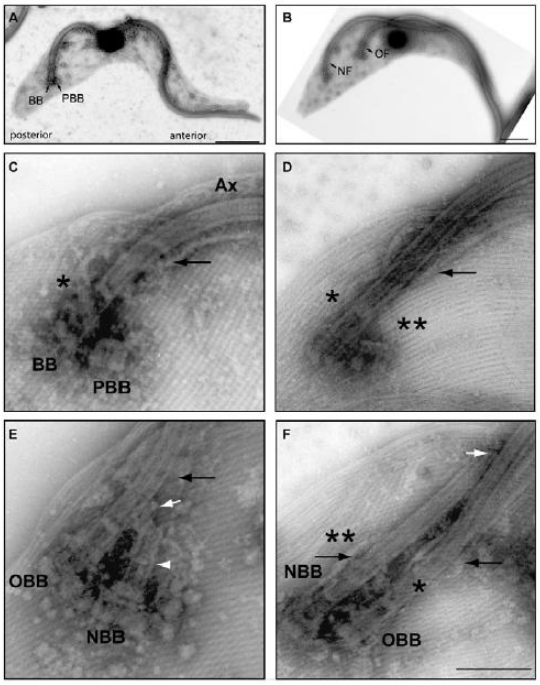

Figure 1. 19 – Repositioning of the BB during cell division, shown by a series of negatively stained cytoskeleton extracts. (A) – G_1 cell with one BB and a proBB (PBB) anterior to it. (B) – Pre-mitotic cell with the new flagellum (NF) anterior to the old flagellum (OF). (C) – Higher magnification over a G_1 cell showing the axoneme (Ax), the flagellar collar (arrow) and the MtQ (*). (D) – Formation of the new MtQ (**). (E) – The new mature BB can now form a new flagellum. The new flagellum basal body (NBB) is anterior to the old flagellum basal body (OBB). (F) – The NBB undergoes rotational movement and is now posterior to the OBB. (Lacomble *et al.*, 2010)

The correct positioning of the BBs is also dependent on correct flagellum formation, which means that BB migration during cell cycle is directly linked to the existence of a proper flagellum (Kohl *et al.*, 2003, Absalon *et al.*, 2007). Absence of a flagellum does not only affect BB separation, but also blocks kDNA segregation, and inhibition of new flagellum elongation leads to the loss of cell polarity and shape (Kohl *et al.*, 2003). Such data proves that correct flagellum elongation is necessary for formation of other cytoskeletal structures that in turn organize the molecular architecture of the cell. The new growing flagellum contributes to BB positioning by three factors: elongation, connection to existing flagellum and base-to-tip wave propagation (Absalon *et al.*, 2007). In the end, the flagellum contributes to its own positioning in the cell.

BB is thus involved in cell morphogenesis and correct organelle division.

1.4.7. Flagellum

Trypanosomatids possess a single flagellum, which in *Trypanosoma* spp. is attached to the cell body for most of its length. The *T. brucei* flagellum is essential for disease pathogenesis in the mammalian host, and also parasite development in the insect vector. It is a multifunctional organelle with roles in motility, cellular morphogenesis, cell division and immune evasion; making it the subject of several studies and reviews (Bastin *et al.*, 2000, Vaughan and Gull, 2003, Ralston *et al.*, 2009).

Different cytoskeleton complexes are part of the flagellum structure (Figure 1. 12) and are essential for its proper function. The single flagellum emerges from the BB (section 1.4.6) and exits the cell from the FP, an invagination present at the posterior end of the cell. Along the length of the cell, the flagellum remains attached to the cell via a specialized structure called the FAZ (section 1.4.4). The flagellum is made from a canonical 9+2 axoneme and an adjacent PFR (section 1.4.5).

The trypanosome axoneme has been characterised over the years and its importance for motility has been revealed by different techniques (Koyfman *et al.*, 2011). Structurally, the axoneme consists of 9 outer doublet microtubules, with 2 central single microtubules (Figure 1. 16 C), originating at the basal plate and extending to the distal end of the flagellum. Radial spokes connect the outer doublets with the central pair, and are essential for normal motility (Branche *et al.*, 2006, Ralston *et al.*, 2006). Inner and outer dynein arms provide the driving force for motility, requiring a coordinate regulation of several dynein motor proteins to correctly propagate flagellar waveforms along the axoneme (Branche *et al.*, 2006, Baron *et al.*, 2007a). Nexin links connect the outer doublets (Lindemann and Kanous, 1997).

The trypanosome FP participates in many cellular processes. It is the only site of exocytosis and endocytosis (Overath and Engstler, 2004) (section 1.3.2) and part of a multiorganelle complex that is involved in cell polarity and cell division, having an important role in host immune evasion as it enables the parasites to protect surface proteins from exposure to the host immune system (section 1.3.2).

The FP comprises less than 5% of the cell surface and is present in all life cycle stages (Overath and Engstler, 2004), although its positioning varies. In PCF trypanosomes, the FP is located midway between the cell midpoint and the posterior end, while in BSF parasites, it localises to the extreme posterior end.

This structure must be able to allow the export of several VSG or procyclin proteins and simultaneously mediate the uptake of different extracellular molecules that need to be transported to intracellular compartments (Field and Carrington, 2009). The rates of endocytosis are developmentally regulated, resulting in a 10 times higher rate in BSF than in PCF trypanosomes (Morgan *et al.*, 2002a). In both stages, a basal level of endocytosis is observed for acquisition of nutrients. The distinct rates are related with the need to remove antibody-VSG complexes from the cell surface of the BSF trypanosomes, which are propelled to the posterior end of the cell (Engstler *et al.*, 2007) and internalised in the FP in only 2 minutes. These complexes are further endocytosed and while antibodies are degraded the VSG molecules are recycled to the cell surface. Despite the higher endocytic rate, the FP of the mammalian form is much smaller than that of the insect form. When adapting for re-entry into a mammalian host, the endocytic activity of the PCF is increased 5-fold (Natesan *et al.*, 2007). More detailed analysis on the mechanism of action of the endocytic apparatus was made in section 1.3.2.

New insights into the organization of the FP were provided by electron tomographic studies among others (Lacomble *et al.*, 2009). The FP appears as an asymmetric compartment (Figure 1. 20 A), closely associated with the Golgi complex and cytoskeletal elements. The FP is divided into clear structural subdomains, the two more distinct being the flagellar pocket collar (FPC) – found at the neck of the FP, where the flagellum exits - and the collarette – referring to the point where the flagellum enters the FP, proximal to the BB (Figure 1. 20 B). Although the FP is not completely enclosed, these structures make it an extracellular compartment that is however segregated from the host environment (Gull, 2003).

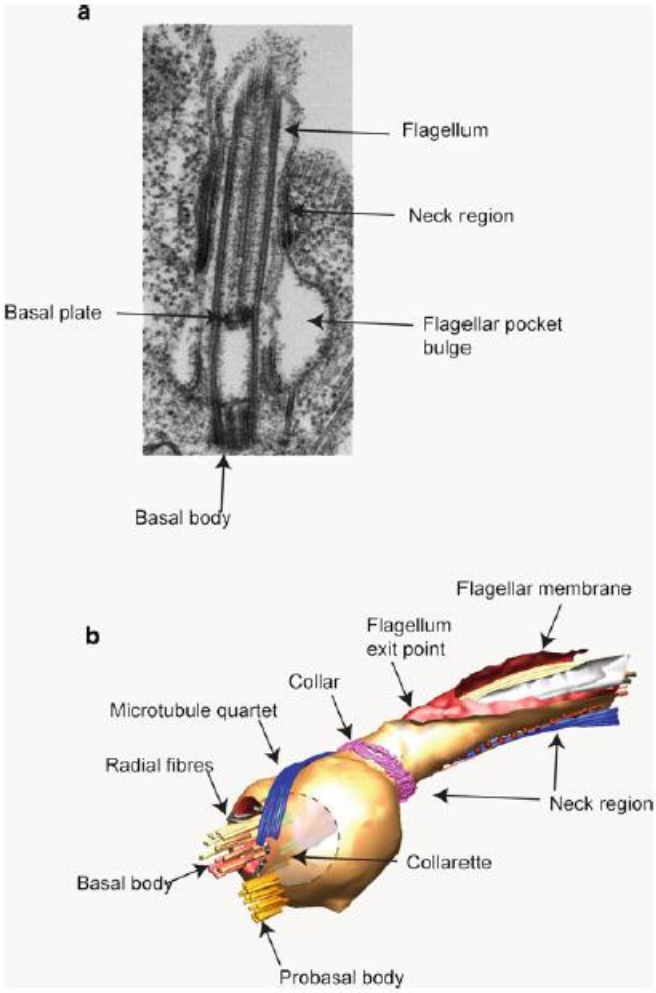

Figure 1. 20 – Architecture of the FP. (a) TEM of the *T. brucei* FP. (b) Model of the major cytoskeleton components that define the FP. (McKean and Gull, 2010)

Identification of FP components has been rather limited, but in 2008 a novel cytoskeletal protein – BILBO1 - was identified that specifically localises to the *T. brucei* FP (Bonhivers *et al.*, 2008b). Immunogold EM located BILBO1 specifically to the FPC; and RNAi ablation proved it to be essential for FP biogenesis and cellular viability, for both life cycle stages (Bonhivers *et al.*, 2008b). Different phenotypes are observed between the different stages, as in PCF cells, the mutants create a new flagellum but lack the pocket and a normal FAZ, resulting in a detached flagellum. In comparison, BILBO1 ablation in BSF trypanosomes results in morphological defects at the level of cell shape, resulting in the appearance of spherical shaped cells but no flagellum detachment is visualised.

The influence of the developing flagellum on FP formation has also been analysed, and results prove that elongation of the new flagellum is not required for FP formation, but for its organization, orientation and function (Absalon *et al.*, 2008a).

The correct assembly of the flagellum is critical for cell division (Kohl *et al.*, 2003). The elongation of the new axoneme begins after BB duplication, making flagellum assembly one of the earliest events in cell cycle (Sherwin and Gull, 1989a). All components needed for maintenance and construction of the flagellum are synthesized in the cytoplasm and must be transported throughout the length of the flagellum to the site of incorporation, the distal tip. This is dependent upon intraflagellar transport (IFT), essential for flagellar growth and maintenance (Rosenbaum *et al.*, 1999, Kohl *et al.*, 2003). The IFT is a bidirectional transport system, powered by kinesin motor proteins for transport to the tip of the flagellum (Kozminski *et al.*, 1995), and by dynein proteins for retrograde transport (Pazour *et al.*, 1999).

The IFT pathway is conserved among organisms that build an extracytoplasmic flagellum and related genes have been identified in *T. brucei* (Kohl *et al.*, 2003, Absalon *et al.*, 2008b). IFT proteins have been localised to both the old and new flagellum, suggesting a role not only in formation but in flagellum maintenance (Absalon *et al.*, 2008b). Depletion of IFT components affects cell size, shape and polarity, while preventing the new flagellum growth (Kohl *et al.*, 2003, Absalon *et al.*, 2008b). The old flagellum is not affected and retains IFT proteins, suggesting it is maintained by the existent and functional proteins present (Kohl *et al.*, 2003). Data suggests there is a connection between flagellum length and cell size.

As the flagellum extends, it remains in a specific path alongside the existing flagellum, defined by the flagellar connector (Moreira-Leite *et al.*, 2001, Briggs *et al.*, 2004). This structure, specific for the insect stage, forms within the FP and moves together with the tip of the growing flagellum, not detaching from the old flagellum until approximately halfway along. Its components remain unknown.

A large number of flagellar proteins have been identified in *T. brucei* (Broadhead *et al.*, 2006, Baron *et al.*, 2007b, Hart *et al.*, 2009), some located to the PFR (section 1.4.5), the BBs (section 1.4.6) or the axoneme itself.

The flagellum is mainly responsible for the trypanosome's motility. It beats in a helical way and two types of waves can be detected. The forward movement of the cell is achieved by a distal tip to base beating; the other beating starts at the base and propagates to the distal tip, and is responsible for cellular reorientation. Parasite migration is not random, but is instead critical for development and disease pathogenesis (Gibson and Bailey, 2003). Besides a functional role in cellular movement, the flagellum mediates attachment to specific tissues of the host (Tetley and Vickerman, 1985), it is the main apparatus for endocytosis and thus is central for immune evasion, and studies also link this cytoskeleton structure with sensory perception.

Another major role of the flagellum is mediation of cell morphogenesis, resulting from the fact that the flagellum is connected to other subcellular organelles. One example can be taken from the role of the flagellar connector in the correct positioning of the flagellum-associated organelles (Moreira-Leite *et al.*, 2001). Other flagellar components have also been functionally related to defects in cell morphogenesis and polarity (Ralston and Hill, 2006, Broadhead *et al.*, 2006, Absalon *et al.*, 2008b, Bonhivers *et al.*, 2008b). Despite the fact that flagellar mutations affect both life cycle stages, the BSF motility mutants are inviable.

1.4.8. Microtubule Associating Proteins

The subpellicular microtubules are regularly spaced and linked to each other and to the plasma membrane by several cross-bridges. The proteins associated with these connections are known as microtubule associating proteins (MAPs), and have been identified over the years mainly due to the use of antibodies generated using cytoskeleton preparations as immunogens, as is the case of the WCB210 (Woods *et al.*,

1992). This high molecular weight protein is present in the bridges lying between the microtubules, being absent from the flagellum and spindle microtubules.

A subclass of MAPS denoted microtubule associated repetitive proteins (MARPs) has been described (Hemphill *et al.*, 1992, Affolter *et al.*, 1994). This family of high molecular weight proteins is characterised by the presence of several repetitive elements.

Over the years different MAPs have been identified (Kohl and Gull, 1998) and subjected to several studies. Among them, the 28 kDa MAP identified as Gb4 demonstrated to have a restricted location at the posterior end of the cell (Rindisbacher *et al.*, 1993). On the other hand, cytoskeleton associated proteins CAP15 and CAP17 show colocalisation with tubulin, restricted however to the anterior end of the cell (Vedrenne *et al.*, 2002). Overexpression of these CAP proteins leads to morphological disorders, subsequently creating cytokinesis defects.

1.5. THE CELL CYCLE

Life cycle progression is intimately linked to cell cycle regulation, with replicating forms alternating with cell cycle arrested forms that are adapted for transmission into the new host (Matthews, 1999, Hammarton *et al.*, 2003b). As the cell cycle of trypanosomes is quite distinct from the mammalian one, authors have proposed that the different proteins involved in regulation of the different pathways could be used as drug targets (Hammarton *et al.*, 2003b, Naula *et al.*, 2005). The existence of two sets of DNA, two distinct S phases and segregation events (Woodward and Gull, 1990), with only one cytokinesis event, suggests the existence of a complex regulatory machinery that controls the different events during cell division. In parallel, the use of anti-microtubule agents and DNA synthesis inhibitors has proved that *T. brucei* cytokinesis is not dependent on either mitosis or nuclear DNA synthesis in PCF cells (Ploubidou *et al.*, 1999), suggesting the existence of novel cell cycle checkpoints in this organism. Such regulatory machinery and general cell cycle progression have been reviewed by several authors (McKean, 2003, Hammarton, 2007, Hammarton *et al.*, 2007b).

The typical eukaryotic cell cycle phases are seen in *T. brucei* – G_1, S, G_2 and M (Figure 1. 21), although containing unique features. The existence of several single copy organelles and their concentration at the posterior end of the cell imposes the need for an accurate duplication and segregation, in order to generate viable progeny. Thus, organelle duplication occurs in a precise order, and cytokinesis is precisely controlled in order to occur after mitosis. The segregation of the kinetoplast before mitosis constitutes an additional cell cycle marker (Sherwin and Gull, 1989a, Woodward and Gull, 1990), while entry into cytokinesis depends on the progression of kinetoplast division and segregation (Woodward and Gull, 1990, Ploubidou *et al.*, 1999). The trypanosome cell cycle has been interlinked with microtubule events (Figure 1. 21), as various microtubule mediated processes can be selectively inhibited and lead to different cell cycle defects (Robinson *et al.*, 1995, Ploubidou *et al.*, 1999, Kohl *et al.*, 2003, Broadhead *et al.*, 2006, Pradel *et al.*, 2006, Gluenz *et al.*, 2011). Major events such as kinetoplast segregation, BB duplication, flagellar axoneme growth, mitosis and cytokinesis have been proved to depend on microtubule polymerization/depolymerization (sections 1.4.2 to 1.4.8).

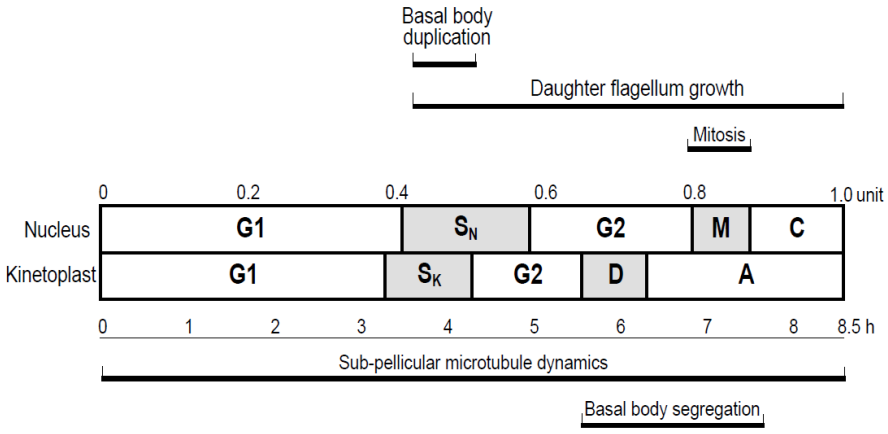

Figure 1. 21 – Schematic representation of *T. brucei* cell cycle in PCF cells. The microtubule and DNA mediated events are represented in this scheme in relation to their relative order and time (hours). SK, kinetoplast S phase; D, kinetoplast division; A, kinetoplast segregation; SN, nuclear S phase; M, mitosis; C, cytokinesis. (Ploubidou *et al.*, 1999)

The order of cell cycle events is common between the two life cycle stages, although studies have mainly been based on the PCF trypanosomes (Woodward and

Gull, 1990, Ploubidou *et al.*, 1999, Kumar and Wang, 2006). Besides subtle differences in the kinetics and the fact that the length of the cell cycle is longer for PCF trypanosomes, the general progression of cellular division has been established (Figure 1. 21). The first morphological event in the *T. brucei* cell cycle is the elongation and maturation of the proBB. As seen previously, this step allows the nucleation of a new flagellum (section 1.4.6). Kinetoplast S phase (S_K) initiates before nuclear S phase (S_N), and the existence of shorter S and G_2 phases for the kinetoplast contributes to the fact that, once mitosis starts, kinetoplast segregation (D) is already completed. As such, during the nuclear G_2 phase, BBs separate and, in conjunction with several microtubule structures such as the TAC (section 1.4.6), lead to a correct kinetoplast segregation (Robinson and Gull, 1991). As mentioned in section 1.4.6, the assembly and movements of the BB are directly connected to kDNA segregation (Ogbadoyi *et al.*, 2003). The replicated nucleus then undergoes mitosis, without chromosome condensation or disruption of the nuclear envelope (Ogbadoyi *et al.*, 2000). One major difference between the two life cycle stages is that, once replicated, one of the nuclei re-positions between the two divided kinetoplasts in the insect form (Tyler *et al.*, 2001, Hammarton *et al.*, 2003b).

Fundamental differences are seen in cell cycle control between life cycle stages. One important feature is the mitosis to cytokinesis checkpoint, which causes differential phenotypes between the two life cycle stages. For example, in studies with PCF cells using microtubule inhibitors to block mitosis, cytokinesis still occurs despite inhibition of mitosis, suggesting these cells lack the mitosis to cytokinesis checkpoint (Ploubidou *et al.*, 1999). Similar results were seen for the same life cycle stage using knockdown of proteins that blocked mitosis (Hammarton *et al.*, 2003a, Li and Wang, 2003), indicating that key cell cycle checkpoints present in higher eukaryotes are absent from trypanosomes. On the contrary, depletion of CYC6 in BSF trypanosomes for example (Hammarton *et al.*, 2003a) blocks both mitosis and cytokinesis, suggesting the existence of the mitosis to cytokinesis checkpoint in this stage. BSF but not PCF reinitiate nuclear S phase in the absence of mitosis. Therefore, in the mammalian form, inhibition of mitosis prevents cytokinesis, although not re-replication of nuclear and kinetoplast DNA (kDNA), or segregation of the replicated kinetoplasts. In fact, a block in mitosis in this stage cause the appearance of “monster” cells with multiple kinetoplasts and an

enlarged nucleus, corresponding to a cytokinesis defect while other cell cycle segregation events still occur (Hammarton *et al.*, 2003a). In PCF cells, cytokinesis occurs despite inhibition of mitosis, generating asymmetric daughter cells, where one lacks the nucleus and contains only one kinetoplast, termed "zoid", and the other contains a tetraploid nucleus and a kinetoplast (Hammarton *et al.*, 2003a). As such, besides differences in regulation between the insect and the mammalian stages, mitosis and cytokinesis appear to be regulated separately.

Cytokinesis in trypanosomes is quite unique, as it does not depend on an actomyosin ring as for mammalian cells. Instead, cell division occurs via the ingression of a cleavage furrow, from the anterior to the posterior end, along the helical axis of the cell. The furrowing event also distinguishes BSF from PCF cells, as it seems to be longer for the latter form. Cytokinesis consists mainly of three stages: signalling, cleavage furrow ingression and abscission. The signalling stage ensures initiation of cell division at the appropriate time, also occurring throughout the cell cycle, while ingression allows bisection of the cell, involving remodelling of the trypanosome cytoskeleton. In order to guarantee an accurate furrow ingression, and as mentioned in sections 1.4.6 and 1.4.7, BB and flagellum separation are vital (Kohl *et al.*, 2003, Hammarton *et al.*, 2007a). Abscission allows the final separation into two daughter cells (Hammarton *et al.*, 2007b).

The correct progression through the cell cycle is guaranteed by a complex set of regulatory proteins. Identification of such proteins has been possible due to sequencing of the *T. brucei* genome (Berriman *et al.*, 2005), together with transcriptome-wide scale analyses of gene expression over the cell cycle (Archer *et al.*, 2011) and RNAi screens (Tu and Wang, 2005b, Tu and Wang, 2005a, Monnerat *et al.*, 2009). Data obtained so far show that molecular regulation of the *T. brucei* cell cycle has unique and unusual features, involving different proteins at different phases (Figure 1. 22), and that progression is monitored by specific signalling checkpoints.

Several cdc2-related kinases (CRKs) and their interacting cyclin partners are among the several regulatory proteins that guarantee an accurate progression through the different cell cycle boundaries (section 1.5.1).

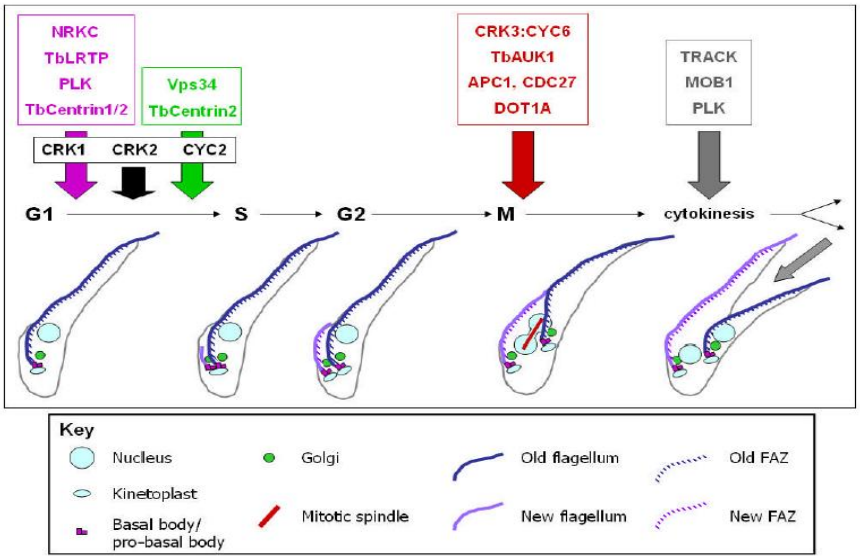

Figure 1. 22 – Cell cycle regulation in *T. brucei*. The schematic representation depicts the general cell cycle progression and different regulators identified in BB duplication (pink), G_1 phase (black), Golgi duplication (green), mitosis (red) and cytokinesis (grey). (Hammarton, 2007)

Regulation of G_1 phase is vital to ensure that the earliest detectable events, like BB duplication and outgrowth of a new flagellum, occur normally. Among other regulatory proteins, *T. brucei* polo-like kinase (TbPLK) has been shown to be essential for BB duplication and for the correct formation of the bilobe and Golgi structures (Hammarton *et al.*, 2007a, de Graffenried *et al.*, 2008). In fact, depletion of PLK in PCF trypanosomes generates abnormal cells containing two nuclei but only one kinetoplast, one BB and one flagellum. Recent results have shown that, besides its functional role in BB duplication, PLK is necessary for correct flagellum positioning (Ikeda and de Graffenried, 2012). In fact, localisation assays have shown that PLK has a dynamic localisation pattern, suggesting a direct link between its position in specific structures and their biogenesis (Ikeda and de Graffenried, 2012). Previous results had suggested that PLK is necessary for cytokinesis initiation (Kumar and Wang, 2006). Later in 2010 the use of a PLK inhibitor and HU synchronization showed that this kinase is able to perform its role in guiding cytokinesis before late S phase, playing a crucial role in subsequent cytokinesis (Li *et al.*, 2010). In fact, if PLK is inhibited in cells synchronized before S-phase, cytokinesis initiation is arrested in that cycle; but if PLK inhibition is performed in cells synchronized in late S-phase, they undergo a full cycle and only the cytokinetic initiation of the following cycle is blocked (Li *et al.*, 2010).

The first identified protein with dual roles in mitosis and cytokinesis is the aurora kinase 1 (AUK1), which seems to be vital for both mitosis and kinetoplast duplication, together with cytokinesis (Tu *et al.*, 2006, Li *et al.*, 2009). TbAUK1 depletion in PCF causes a cell cycle arrest in the G_2/M phase, resulting from an inhibited kinetoplast duplication and a failed mitosis, connected with the absence of a mitotic spindle (Tu *et al.*, 2006). Analyses of AUK1 depletion in synchronized cells have shown it to be essential for the metaphase-anaphase transition in both life cycle stages, being required also for initiation of cytokinesis at least in the insect form (Li *et al.*, 2009). The two regulatory functions coupled by this protein seem to be separated into two clearly distinct time frames within the cell cycle.

In terms of cytokinesis, different proteins have been identified to be essential for the different phases, like for example FLA1 (section 1.4.4), AUK1, MOB1, among others. As opposed to AUK1 which blocks cytokinesis initiation, MOB1 is necessary for furrow ingression in BSF trypanosomes (Hammarton *et al.*, 2005). In fact, MOB1 depletion in this life cycle stage leads to accumulation of post-mitotic cells, most of which containing a visible cleavage furrow. Different phenotypes are observed for PCF trypanosomes, where it impedes an accurate cytokinesis by allowing mispositioning of the cleavage furrow, instead of affecting the actual ingression of the furrow (Hammarton *et al.*, 2005).

As cellular division in trypanosomes involves serious remodelling of the microtubule cytoskeleton, several proteins e.g. katanins and spastin are necessary at different stages of cytokinesis (Benz *et al.*, 2012). So far, no proteins have been indentified to have a direct regulatory role in the final stage of cytokinesis, abscission, involving the final separation into two daughter cells.

1.5.1. Cell cycle regulators: CRKs and cyclins

Cyclin-dependent kinases (CDK) are fundamental for cell cycle control, and their involvement in cellular division has been established in yeast and higher eukaryotes (Mottram, 1994, Nigg, 1995, Satyanarayana and Kaldis, 2009). CDKs are

proline-directed serine-threonine kinases whose activation is dependent upon phosphorylation of specific residues and binding of a cyclin (CYC) partner (Morgan, 1995, Bloom and Cross, 2007). CYC expression displays an undulating pattern, being transcribed and degraded at specific points during cell cycle, reflecting the level of their partner kinase activation. The interaction between a kinase and its CYC partner determines not only the CDK localisation but also its substrate. Such interaction is not however restricted to specific kinases/CYCs, being that one CDK can be activated by different CYCs, and thus target different substrates (Morgan, 1995, Bloom and Cross, 2007, Satyanarayana and Kaldis, 2009). The opposite also occurs, where a specific CYC can bind and activate different CDKs and consequently regulate several cell cycle phases.

To date, eleven CRKs (CRK1-4 and CRK6-12) and ten CYCs (CYC2-11) have been identified in *T. brucei* (Naula *et al.*, 2005, Hammarton, 2007). Although phylogenetically all CRKs cluster with those of other eukaryotes, some insertions and extensions have been observed in the sequences of trypanosomatids. This might indicate that trypanosomes have evolved the regulatory activation of their CRKs. The presence of two different forms, where the parasite has to adapt to living freely in the bloodstream of the mammalian host and surviving in the insect host, leads to quite a differential expression and function of the different CRKs/CYCs (Hua *et al.*, 1997).

Establishing a function for the different kinases and CYCs has been accomplished by generating RNAi cell lines, specific for the different proteins or even targeting two putative regulators at the same time (Tu and Wang, 2005b, Tu and Wang, 2005a). However, a functional role has not yet been established for all of them (Tu and Wang, 2004). The lack of a detectable phenotype does not rule out a vital role for cellular viability, since RNAi knockdown is never absolute, and it is possible that some kinases/CYCs can functionally replace others (functional redundancy).

The first CRKs for which functions were established were CRK1 and CRK3. Similar knockdown assays involving CRK2, CRK4 and CRK6, did not show a role for these CRKs in cell growth or cell cycle progression (Tu and Wang, 2004). CRK1 depletion leads to accumulation of cells in G_1 phase, while CRK3 seems to be essential for the G_2/M transition (Tu and Wang, 2004). The presence of different observable

phenotypes between PCF and BSF forms once again suggests the existence of a mitosis to cytokinesis checkpoint for the latter form. In fact, PCF cells depleted of CRK3 displayed an increase number of anucleate cells, while a small number of cells with aggregated multiple nuclei and multiple kinetoplasts were seen in the BSF (Tu and Wang, 2004). Recently, CRK9 was shown to be involved in regulation of both mitosis and cytokinesis in PCF *T. brucei* (Gourguechon and Wang, 2009). Pairwise knockdown analyses performed in 2005 suggest that CRK2 is involved in cytoskeletal morphogenesis of PCF trypanosomes stalled in G_1 phase (Tu and Wang, 2005b, Tu and Wang, 2005a). In fact, elongation of the posterior end is observed for cell lines depleted of CRK2 and CRK1, and thus blocked in G_1/S transition (Tu and Wang, 2005a). On the contrary, this does not occur in knockdown cell lines of both CRK2 and CRK3, where cells are arrested in G_2/M transition which corresponds to depletion of CRK3 as mentioned above (Tu and Wang, 2005b).

In terms of *T. brucei* CYCs, functional roles have only been identified for CYC2 and CYC6 (Li and Wang, 2003, Hammarton *et al.*, 2004). CYC2 has been proved to be involved in regulation of the G_1/S transition, causing an accumulation of cells in G_1 phase for both life cycle stages once depleted (Li and Wang, 2003, Hammarton *et al.*, 2004). An additional role is observed in PCF cells, but not in BSF trypanosomes, where CYC2 depletion leads to cell elongation at the posterior end, meaning that this protein is required for the maintenance of cell morphology. Double knockdown studies have demonstrated that this CYC has multiple roles in cell cycle progression and cellular morphology (Gourguechon *et al.*, 2007). Once depleted together with CRK1 and CRK3, the arrest in the G_1/S and G_2/M transitions, respectively, was stronger (Gourguechon *et al.*, 2007). Knockdown of both CRK2 and CYC2 causes once again an abnormal cytoskeletal morphology, where longer posterior ends are observed (Gourguechon *et al.*, 2007). Knockdown of CYC6 generates a mitotic block in both the insect and mammalian form (Hammarton *et al.*, 2003a, Li and Wang, 2003), although flow cytometry data shows that BSF cells re-initiate S-phase while mitosis is blocked, which does not occur in PCF cells. As mentioned in section 1.5 the distinct phenotypes observed are due to differences in key cell cycle checkpoints between the two life cycle forms.

As CRK activity is cyclin-dependent, regulation through the different cell cycle boundaries should involve the formation of several CRKs/CYC complexes. So far, *in vivo* interactions between *T. brucei* CRKs and CYCs have not been successfully established, with only two complexes identified. The first complex identified was CRK3:CYC2, first discovered by yeast two-hybrid assay and further confirmed *in vivo* by immunoprecipitation (IP) (Van Hellemond *et al.*, 2000). This complex is suggested to be involved in regulating the G_1/S transition (Gourguechon *et al.*, 2007), although CRK3 is known to regulate the boundary G_2/M. Alternatively, CRK3 was found to interact with CYC6 and regulate the G_2/M transition (Hammarton *et al.*, 2003a), forming an active complex both *in vitro* and *in vivo*. One important aspect of such data is that CRK3 is activated by two different CYCs (CYC2 and CYC6), thus regulating two different phases of the *T. brucei* cell cycle.

In vitro interactions involving GST-pull down assays with recombinant proteins and yeast-two hybrid assays have shown three other complexes: CRK1:CYC2 (Gourguechon *et al.*, 2007); CRK2:CYC2 (Gourguechon *et al.*, 2007) and CRK9:CYC6 (Gourguechon and Wang, 2009). However, data obtained by the different methods was sometimes inconsistent (Gourguechon *et al.*, 2007), and none of these interactions have yet been proved to occur in the trypanosome cell.

Besides the lack of information on the functional role of all identified CRKs and CYCs and their interaction, many proteins remain to be identified as cell cycle regulators and much is unknown on cellular division. This project appeared in an attempt to answer some of these questions.

2. MATERIALS AND METHODS

2.1. CULTURE, TRANSFORMATION AND STORAGE OF BACTERIAL CELLS

2.1.1. **Bacterial strains**

For standard cloning techniques and to ensure high transformation efficiency, commercially-prepared cells were used (Strataclone SoloPack Competent cells, genotype Tet^r Δ(*mcr*A)183 Δ(*mcr*CB-*hsd*SMR-*mrr*)173 *end*A1 *sup*E44 *thi*-1 *rec*A1 *gyr*A96 *rel*A1 *lac*Hte [F' *pro*AB *lac*I^q ZΔM15 Tn10 (Tet^r) Amy Cam^r]). This strain supports blue-white screening with plasmids pSC-A and pSC-B.

E. coli XL1Blue cells (genotype *rec*A1 *end*A1 *gyr*A96 *thi*-1 *hsd*R17 *sup*E44 *rel*A1 lac (F' *pro*AB *lac*I^q ZΔM15 Tn10 (Tet^r)) from Stratagene were used for amplification and maintenance of plasmid DNA, and during plasmid sub-cloning procedures. Recombinant proteins were expressed from one of two *E. coli* host strains: BL21 (DE3) (Stratagene, genotype *E. coli* B F^- *omp*T *hsd*S($r_B^-m_B^-$) *gal dcm* λ(DE3[*lac*I *lac*UV5-T7 gene 1 *ind*1 *sam*7 *nin*5])) and BL21 (DE3) pLysS (Invitrogen, genotype *E. coli* B F^- *omp*T *hsd*Sb($r_B^-m_B^-$) *gal dcm* λ(DE3) [pLysS (Cam^r)]). DE3 strains contain an Isopropyl β-D-1-thiogalactopyranoside (IPTG)-inducible T7 RNA Polymerase gene, making them suitable for expression of proteins from target genes cloned into pET vectors (Novagen) which due to the high selectivity of the polymerase to the promoter sequence guarantees a high-level transcription and translation. pLysS encodes T7 lysozyme, a natural inhibitor of T7 RNA polymerase, allowing suppression of basal expression prior to induction and stabilizing production of possible toxic proteins.

2.1.2. **Bacterial culture and storage**

Prior to use, all media and solutions were autoclaved at 121ºC, 15 psi for 20 minutes or filter sterilised using either a 0.1 µm syringe filter (Sartorius) or a 0.1 µm bottle top filters (Millipore).

When necessary, media was supplemented with the correct antibiotics at a final concentration of 100 µg.ml^{-1} ampicillin, 50 µg.ml^{-1} kanamycin, or 40 µg.ml^{-1} chloramphenicol, made up in dH_2O and kept at -20ºC.

Individual colonies were inoculated in liquid medium. For long term storage, overnight cultures were centrifuged at 3500 rpm for 5 minutes at 4ºC, before the cell pellet was resuspended in 0.5 ml Luria bertani medium (LB), mixed with an equal volume of 2% (w/v) peptone, 40% (v/v) glycerol and kept at -80ºC.

2.1.3. **Production of competent cells**

Cells were made competent by treatment with rubidium chloride. An overnight inoculum, grown at 37ºC with agitation at 200 rpm, was diluted 100x in 50 ml of Luria-Bertani broth (L-Broth- 86 mM NaCl, 10 g.l^{-1} tryptone, 5 g.l^{-1} yeast extract, adjusted to pH 7.0 using NaOH (Miller, 1972) and grown at 37ºC until an optical density (OD_{600nm}) of 0.6 as measured using a spectrophotometer (Shimadzu Biospec-mini DNA/RNA/protein analyser) was reached. The culture was put on ice for 10 minutes and centrifuged at 2000 x *g* for 15 minutes, after which the cell pellet was gently resuspended in 16 ml chilled RF1 buffer (100 mM rubidium chloride, 50 mM $MnCl_2.4H_2O$, 30 mM potassium acetate, 10 mM $CaCl_2$, 15 % glycerol, adjusted to pH 5.8 using acetic acid) and maintained on ice for further 15 minutes. After centrifugation at 1800 x *g* for 15 minutes, the pellet was resuspended in 4 ml of cold RF2 buffer (10 mM 3-(N-morpholino)propanesulfonic acid (MOPS) pH 6.8, 10 mM rubidium chloride, 75 mM $CaCl_2$, 15 % glycerol adjusted to pH 6.8 with NaOH), and incubated on ice for 1 hour. 200 µl aliquots were stored at -80ºC.

2.1.4. **Bacterial transformation**

Insertion of plasmids into *E. coli* competent cells was performed by heat-shock treatment. 50 µl aliquots of competent cells were thawed on ice and incubated for 20 minutes with 1 µl or 2 µl of the cloning reaction mixture, whether the expected plasmid

was smaller or larger than 5 kbp, respectively. Cells were heat shocked at 42ºC, for approximately 45 seconds, and returned to ice for 2 minutes, before adding 250 µl of pre-warmed LB and incubating at 37ºC for an hour. 100 µl of transformed cells were plated out on LB agar plates (L-broth supplemented with 15 $g.l^{-1}$ agar), containing the appropriate antibiotics.

2.2. CULTURE, TRANSFECTION, STORAGE AND ANALYSIS OF *T. BRUCEI* CELLS

2.2.1. *T. brucei* strains

Table 2. 1 and Table 2. 2 show *T. brucei* strains used and generated during this study.

Table 2. 1 - *T. brucei* strains used in this study.

Life cycle stage	Genotype	Description	Drug resistance
BSF	Lister 427	wildtype	---
PCF	Lister 427		---
PCF	Lister 427 pGL1217 pGL1125 clone 1-10-B2 and clone 1-10-G1	Single allele knockout of *CYC9* and second allele replaced by *CYC9:TAP** - Expression of CYC9:TAP from endogenous locus (Mottram lab)	Neomycin Blasticidin
PCF	Lister 427 pLew13 pLew29 pGL1759 clone 10-2-D9 and 10-1-C10	Tetracycline-inducible RNAi of *CYC9* (Mottram lab)	Zeocin
BSF	Lister 427 pLew13 pLew90 pGL1759 clone 1 and clone 2	Tetracycline-inducible RNAi of *CYC9* (Mottram lab)	Phleomycin
BSF	Lister 427 2T1 MITat1.2 pGL1986 clone 4 and clone 5	Tetracycline-inducible RNAi of *CRK12* - stem-loop vector (Mottram lab)	Hygromycin
BSF	Lister 427 pHD449 pHG230 clone C2	Tetracycline-inducible overexpression of ty:CRK12 WT (Hammarton lab)	Hygromycin
PCF	Lister 427 pHD449 pHG230 pool 1	Tetracycline-inducible overexpression of ty:CRK12 WT (Hammarton lab)	Hygromycin
PCF	Lister 427 pHD449 pHG231 pool 1	Tetracycline-inducible overexpression of ty:CRK12 Kinase Dead (K358M) (Hammarton lab)	Hygromycin

* - TAP - Tandem affinity purification

Table 2. 2 - *T. brucei* strains generated in this study.

Life Cycle Stage	Genotype	Description	Drug resistance
PCF	Lister 427 pHG69 pool 1	Expression of ty:GFP*:CRK12 from endogenous locus	Hygromycin
PCF	Lister 427 pGL1217 pGL1125 pHG69 clone D9	Single allele knockout of *CYC9*; expression of CYC9:TAP and ty:GFP:CRK12 from endogenous locus	Neomycin Blasticidin Hygromycin
BSF	Lister 427 pHG69 clone C6	Expression of ty:GFP:CRK12 from endogenous locus	Hygromycin
BSF	LLister 427 pHD449 pHG230 pGL1125 clone A1	Tetracycline-inducible overexpression of ty:CRK12 WT; Expression of CYC9:TAP from endogenous locus	Hygromycin Blasticidin

* - GFP - green fluorescent protein

2.2.2. *T. brucei* culture and storage

BSF parasites were grown at 37ºC in 5% carbon dioxide, in HMI-9 (Hirumi and Hirumi, 1989) media supplemented with 10% (v/v) heat-inactivated tetracycline-free (tet-free) Foetal Bovine Serum (FBS;Biosera), 10% (v/v) Serum Plus (JRH Biosciences), 500 $U.ml^{-1}$ penicillin and 50 $\mu g.ml^{-1}$ streptomycin. PCF parasites were cultured at 27ºC in 5% carbon dioxide, in SDM-79 (Brun and Schönenberger, 1979) containing 10% (v/v) heat-inactivated tet-free FBS, 500 $U.ml^{-1}$ penicillin and 50 $\mu g.ml^{-1}$ streptomycin. Parasites were maintained at mid-log phase growth, at a cell density of 1 x 10^5 – 1 x 10^6 $cells.ml^{-1}$ for BSF, and 1 x 10^6 – 1 x 10^7 $cells.ml^{-1}$ for PCF parasites. Where appropriate, antibiotics were added to medium (Table 2. 3).

Table 2. 3 - Final antibiotic concentrations for *T. brucei* culture.

Drug\Final concentration ($\mu g.ml^{-1}$)	BSF	PCF
Blasticidin (Calbiochem)	10	20
Hygromycin (Calbiochem)	5	50
Neomycin (Calbiochem)	2.5	10
Phleomycin (Invivo Gen)	2.5	-
Zeocin (Calbiochem)	-	10

Cell density was determined by analysis of 10 µl of culture, using an Improved Neubauer Haemocytometer counting chamber (Weber Scientific). When monitoring parasite growth, cell density was determined at regular intervals, every 6 hours for BSF parasites and every 24 hours for PCF parasites, approximately.

Induction of RNAi and overexpression cell lines was performed by addition of 1 $\mu g.ml^{-1}$ tet to the culture medium. For downstream analyses, parasite cultures were centrifuged at 1500 x *g* or 600 x *g*, for BSF or PCF, respectively, and when needed were washed in Trypanosome dilution buffer (TDB: 20 mM Na_2HPO_4, 2 mM $NaH_2PO_4.2H_20$, 80 m NaCl, 5 mM KCl, 1 mM $MgSO_4.7H_2O$, and 20 mM glucose, adjusted to pH 7.4; BSF parasites), or phosphate buffered saline (PBS: 137 mM NaCl, 2.7 mM KCl, 8 mM Na_2HPO_4 and 1.8 mM KH_2PO_4, adjusted to pH 7.4; PCF parasites).

For long term preservation, 10 ml of mid-log phase BSF and PCF cells were harvested and resuspended in 4 ml of their respective media containing 10% (v/v) glycerol. Aliquots of 1 ml were transferred to cryotubes and stored at -80ºC for 24 hours, before transfer to liquid nitrogen tanks for long term storage. Stabilates removed from liquid nitrogen were allowed to slowly defrost at room temperature before transferring to pre-warmed medium without selective drugs and being cultured as described above. Appropriate drugs were added 1 day after defrosting.

2.2.3. **BSF transfection**

T. brucei BSF cells were cultured as described in section 2.2.2. 1 x 10^7 to 3 x 10^7 cells were harvested at mid-log phase by centrifugation at 1500 x *g* for 10 minutes. The supernatant was carefully removed and cells were resuspended in 100 µl of ice-cold Human T Cell Nucleofector solution (Lonza) and transferred to an electroporation cuvette (Lonza) (Burkard *et al.*, 2007).

To prepare DNA for transfection, plasmid DNA was linearized overnight by restriction digestion (section 2.3.3). Complete digestion of plasmid DNA was confirmed by analysing 1 µl of digested plasmid on a 1% agarose gel (section 2.3.2), and the remainder of plasmid DNA was purified using phenol-chloroform purification (section 2.3.7). 10 µg of linearized purified plasmid DNA was added to the cells before they were transfected using the programme X-001 in the Nucleofector machine (Amaxa). As a control, a second aliquot of cells was pulsed without any DNA present. Transfected cells were transferred immediately to 30 ml pre-warmed HMI-9 medium, or to 10 ml medium for the mock transfected cells. Selection of transfected clones was performed by limiting dilution; the transfected cells were diluted 50x, 250x and 1000x before 1 ml of each dilution and of the neat cells were plated out into wells of a 24 well plate. Cells were allowed to recover at 37ºC in 5% CO_2 for 6 hours, after which fresh medium containing a 2x concentration of the appropriate selective drug was added to all wells, including the control. Cells were observed at regular intervals to check for the emergence of clones which were detected typically after 6-8 days. When less than 10%

of the wells contained live cells, the emerging cells were considered clones and were transferred to 25 cm^3 flasks, cultured and stored as described in section 2.2.2.

2.2.4. **PCF transfection**

Similarly to BSF cells, PCF cells were harvested at mid-log phase. 6 x 10^7 to 1 x 10^8 cells were centrifuged at 600 x *g* for 10 minutes. Pelleted cells were resuspended in 100 µl of Human T Cell Nucleofector solution, transferred to a cuvette (Lonza), mixed with 10 µg of linearized DNA and pulsed in the Amaxa Nucleofector machine using X-001 programme. A no-DNA control was performed as described previously (section 2.2.3). The entire transfection mixture was added to 10 ml of pre-warmed SDM-79 without selective drugs and containing 30% conditioned medium, consisting of the supernatant from a concentrated PCF culture previously filter sterilised. Transfected cells were incubated overnight at 27ºC. Following recovery, cells were split into 3 aliquots, diluted 10x, 100x and 1000x in SDM-79 supplemented with conditioned medium, and selective antibiotics were added. Neat and diluted cultures were plated out in 96 well-plates (100 µl per well), and clones were detected 14-21 days post-transfection. Culture volumes were gradually increased and stabilates were produced as described in section 2.2.2.

2.2.5. **Hydroxyurea synchronization**

Both BSF and PCF cultures were synchronized in S-phase by the addition of 0.2 mM hydroxyurea (HU, Sigma), which blocks DNA replication by inhibiting a ribonucleotide reductase (Chowdhury *et al.*, 2008, Forsythe *et al.*, 2009). Before starting HU treatment, cell growth was followed to ascertain the doubling time (usually 6 hours or 12 hours, for BSF or PCF cultures, respectively). HU solution was freshly prepared on the day of use, filter sterilized and kept at 4ºC until use. Parasite cultures at a cell density of 5 x 10^5 (BSF) or 2 x 10^6 (PCF) cells.ml^{-1} were incubated with hydroxyurea for one doubling time, after which cells were centrifuged for 10 minutes at 1500 x *g*

(BSF) or 600 x *g* (PCF) and washed twice in medium without HU to remove the HU. Cells were re-incubated in fresh HMI-9/SDM-79, allowing them to proceed through the cell cycle in a synchronous manner. Samples were taken at time 0, at the doubling time, and at regular intervals thereafter to check cell cycle progression by flow cytometry (section 2.2.6) and microscope analyses (section 2.6.1). The time points to maximise the proportion of cells in mitosis and cytokinesis were optimized for both BSF and PCF form cells, after which cytoskeleton protein samples were prepared (section 2.2.8) for each culture and stored at -80ºC until required for antibody production (section 2.7) and protein analyses (section 2.4).

2.2.6. **Flow cytometry**

Approximately 3 x 10^6 trypanosome cells were collected and washed twice in one culture volume of PBS/TDB (section 2.2.2), for PCF/BSF cells, respectively. Cell pellets were resuspended in 1 ml 70% methanol/30% PBS, and stored at 4ºC overnight or up to 1 month. On the day of the analysis, fixed cells were washed once in PBS and resuspended in 1 ml of PBS containing 10 µg.ml^{-1} of propidium iodide (Sigma) and 10 µg/ml RNAse A (Sigma), and incubated at 37ºC for 45 mins, in the dark. DNA content was analysed using a Becton Dickinson FACSCalibur with the software CellQuest Pro 6.0, and for each sample 10,000 cells were analysed.

2.2.7. **Preparation of whole cell extracts**

Whole cell extracts were purified from *T. brucei* cultures for protein analysis and immunoprecipitations (IPs). Parasite cells were centrifuged for 10 minutes at 1500 x *g* and 600 x *g* for BSF and PCF cells, respectively. For each IP, a total of 5 x 10^8 cells were washed in 20 ml PBS/TDB for BSF/PCF forms respectively, and stored at -80ºC until required. For protein analysis by sodium dodecyl sulfate Polyacrylamide gel electrophoresis (SDS-PAGE) gels, parasite pellets were washed twice in 10 ml PBS and resuspended in equal volumes of PBS and 2x Laemmli loading buffer (0.25 M Tris.HCl

pH 6.8, 2% (w/v) SDS, 25% (v/v) glycerol, 5% (v/v) β-mercaptoethanol, 0.01% (w/v) bromophenol blue), to a final concentration of 2 x 10^5 cells.μl^{-1}.

2.2.8. **Preparation of cytoskeletal fractions**

Parasite cells were harvested at 1000 x *g* for 15 minutes, washed once in PBS (pH7) and centrifuged again at room temperature. Cell pellets were resuspended in 10 ml cold PEME (100mM PIPES, pH6.9, 2mM ethylene glycol tetraacetic acid (EGTA), 1mM MgSO4, 0.1mM EDTA (ethylene diamine tetra acetic acid)) supplemented with 1x EDTA-free protease inhibitor cocktail (Roche) and 1% Nonidet P40 detergent (NP40 - octylphenyl-polyethylene glycol) (PCF) or 0.5% NP40 (BSF). Cells were lysed on ice for 5 minutes (BSF) or 10 minutes (PCF), and centrifuged at 4ºC at 1000 x *g* for 10 minutes (PCF) or 250 x *g* for 30 minutes (BSF), to separate cytoskeletons from cytosolic proteins. The pellet containing the cytoskeleton fraction was resuspended in 1x Laemmli buffer to a final concentration of 2 x 10^5 cells.μl^{-1} and stored at -80ºC.

For antibody production (section 2.7) cytoskeletons were prepared from 1 x 10^9 BSF cells synchronized at mitosis or cytokinesis (section 2.2.5), lysed in 50 ml of PEME buffer and resuspended in 1x Laemmli buffer at 1 x 10^7 cells.μl^{-1}. The obtained cytoskeleton mixture was electrophoresed on 10% SDS-PAGE gels (section 2.4.5) (1 x 10^8 cells per well) and stained with Zinc Sulphate according to the manufacturer's protocol (Zinc staining Kit, BIORAD). Several slices of different molecular weights were cut from the gel (Table 2. 4), incubated for 20 minutes with 1/10 destain solution and stored at -80ºC. Prior to injection into Balb/c mice (section 2.7.1), gel slices were frozen in liquid nitrogen, ground up and mixed with small volumes of PBS (approximately 100 µl).

Table 2. 4 - Protein molecular weight characteristics of the different polyacrylamide gel slices obtained for synchronized BSF samples.

Polyacrylamide gel slices ID	Mitotic cytoskeleton	Cytokinesis cytoskeleton
1	Above 160 kDa	Above 160 kDa
2	100 to 160	100 to 160
3	80 to 100	80 to 100
4	60 to 80	60 to 80
5	35 to 40	35 to 40
6	30 to 35	30 to35
7	25 to 30	25 to 30
8	20 to 25	Below 25 kDa
9	Below 20 kDa	--

2.3. MOLECULAR BIOLOGY

2.3.1. **Amplification and cloning of DNA**

Specific gene fragments were amplified from *Trypanosoma brucei brucei* 427 genomic DNA by Polymerase Chain Reaction (PCR), using a pX2 Therma Cycler PCR machine (Thermo Electron Corporation). PCR was also used for colony screening and site-directed mutagenesis. Standard PCRs were performed using Taq Polymerase (NEB), and for high fidelity cloning, the proof reading enzymes Pfu Turbo (Stratagene) and Phusion DNA Polymerase (Finnzymes) were used. All polymerases were used according to the manufacturer's guidelines. Oligonucleotide primers were designed (using Vector NTI version 11 software, Invitrogen) to contain specific restriction sites, that allowed further sub-cloning into vectors of interest, and were obtained from Eurofins MWG (Germany). Table 2. 5 lists the primers used in this study.

Table 2. 5 - Oligonucleotides used during this study.

ID	Sequence (5`-3`) and restriction sites	Description
PR54	GGGAAGATCTCGGGTATGGCAACACGTTC BglII	Sense oligonucleotide to amplify *CRK12* (bases 2-2310)
PR53	GGGGCTCGAGTTACGCAGCGCTTGGATAAG XhoI	Antisense oligonucleotide to amplify *CRK12* up to the stop codon (bases 2-2310)
PR52	GGGGGAATTCGACGGAGCGGGCG EcoRI	Sense oligonucleotide to amplify C-terminal *CRK12* (bases 1674-2310)
PR55	GGGGCATATGGGTATGGCAACACGTTCGC NdeI	Sense oligonucleotide to amplify *CRK12* (bases 0-2310)
PR53	GGGGCTCGAGTTACGCAGCGCTTGGATAAG XhoI	Antisense oligonucleotide to amplify full length *CRK12* (bases 0-2310) or C-terminal *CRK12* (bases 1674-2310) up to the stop codon
PR206	BglII CGCGAGATCTATGGAGGTCCATACTAACCAAG ATCCACTTGACGGTATGGCAACACGTTCGCCT TCGCC	Sense oligonucleotide to amplify *CRK12* (bases 5-2310). Introduction of a start codon (bold) and a TY tag (double underlined)
PR207	GTTGAGATCTTTACGCAGCGCTTGGATAAGG BglII	Antisense oligonucleotide to amplify *CRK12* up to stop codon (bases 5-2310).
PR208	GGTGAGTATGTTGCGTTGATGCGACTTAAAGT TTTAGAGG K358M	Sense oligonucleotide for site directed mutagenesis of *CRK12* base 1073 (A→T; in bold)
PR209	CCTCTAAAACTTTAAGTCGCATCAACGCAACA TACTCACC K358M	Antisense oligonucleotide for site directed mutagenesis of *CRK12* base 1073 (A→T; in bold)

Approximately 100 ng of genomic DNA from *T.b.brucei* 427 were used in each amplification reaction (Table 2. 6), except for colony PCRs where DNA was obtained by directly incubating part of the colony with the reaction mix for a few seconds. The reaction mix was optimized for high fidelity amplifications (Table 2. 6).

Table 2. 6 - Composition of the PCR reaction mixes used in this study.

	PCR Enzyme		
Reagents	**Taq Polymerase**	**Pfu Turbo**	**Phusion**
Buffer	1x Taq PCR mix*	1x PfuTurbo buffer	1x Phusion HF buffer
DNA	100 ng or small portion of *E.coli* colony	100 ng	100 - 200 ng
Each oligonucleotide	20 ng	20 - 40 ng	40 ng
Enzyme	1 U	2.5 U	0.4 - 1 U
NTPs	Included in the PCR mix	200 µM	200 µM
DMSO	--	--	3%
Final volume	20	20	50

** Taq PCR mix - 1.13 $mg.ml^{-1}$ bovine serum albumin (BSA), 450 mM Tris (pH 8.8), 110 mM $(NH_4)_2SO_4$, 45 mM $MgCl_2$, 0.47 % (v/v) β-mercaptoethanol, 44 µM EDTA (pH 8) and 10 mM dNTPs (dCTP, dATP, dGTP, dTTP) (Invitrogen)

Typically, cycling conditions using Taq polymerase were as follows: initial denaturation step of 95ºC for 30 secs; 30 cycles of denaturation (95°C, 50 secs), annealing (50°C, 50 secs) and extension (72°C, 2.5 mins), followed by a final extension at 72°C for 5 mins. When used for colony PCR, an extra 5 minute denaturation step was added at the beginning of the reaction.

For long fragments (open reading frame (ORF) for *CRK12* ~ 2.3 kbp), the amplification programme consisted of: 1x 98°C for 30 seconds, 30x 98°C for 10 seconds; 60°C or 68°C for 30 seconds (for amplifications with PR53+PR54 or PR53+PR55 and PR206+PR207 (Table 2. 5) respectively); 68°C 2 minutes and 30 seconds, and 1x 72°C for 5 to 7 minutes. Due to the longer size of the fragments (2.3 kb when compared to 650 bp of the C-terminus CRK12) the colony PCR programme was also optimized by decreasing the denaturation and extension temperatures to 92ºC and 68ºC, respectively.

Amplified DNA was visualised by gel electrophoresis (section 2.3.2), and where successful, the required fragment was excised from the gel with a clean scalpel blade under a blue light and purified using a Qiaex Gel Extraction Kit (Qiagen). 2 µl of the DNA product were cloned into the pSC-B vector (Strataclone Blunt PCR Cloning Kit,

Stratagene) and 1 µl to 2 µl of the ligated product was transformed into Strataclone SoloPack Competent cells (Stratagene) according to the manufacturer's instructions. 100 µl of the transformation mix were plated onto LB Agar plates containing 100 $\mu g.ml^{-1}$ ampicillin and 40 µl 5-bromo-4-chloro-3 indolyl-β-D galactopyranoside (X-gal; 2% in dimethylformamide), and incubated at 37^{o}C overnight. White colonies were analysed by colony PCR using M13 forward and reverse primers to confirm they contained pSC-B with the expected insert, with cycling conditions optimized according to the expected fragment size. Plasmid DNA was then purified from colony PCR positive colonies and analysed by restriction endonuclease analysis to confirm plasmids contained the correct insert (section 2.3.3). Plasmids were further analysed by sequencing of their insert (section 2.3.6), to rule out the presence of any mutations introduced during the PCR.

2.3.2. **DNA gel electrophoresis**

DNA samples were electrophoresed in a 1% (w/v) agarose/(Ultrapure, Invitrogen) 0.5x TBE (44.6 mM Tris base, 44.5 mM boric acid and 1 mM EDTA) gel. Agarose was dissolved by heating, allowed to cool before adding SYBR Safe stain (Invitrogen, diluted 1:30,000) and poured into an appropriate gel tray with comb to set. The gel was then transferred to an electrophoresis tank and immersed in 0.5x TBE. DNA samples were prepared by the addition of 6x loading buffer (15% Ficoll, 0.25% Xylene cyanol and 0.25% bromophenol blue) to give a final concentration of 1x, and loaded into the wells, together with a reference sample (1 kb^{+} DNA ladder, Invitrogen). Typically, DNA was electrophoresed at 100 V for approximately 45 minutes and visualised under UV light (BioRad Gel-Doc imager and Quantity One software).

2.3.3. **Restriction endonuclease analysis**

Endonucleases (New England Biolabs – NEB) were used to confirm insertion of the correct DNA fragment, sub-cloning into other vectors of interest (section 2.3.4) and

for preparation of linearized DNA for transfection (section 2.3.7). Typically, 0.2 µg of DNA was cut with 10 U of each of the desired enzymes in a 10 µl mixture, containing 1x Buffer (NEB) and, if required, 1x BSA. The reaction mix was incubated at 37ºC for 1 hour, electrophoresed on a 1% agarose gel and visualised under UV light (section 2.3.2).

When sub-cloning, a total of 2 µg of DNA were digested in a 20 to 50 µl reaction (as above), with 20 U of restriction endonuclease and for approximately 2 hours at 37ºC. Digested DNA was analysed by DNA gel electrophoresis, the desired fragment was excised from an agarose gel using a clean scalpel blade and purified using a Gel Extraction kit (Qiagen) according to the manufacturer's protocol.

For linearization of DNA for transfection, 100 µg of DNA were digested at 37ºC overnight, with 40 U of enzyme, in a total volume of 500 µl. To verify digestion efficiency, 1 µl of the digestion product was analysed by agarose gel electrophoresis and the remaining DNA was used for phenol/chloroform purification (section 2.3.7).

2.3.4. **Sub-cloning of DNA fragment into vectors of interest**

When cloning into the final destination vectors, both the plasmid containing the desired insert and the vector were digested at 37ºC for 2 hours (section 2.3.3), with the appropriate restriction enzymes, and analysed by agarose gel electrophoresis (section 2.3.2). To prevent religation of the empty vector, 1U of CIP (calf intestinal alkaline phosphatase, NEB) was added after restriction endonuclease digestion, incubated at 37ºC for 30 minutes and then inactivated by heating to 65ºC for 30 minutes, prior to gel analysis. After extraction and purification of the required DNA fragments from the agarose gel, insert and vector were ligated in a 10 µl reaction mix, using 0.4 U of T4 DNA ligase and 1x T4 Ligase Buffer (NEB), at different ratios (vector:insert 1:3, 1:6). The ligation reaction was incubated at room temperature for 2 hours and further ligated at 16ºC overnight, before half of the reaction volume was transformed in XL1Blue competent cells by heat-shock (section 2.1.4) and cells which had taken up plasmid selected by plating on appropriate antibiotics. Individual colonies were screened for the

presence of the correct plasmid by colony PCR (section 2.3.1) and/or restriction digestion of purified bacterial DNA (section 2.3.3).

2.3.5. **Site-directed mutagenesis**

In order to mutate specific amino acids in proteins, primers were designed according to the QuickChange Site-directed Mutagenesis kit (Invitrogen), containing specific nucleotide changes. The mutagenesis reaction was carried out according to the manufacturer's instructions, and sequencing analysis (section 2.3.6) confirmed the presence of the desired mutation and the absence of undesired changes introduced in the PCR.

2.3.6. **Sequencing**

DNA sequencing was performed by the DNA Sequencing Service at the University of Dundee (http://www.dnaseq.co.uk/home.html), and results were analysed using Vector NTI ContigExpress (Invitrogen) to compare the obtained sequence against the expected sequence.

2.3.7. **Preparation of DNA for transfection into parasites**

The remainder of the digested DNA was purified by the addition of one volume of a 1:1 solution of phenol:chloroform:isoamyl alcohol 25:24:1, and vortexing for a few seconds prior to being centrifuged at 17,968 x *g* for 2 minutes. The upper aqueous phase containing the DNA was decanted from the organic phase, containing precipitated proteins, and mixed with an equal volume of chloroform. The mixture was vortexed and centrifuged as before, and the aqueous phase was decanted. After a second chloroform extraction, DNA was precipitated by addition of a 1/10 volume of 3 M sodium acetate and 1 volume of isopropanol, vortexed and centrifuged at 17,968 x *g* for 15 minutes.

The supernatant was carefully removed, and the DNA pellet was washed with 70% ethanol and allowed to air dry in a sterile environment. DNA was resuspended in sterile water, to a final concentration of 1 $\mu g.ml^{-1}$, and stored at -20ºC.

2.3.8. **Plasmid generation**

All plasmids used in this study are detailed in Table 2. 7 and Table 2. 8.

Table 2. 7 – **Plasmids generated in this study**. Description includes the resistance marker (Kan – Kanamycin; Amp – Ampicillin).

Plasmid ID	Description
pHG97	C-terminal end of *CRK12* (bases 1674 to 2310) in pSC-B, amplified using PR52 and PR53. Amp^r
pHG98	ORF for *CRK12* (bases 2 to 2310) in pSC-B, amplified using PR53 and PR54. Amp^r
pHG110	ORF for *CRK12* (bases 0 to 2310) in pSC-B, amplified using PR53 and PR55. Amp^r
pHG178	C-terminal end of *CRK12* sub-cloned from pHG97 into $pET28a^+$, for protein expression. Kan^r
pHG180	*CRK12* sub-cloned from pHG110 into $pET28a^+$, for protein expression. Kan^r
pHG298	*CRK12* sub-cloned from pHG98 into pGEX5X1, for protein expression. Amp^r
pHG199	ORF for *CRK12* (bases 5 to 2310) in pSC-B amplified using PR206 and PR207, for tet inducible expression of N-terminal TY. Amp^r
pHG218	Site-directed mutagenesis of pHG199 using PR208 and PR209 to generate CRK12 K358M in pSC-B, for tet inducible expression of N-terminal TY. Amp^r

Table 2. 8 - Plasmids used in this study. Description includes the resistance marker (HYG – hygromycin; NEO – neomycin; BLAS – blasticidin).

Plasmid ID	Description
pHG69	ty:GFP:CRK12 (Tb11.01.4130) fusion protein construct for expression at the endogenous locus. HYG^r
pGL1217	CYC9 (Tb11.01.5600) knockout. NEO^r
pGL1125	CYC9:TAP (Tb11.01.5600) expression from endogenous locus. $BLAS^r$
pHG230	tet-inducible expression vector of ty:CRK12 WT (Tb11.01.4130). HYG^r
pHG231	tet-inducible expression vector of of ty:CRK12 kinase dead (K358M). HYG^r

2.4. PROTEIN BIOCHEMISTRY

2.4.1. **Recombinant protein expression**

Recombinant proteins were expressed fused to different tags, to increase solubility and allow purification, and used for production of MAbs (section 2.7) or for further analyses including kinase assays (section 2.4.11).

The following plasmids were generated for protein expression: pHG178 (C-terminal end of *CRK12* sub-cloned from pHG97 into pET28a^{+}); pHG180 (full length ORF for *CRK12* sub-cloned from pHG110 into pET28a^{+}) and pHG298 (full length ORF for *CRK12* sub-cloned from pHG98 into pGEX5X1) (Table 2. 7).

Plasmids generated for protein expression were transformed (section 2.1.4) into different *E.coli* cell lines: pHG178 and pHG180 (Table 2. 7) were transformed into BL21 (DE3) pLysS cells (section 2.1.1), while pHG298 (Table 2. 7) was transformed into BL21 (DE3) cells (section 2.1.1), for inducible expression of recombinant proteins. Overnight cultures were grown at 37°C with shaking at 200 rpm in LB supplemented with the appropriate antibiotics, and diluted the next day 1/100. Cultures were allowed to grow until the OD_{600nm} reached 0.6-0.8, determined using a spectrophotometer (Shimadzu Biospec-mini DNA/RNA/Protein analyser), at which time, protein expression was induced by the addition of 1 mM isopropyl-beta-D-thiogalactopyranoside (IPTG). Expression conditions were optimized individually for each protein: 18°C overnight, 20°C for four hours, and 37°C for two or four hours; and after growth at optimum conditions, cells were harvested by centrifugation at 6654 x *g* for 10 minutes at 4°C. The cell pellet was resuspended in 1/20 of the original culture volume of cold lysis buffer, performing all downstream processing in cold environments to prevent protein degradation. For GST-tagged proteins, the lysis buffer was PBS supplemented with 0.1% Triton X-100, while for His-tagged proteins, different buffers were used: a guanidium lysis buffer was used for cells expressing the C-terminus of CRK12 (6 M guanidine HCl, 20 mM sodium phosphate, 500 mM NaCl, adjusted to pH 7.8), and for cells expressing the full length protein, the buffer comprised 50 mM Na_2HPO_4 pH 8, 0.3 M NaCl and 10 mM Immidazole. All buffers were

supplemented with 1x complete EDTA free protease inhibitor cocktail (Roche), and in some cases, the cell suspension was incubated with 1mg.ml^{-1} lysozyme for an hour to degrade the cell wall, prior to sonicating for 10 to 20 cycles, 10 seconds on, 10 seconds off, at 80% power (Soniprep 150 sonicator/Bandelin sonicator). Centrifugation at 6654 x *g* for 20 minutes allowed separation of the soluble and insoluble fractions.

Analysis of expression and solubility of the recombinant proteins was performed by electrophoresing the samples on an SDS-PAGE gel (section 2.4.5). For uninduced and induced samples, 0.5 ml of culture were centrifuged at 17900 x *g* for 2 minutes, the pellet was resuspended in 100 µl 1x Laemmli buffer (section 2.2.7) and boiled for 5 minutes. Aliquots of the soluble and insoluble fractions were mixed with an equal volume of 2x loading buffer, boiled as previously and analysed by protein electrophoresis (section 2.4.5).

2.4.2. **Purification of His-tagged proteins**

Purification of His-CRK12 proteins used a ProBond Nickel-Chelating resin (Invitrogen) and was optimized for the C-terminal end and for the full length protein, such that the recombinant proteins were eluted from the beads by pH variation or with imidazole, respectively.

For both constructs, protein expression was induced for 4 hours at 37ºC and solubility tests (section 2.4.1) showed that both recombinant proteins remained in the insoluble fraction. Buffers were changed to include 8M or 6M urea for solubilization of the C-terminal end of CRK12 or for the full length, respectively; leading to approximately 50% of the recombinant protein in the soluble fraction after sonication (section 2.4.1). 10 ml of 50% slurry were used per 50 ml of clear lysate, applied to a disposable column and allowed to settle. The supernatant was drained and the beads were washed first with sterile dH_20 and then twice with binding buffer (500 mM NaCl, 20 or 50 mM sodium phosphate, 8 M or 6M urea, for purification of the C-terminal end of CRK12 or for the full length, respectively). The clear soluble lysate was incubated with the resin for one to two hours at 4ºC, to allow binding of the His-tagged proteins,

after which the flow through was collected for further analysis (unbound sample). The column was washed two to three times with the appropriate wash buffer (same composition as the binding buffer, pH 6 for purification of the C-terminal end of CRK12), by inverting the column, allowing the resin to settle and aspirating the supernatant. For the C-terminal end of CRK12, a last wash was carried out as above, at pH 5.3. Elution was performed by incubating 5 ml of elution buffer (8 M urea, 20 mM sodium phosphate, 500 mM NaCl, pH 4.0 for purification of the C-terminal end of CRK12; 6 M Urea, 20 mM Tris pH 7.5, 100 mM NaCl, 300 mM Imidazole for purification of the full length CRK12) for 15 minutes, before collecting 1 ml fractions. All elution fractions, together with the flow through and washing samples, were monitored by SDS-PAGE (section 2.4.5) and/or Western Blotting (WB) (section 2.4.7), using an anti-His antibody (Sigma). The elution fractions containing the desired protein were combined and dialyzed against PBS overnight at 4°C (section 2.4.3).

2.4.3. **Dialysis of proteins**

Recombinant proteins and MAbs were dialysed using a Dialysis Tubing Visking membrane (Carl Roth GmbH), boiled previously in dH_20 to make it easier to manipulate. The samples were filtered using a 0.45 µm syringe filter, inserted on the dialysis tubing, sealed and dialysed against 1 L of PBS or Equilibrium Buffer (section 2.7.9), for recombinant protein or MAbs, respectively. After 1-2 hours, the samples were placed into fresh buffer and dialysed overnight. All dialysis were performed at 4°C with stirring.

2.4.4. **Determination of protein concentration**

Protein concentration was determined using a Bradford assay (Bio Rad protein Assay), and following the manufacturer's standard procedure for microtitre plates. First, the dye reagent was prepared by mixing 1 part Dye Reagent Concentrate with 4 parts dH_20 and filtered. As a control, a protein standard dilution set was prepared, using bovine serum albumin (BSA) at concentrations ranging from 0.05 $mg.ml^{-1}$ to 0.5 $mg.ml^{-}$

[1]. In general, 10 µl of the protein sample or standard were applied to a 96 well plate, and mixed thoroughly with 200 µl of the prepared reagent mix by pipetting up and down. Protein samples in triplicate were added neat, 10x and 100x diluted. The plate was incubated at room temperature for approximately 5 minutes and analysed at a wavelength of 595 nm, using the software Microplate manager 4.0 (BioRad) in a microplate reader (BioRad model 550). The standard values were used to plot a calibration curve of absorbance versus BSA concentration, and the regression line was used to determine the concentration of the different samples.

2.4.5. **Protein electrophoresis**

Recombinant proteins, whole cell and cytoskeleton extracts were separated by SDS-PAGE (sodium dodecyl phosphate polyacrylamide gel electrophoresis). Typically, 12% or 14% gels (Table 2. 9 and Table 2. 10) were used, 8% gels were also used for visualisation of large proteins; and proteins were electrophoresed with SDS-PAGE running buffer (25 mM Tris, 192 mM glycine and 0.1% SDS) at 90 V while in the stacking gel and 200 V in the resolving gel.

Table 2. 9 – Reagents used for preparation of the separating gel for SDS-PAGE at different concentrations.

Reagent (ml)	8%	12%	14%
dH_20	4.6	3.3	2.6
30% / 0.8% acrylamide/Bis acrylamide	2.7	4	4.7
1.5 M Tris pH 8.8	2.5	2.5	2.5
10% (w/v) SDS	0.1	0.1	0.1
10% (w/v) APS	0.1	0.1	0.1
TEMED	0.004	0.004	0.004

Table 2. 10 - Reagents used for preparation of the stacking gel for SDS-PAGE.

Reagent (ml)	Stacking gel
dH_20	1.4
30% / 0,8% acrylamide/Bis acrylamide	0.33
1,5 M Tris pH 8,8	0.25
10% (w/v) SDS	0.02
10% (w/v) APS	0.02
TEMED	0.002

Before applying to the wells, 1 volume of 2x loading buffer was added to protein samples (0.2 M Tris.HCl pH 6.8, 2.5% (w/v) SDS, 20% (v/v) glycerol, 5% (v/v) β-mercaptoethanol, 0.05% (w/v) bromophenol blue) and boiled for five minutes. As a reference and to allow determination of molecular sizes, a protein marker was electrophoresed with each gel, differing whether the gel was for Coomassie staining (Benchmark protein ladder (Invitrogen) or Amersham Low Molecular Weight calibration kit for SDS electrophoresis (GE Healthcare)), or for WB (See Blue Plus 2 ladder (Invitrogen); Novex Sharp Pre-stained Protein Standard (Invitrogen); Broad Range Prestained protein marker (7-175 kDa, NEB); Amersham Low (LMW) and High Molecular Weight (HMW) calibration kit for SDS electrophoresis (GE Healthcare)).

To better separate small proteins, a NuPAGE® Novex 4-12% Bis-Tris gradient gel (Invitrogen) was used with NuPAGE® MES running buffer and 10x Transfer Buffer (Invitrogen). Samples were prepared in NuPAGE® LDS Sample Buffer and Reducing Agent (Invitrogen).

2.4.6. **Coomassie staining**

Protein gels were stained for one hour at room temperature with shaking with Coomassie stain solution (0.25% (w/v) Coomassie Blue R-250, 50% (v/v) methanol, 10% (v/v) acetic acid). Polyacrylamide gels were incubated in destain solution (40% (v/v) methanol, 10% (v/v) acetic acid) for 15 minutes, and then transferred to fresh destain solution and incubated until a high contrast was observed between protein bands and background, following which they were washed in distilled water and photographed and/or dried (BioRad gel dryer model 583).

2.4.7. **Western Blotting**

To analyse proteins by WB, SDS-PAGE gels were transferred to a Hybond ECL nitrocellulose membrane (Invitrogen), pre-incubated with transfer buffer (Running buffer with 20% methanol) for 10 minutes prior to electrotransfer. The transfer module

(Invitrogen/BioRad) was assembled by placing a layer of sponges, two layers of filter papers, the protein gel, covering with the prepared membrane, two filter papers and another layer of sponges. All filter papers and sponges were pre-soaked in transfer buffer, prior to assembly with the gel and the membrane, placed on a gel tank, where transfer buffer was added to cover the membrane, gel and sponges, before filling the outer compartment with water or ice, according to the transfer module used (Invitrogen/BioRad). Proteins were transferred for two hours at 32 V at room temperature or overnight at 90 mA at 4ºC and transfer efficiency was determined by staining the membrane with Ponceau S (Sigma) for 10 minutes, before being washed with dH_20 to visualise the transferred proteins and removed by washing with PBST.

A blocking step was carried out by incubating the membrane for one hour in 5% milk in washing buffer (PBS/0.1% Tween 20; PBST), prior to incubating with the primary antibody (Table 2. 11) for one hour at room temperature or overnight at 4ºC, followed by three washes with PBST for 15 minutes each. Secondary antibodies were either conjugated with horse radish peroxidase (HRP) and blots developed using a chemiluminescent detection agent (West Dura, West Pico or West Femto reagents, Pierce) before exposing the membrane to photographic film and developing the film using a Kodak film processor, or with alkaline phosphatase (AP) which was developed using the AP conjugate substrate kit (BioRad) before being visually analysed until it was appropriate for the reaction to be stopped by the addition of water.

Table 2. 11 - Antibodies used for WB.

Name / target	Antibody type	Source	Stock Concentration	Working dilution
Primary antibodies used				
Polyclonal serum against cell cycle proteins in mouse	Mouse	Produced during this study	--	1:10,000
Antibodies produced against cell cycle proteins in mouse	Mouse monoclonal	Produced during this study	--	Neat
Anti β-tubulin (KMX)	Mouse Monoclonal IgG2b	Millipore	1 $mg.ml^{-1}$	1:10,000
Anti-TY (Clone BB2)	Mouse monoclonal IgG1	Matthews laboratory		1:50 – 1:20
Anti-GFP	Mouse monoclonal IgG2a	Santa Cruz Biotechnology	200 $\mu g.ml^{-1}$	1:1,000
Peroxidase anti-peroxidase soluble complex antibody	Rabbit	Sigma		1:200
Anti-GST (B-14)	Mouse monoclonal IgG1	Santa Cruz Biotechnology	0.1 $\mu g.ml^{-1}$	1:10,000
Anti-tetra-his	Mouse monoclonal IgG1	Qiagen	0.2 $\mu g.ml^{-1}$	1:1,000
Monoclonal anti-polyHistidine-AP	Mouse monoclonal Ig2a	Sigma	--	1:2,000
Anti-EF1-α (clone CBP-KK1)	Mouse monoclonal IgG1κ	Millipore	1 $mg.ml^{-1}$	1:25,000
Anti-α-tubulin antibody (TAT1)	Mouse IgG2b	Gull laboratories (Woods *et al.*, 1989)	Neat antibody	1:5,000
Secondary antibodies used				
Anti-mouse polyvalent Immunoglobulins (IgG, IgA, IgM)	Produced in goat; AP conjugate	Sigma	--	1:10,000
Anti-mouse IgG	Produced in goat; HRP conjugate	Promega	1 $mg.ml^{-1}$	1:10,000
Anti-rabbit IgG	Produced in goat; HRP conjugate	Promega	1 $mg.ml^{-1}$	1:50,000
Anti-mouse IgM (μ-chain specific)	Produced in goat; HRP conjugate	Invitrogen	--	1:4,000
AffiniPure anti-mouse IgG + IgM (H+L)	Produced in goat; HRP conjugate	Jackson Immunoresearch	0.8 $mg.ml^{-1}$	1:10,000

2.4.8. **Dot-blot**

Dot-blots were performed using cytoskeleton samples of un-synchronized cultures, as well as from cultures synchronized in mitosis and in cytokinesis using HU (section 2.2.5). Cytoskeleton preparations from 4 x 10^5 cells were directly applied to a nitrocellulose membrane (Invitrogen), allowed to dry and blocked in 5% milk for 1 hour. Primary antibodies were incubated with the membrane for 1 hour at room temperature or overnight at 4ºC, before the membrane was washed three times with PBST for 10 minutes each and incubated with an anti-mouse HRP-conjugated secondary antibody IgG+IgM (Jackson Immunoresearch, Table 2. 11) for one hour. After washing three times in PBST for 10 minutes each wash, the blots were developed as before (section 2.4.7).

2.4.9. **Immunoprecipitaton using protein G agarose beads**

IP assays were used to check for an interaction between two proteins *in vivo*, to analyse kinase activity of the immunoprecipitated protein, and also to test the ability of the antibodies generated in this study to pull down a specific protein. For this test, a large number of parasite cells were used, typically between 1 x 10^8 and 1 x 10^9 cells per reaction (section 2.2.7).

Cells were lysed with 1 ml LSGI buffer (Lysis Solution with Glycerol and Inhibitors), comprising of LSG (Lysis Solution with Glycerol) Buffer (50 mM MOPS pH 7.4, 100 mM NaCl, 1 mM EGTA, 1 mM EDTA, 10 mM NaF, 1 mM NaOVa, 1% (v/v) Triton X-100 and 10% (v/v) glycerol) supplemented with different protease inhibitors (0.1 mg.ml^{-1} Leupeptin, 0.5 mM phenylmethanesulfonylfluoride (PMSF), 5 µg.ml^{-1} Pepstatin, 0.5 mg.ml^{-1} Pefabloc and 1 mM 1,10-Phenanthroline). A clear lysate was obtained after centrifugation at 10,000 x *g* for 45 minutes at 4ºC to pellet cell debris, and then incubated overnight at 4ºC with either PBS (negative control) or with a specific antibody (anti-TY mouse monoclonal IgG1 clone BB2 (Woods *et al.*, 1989), or one of the MAbs raised during this study).

The following day, 100 µl of Protein G beads (Pierce), previously washed and resuspended in PBS as a 50% slurry, were incubated with the antibody-lysate mix for a further two hours at 4ºC. The beads were transferred to a 2 ml disposable column, drained and washed sequentially, at 4ºC for 5 minutes, with 1 ml of 3 different buffers: 1x with LSGI, 1x with LSG and 2x with High Salt Lysis Solution (HSLS - 50 mM MOPS pH 7.4, 100 mM NaCl, 1 mM EGTA, 1 mM EDTA, 10 mM NaF, 1 mM NaOVa, 1% (v/v) Triton X-100), before a stopper was placed on the bottom of the column and the beads were resuspended in 1 ml Kinase Assay Buffer (KAB: 50 mM MOPS, 20 mM $MgCl_2$, 2 mM dithiothreitol (DTT), 10 mM EGTA) and transferred to an Eppendorf tube. An aliquot (half the volume) of the beads/KAB mix was centrifuged at 17,968 x *g* for 2 minutes, and the beads resuspended in 40 µl of 1x Laemmli buffer, boiled and used for WB (section 2.4.7), while the remaining solution was used for kinase assays (section 2.4.11).

2.4.10. **IP using Dynabeads®**

Magnetic Dynabeads®-protein G beads (Invitrogen) were used following the manufacturer's protocol, and lysates were obtained and treated as in section 2.2.7. The beads used are coupled with protein G to their surface, which binds to IgG antibodies. For each IP, 1.5 mg of Dynabeads® were transferred to an Eppendorf tube, incubated with 200 µl of antibody at room temperature for 30 minutes, and cross-linked for one hour using Bis(sulfosuccinimidyl)suberate (BS^3) (Thermo Fisher Scientific), according to the manufacturer's protocol.

Antibody-coupled beads were washed with PBST, separating the beads from the wash buffer by using the magnet, which pulled down the beads allowing the supernatant to be removed by gently pipetting. The beads were incubated with the sample containing the antigen of interest for 10 minutes at room temperature or one hour at 4ºC, in order to obtain optimal binding. The sample was placed on the magnet and the supernatant was removed, representing the unbound sample which was kept for further analysis, and the Dynabeads®-antibody-antigen complex was washed three times with PBST, separating the beads from the wash buffer using the magnet to allow removal of

the wash solution each time, and finally resuspended in 100 µl PBS and transferred to a clean tube for elution. To elute the bound proteins, denaturing conditions were applied, by heating the beads for 10 minutes at 70ºC in protein loading buffer (section 2.4.5). Using the magnet, the beads were separated from the supernatant containing the bound proteins, which was used for further analysis. If desired, a kinase assay was performed prior to elution by resuspending the beads-antibody-protein complex in 1 ml KAB instead of PBS, and using 0.4 ml for the kinase assay (section 2.4.11) and pelleting the remaining 0.6 ml again and resuspending in PBS before eluting as described above.

2.4.11. **Kinase assays**

Kinase assays were performed with recombinant proteins or using proteins immunoprecipitated from parasite lysates.

IP beads or recombinant proteins were resuspended in KAB or dialysed into this buffer, respectively, before being divided in four aliquots to assay against generic kinase substrates: Histone H1 (Calbiochem), α- or β-casein (Invitrogen), or myelin basic protein (MBP;Invitrogen). Both the beads and the kinase assay mix (KAM; 4 µM ATP, 5 µg substrate and 0.37 MBq γ32P-ATP per reaction in KAB, for a total volume of 20 µl) were prewarmed at 30ºC for 5 minutes with shaking, before 20 µl KAM were added to the beads and incubated for a further 20 minutes. The reaction was stopped by the addition of 20 µl of 1x Laemmli buffer, heated at 70ºC for 5 minutes, loaded on an SDS-PAGE gel and electrophoresed (section 2.4.5) until the dye front (containing unincorporated radiolabelled nucleotides) just ran off the bottom of the gel. The gel was then stained with Coomassie Blue (section 2.4.6) before being dried, exposed overnight to a phosphor-imaging screen and scanned using a Typhoon scanner.

2.5. UPTAKE ASSAYS

2.5.1. **FM4-64 uptake assay**

To investigate endocytosis in BSF cell lines, uptake of the fluorescent lipophilic stain FM4-64FX (Invitrogen) was followed both at 4ºC and 37ºC. All centrifugation

steps were performed at 600 x *g* for 5 minutes. Briefly, cells were washed in TES buffer (120 mM NaCl, 5 mM KCl, 3 mM $MgSO_4$, 16 mM Na_2HPO_4, 5 mM KH_2PO_4, 30 mM TES, 10 mM glucose, 0.1 mM adenosine) and resuspended in fresh TES buffer at 1 x 10^7 cells.ml^{-1}. Samples were pre-incubated at the desired temperature for 10 minutes, after which 40 µM FM4-64FX was added and cells were incubated at the same temperature for a further 5 minutes. Uptake was stopped by placing the cells on ice and the remaining protocol was performed at 4ºC in the dark. Cells were washed once in PBS and allowed to settle on a poly-L-lysine coated slide (section 2.6.1) for 10 minutes, after which they were fixed in 4% paraformaldehyde (PFA) for 30 minutes. Slides were washed twice in PBS before being mounted with Vectashield (Vector Laboratories) containing 4,6-diamidino-2-phenylindole (DAPI) and analysed using a Zeiss Axioskop fluorescent microscope and OpenLab version 3.5 software.

2.5.2. **Transferrin uptake assay**

Endocytosis analyses were also performed by following the uptake of Alexa Fluor 594 conjugated Tf (AF594-transferrin) (Invitrogen). Cells were washed in HMI9-1% BSA, and resuspended in the same medium at 1 x 10^7 cells.ml^{-1}, before being incubated at 37ºC for 15 minutes. AF594- transferrin was added to a final concentration of 50 µg.ml^{-1} and cells were incubated for a further five minutes at 37^{o}C. The reaction was stopped by the addition of 5 volumes of Voorheis's modified PBS (vPBS: 137 mM NaCl, 2.7 mM KCl, 8 mM Na_2HPO_4 and 1.8 mM KH_2PO_4, 15.7 g.l^{-1} sucrose, 1.8 g.l^{-1} glucose) and kept on ice. The remaining protocol was carried out at 4ºC and in the dark. Cells were fixed on ice for 1 hour in 4% PFA, before being washed twice in PBS and allowed to adhere to a poly-L-lysine coated slide, before being mounted with Vectashield and analysed using a Zeiss Axioskop fluorescent microscope and OpenLab version 3.5 software.

2.6. MICROSCOPY TECHNIQUES

T. brucei cells were analysed with different microscopy methods. Fluorescence microscopy was used to visualise DNA-containing organelles (section 2.6.1), proteins

tagged with fluorescent markers (section 2.6.2) and specific proteins using antibodies (IFA; sections 2.6.3 and 2.6.4), while TEM was used where higher resolution was required to visualise cell content (section 2.6.5).

2.6.1. **DAPI staining**

Analysis of DNA content involved staining parasite cells with DAPI, and was performed to monitor cell cycle progression in cell lines under investigation. Typically, 5 x 10^5 cells were harvested by centrifugation, most of the supernatant was removed and cells were resuspended in the remaining medium. Cells were spread over a glass microscope slide (previously incubated in a 1/10 dilution of poly-L-lysine solution for 10 minutes and air dried) and allowed to dry before being fixed in methanol overnight at -20ºC. Methanol was then allowed to evaporate and slides were kept at room temperature until further use. Prior to staining, cells were re-hydrated in PBS for 10 minutes at room temperature, after which the slides were drained and 50 µl 1 µg.ml^{-1} of DAPI in PBS supplemented with 1 µl of 2.5% 1,4-diazabicyclo[2.2.2]octane (DABCO), an anti-fading agent was added. Alternatively, cells were stained using Vectashield (Vector Laboratories), a mounting media containing DAPI. All slides were fitted with a coverslip and sealed with nail varnish.

Cells were visualised under a Zeiss Axioskop fluorescent microscope at 100 X magnification with immersion oil, using the differential interference contrast (DIC) filter to examine cell morphology and a UV light filter at 480 nm (λEx 360 nm / λEm 457 nm) to visualise DAPI staining of DNA. Images were captured using a Hamamatsu ORCA-ER digital camera and processed using Openlab version 3.5 software.

2.6.2. **Visualising direct-cell fluorescence**

Several parasite cell lines used or generated in this study harboured a gene of interest fused to a fluorescent tag (e.g. *GFP:CRK12*, Table 2. 1 and Table 2. 2). Cells

were fixed on poly-lysine slides and stained with Vectashield as previously described (section 2.6.1).

Fluorescently tagged proteins were visualised under UV light, on either the Zeiss Axioskop with a FITC (Fluorescein isothiocyanate) filter set at 540 nm, or using an Applied Precision DeltaVision Deconvolution microscope. In the latter case, images were taken with a CoolSnap HQ camera and processed using SoftWoRx® software. Z-stacks of 10 images 0.2 µm apart were generally taken for each filter: DAPI (λEx 360 nm /λEm 457 nm), FITC (λEx 490 nm /λEm 528 nm) and RD-TR-PE filter (λEx 555 nm / λEm 617 nm). A reference DIC image at the midpoint of the Z stack was also taken.

2.6.3. **IFA microscopy using whole cells**

The protocol used originated from the laboratory of Derrick Robinson and was optimized according to whether the cell lines under investigation were BSF or PCF, whether whole cells or cytoskeleton preparations (section 2.6.4) were desired, and the fixative required.

Mid-log phase cells were harvested by centrifugation at 800 x *g* or 1000 x *g* for 5 minutes at room temperature, for BSF (10 ml) or PCF (1 ml) cells respectively, washed 1x in vPBS and resuspended in 100 µl (BSF) or 200 µl (PCF) vPBS. Cells were applied to poly-L-lysine coated slides with 4 mm diameter wells. For BSF cultures, 10 µl were applied to each well and allowed to dry. For PCF cultures, 20 µl were added to each well, cells were allowed to settle onto the slides for 4 minutes and then the majority of the supernatant was removed. The slides were fixed in -20ºC methanol for one hour to overnight, before being immersed in a PBS bath for 5 minutes (without allowing to dry out) to remove the methanol, and then washed for another 5 minutes in fresh PBS, before proceeding to incubation with primary antibody. To fix cells in PFA rather than methanol, after applying the samples to the slides 25 µl of 2% (BSF) or 4% (PCF) PFA were added for 10 minutes (BSF) or 4 minutes (PCF), after which the majority of the PFA was removed and cells were permeabilised with 0.1% Triton X-100

in PBS for 10 minutes. After detergent removal, 50 µl of 100 mM glycine were added to each well and incubated for 10 minutes, twice. The wells were washed in PBS twice for 5 minutes each, before continuing to incubation with primary antibody.

20 µl of primary antibody were applied to each well (Table 2. 12) and incubated for one hour in a moist chamber. Antibodies were removed being careful to not cross-contaminate the different wells, and wells were washed twice in PBS for 5 minutes each. Similarly, 20 µl of secondary antibody (Table 2. 12) were added to each well and incubated for one hour in a dark and moist chamber, before being removed by two 5 minute washes in 100 mM HEPES pH 7.5. 25 µl of DAPI in HEPES pH 7.5 (10 $\mu g.ml^{-1}$) were added to each well and incubated for 4 minutes before wells were washed as before in HEPES buffer. 10 µl of SlowFade Gold antifade reagent (Invitrogen) were added and wells covered with a cover slip before being analysed under the Zeiss Axioskop or/and the Deltavision microscope.

Table 2. 12 - Antibodies used for IFA microscopy.

Antibody	Source Concentration	Working dilution
Primary antibodies used		
Polyclonal serum against cell cycle proteins in mouse	Produced during this study	1:100
Antibodies produced against cell cycle proteins in mouse	Produced during this study	Neat
Anti β-tubulin mouse monoclonal IgG2b (KMX)	Millipore 1 $mg.ml^{-1}$	1:20
Anti-TY mouse monoclonal IgG1 (Clone BB2)	Matthews laboratory	Neat
Anti-Protein A rabbit polyclonal antibody	Sigma 2 ml lyophilized powder	1:5000
Secondary antibodies used		
Alexa Fluor 488-conjugated goat anti-mouse IgG	Molecular Probes/Invitrogen 2 $mg.ml^{-1}$	1:100
Alexa Fluor 594-conjugated goat anti-mouse IgG	Molecular Probes/Invitrogen 2 $mg.ml^{-1}$	1:100
Alexa Fluor 488-conjugated goat anti-mouse IgM	Molecular Probes/Invitrogen 2 $mg.ml^{-1}$	1:100
Alexa fluor 594-conjugated goat anti-rabbit IgG	Molecular Probes/Invitrogen 2 $mg.ml^{-1}$	1:100

2.6.4. **IFA microscopy using cytoskeletons**

IFA using cytoskeletons from BSF cells was similar to the protocol described above (section 2.6.3). After washing the cell pellet in vPBS, cells were resuspended in 200 µl 0.25% NP40 in 100 mM PIPES pH 6.8, 1 mM $MgCl_2$, and 20 µl were immediately applied to each well for 10 minutes. The remaining buffer was removed and wells were washed twice for 5 minutes in 100 mM PIPES pH 6.8, 1 mM $MgCl_2$, before removing the majority of the liquid and fixing in methanol as described in section 2.6.3. The remaining protocol was performed as described in section 2.6.3.

2.6.5. **Transmission Electron Microscopy**

To analyse intracellular structure at high resolution, 10^7 cells were harvested at 1000 x *g* for 10 minutes, and the medium was carefully removed. A fixative solution (2.5% glutaraldehyde in 0.1 M sodium cacodylate buffer) was added slowly to the cell pellet, in order to prevent its resuspension, and the sample incubated for 1 hour at room temperature. Downstream processing was performed by Dr Laurence Tetley and Margaret Mullin in the Integrated Microscopy Facility, University of Glasgow, where cells were post-fixed in 1% (w/v) osmium tetroxide/0.1 M sodium cacodylate buffer for 1 hour. Cells were then rinsed 3 times (10 minutes each) in dH_2O, dehydrated using an alcohol series and embedded in pure Epon resin. Samples were sectioned (60-70 nm) and stained with 2% uranyl acetate (10 minutes) and Reynold's lead citrate (5 minutes). Cells were analysed under a Leo 912 AB transmission electron microscope, and images were processed using Olympus SIS software.

2.7. ANTIBODY PRODUCTION

2.7.1. **Immunisation of Balb/c mice**

Antibodies were generated against purified recombinant proteins (His-CRK12) or polyacrylamide gel slices containing purified cytoskeleton preparations of BSF

synchronized cultures (Mitosis and Cytokinesis). Injections were given intraperitoneally to 2 mice (recombinant proteins) or to a single mouse (polyacrylamide slices), in a total volume of 200 µl per injection. For recombinant proteins, a total of 10 µg were injected, mixed with 100 µl of Incomplete Freund´s Adjuvant (Sigma) to increase the immune response. As cytoskeleton proteins remain insoluble, gel slices from a 10% SDS-PAGE gel containing different unknown proteins (section 2.2.8 and Table 2. 1) were directly injected in the mouse after being frozen in liquid nitrogen and ground up. As no adjuvant was used for cytoskeleton proteins, a minimum volume of PBS was mixed with the samples to facilitate injection.

Injections were given regularly at two week intervals, and after the third injection, antibody production was analysed (section 2.7.2) and mice were sacrificed or injected again depending on the strength of the immune response observed.

2.7.2. **Antibody titre monitoring of mouse serum using ELISA**

Antibody production was determined for mice injected with recombinant proteins, as cytoskeleton proteins are insoluble and, as such, cannot be used in an ELISA assay. Approximately 50 µl of blood was removed from the tail of the mice to be analysed and, after being kept overnight at 4ºC to allow it to clot, the serum was obtained by centrifugation at 2000 x *g* for 20 minutes. A high binding ELISA plate (Costar® 96-Well EIA/RIA plate) was incubated overnight at 4ºC with 0.1 µg of recombinant protein per well, diluted in 100 µl PBS, to allow binding of the antigen to the bottom of the plate, leaving a column with only PBS as a negative control.

After antigen incubation, the plate was blocked with 200 µl of 1% gelatine (Merck) at room temperature for one hour, then washed three times Tris Buffered Saline / 0.05% Tween 20 (TBST), by adding approximately 200 µl of washing buffer and flicking the contents over a sink. The remaining drops were removed by patting the plate on a paper towel.

A dilution series of the serum was added to the wells containing the antigen, starting at 1:200 and diluting 2x between wells, reaching a minimum dilution of

1:204800. The most concentrated sample was also added to the negative control well. The serum was incubated with the wells for one hour at 37ºC, before being removed and wells were then washed three times with TBS/T as before. Secondary antibody, Anti-Mouse Polyvalent Immunoglobulins AP conjugated (Sigma), was diluted 1:10,000 in TBST supplemented with 0.1% BSA (Sigma), added to all wells and incubated for one hour at 37ºC. The plate was washed three times with TBST and once with dH_2O, prior to incubation with 100 µl of substrate, 4-nitrophenyl phosphate disodium salt hexahydrate (4NPP;Applichem), diluted to 1 $mg.ml^{-1}$ in substrate buffer (2% diethanolamine, 10 $mg.ml^{-1}$ $MgCl_2.6H_2O$, pH 10.4). The plate was kept at 37ºC in the dark, checked after 30 minutes for colour change, and every 30 minutes until the wells turned yellow. Absorbance was measured at 405 nm using a microplate reader (BioRad model 550) and the software Microplate manager 4.0 (BioRad). Antibody production was considered positive when a titre greater than 1:3200 was obtained, and the mouse was then sacrificed (section 2.7.3). If the titre was negative (less than 1:3200), more rounds of injections were performed as described in section 2.7.1 until a positive titre was obtained.

2.7.3. **Production of hybridoma cell lines**

Mice were sacrificed by cervical dislocation when the antibody titre was high enough or, in the case of mice injected with polyacrylamide slices, after a minimum of four injections. All of the blood of the animal was removed in order to purify antiserum. Mice were sprayed with 70% ethanol under a laminar flow hood and the spleen was removed and kept in Dulbecco Modified Eagle's Medium (DMEM: 13.42 $g.l^{-1}$ DMEM (AppliChem/Gibco), 2.1 mM HEPES, 23.8 mM sodium bicarbonate, 57 µM ascorbic acid, 92 µM Alanyl-glutamine (Ala-Gln), 86.7 µM gentamycin sulphate, supplemented with 25 µl sodium selenite (100 $µg.ml^{-1}$), 250 µl BSA-oleic-linoleic, 500 µl putrescine (0.32 $mg.ml^{-1}$) per litre). Downstream processing was performed under sterile conditions in a horizontal flow hood.

The spleen was transferred to a Petri dish and cells were removed with the help of syringes and needles, being careful not to dissociate the spleen. The medium

containing the cells was transferred to a clean 50 ml Falcon tube, where debris was allowed to settle, and the clarified supernatant was transferred to a new tube.

Meanwhile, myeloma SP2/0 AG14 adherent cells were grown in DMEM supplemented with 5% FBS (Gibco), at 37ºC in the presence of 5% CO_2. This cell line lacks the enzyme hypoxanthine guanine phosphoribosyltransferase (HGPRT), involved in nucleotide synthesis through the purine salvage pathway (Zaharevitz *et al.*, 1992). Myeloma cells were kept in medium containing 8-azaguanine, an analog of guanine, which is normally incorporated by normal cells through HGPRT enzyme and inhibits purine nucleotide synthesis leading to cell death. In $HGPRT^-$ cells, this compound is not incorporated, allowing selection of cells without this enzyme. A few days prior to fusion, azaguanine was removed from the medium by centrifugation and resuspension of the cells in fresh medium. On the day of the sacrifice, myeloma cells in mid-log phase ($1 \times 10^5 - 5 \times 10^5$ cells.ml^{-1}) were removed from the bottom of the flask and transferred to a clean falcon tube.

Both spleen and myeloma cells were centrifuged at 1200 x *g* for 10 minutes, and resuspended in 10 ml of fresh medium with no FBS. Cell density was determined using a Neubauer chamber and both suspensions were mixed at a ratio of 1:10 SP2/0 : Spleen cells. Cell fusion was induced by using polyethylene glycol–dimethyl sulfoxide (PEG-DMSO: 50% (w/v) PEG mol wt 1,450 in 10% (v/v) DMSO; Sigma) to produce hybridoma cells. In general, the pellet containing the mixture of spleen/myeloma cells was resuspended in 0.8 ml PEG-DMSO with slow mixing for one minute, and allowed to rest for another minute. 1 ml of DMEM medium with no FBS was added for approximately one minute, with continuous agitation, and another 20 ml was added for 5 minutes, followed by centrifugation at 1200 x *g* for 10 minutes. The hybridoma cell pellet was resuspended in 25 ml of complete medium, i.e. DMEM supplemented with 10% FBS and 1x hypoxanthine aminopterin thymidine (HAT, Sigma), and distributed across 96 well plates (100 µl per well). Selection of hybridoma cells is made by growing them in the presence of HAT, which contains aminopterin, a drug that blocks de *de novo* pathway for nucleotide synthesis. As *in vivo* nucleotides are synthesized either *de novo* or recycled through salvage pathways (Zaharevitz *et al.*, 1992), the presence of HAT in the medium makes cells dependent on the purine salvage pathway,

and as such on the presence of the enzyme HGPRT (Köhler and Milstein, 1975). Therefore, myeloma cells that do not fuse with the spleen cells do not survive since they are HGPRT negative, and spleen cells not fused eventually die as they lack immortal growth. HAT medium thus allows selection of hybridoma cells, which inherit HGPRT gene from B cells and tumorigenic properties from myeloma cells.

Plates containing hybridoma cells were incubated at 37ºC overnight, and 100 µl of fresh complete medium was added the next day to each well. After 5 to 7 days, 100 µl of medium were replaced with fresh medium, being careful not to remove the growing hybridoma cells adherent to the bottom of the plates.

2.7.4. **Hybridoma cell culture and storage**

Hybridoma cells were allowed to develop in the 96-well plates and, when large amounts of cells were visible, the supernatant of the culture was used to screen against the recombinant antigen by ELISA (section 2.7.6). Wells that showed a positive result by ELISA were transferred to 24-well plates containing 1 ml of fresh complete medium, re-tested by ELISA and further tested by WB (section 2.7.7), and confirmed positive cultures were further transferred to 25 cm^3 flasks in a total volume of 5 ml. For fusions from mice injected with polyacrylamide slices, 96-well plate cultures were automatically transferred to 24-well plates, where the supernatant could be tested by WB against cell lysates. Once in the flasks, the amount of FBS used for culturing the cells was lowered gradually until a final amount of 2.5% (v/v) was reached, at which time glycerol stocks were made and the remaining culture was either cloned (section 2.7.5) or used to produce large amounts of supernatants containing the desired antibody, for further classification and purification (sections 2.7.8 and 2.7.9).

For cell storage, hybridomas were removed from the flasks with the help of cell scrapers, and 5 ml of culture were centrifuged at 1200 x *g* for 5 minutes. The supernatant was removed and the cell pellet was resuspended in freezing medium (960 µl of FBS plus 40 µl DMSO) and transferred to cryovials which were placed

immediately at -80ºC, where they were stored for 24-48 hours until they were transferred to liquid nitrogen.

To reculture, cells were defrosted rapidly and ressuspended in 20 ml of DMEM medium with no serum or HAT, and centrifuged at 1200 x *g* for 10 minutes. The pellet was then resuspended in 5 ml of complete medium and incubated at 37ºC and 5% CO_2, and cell growth was monitored at regular intervals.

To obtain the supernatant containing the antibodies, cells were allowed to grow in complete medium without subpassage, until the medium turned yellow and almost all cells were dead. The culture was centrifuged, the cell pellet discarded and the supernatant was passed through a 0.45 µm syringe filter (Carl Roth GmbH) and kept at 4ºC or -20ºC.

2.7.5. **Cloning by limiting dilution**

Hybridomas screened and considered positive were further cloned, in order to produce cell lines with higher specificity towards the desired antigen. In general, the cell suspension was serial diluted, to a final concentration of 2.5 cells.ml^{-1}, allowing an average of one cell per two wells (plating a 200 µl aliquot/well), and cells were distributed across 96-well plates. Cell growth was followed closely, in order to distinguish between wells with a high amount of hybridomas ("fake clones") or wells with approximately one hybridoma cell ("true clones"). Cells were expanded to flasks and cultured as previously described (section 2.7.4). Supernatants were screened (section 2.7.6 and 2.7.7) and stored, and glycerol stocks of positive hybridomas were made as described above (section 2.7.4).

2.7.6. **Screening of hybridoma supernatants by ELISA**

Hybridomas from fusions from mice injected with recombinant proteins were first tested by ELISA against the recombinant protein. The assay plate was prepared as

described previously (section 2.7.2), including a well with no antigen (PBS only) to account for non-specific reaction of the primary antibody (antiserum). Four different controls were performed against the recombinant protein: a positive control using the antiserum diluted according to its titre; and three negative controls (primary antibody (antiserum) with no secondary; no primary antibody with secondary antibody; no primary or secondary antibodies). The assay was performed as previously described (section 2.7.2), using 100 µl of the hybridoma supernatant as primary antibody.

2.7.7. **Screening of hybridoma supernatants by WB**

Supernatants from hybridoma cultures were screened by WB against recombinant proteins (0.5 µg/lane), where possible. Positive antibody supernatants were further tested against *T. brucei* cell lysates (2 x 10^6 cells/lane). Hybridomas generated from mice injected with polyacrylamide samples were tested against cytoskeleton samples of asynchronous and/or synchronized parasite populations (2 x 10^6 cells/lane). WBs were carried out as described previously (section 2.4.7).

2.7.8. **Antibody classification**

Using a commercial kit (Zymed's Mouse MonoAB ID Kit Alkaline Phosphatase, Invitrogen), MAbs were classified according to their class and subclass, using the culture supernatant and a set of ELISA reagents designed for isotyping mouse immunoglobulins.

On the day prior to the assay, the microtiter plate was coated with the antigen, using 0.5 µg per well for recombinant proteins or 50 µl of 1x goat anti-mouse IgGAM (mix of IgG, IgA and IgM), as a capture method for insoluble proteins as is the case for cytoskeleton proteins. After binding overnight at 4ºC, the plate was blocked with 200 µl of 1% BSA for one hour at 37ºC, and the solution decanted before adding each hybridoma supernatant to all wells in duplicate (Table 2. 13).

Table 2. 13 - Schematic representation of the distribution of reagents in the ELISA plate used for antibody classification.

	PBS	NSR	IgG1	IgG2a	IgG2b	IgG3	IgM	IgA	κ	λ
Supernatant 1										
Supernatant 1										

The primary antibodies in the hybridoma supernatant were incubated in the plate for one hour at 37ºC, before being removed and the wells washed 4 times with 200 µl TBST. Secondary antibodies were then added to the wells, using a different antibody for each column of the plate. As a negative control, normal rabbit serum (NSR) was used, and PBS was used as a blank (Table 2. 13). To the remaining columns different rabbit anti-mouse antibodies were added, recognising different immunoglobulins: IgG_1, IgG_{2a}, IgG_{2b}, IgG_3, IgM, IgA, kappa light chain and lambda light chain (Table 2. 13). After another wash with TBST, the final step was to add 50 µl of diluted AP-Goat Anti-rabbit IgG in all wells (diluted by addition of one drop of concentrated antibody to 2.5 ml of TBST), and incubate for another hour at 37ºC. A final wash was performed and results revealed by using the provided substrate *p*-nitrophenyl phosphate disodium salt (PNPP). The plate was incubated at room temperature in the dark, monitored after 30 minutes for colour change and absorbance was measured at 405 nm on an ELISA plate reader.

2.7.9. **Antibody purification**

Supernatants obtained from hybridoma cultures were first classified according to their class (section 2.7.8), dialysed and purified with the appropriate buffers and columns (see below), and antibody concentration was calculated using the Bradford method (section 2.4.4). General purification protocols were similar between antibodies from classes IgG and IgM, except for the columns and buffers used, and all purifications were performed according to the manufacturer's protocol (GE Healthcare) on an ÄKTAprime Plus purification system (GE Healthcare).

On the day prior to the purification, supernatants were dialysed against 1 L of binding buffer overnight at 4 ºC, which consisted of 20 mM sodium phosphate pH 7.0 for IgG antibodies, and for IgM antibodies this buffer was supplemented with 0.8 M

ammonium sulphate pH 7.5. All buffers used during the purification were filtered and degassed prior to use, and applied at a flow rate of 1ml.minute^{-1}.

To enable purification of IgG or IgM antibodies, the supernatant was applied to a HiTrap^{TM} ProteinG HP or a HiTrap^{TM} IgM HP purification column (GE Healthcare) respectively, using an injection column. The purification columns were pre-washed with 5 column volumes of binding buffer, and the sample was applied at a flow rate of 1ml.minute^{-1}, loading 10 column volumes at a time and collecting the flow through material to analyse the efficiency of purification. Washing of the column to remove unbound material was performed with binding buffer, using either 5 ml or 15 ml for purification of IgG or IgM antibodies, respectively. Elution of the bound antibodies was performed using 5 column volumes of 0.1 M glycine-HCl pH 2.7 for IgG antibodies and 12 column volumes of 20 mM phosphate buffer pH 7.5 for IgM antibodies. For antibodies eluted in low pH conditions, 100 µl of neutralization buffer consisting of 1 M Tris-HCl pH 9 was mixed with the elution fractions, to prevent antibody precipitation.

Elution pools were analysed using the PrimeView software and the most concentrated fractions were combined and precipitated with 2 M ammonium sulphate overnight at 4ºC. Precipitated antibodies were obtained by centrifugation at 3000 x *g* for 30 minutes, resuspended in 1/10 elution volume of PBS and dialysed overnight at 4ºC in PBS. The purified antibodies were stored at 4ºC.

3. RESULTS AND DISCUSSION

3.1. *T. BRUCEI* CRK12: PROJECT AIMS

As mentioned in previous chapters, regulation and progression throughout the cell cycle is regulated by several kinases and their interaction with their CYC partners. So far, 11 CRKs and 10 CYCs have been identified in *T. b. brucei* (Hammarton, 2007). However, the only partners identified so far to interact *in vivo* are CRK3:CYC2 and CRK3:CYC6 (Van Hellemond *et al.*, 2000, Hammarton *et al.*, 2003a). Previous work in the Hammarton lab using yeast-two hybrid assays and TAP suggests that CRK12 and CYC9 are interacting partners (Monnerat *et al.*, 2012). Phylogenetic analyses were performed for each protein and results revealed that CYC9 is a putative transcriptional CYC, clustering phylogenetically with Cyclin C (Monnerat *et al.*, 2012). As for CRK12, comparison of its kinase domain with all of the *T. brucei* CRKs, other kinetoplastid CRK12 kinases, human CDKs and selected CDKs from *Drosophila melanogaster* and *Caenorrhabditis elegans*, indicated that CRK12 forms a separate kinetoplastid clade, with high similarity to *T. brucei* CRK8 and CRK11 (Monnerat *et al.*, 2012).

In order to investigate CYC9 function in *T. brucei*, several attempts were made to knockout the gene in both BSF and PCF life cycle stages, although they turned out to be unsuccessful (Monnerat *et al.*, 2012). Functional investigation was performed by generating tet-inducible *CYC9* RNAi PCF and BSF cell lines, proving CYC9 to be essential for cell viability in both life cycle stages (Monnerat *et al.*, 2012). Although *CYC9* knockdown in PCF cells caused only minor changes in cell cycle progression, as visualised by DAPI staining and flow cytometry, results were quite different for the BSF cell line. An abnormal cell cycle progression was visible, demonstrating that *CYC9* knockdown in BSF trypanosomes seems to inhibit completion of cytokinesis, leading to an increase of cells undergoing furrow ingression, as was confirmed more thoroughly during this study. Additionally, recombinant CYC9 was produced (GST and 6xHis fusions), and although insoluble, was used to generate anti-CYC9 antibodies in rabbit. However, the generated antibodies did not detect the desired protein in cell lysates.

As for CRK12, no attempts had been previously made to generate antibodies against it, and to date not much is known about this kinase. Some data obtained for this kinase were published in 2009 (Gourguechon and Wang, 2009), where RNAi

knockdown was used to investigate the potential function of several CRKs in PCF cells of *T. brucei*. Although a significant reduction in corresponding mRNA following RNAi induction was observed in each case, cell growth was unaffected in most cases, including for CRK12 knockdown. In 2011, an RNAi screen of the *T. brucei* kinome using a luciferase-based assay proved CRK12 to be essential for BSF cell proliferation (Mackey *et al.*, 2011).

In this project, we attempt to study the role of this CRK/CYC complex in cell cycle regulation, by:

- Confirming the interaction between CRK12 and CYC9 *in vivo* using IP
- Determining the subcellular localisation of CRK12 by generating anti-CRK12 MAbs
- Investigating the function of CRK12 and CYC9 by using RNAi to downregulate their expression.

3.1.1. **Generation of plasmids for production of recombinant CRK12**

The *CRK12* sequence (Tb11.01.4130) was amplified from *T. brucei* 427 genomic DNA, using 3 different sets of primers (Table 2. 5), designed to contain specific restriction sites, and optimized reaction conditions (section 2.3.1). Amplification of the gene sequence encoding the C-terminal end of CRK12 was achieved using primers PR52 and PR53 (Table 2. 5) and PfuTurbo (Invitrogen, section 2.3.1), generating a 652 bp fragment (Figure 3. 1, lane 1). The ORF for *CRK12* was PCR-amplified using Phusion Polymerase (Finnzymes) and primers PR53 and PR54 (Table 2. 5; Figure 3. 1, lane 2) or PR53 and PR55 (Table 2. 5; Figure 3. 1 lane 3), to allow sub-cloning into pGEX5X1 or pET28a^{+}, respectively. The amplified fragments are visible in Figure 3. 1.

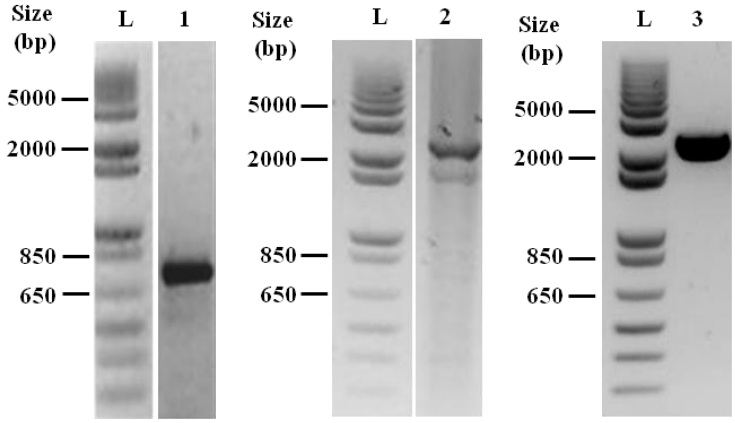

Figure 3. 1 - DNA gel electrophoresis of *CRK12* fragments amplified from *T. brucei* 427 genomic DNA. Amplified fragments of the gene sequence encoding the C-terminal end of CRK12 (lane 1, predicted size 652 bp) and of the full length sequence (lane 2, with a predicted size of 2328 bp and lane 3 with a predicted size of 2327 bp) were visualised on a 1% agarose gel. L – 1 kb Plus DNA Ladder (Invitrogen).

The PCR products were ligated into pSC-B (section 2.3.1) and the presence of the correct insert was confirmed by colony PCR using M13 forward and reverse primers (section 2.3.1, results not shown) and restriction endonuclease digestion of DNA obtained from individual PCR positive colonies (section 2.3.1). Table 3. 1 and Figure 3. 2 show the expected sizes of fragments after endonuclease digestion and DNA gel electrophoresis of the obtained reactions for the different constructs, respectively.

Table 3. 1 - Expected sizes of fragments obtained after restriction endonuclease digestion of CRK12 constructs. Construct (1): pSC-B containing the C-terminus of *CRK12*; construct (2): pSC-B containing the full ORF for *CRK12* for sub-cloning into pGEX5X1; and construct (3): pSC-B containing the full ORF for *CRK12* for sub-cloning into pET28a^{+}).

Construct	Restriction Enzyme	Expected Sizes (bp)	Restriction Enzymes	Expected Sizes (bp)
Construct (1)	BamHI	260 + 3857 / 459 + 3658	EcoRI + XhoI	40 + 16 + 16 + 652 + 3393
Construct (2)		260 + 5537 / 2137 + 3660	BglII + XhoI	57 + 2328 + 3411
Construct (3)		262 + 5534 / 2138 + 3658	NdeI + XhoI	57 + 2327 + 3412

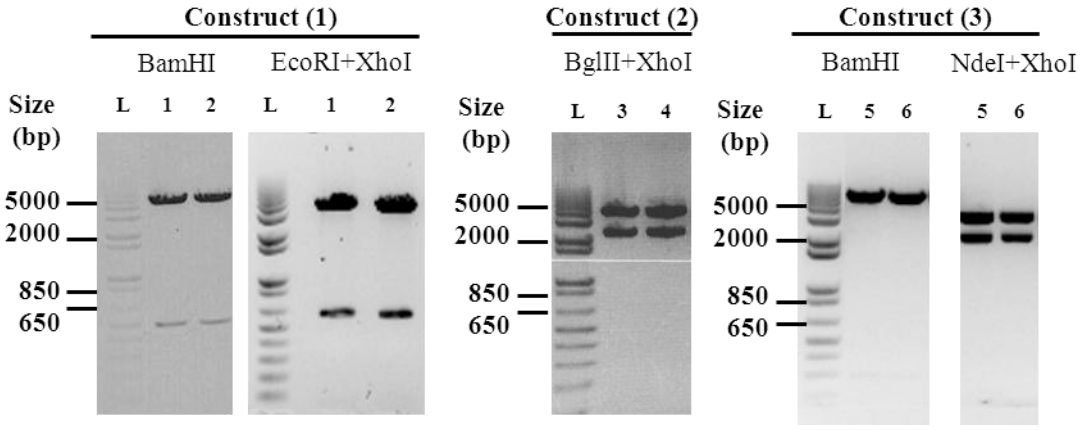

Figure 3. 2 - DNA gel electrophoresis of restriction endonuclease reactions performed for CRK12 constructs to confirm the presence of the correct insert. Different reactions were carried out using DNA obtained from two different colonies of each construct: lane 1 and 2 – colonies from construct (1) (pSC-B containing the C-terminus of *CRK12*); lane 3 and 4 – colonies from construct (2) (pSC-B containing the ORF of *CRK12* for sub-cloning into pGEX5X1); lane 5 and 6 – colonies from construct (3) (pSC-B containing the ORF of *CRK12* for sub-cloning into pET28a^{+}). Fragments obtained were visualised on a 1% agarose gel and and the sizes of bands obtained were compared to the expected sizes (Table 3. 1). L – 1 kb Plus DNA Ladder (Invitrogen).

DNA from positive colonies (Table 3. 1 and Figure 3. 2) was confirmed by sequencing (section 2.3.6). The obtained sequences were analysed by BLAST analysis to compare them with genomic DNA from *T. b. brucei* 927 at GeneDB (www.genedb.org), revealing a total of 16 nucleotide differences, 7 of which translate as silent mutations (Table 3. 2).

Table 3. 2- Nucleotide point mutations observed by DNA sequencing and corresponding changes at the protein level. The nucleotide position refers to the changed nucleotide, counting from the start codon.

Nucleotide number	Nucleotide change	Amino acid change	Nucleotide number	Nucleotide change	Amino acid change
113	C>T	Ser>Leu	1380	T>C	Ile
143	G>A	Arg>His	1398	A>G	Leu
426	T>C	Asp	1575	C>T	Ala
433	C>T	Pro>Ser	1644	G>A	Val
513	A>G	Leu	1656	C>G	Ala>Gly
740	A>G	His>Arg	1772	A>G	Gln>Arg
748	A>C	Arg	1790	C>A	Ala>Glu
1348	A>C	Lys>Gln	2216	T>G	Val>Gly

While some mutations are conservative, resulting in an amino acid with the same properties, most of them result in changes in polarity and charge. Since these changes are present in all of the PCR products sent for sequencing, they were considered to be due to strain-specific differences, as they were amplified from *T. b brucei* 427 genomic DNA and compared with genomic DNA from *T. b. brucei* 927. The following plasmids were generated: pHG97 (previously construct (1)) and pHG110 (previously contruct (3)), containing the gene sequence encoding the C-terminal end of CRK12 and the full length ORF, respectively, for sub-cloning into pET28a^{+}; and pHG98 (previously construct (2)) for sub-cloning the full length ORF into pGEX5X1.

Using the restriction endonuclease sites introduced by the primers used for amplification (Table 2. 5), plasmids pHG97, pHG98 and pHG110 were digested (section 2.3.3) to release the *CRK12* products, visualised by DNA gel electrophoresis (Figure 3. 3) and the required fragments were excised from the gel and purified (section 2.3.1). The final destination vectors (pGEX5X1 and pET28a^{+}) were digested with the same enzymes or enzymes creating cohesive ends (section 2.3.3), electrophoresed on a 1% agarose gel (section 2.3.2), and the digested vector (Figure 3. 3) was excised from the gel and purified (section 2.3.1).

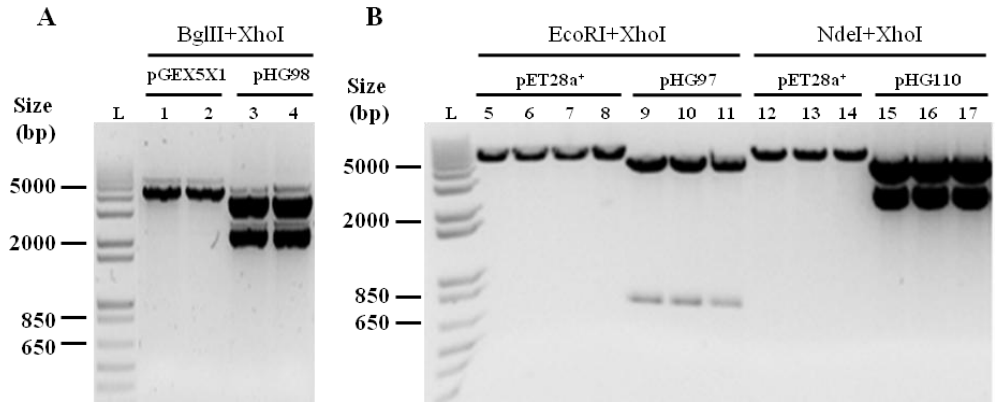

Figure 3. 3 - DNA gel electrophoresis of restriction endonuclease digestion of pHG97, pHG98, pHG110 and expression vectors pET28a^{+} and pGEX5X1. Panel A – digestion of pHG98 (2328 bp of insert + 3411 bp of pSC-B vector) and pGEX5X1 (single fragment of 4900 bp) with BglII and XhoI. Panel B – digestion of pHG97 (652 bp of insert + 3393 bp of pSC-B vector) and pET28a^{+} (single fragment of 5369 bp) with EcoRI and XhoI; and digestion of pHG110 (2327 bp of insert + 3412 bp of pSC-B vector) and pET28a^{+} (single fragment of 5369 bp) with NdeI and XhoI. Results were visualised on a 1% agarose gel. L – 1 kb Plus DNA Ladder (Invitrogen).

The gene sequence encoding the C-terminal end of CRK12, digested with BglII and XhoI (Figure 3. 3 panel B), and the full length ORF for *CRK12*, digested with NdeI and XhoI (Figure 3. 3 panel B) were cloned into expression vector pET28a^{+}, previously digested with the same enzymes (Figure 3. 3 panel B) in a reaction mix containing a 1:6 ratio of vector:insert (section 2.3.4). After confirmation of a successful ligation by digestion with the enzymes used for sub-cloning (results not shown), the obtained plasmids were named pHG178 and pHG180, containing the gene sequence encoding for the C-terminus and the full length sequence of *CRK12*, respectively; and transformed into BL21 (DE3) pLysS *E.coli* competent cells (section 2.1.4). For generation of a GST-tagged protein, the *CRK12* ORF was obtained by digestion of pHG98 with BglII and XhoI (Figure 3. 3 panel A), and ligated to the digested vector pGEX5X1 (Figure 3. 3 panel A) in a 1:3 ratio (vector:insert). The generated plasmid, pHG298, was checked by restriction endonuclease analysis for a correct ligation and further transformed into the expression *E.coli* cell line BL21 (DE3).

3.1.2. **Purification of recombinant His:CRK12**

To enable immunisation of Balb/c mice (section 2.7.1), the full length CRK12 fused to the His tag was expressed and purified. Expression of 6xHis:CRK12 (expected size ~ 85 kDa) was tested under different conditions (section 2.4.1), with cultures being grown in the presence of IPTG for different periods of time and at different temperatures (Figure 3. 4). Samples were taken at the appropriate times and analysed by SDS-PAGE (section 2.4.5 and 2.4.6) and by WB (section 2.4.7), using an anti-His antibody (Table 2. 11) to probe for optimal conditions for protein expression, which were established to be induction at 37ºC for 4 hours (Figure 3. 4 lane 4). As seen in Figure 3. 4, after protein induction several degradation products of 6xHis:CRK12 appear, recognised by the anti-His antibody (Figure 3. 4 WB results).

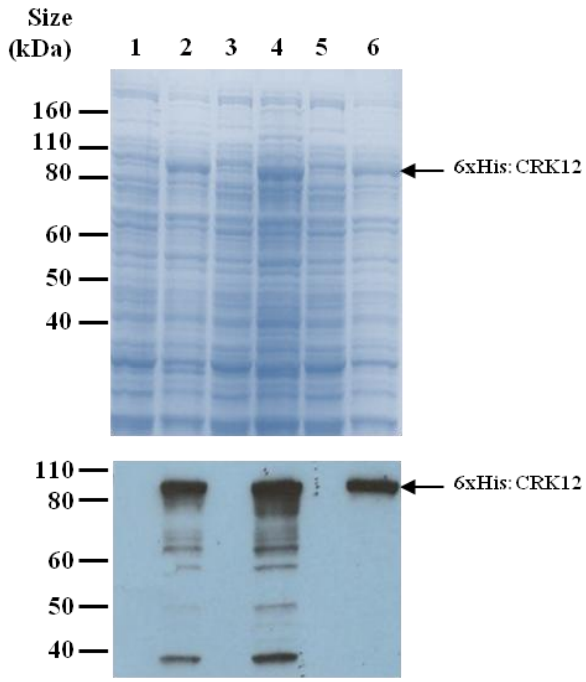

Figure 3. 4 - Expression of 6xHis:CRK12 under different conditions. Uninduced (lanes 1, 3, 5) and induced (lanes 2, 4, 6) whole cell lysates of 6xHis:CRK12 expression (predicted size 84.6 kDa) were separated on a 14% SDS-PAGE gel (top panel); and probed by WB (bottom panel) with an anti-His antibody. Lanes 1 and 2 – protein induction at 37ºC for 2 hours; lanes 3 and 4 – protein induction at 37ºC for 4 hours; lanes 5 and 6 – protein induction at 20ºC for 4 hours. Ladder – Novex Sharp Pre-stained Protein Standard (Invitrogen).

Cell pellets obtained after growth in optimal conditions were solubilized by lysozyme incubation followed by sonication (section 2.4.1), allowing separation of the soluble and insoluble protein fractions. Samples were separated and analysed by SDS-PAGE (section 2.4.5 and 2.4.6) and WB (section 2.4.7), revealing the presence of the desired recombinant protein in the insoluble fraction (Figure 3. 5). Solubilization of approximately 50% of recombinant 6xHis:CRK12 (Figure 3. 5) was achieved by supplementing buffers with 6 M urea. This soluble sample was further used for purification of the desired protein by affinity chromatography (section 2.4.2).

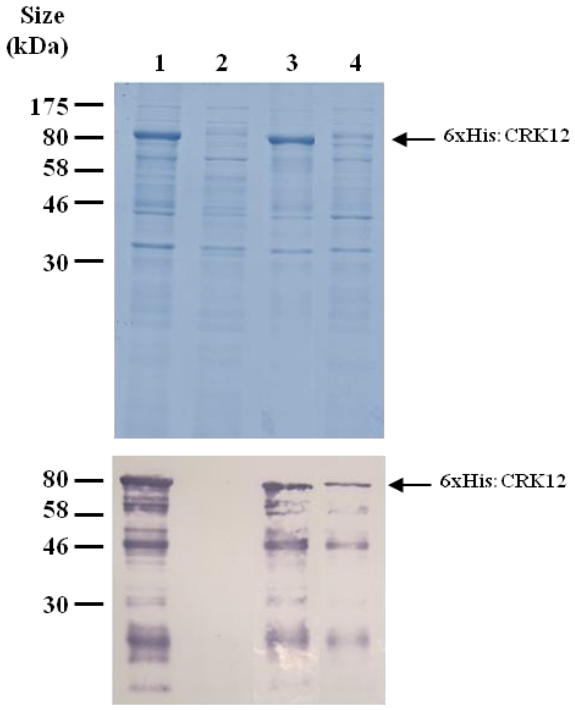

Figure 3. 5 - Solubilization of 6xHis:CRK12. The insoluble (lanes 1 and 3) and soluble (lane 2 and 4) fractions before (lanes 1 and 2) and after (lanes 3 and 4) urea treatment were electrophoresed on a 12% SDS-PAGE gel (top panel) and probed with an anti-his antibody by WB (bottom panel) to check for solubilization of 6xHis:CRK12 (predicted size 84.6 kDa). Ladder - Broad Range pre-stained marker (NEB).

Purification of recombinant 6xHis:CRK12 was carried out using a Nickel resin and under denaturing conditions, which meant that all buffers were supplemented with 6 M urea (section 2.4.2). Elution of 6xHis:CRK12 was obtained by increasing the imidazole concentration (section 2.4.2), and elution fractions were dialysed against PBS (section 2.4.3) to allow the protein sample to be used for mice immunisation (section 2.7.1) and to decrease the possible effect of urea on antibody screening assays, such as ELISA (section 2.7.6). As visible in Figure 3. 6 by Coomassie staining (section 2.4.6) and by WB (section 2.4.7), purification efficiency is quite low, ~ 1 mg per 200 ml of *E.coli* culture. This inefficient purification is most likely due to degradation problems and because of the low interaction observed between 6xHis:CRK12 and the Nickel resin (Figure 3. 6).

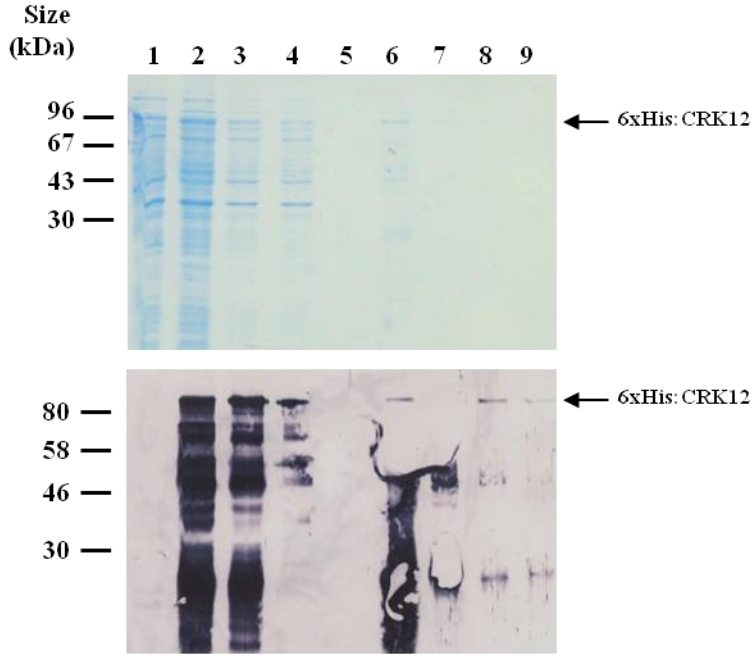

Figure 3. 6 - Purification of 6xHis:CRK12 by affinity chromatography. Lanes 1 and 2 - Uninduced and induced total bacterial extract, respectively; lane 3 - soluble fraction after urea treatment; lane 4 – flow through; lane 5 – washes; lanes 6 to 9 – elution fractions. Protein loading relative to the cell extract corresponds to the ratios: 1:20 (lanes 1-2); 1:1 (lanes 3-5); 1:5 (lanes 6-9). The different protein samples obtained during purification of 6xHis:CRK12 (predicted size 84.6 kDa) were analysed by electrophoresis through 12% gels, stained with Coomassie (top panel, Ladder – LMW, GE Healthcare) or transferred to a nitrocellulose membrane to probe with anti-His antibody by WB (bottom panel, Ladder – Broad Range pre-stained marker, NEB).

A degradation product of approximately 48 kDa is recognised strongly by the anti-His antibody in the elution fractions (Figure 3. 6). Continuous freezing and thawing and over time degradation lead to an accumulation of the 48 kDa product and a progressive disappearance of the initial 86 kDa protein (see Figure 3. 8). In conclusion, the stability of recombinant 6xHis:CRK12 is very low, with precipitates being visible as soon as one week after dialysis; and consequently some protein samples were stored under denaturing conditions to increase protein half-life.

3.1.3. **Production of MAbs against CRK12**

The purified recombinant 6xHis:CRK12 (section 3.1.2) was used to generate antibodies by injecting intraperitoneally two Balb/c mice (section 2.7.1) with 10 µg of

recombinant protein, in a total volume of 200 µl per injection, every 2 weeks. Antibody production was monitored by titring (section 2.7.2) the antiserum obtained from a tail bleed of the injected mice, and one mouse with a titre of 1:51,200 was sacrificed and used for production of a hybridoma cell line (section 2.7.3). Approximately 12 days after cell fusion (section 2.7.3), supernatants from the 96 well plates were used to screen for antibody production against recombinant protein by ELISA (section 2.7.6).

From a total of 240 supernatants from cultures in 96 well plates, 199 were tested by ELISA (section 2.7.6) against 6xHis:CRK12, identifying 34 positive supernatants (17% efficiency, calculated as indicated in Table 3. 3). Stringent criteria were used to determine whether a supernatant was positive, as most Abs_{405nm} were high (> 0.4) after one hour incubation with the substrate. For this particular fusion, supernatants were considered positive when showing absorbances higher than 0.8 or 1.0, for 96 or 24 well plates, respectively, measured one hour after incubating with 4-NPP, meaning that efficiencies could have been increased if a lower limit was set.

Table 3. 3 - Results from supernatant screening against recombinant 6xHis:CRK12. Recombinant protein was used to cover a high-binding ELISA plate, and supernatants from hybridoma cultures were used as primary antibodies. Efficiency of antibody production is presented as a ratio between positive results and the total number of supernatants tested.

	Supernatants tested	Positive supernatants
96 well plates	199	34
Efficiency*		17%
24 well plates	34	15
Efficiency*		44%

* - calculated as Efficiency= $\frac{\text{Positive sup.}}{\text{Sup. tested}} \times 100$.

Antibody production efficiency increased from 17% to 44% for 96 to 24 well plates, respectively (Table 3. 3), and a total of 15 hybridomas (Figure 3. 7) with Abs_{405nm} higher than 1.0 were transferred to 25 cm^3 flasks (section 2.7.4) for further screening by WB (section 2.7.7). Although only 15 cultures from the 24 well plates were grown at higher volumes, 5 other hybridomas that showed strong positive results (Abs_{405nm} ~ 0.6) (Figure 3. 7) were also tested by WB (section 2.7.7) against recombinant protein, but were discarded later due to cross-reaction with the His-tag (results not shown).

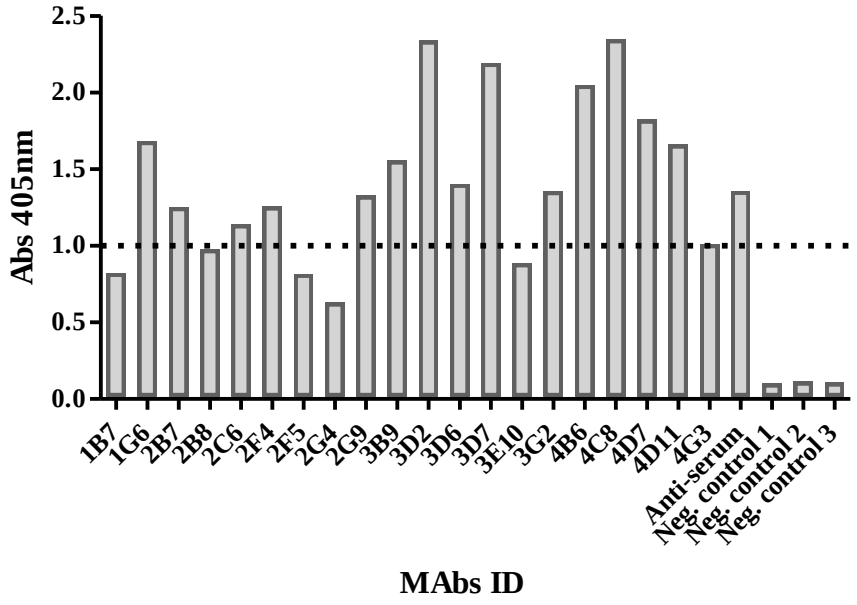

Figure 3. 7 - ELISA results for supernatants from 24 well plates. Absorbance at 405 nm is presented for each of the 15 supernatants that showed positive results (> 1.0), for the 5 supernatants with absorbances between 0.6 and 1.0, for the antiserum diluted 1:50,000 and for the negative controls: Control 1 – no secondary antibody; Control 2 – no primary antibody; Control 3 – no primary and no secondary antibody.

When screening by WB (section 2.7.7), and in order to check for cross-reaction with the His-tag, a negative control was performed using another recombinant protein tagged with a 6xHis tag, 6xHis:PLK, provided by the Hammarton lab (Figure 3. 8 bottom panel). Due to the high degradation rate of 6xHis:CRK12 and to the low sensitivity of the AP developing method, supernatants were considered positive when recognising the 48 kDa degradation product of 6xHis:CRK12 and not 6xHis:PLK. A total of 8 hybridomas were selected that recognised CRK12 and showed no or little interaction with the His-tag (Figure 3. 8): 1G6; 2B7; 2C6; 2F4; 2G9; 3G2; 4C8; 4D7; 4D11. Hybridoma cell stocks (section 2.7.4) were made for these cultures.

The overall efficiency of the fusion, when considering the 8 final positive hybridomas from the 25 cm^3 flask cultures and the initial 199 tested supernatants from the 96 well plates, was 4%. The decrease in the number of positive hybridomas (34 in 96 well plates) was due first of all to application of more stringent criteria with the

increase of culture volumes, and in parallel to elimination of supernatants cross-reacting with the protein tag.

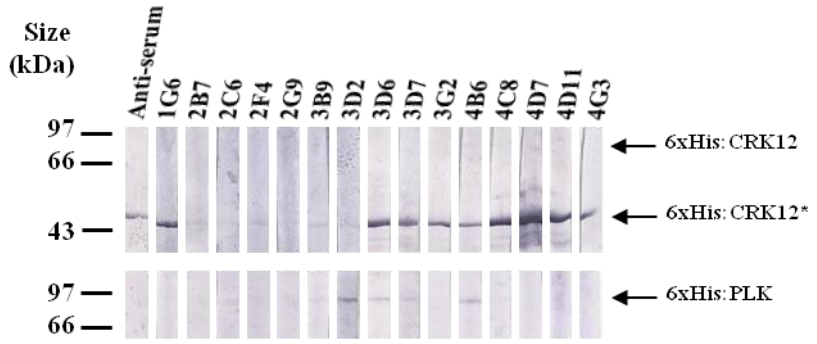

Figure 3. 8 - Screening of supernatants from hybridoma cultures by WB against recombinant 6xHis:CRK12 and a negative control – 6xHis:PLK. 0.5 µg of recombinant 6xHis:CRK12 (top panel, predicted size 84.6 kDa) and 6xHis:PLK (bottom panel, predicted size ~ 88 kDa) were electrophoresed on 12% SDS-PAGE gels and transferred to a nitrocellulose membrane for WB with neat hybridoma supernatants as primary antibody and a polyvalent immunoglobulin Anti-mouse antibody as secondary antibody. A positive control was performed, using anti-CRK12 serum diluted 1:50,000 as primary antibody. 6xHis:CRK12* - degradation product with ≈ 48 kDa, Ladder – Low Molecular Weight calibration kit for SDS electrophoresis (GE Healthcare).

Five of the positive hybridomas identified by WB were allowed to grow in large volumes (~ 50 ml) until cell death occurred, which ensures a higher antibody concentration. These supernatants were further selected by WB analyses (section 2.7.7), using a tet inducible ty:CRK12 overexpression cell line (Lister 427 pHD449 transfected with pHG230, Table 2. 1), following preparation of total cell extracts (section 2.2.7) of uninduced and induced cell lines at 48 hours post-addition of 1 $\mu g.ml^{-1}$ of tet. Given that only supernatant 4D7 is able to specifically detect a band of the expected size in the induced protein sample (Figure 3. 9), which is absent from the uninduced sample, and considering that there is equal loading between uninduced and induced lanes (Figure 3. 9 bottom panel), this supernatant was used for further experiments.

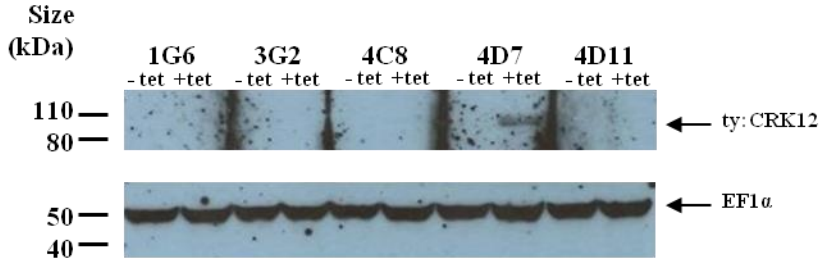

Figure 3. 9 - Screening of anti-CRK12 supernatants against tet induced ty:CRK12 expression. PCF cells were grown for 48 hours in SDM79 supplemented or not with 1 μg ml^{-1} tet (–tet/+tet) for overexpression of ty:CRK12 (predicted size ~ 86 kDa). 2 x 10^6 cells were loaded per lane, electrophoresed on 14% SDS-PAGE gels, WB and probed with MAbs against CRK12 (top panel). To demonstrate equal loading of samples, the membrane was cut at 60 kDa and probed with anti-EF1α antibody (bottom panel; predicted size ~ 51 kDa). Ladder - Novex Sharp Pre-stained Protein Standard (Invitrogen).

3.1.4. **Characterisation of 4D7: anti-CRK12 MAb**

All previous screening assays were carried out using polyvalent secondary antibodies (against IgG, IgA and IgM), to account for the different classes of the primary antibodies that could have been generated. Determination of Immunoglobulin isotype was performed using a commercial kit (section 2.7.8), based on an adapted ELISA assay with 3 antibody incubations, where the antibody to be analysed is captured, recognised by secondary rabbit antibodies directed against different isotypes of anti-mouse immunoglobulins, which are finally recognised by a third conjugated anti-rabbit antibody. Results showed that 4D7 consists of an IgG antibody, containing as such two heavy chains γ (results not shown). As to characterisation of 4D7 MAb light chains, although the absorbances were of low magnitude, the two light chains appear to be of the kappa (κ) isotype. Further analyses using this antibody were carried out using anti-mouse IgG secondary antibodies.

Classification of 4D7 as an IgG antibody enabled antibody purification by affinity chromatography using a protein G HP purification column (section 2.7.9). Although chromatographic results indicated a high purification efficiency, as demonstrated by a clear absorbance peak appearing after loading of the elution buffer (Figure 3. 10 blue curve at approximately minute 30), the obtained fractions did not present any signal against recombinant protein or parasite cell extracts by WB (results

not shown). This could be due to the low concentration of the sample used for purification, and consequently further work was performed with the un-purified supernatant.

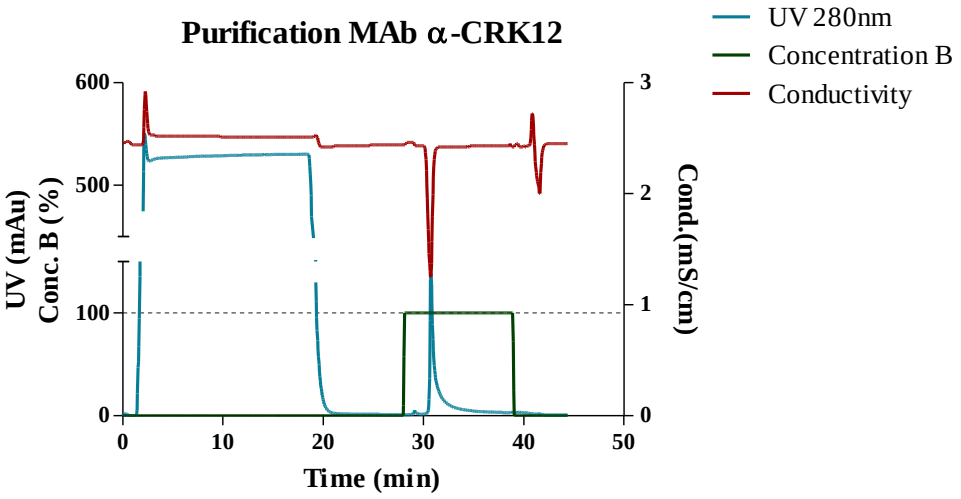

Figure 3. 10 - Purification of MAb anti-CRK12 4D7 by affinity chromatography, using a protein G HP purification column. Absorbance at 280 nm showing protein presence (blue); concentration of elution buffer (B) (green) and conductivity (red) were represented in function of the purification time (minutes).

To investigate the specificity of the 4D7 supernatant, and in line with other experiments developed during this study (section 3.2), several *T. brucei* cell lysates (Table 2. 1 and Table 2. 2) were used for WB (section 2.4.7). Cells expressing ty:CRK12 were grown for 24 (BSF) or 48 (PCF) hours in the presence or absence of tet (1 $\mu g.ml^{-1}$), before harvesting the cells and preparing cell lysates (section 2.2.7). *CRK12* BSF RNAi cell lysates were also prepared (section 2.2.7), by allowing the cells to grow in the presence of tet (1 $\mu g.ml^{-1}$) for 12 and 24 hours.

For wildtype (WT) cell extracts, prepared as described in section 2.2.7, a specific band is recognised by 4D7 corresponding to CRK12 (Figure 3. 11 lanes 1 and 4) and no cross-reaction is observed. When tested against overexpression cell lines (Figure 3. 11 lanes 2 and 3 for BSF, lanes 4 and 5 for PCF), the antibody recognises a band of the expected size in induced lysates and more weakly in the un-induced lysates, confirming an efficient overexpression of CRK12 in these cell lines. Interestingly, the

band in the induced lanes (Figure 3. 11 lanes 3 and 5) corresponds to a protein doublet, which could be related to the presence of both native CRK12 and overexpression of the tagged version of the protein (section 3.2.1). In parallel, the 4D7 antibody recognises a band at ~ 65 kDa or ~ 75 kDa, in BSF (Figure 3. 11 lane 3) or PCF (Figure 3. 11 lane 5) overexpression cell lines respectively, mainly in the induced samples, which could imply the occurrence of protein degradation.

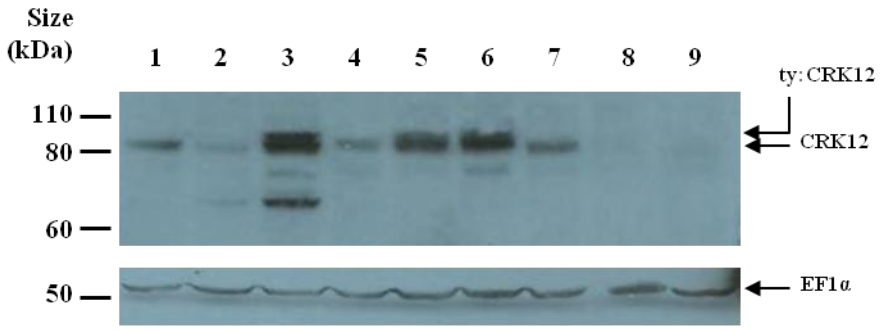

Figure 3. 11 - WB analysis of specificity of 4D7 against *T. brucei* CRK12. Total cell extracts of 2 x 10^6 *T. brucei* cells were loaded on 14% SDS-PAGE gels: Lane 1 – BSF WT; lanes 2 and 3 – BSF ty:CRK12 overexpression cell line, uninduced and induced for 24 hours, respectively; lane 4 – PCF WT; lanes 5 and 6 - PCF ty:CRK12 overexpression cell line, uninduced and induced for 48 hours, respectively; lanes 7, 8 and 9 – BSF *CRK12* RNAi cell line at 0, 12 and 24 hours post-induction, respectively. Neat 4D7 supernatant was used as primary antibody against CRK12 (predicted size ~ 85 kDa) and the membrane was re-probed after stripping with anti-EF1α (predicted size ~ 51 kDa) as a loading control. Ladder - Novex Sharp Pre-stained Protein Standard (Invitrogen).

In order to study the functional role of this kinase in BSF *T. brucei* (section 3.2.3), *CRK12* RNAi cell lines (Table 2. 1) were provided by the Mottram lab, and the anti-CRK12 antibody generated was used to confirm how gene knockdown was translated at a protein level (Figure 3. 11 lanes 7, 8 and 9). A clear decrease in protein amount is visible already at 12 hours post-induction (Figure 3. 11 lane 8).

Taking all these results into account, 4D7 MAb recognises CRK12 in distinct *T. brucei* cell extracts in a specific way.

3.1.5. **Ability of 4D7 to pull-down CRK12 from *T.brucei* cell lysates**

To verify the ability of 4D7 to pull-down CRK12 from *T. brucei* cells, the inducible ty:CRK12 BSF cell line (Table 2. 1) was allowed to grow for 24 hours in the presence of tet (1 µg.ml^{-1}), after which cells were harvested and prepared for IP with Dynabeads® Protein G (section 2.4.10). The undiluted MAb was incubated with the beads for 30 minutes, to allow interaction between the Protein G and the immunoglobulin; and the complex was incubated for 20 minutes with the cell lysate, enabling interaction of the antibody with specific proteins and minimizing non-specific binding. IP efficiency was determined by WB analysis (section 2.4.7) of the different protein samples obtained, using 4D7 as a primary antibody (Figure 3. 12).

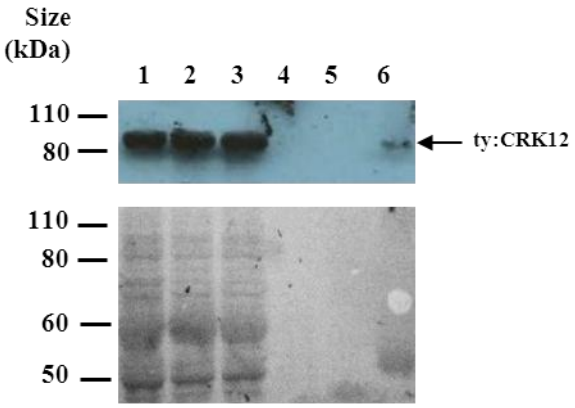

Figure 3. 12 - Ability of 4D7 anti-CRK12 antibody to pull-down ty:CRK12 from BSF *T. brucei*. 5 x 10^8 ty:CRK12 (predicted size ~ 86 kDa) overexpression BSF cells induced with tet for 24 hours were lysed and incubated with Dynabeads® to allow pull-down of proteins recognised by the MAb. Different fractions of the IP were loaded onto 14% gels: 1/100 of the total cell lysate (lane 1); 1/100 of the clarified lysate (lane 2); 1/100 of the unbound fraction (flow through, lane 3); 1/20 of first and last washes (lanes 4 and 5); and 1/3 of the elution (lane 6). Following WB, transfer efficiency was checked by Ponceau staining (lower panel) before the blot was probed with 4D7 neat antibody (upper panel). Ladder - Novex Sharp Pre-stained Protein Standard (Invitrogen).

Although 4D7 is capable of pulling-down CRK12 from the cell lysate (Figure 3. 12 lane 6), the efficiency is quite low as most of the protein is lost in the flow through, indicating it does not bind strongly to the antibody (Figure 3. 12 lane 3). Optimization could in future be achieved by increasing the incubation periods, risking however non-specific reactions.

3.1.6. **Localisation of CRK12 by IFA using 4D7**

IFA microscopy (section 2.6.3) using 4D7 as a primary antibody was carried out to determine the localisation of CRK12. Cells were co-stained with DAPI (section 2.6.1) to visualise DNA content, and fluorescence was analysed for cells in different cell cycle stages (Figure 3. 13). To analyse the specificity of the antibody by IFA, 4D7 was also tested using lysates from *CRK12* RNAi (Table 2. 1) uninduced and induced cultures (Figure 3. 14), after 18 hours of addition of tet (1 µg.ml^{-1}).

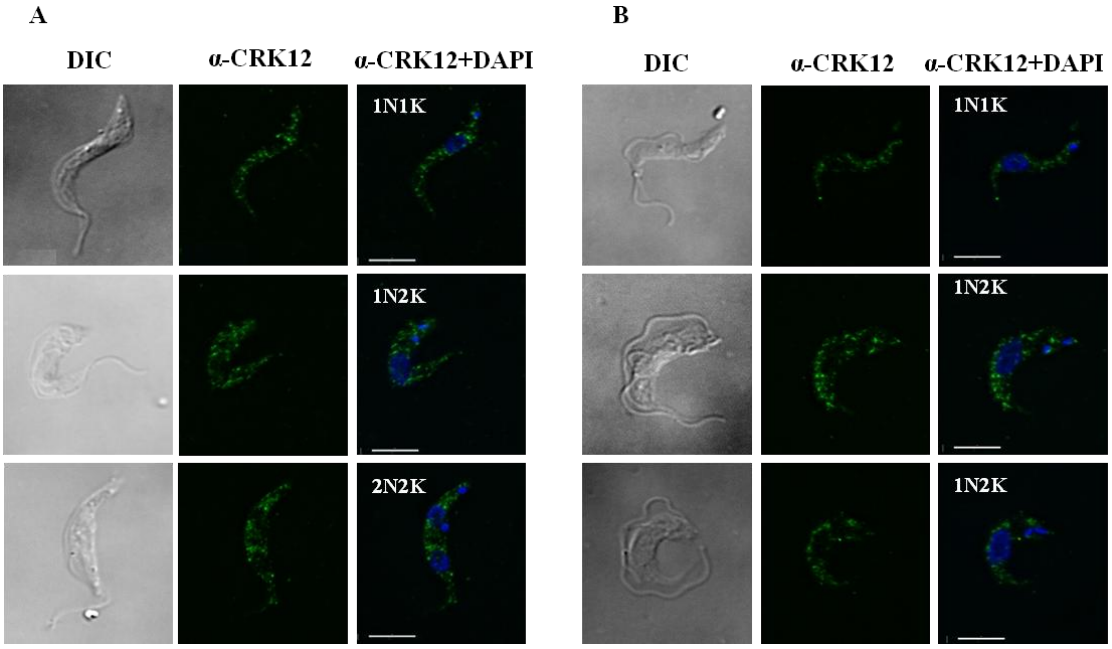

Figure 3. 13 - Localisation of CRK12 in PCF and BSF parasites. PCF WT (A) and BSF WT (B) cells were examined by IFA using 4D7 MAb as a primary antibody and fluorescent images were deconvolved. Panels from left to right: DIC images; anti-CRK12 (green); DAPI (blue)/anti-CRK12 (green) merge. The number of nuclei (N) and kinetoplasts (K) per cell are indicated. Scale bars – 5 µm.

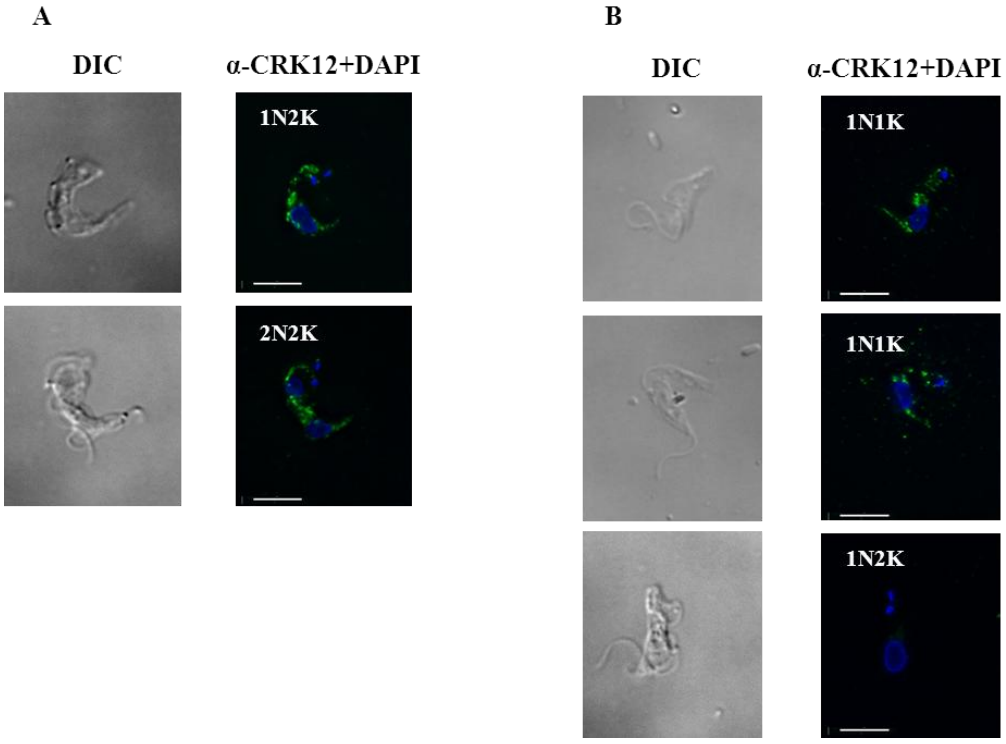

Figure 3. 14 – Specificity of anti-CRK12 4D7 antibody for IFA. Uninduced (A) and induced (B) BSF *CRK12* RNAi cells were examined by IFA using 4D7 MAb as a primary antibody. Fluorescent images were deconvolved; cell morphology is shown by DIC (left panels), fluorescent results as anti-CRK12 images (middle panels) and as a merge of DAPI (blue) and anti-CRK12 (green) (right panels). The number of nuclei (N) and kinetoplasts (K) per cell are indicated. Scale bars – 5 µm.

Cells at different cycle stages display a similar punctate distribution, for both BSF (Figure 3. 13 B) and PCF (Figure 3. 13 A) cell lines, not exhibiting a pronounced staining at any particular subcellular location. Despite the fact that knockdown of *CRK12* is accompanied by a clear reduction at a protein level (Figure 3. 11); not all induced cells present a decrease in fluorescence signal (Figure 3. 14 B) when compared to the uninduced or WT cultures. It is likely that 4D7 supernatant is neither concentrated nor pure enough to be suitable for IFA. The cellular localisation of CRK12 was instead determined by overexpressing ty:CRK12 (Table 2. 1) and performing IFA with antibodies directed against the TY tag (Figure 3. 20 and Figure 3. 21).

3.2. CHARACTERISATION OF CRK12:CYC9 – A NOVEL CRK:CYC COMPLEX IDENTIFIED IN *T. BRUCEI*

3.2.1. **CRK12 interacts with CYC9**

CRK activation is dependent on the binding of a CYC partner. Due to the fluctuation in CYC gene expression and protein destruction, CDK activity displays cyclin-dependent oscillations. So far, no interacting partners have been identified for CRK12 and neither has its function been analysed.

Previous results from the University of Glasgow labs have established that CRK12 and CYC9 are interacting partners. A yeast-two hybrid study including all the CYCs and CRKs identified in *T. brucei* proved that CRK12 and CYC9 interact in *S. cerevisiae* (Monnerat *et al.*, 2012). These preliminary results needed further confirmation using parasite cell lines. As such, several PCF cell lines were generated expressing *CYC9* tagged with a TAP tag at its C-terminus (Table 2. 2) and/or expressing ty:GFP:CRK12 (Table 2. 2), and used for further confirmation experiments (Monnerat *et al.*, 2012). CYC9:TAP cell lines were previously generated by other lab members, by deleting one allele of *CYC9* and replacing the second allele with the tagged version (Table 2. 1), allowing detection of CYC9 as previously generated antibodies do not recognise the protein effectively. Tagging of *CYC9* allows the use of commercial antibodies (Peroxidase anti-peroxidase (PAP) soluble complex antibody) to follow protein expression, without the tag affecting protein activity. As knockout experiments concluded that this gene is most likely essential for parasite proliferation (Monnerat *et al.*, 2012), the only copy of CYC9 present in the generated cell line, which is tagged with a TAP tag at its C-terminus, has to be active.

Cell lines containing *CRK12* tagged with ty:GFP at its N-terminus were generated by transfecting (section 2.2.3 and 2.2.4) pHG69 (Table 2. 8) (previously linearized with XhoI (section 2.3.3) and purified (section 2.3.7)) into three cell lines: PCF WT (Figure 3. 15 panel A); BSF WT (Figure 3. 15 panel B); and PCF parasites already expressing CYC9:TAP (Figure 3. 15 panel C). Insertion of this tag facilitates

different protein studies, including those determining localisation and expression profiles (Bastin *et al.*, 1996a). Transfection efficiency was confirmed by WB (section 2.4.7, Figure 3. 15). Most of the clones tested were positive for ty:GFP:CRK12 indicating a successful transfection, except one clone from the transfected PCF CYC9:TAP cell line, which did not show a band corresponding to ty:GFP:CRK12 (Figure 3. 15 panel C lane 5). Glycerol stocks were prepared for at least two different clones of each transfected cell line.

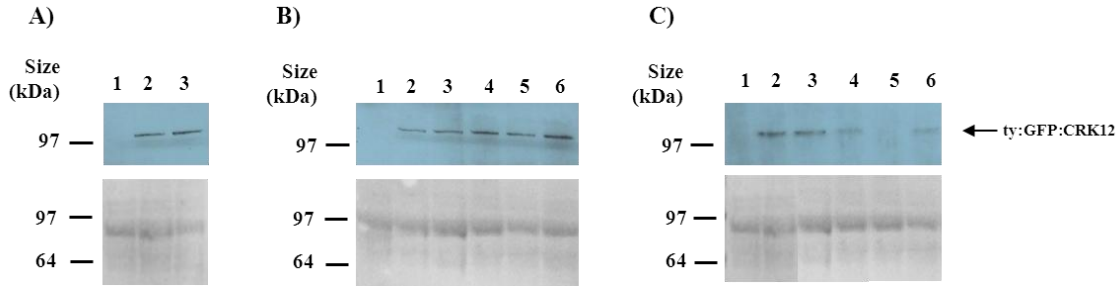

Figure 3. 15 - WB analysis to confirm expression of ty:GFP:CRK12 in transfected cell lines. Cell lysates of PCF WT (panel A), BSF WT (panel B) and PCF CYC9:TAP (panel C) cell lines transfected with pHG69 for endogenous expression of ty:GFP:CRK12 were prepared for SDS-PAGE, electrophoresed on 12% gels, transferred to nitrocellulose membranes and probed with anti-TY antibody. A loading control was performed by staining with Ponceau reagent prior to adding the antibody (lower panels). Lane 1 of all panels corresponds to the untransfected cell lines (negative control) and the remaining lanes contain the different clones tested. The signal corresponds to the predicted size of 113.5 kDa for ty:GFP:CRK12. Ladder – See blue plus2 (Invitrogen).

Analysis of interacting partners was primarily performed using cell lysates from PCF CYC9:TAP cell line, by purifying CYC9 and analysing by mass spectrometry the elution fractions (Monnerat *et al.*, 2012). Such results gave the first indication of *in vivo* interaction between CRK12 and CYC9 in PCF parasites. IP was used to corroborate this, using the tagged PCF cell lines (Figure 3. 15 panel C). Whether CYC9:TAP or ty:GFP:CRK12 were pulled down, ty:GFP:CRK12 or CYC9:TAP, respectively, were copurified and appeared in the elution fractions (Monnerat *et al.*, 2012), indicating that these proteins interact in PCF cell lines. Parallel experiments have also shown that, although CRK12 is active *in vivo* and undergoes auto-phosphorylation, it does not phosphorylate any common kinase substrates (α-casein, β-casein, MBP and histone H1) (Monnerat *et al.*, 2012).

Confirmation of the CRK12:CYC9 interaction was further needed for the BSF, and cell lines with tagged versions of each protein were once again used. In this case, inducible expression cell lines were employed, expressing ty:CRK12 under the control of a tet promoter (Table 2. 1). To allow detection of CYC9, the ty:CRK12 overexpression cell line was transfected (section 2.2.3) with pGL1125 (linearized with XhoI (section 2.3.3) and purified (section 2.3.7)), the CYC9:TAP endogenous expression construct. Transfectants were analysed by WB to confirm expression of CYC9:TAP (Figure 3. 16).

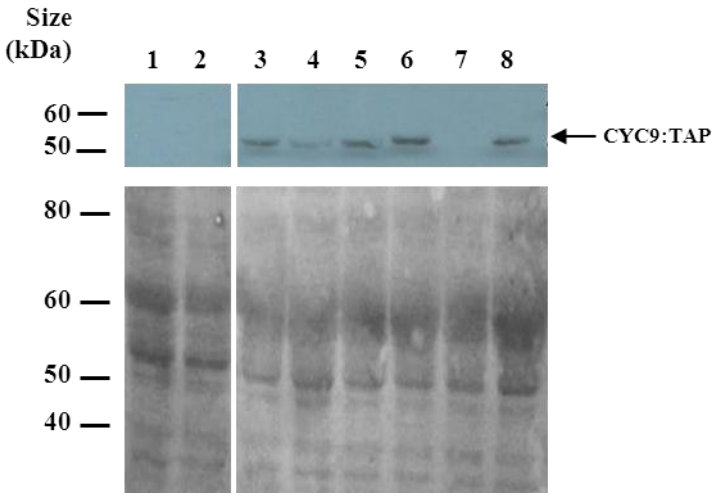

Figure 3. 16 -Analysis of CYC9:TAP expression in BSF transfectants. Cell lysates of BSF ty:CRK12 overexpression cell lines (BSF 427 pHD449 pHG230) transfected with pGL1125 (CYC9:TAP endogenous expression construct, predicted size – 51,6 kDa) were analysed by WB. Lanes 1 and 2 – untransfected ty:CRK12 overexpression cell line, uninduced and induced respectively. Lanes 3 to 8 – cell lysates from different CYC9:TAP transfected clones. Samples were electrophoresed in 12% SDS-PAGE gels, loading was checked by Ponceau staining (lower panel), and expression of CYC9:TAP was probed with anti-PAP antibody (upper panel). Ladder - Novex Sharp Pre-stained Protein Standard (Invitrogen).

Of the six clones tested only one lacked the presence of the CYC9:TAP expression construct (Figure 3. 16 lane 7) and as such glycerol stocks were prepared for three positive clones (Figure 3. 16 lanes 3, 4 and 5). Further work was performed using the clone represented on lane 3 in Figure 3. 16.

Cell lysates co-expressing CYC9:TAP from the endogenous locus and ty:CRK12 under inducible control (corresponding to clone 3 in Figure 3. 16 and panel A in Figure 3. 17) were prepared (section 2.2.7). Prior to IP with Dynabeads® (section

2.4.10), the TY antibody was cross-linked with the beads to prevent the appearance of an extra band at 50 kDa in the elution fractions, corresponding to the heavy chain of the IgG antibody, and approximately with the same size as CYC9:TAP. The lysate was incubated with the TY antibody coupled beads for one hour at 4ºC, in order to pull down ty:CRK12. IP efficiency was followed-up by WB analysis of the input (1/100 loaded), flow through (1/100), washes (1/20) and elution (1/4) fractions (Figure 3. 17 panel B), probing with different antibodies directed against the tags fused to the proteins of interest and using EF1α as the antibody for loading control.

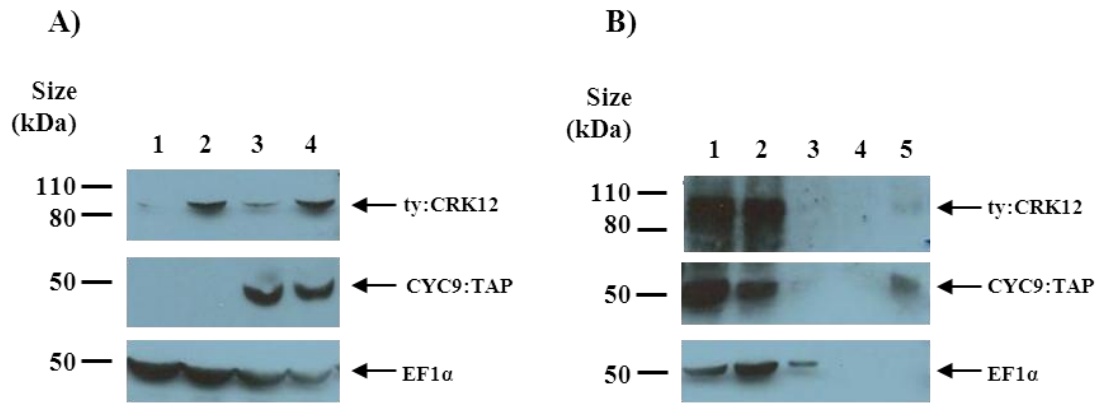

Figure 3. 17 –Analysis of ty:CRK12 IP from BSF parasites co-expressing CYC9:TAP. BSF cell lysates were prepared for SDS-PAGE, electrophoresed on 14% SDS-PAGE gels, transferred to nitrocellulose membranes and WB with different antibodies. A –control WBs to confirm protein expression of ty:CRK12 (predicted size ~ 86 kDa) and CYC9:TAP (predicted size ~ 51.6 kDa). Lane 1: BSF 427 pHD449 pHG230 (ty:CRK12 overexpression construct) uninduced; lane 2: BSF 427 pHD449 pHG230 induced 24 hrs with tet; lane 3: BSF 427 pHD449 pHG230 pGL1125 (ty:CRK12 overexpression construct CYC9:TAP) uninduced; lane 4: BSF 427 pHD449 pHG230 pGL1125 induced for 24 hrs with tet. 2 x 10^6 cells were loaded per lane. Blots were probed with anti-TY (to detect ty:CRK12; top panel), anti-PAP (to detect CYC9:TAP; middle panel) and anti-EF1α as a loading control (bottom panel). B – WB analysis of samples from IP of ty:CRK12 with anti-TY antibody from BSF 427 pHD449 pHG230 pGL1125 (ty:CRK12 overexpression construct CYC9:TAP) cell line induced 24 hours with tet. Lane 1: input (1/100); lane 2: flow through (1/100); lanes 3 and 4: washes 1 and 3 (1/20), respectively; lane 5: elution (1/4). Blots were probed with antibodies as for A. Ladder - Novex Sharp Pre-stained Protein Standard (Invitrogen).

The interaction between ty:CRK12 and the antibody coupled beads is not very efficient, as the majority of the protein is visible in the flow through (Figure 3. 17 panel B top panel), translating to a very low amount of the kinase in the elution fraction. Even so, CYC9 is co-purified (Figure 3. 17 panel B middle panel), appearing as a band of the expected size in the elution fraction accompanied by a reduction of the signal between

the input and the flow through. CYC9 is thus found to interact with CRK12 in the BSF. In conclusion, CRK12:CYC9 constitutes a novel CRK:CYC complex identified in both life cycle stages.

3.2.2. **Localisation of CYC9 and CRK12**

Localisation influences the activity of cell cycle regulators, and their interaction with possible regulatory proteins or substrates. To study the localisation of both CYC9 and CRK12, IFA experiments were carried out (section 2.6.3) in optimal conditions for each cell line, using tagged cell lines and antibodies directed against the tags. Anti-TY was used for analysis of ty:CRK12 localisation in BSF cells (Table 2. 12), fixed in 2% PFA for 7 minutes and incubated with primary antibody overnight at 4ºC. CYC9:TAP cells were fixed in 70% methanol at -20ºC for one hour (section 2.6.3), re-hydrated in PBS and incubated with primary antibody (anti-protein A antibody (Table 2. 12)) for one hour at room temperature.

Localisation of CYC9 in *T. brucei* was analysed by using the CYC9 tagged cell lines from both life cycle stages: PCF 427 pGL1217 pGL1125 pHG69 (TY:GFP:CRK12 CYC9:TAP) and BSF 427 pHD449 pHG230 pGL1125 (ty:CRK12 overexpression construct + CYC9:TAP). An anti-protein A antibody which interacts with the TAP tag was used as a primary antibody, demonstrating a similar localisation of CYC9:TAP for the different life cycle stages and for cells at different cell cycle phases (Figure 3. 18 and Figure 3. 19). A pronounced staining of the nucleus is visible, whether the cell contains one or two nucleus (see "Merge" panel on Figure 3. 18 and Figure 3. 19). The staining seems to be enriched at the periphery of the nucleus, although this would need confirmation by performing a 3D reconstruction of the z-stacks, as the images displayed here correspond to a merge of the different z-stacks. Negative controls performed with no primary antibody or no secondary antibody displayed no fluorescent signal (results not shown), validating the IFA results.

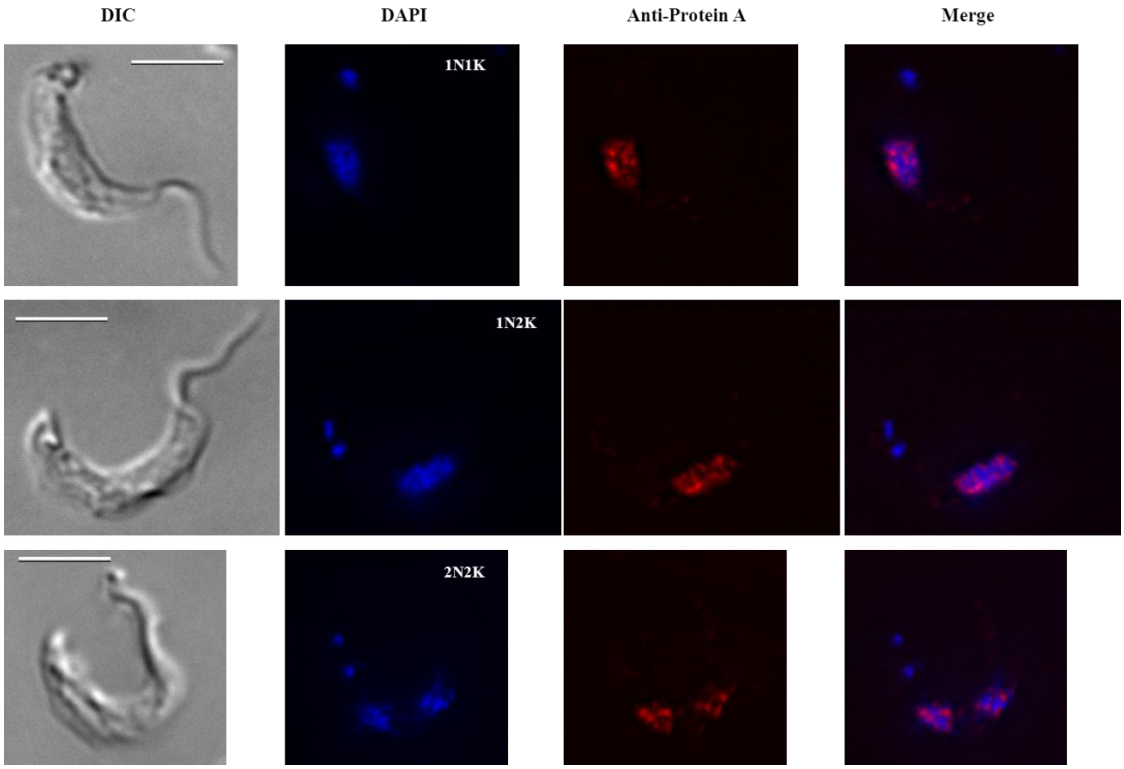

Figure 3. 18 –Localisation of CYC9:TAP in BSF *T. brucei* parasites. IFA analysis of CYC9:TAP BSF cell line (BSF 427 pHD449 pHG230 pGL1125)was performed using an anti-protein A antibody with Alexa fluor 594-conjugated goat anti-rabbit IgG secondary antibody, and fluorescent images were deconvolved. Panels from left to right: DIC images; DAPI staining of DNA (blue); protein A staining of CYC9:TAP (red) and DAPI/protein A merge. The number of nuclei (N) and kinetoplasts (K) per cell are indicated. Scale bars – 5 µm.

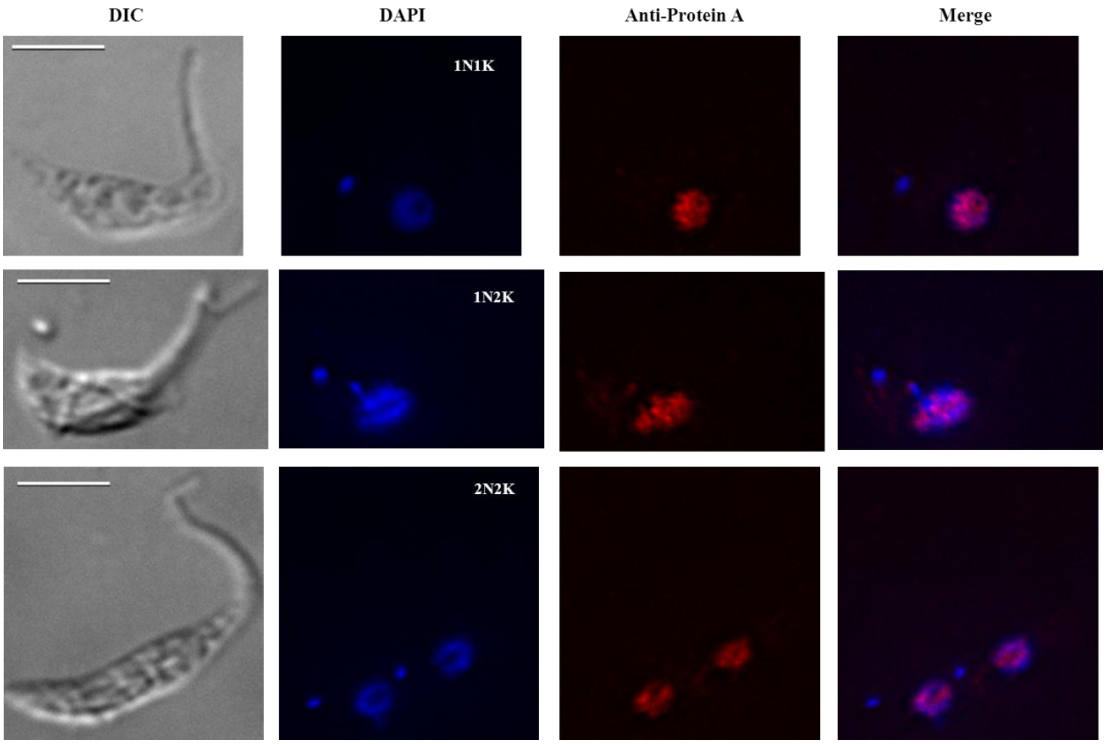

Figure 3. 19 - Localisation of CYC9:TAP in PCF *T. brucei* parasites. IFA analysis of CYC9:TAP PCF cell line (PCF 427 pGL1217 pGL1125 pHG69) was performed using an anti-protein A antibody with Alexa fluor 594-conjugated goat anti-rabbit IgG secondary antibody, and fluorescent images were deconvolved. Panels from left to right: DIC images; DAPI staining of DNA (blue); protein A staining of CYC9:TAP (red) and DAPI/protein A merge. The number of nuclei (N) and kinetoplasts (K) per cell are indicated. Scale bars – 5 µm.

Not much is known about the localisation of the different CYCs in *T. brucei* or in other Trypanosomatids. CYC2 for example (Van Hellemond *et al.*, 2000) presents a cytoplasmic distribution in PCF trypanosomes, as revealed by IFA of CYC2:ty-expressing cell lines. Similarly, CYC1 in *L. donovani* (Banerjee *et al.*, 2006) localises to the cytoplasm of promastigotes, observed by using antiserum raised in rabbit against the his-tagged N-terminal end of LdCYC1. However, no orthologue of LdCYC1 is found in *T. brucei*.

Some other proteins involved in cell cycle regulation in *T. brucei* have been determined to have a nuclear localisation. Recent investigations into the role of CRK9 in *T. brucei* (Gourguechon and Wang, 2009) have localised this protein to the nucleus of both BSF and PCF parasites, despite a function for this protein only having been observed in PCF parasites (Gourguechon and Wang, 2009), where it is proposed to control mitosis and kinetoplast segregation. Such results are similar to the ones obtained

in 2006 and 2009 for TbAUK1 (Tu *et al.*, 2006, Li *et al.*, 2009), which also seems to couple functions in mitosis and cytokinesis, localising to the nucleus but migrating to the mitotic spindles during metaphase. Depletion of CYC9 also causes defects in cytokinesis (section 3.2.5), although only affecting BSF parasites (section 3.2.5), but there are distinct features between CYC9 and TbAUK1 localisation. The latter apparently fills the central portion of the nucleus during interphase and migrates to the cleavage furrow during telophase (Li *et al.*, 2008), while CYC9 always remains associated with the nucleus. It is necessary to take into consideration the fact that CYC9 localisation was visualised by using a tagged cell line, and such tag could alter CYC9 localisation or affect its migration ability. On the other hand, CYC9 is expressed throughout the cell cycle due to the 3` UTR, so any potential cell cycle stage specific differences in expression/localisation would not be visible.

Interestingly, another protein that has been found to localise to the nucleus is Target of rapamycin 1 (TbTOR1) (Barquilla *et al.*, 2008). RNAi experiments show that TbTOR1 is essential for cell proliferation and that this protein controls cell growth by regulating cell cycle, nucleolus structure and protein synthesis. A related protein TbTOR2, with a cytosolic punctate distribution, is required for cytokinesis and demonstrates in parallel a function in polarized cell growth (Barquilla *et al.*, 2008). TbTOR2 binds exclusively to the complex TORC2, while TbTOR1 interacts predominantly with TORC1 but shows a weak interaction with TORC2 (Barquilla *et al.*, 2008). Interestingly, CYC9 has the same localization as TbTOR1, but its role in cytokinesis is similar to TbTOR2. On the other hand, TbTOR2 depletion leads to enlarged FPs, as seen for CRK12 knockdown (section 3.2.6). Although the nucleus localisation and the regulation of cytokinesis is not directly linked in these proteins, one cannot rule out that TbTOR1, which in fact localises to the nucleus, might be linked to the cytokinesis role of TORC2, despite their low interaction *in vivo*.

Localisation of CRK12 was not possible using the MAb generated during this study (section 3.1.6), nor was an endogenously tagged CRK12 (ty:GFP:CRK12) visible by *in situ* fluorescent microscopy (results not shown). Analysis of the parasite's transcriptome profile over the cell cycle reveals that several genes are regulated

periodically (Archer *et al.*, 2011), presenting expression peaks at distinct times in the cell cycle. This might be the case for CRKs that control different phases of the cell cycle exhibiting stage-specific activity, for example CRK1 and CRK3, which are required for the G1/S and G2/M transitions, respectively (Tu and Wang, 2004). Such oscillations in protein levels might interfere with localisation determination, together with a low expression profile exhibited by some cell cycle regulators. For some proteins, inducible expressions systems are necessary to overcome the difficulty in detecting endogenous levels of expression; in spite of the fact that some cell cycle regulators are toxic at high concentrations, and protein localisation should ideally be determined with expression near the endogenous level. Systems for tet inducible expression have been developed for *T. brucei* (Wirtz and Clayton, 1995, Biebinger *et al.*, 1997), lowering in parallel the possible toxic effects of the expressed protein.

For visualisation of CRK12, the BSF ty:CRK12 over-expression cell line (Table 2. 1) was induced for 24 hours with 1 µg.ml^{-1} tet, cells were applied to poly-L-lysine slides (section 2.6.3) and IFA with an anti-TY antibody was performed as described in section 2.6.3 (Figure 3. 21). As a control, uninduced cell lines were also probed with anti-TY antibody (Figure 3. 20), and negative controls with no primary and no secondary antibodies were carried out (results not shown).

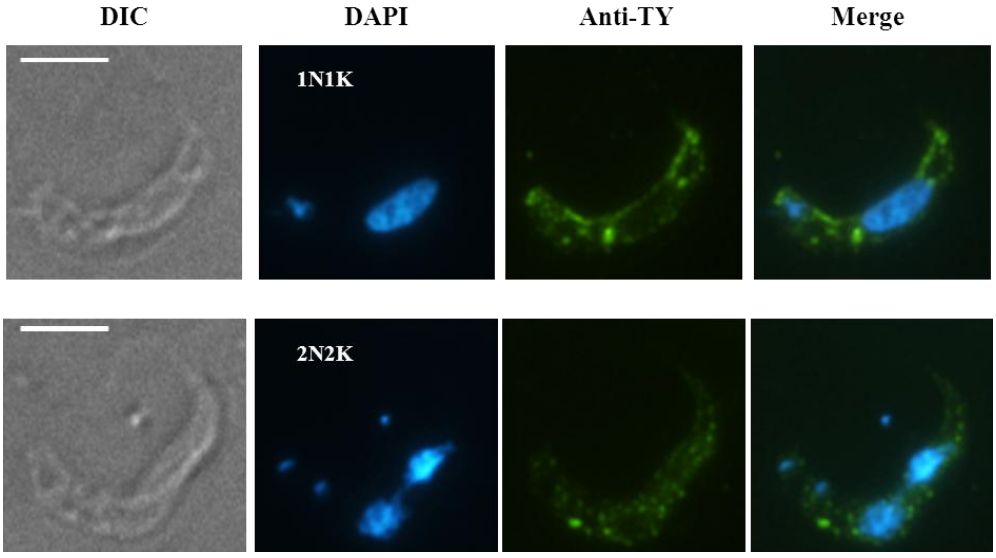

Figure 3. 20 - Localisation of ty:CRK12 in uninduced over-expression BSF cell lines. IFA analysis of uninduced ty:CRK12 BSF cell line (BSF 427 pHD449 pHG230) was performed using an anti-TY antibody with Alexa fluor 488-conjugated goat anti-mouse IgG secondary antibody, and fluorescent images were deconvolved. Panels from left to right: DIC images; DAPI staining of DNA (blue); TY A staining of ty:CRK12 (green) and DAPI/TY merge. The number of nuclei (N) and kinetoplasts (K) per cell are indicated. Scale bars – 5 µm.

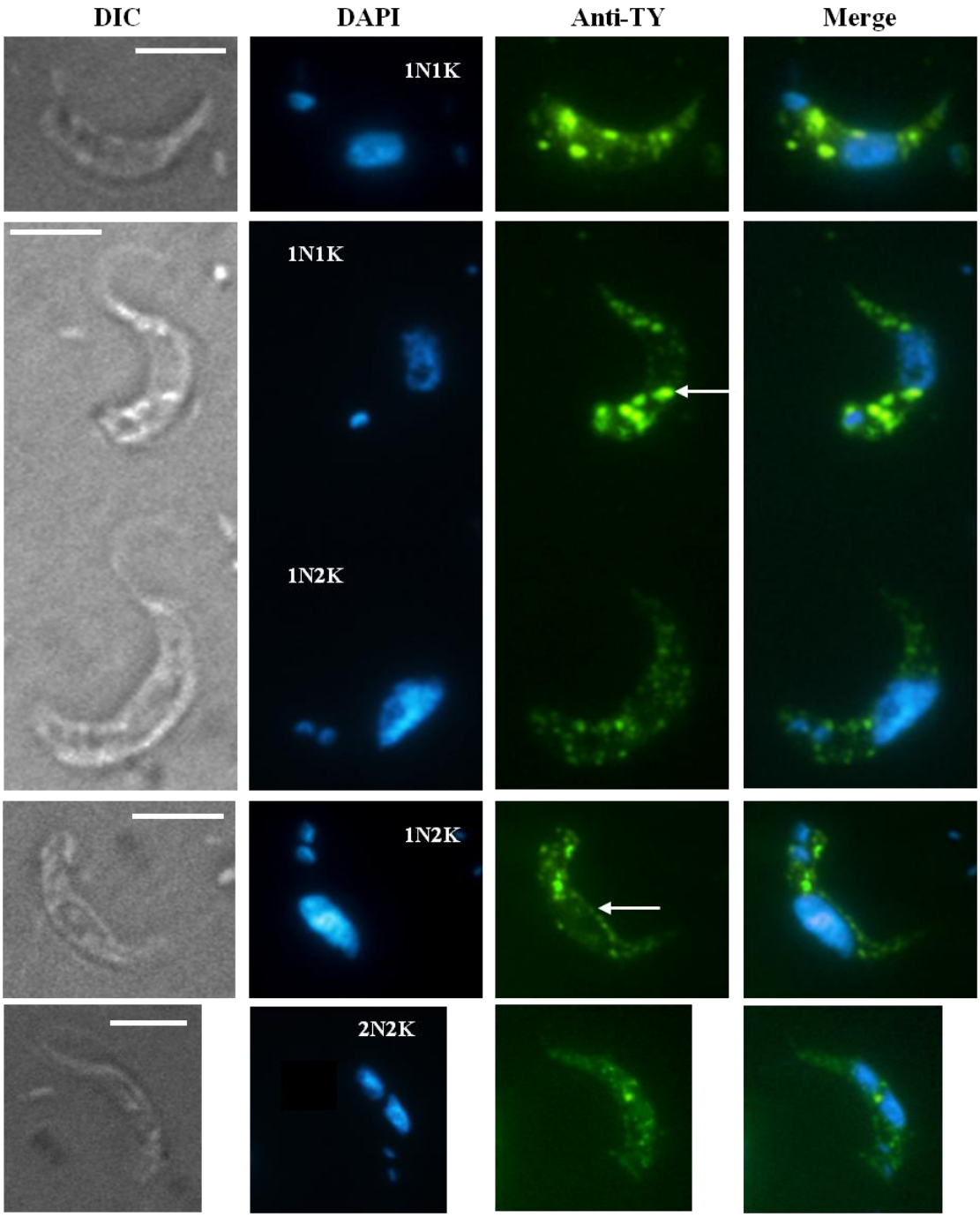

Figure 3. 21 - Localisation of ty:CRK12 in induced over-expression BSF cell lines. IFA analysis of induced ty:CRK12 BSF cell line (BSF 427 pHD449 pHG230) was performed using an anti-TY antibody with Alexa fluor 488-conjugated goat anti-mouse IgG secondary antibody, and fluorescent images were deconvolved. Panels from left to right: DIC images; DAPI staining of DNA (blue); TY A staining of ty:CRK12 (green) and DAPI/TY merge. The number of nuclei (N) and kinetoplasts (K) per cell are indicated. The arrow indicates a possible concentration of ty:CRK12 at the nuclear periphery. Scale bars – 5 µm.

As opposed to its CYC partner, CRK12 remains excluded from the nucleus in all cell cycle stages (Figure 3. 21), presenting a punctate cytoplasmic distribution with brighter staining between the nucleus and the kinetoplast(s) in some cells (Figure 3. 21 1N1K cells). An apparent concentration of ty:CRK12 signal at the nucleus periphery is also visible (Figure 3. 21 arrows). Uninduced cell lines also display fluorescence, most likely corresponding to a basal protein expression, as also visible by WB (Figure 3. 17 panel A).

As mentioned for CYC9, not many cell cycle regulators have had their localisation determined in *T. brucei*, and when considering the 11 CRKs identified so far, only the localisation of CRK9 has been characterised (Gourguechon and Wang, 2009). CRK1 has been localised in *T. cruzi* (Gómez *et al.*, 2001), using immune-gold labelling and an anti-TzCRK1 antibody. The distribution of CRK1 in this trypanosomatid seems to concentrate mainly in the cytoplasm, while 16% stains the nucleus and 24% the kinetoplast (Gómez *et al.*, 2001).

During this study, a novel CRK:CYC complex has been identified with each protein displaying a different localisation. The different distributions of CRK12 and CYC9 do not invalidate the fact that they interact in both life cycle stages of the parasite, and although CRK12 is present mainly in the cytoplasm, it appears in some cells to also localise at the nucleus periphery, potentially allowing it to interact with CYC9 at such points. Confirmation of this nuclear periphery localisation would need future 3D reconstructions of the z-stacks. Considering the cyclic expression of these proteins, interaction between CYC9 and CRK12 might occur at those points during specific stages of the cell cycle, and then when binding is disrupted each protein assumes a different location. On the other hand, the existence of a possible nuclear localisation signal (NLS) might have been distrupted or introduced by insertion of the protein tag into the sequence of CRK12 or CYC9, respectively.

Also, CRK12 localisation was analysed using over-expression cell lines which might not reflect the protein distribution as seen in WT cells, and a potential nuclear localisation of CRK12 might be masked by a stronger cytoplasmic distribution when it is over-expressed. CYC concentration varies in a cyclical fashion, and binding of the CYC to the kinase consequently leads to oscillations in the kinase activity and targets

the latter to specific subcellular locations. When using over-expression cell lines, besides the fact that the oscillations at the protein level are disrupted, the activation of the kinase might not be fully achieved, as CYC9 is expressed at endogenous levels, potentially leading to ambiguous results.

3.2.3. **CRK12 and CYC9 function in BSF**

Advances in RNAi techniques have turned it into the preferred system to investigate the role of certain proteins in trypanosomes. Gene knockout can determine if a specific gene is essential or not to the parasite and validate its possible use as a drug target (Barrett *et al.*, 1999); but for essential genes effects of the depletion on the parasite is better understood with gene knockdown. The first studies on RNAi were done in 1998 by transfection of double-stranded RNA (dsRNA) (Ngô *et al.*, 1998). *T. brucei* cells were transfected with α–tubulin 5' untranslated region (UTR) dsRNA and authors observed that tubulin mRNA was rapidly and specifically degraded. Several improvements have been achieved since, inhibition of gene expression was studied primarily for PCF (Wang *et al.*, 2000) and later on for BSF trypanosomes (Morris *et al.*, 2001), and new systems were developed (Wirtz *et al.*, 1999) to overcome the drawbacks of the old ones.

RNAi screens have been used in the search for new key cell cycle regulators (Monnerat *et al.*, 2009, Mackey *et al.*, 2011), and recently in a high throughput approach to determine the effects of gene knockdown on growth and development profiles (Alsford *et al.*, 2011, Alsford *et al.*, 2012). The roles of CRK12 and CYC9 in *T. brucei* have been determined during this study using RNAi systems, which have been used extensively for functional analysis of CRKs and CYCs over the years.

3.2.4. **The effect of CRK12 and CYC9 knockdown on cell growth and DNA content**

Silencing of CRK12 in PCF *T. brucei* shows no effect on cell cycle progression (Gourguechon and Wang, 2009), although a clear decrease at the mRNA level is

observed with semi-quantitative RT-PCR after 2 days of induction. The effects of CYC9 knockdown of PCF parasites was studied by previous members of the Hammarton lab (Monnerat *et al.*, 2012). Although causing a strong reduction in cell growth 5 days post-induction, no visible cell cycle effect was observed (results not shown).

As no phenotype was observed in PCF, BSF RNAi cell lines (Table 2. 1) were used for functional analysis of CRK12 and CYC9. Two independent clones were induced with 1 µg.ml^{-1} tet and cell density was determined (section 2.2.2) at regular intervals, for both the induced and uninduced cultures of the *CRK12* RNAi (Figure 3. 22) and the *CYC9* RNAi (Figure 3. 23) cell lines. Silencing of either *CRK12* or *CYC9* leads to a clear growth arrest after 12 hours of induction, with consistent results between the two independent clones (Figure 3. 22 and Figure 3. 23), and showing that such depletion is lethal for BSF *T. brucei*. RT-PCR shows a specific reduction at the mRNA level for each gene (Monnerat *et al.*, 2012), and α-CRK12 MAb 4D7 demonstrates that the knockdown also occurred at the protein level, presenting a striking reduction already at 12 hours post-induction (Figure 3. 11). The data obtained leads to the conclusion that CRK12 and CYC9 are essential for cell proliferation *in vitro*.

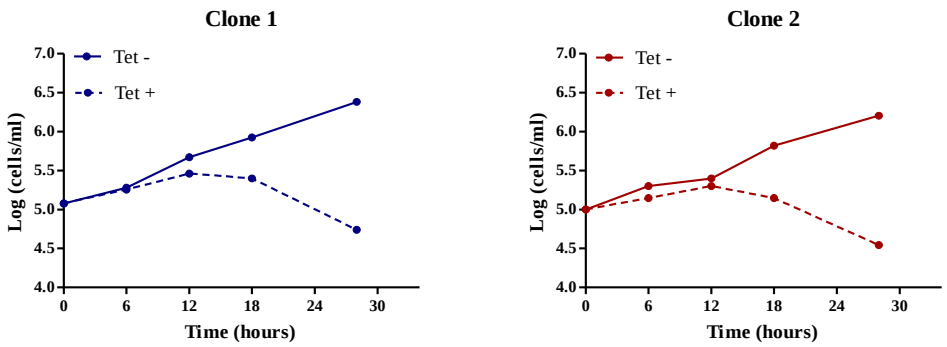

Figure 3. 22 – Cumulative growth curves of BSF *CRK12* RNAi cell lines. Two independent clones were grown in the absence (Tet-) or presence (Tet+) of 1 µg.ml^{-1} tet and cell density was determined over a period of 28 hours.

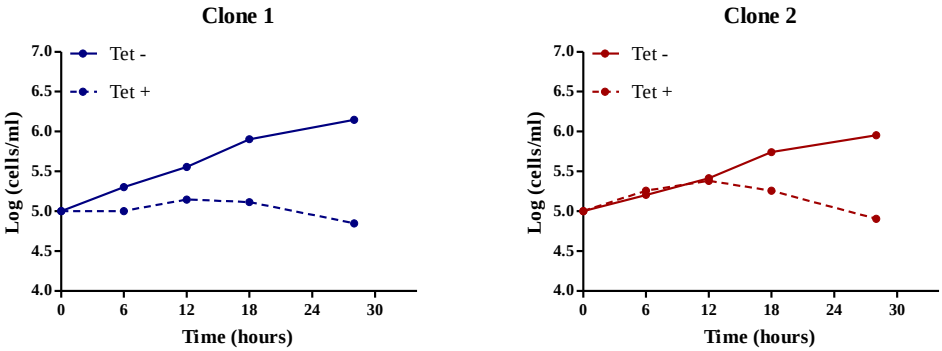

Figure 3. 23 – Cumulative growth curves of BSF *CYC9* RNAi cell lines. Two independent clones were grown in the absence (Tet-) or presence (Tet+) of 1 µg.ml^{-1} tet and cell density was determined over a period of 28 hours.

To determine if the growth defect is caused by cell cycle arrest, RNAi cell lines were analysed by flow cytometry (section 2.2.6), using once again two independent clones for each cell line. Samples were taken at regular intervals for uninduced and induced cultures, fixed with methanol and stained with propidium iodide, prior to analysis by flow cytometry. Cells at time 0 were used for calibration, as they represent a typical DNA profile (Figure 3. 24 and Figure 3. 25 panels "0h"), with the 2C and 4C peaks representing cells in G0/G1 and G2/M phases, respectively. Fluorescence between these 2 points corresponds to cells in S-phase.

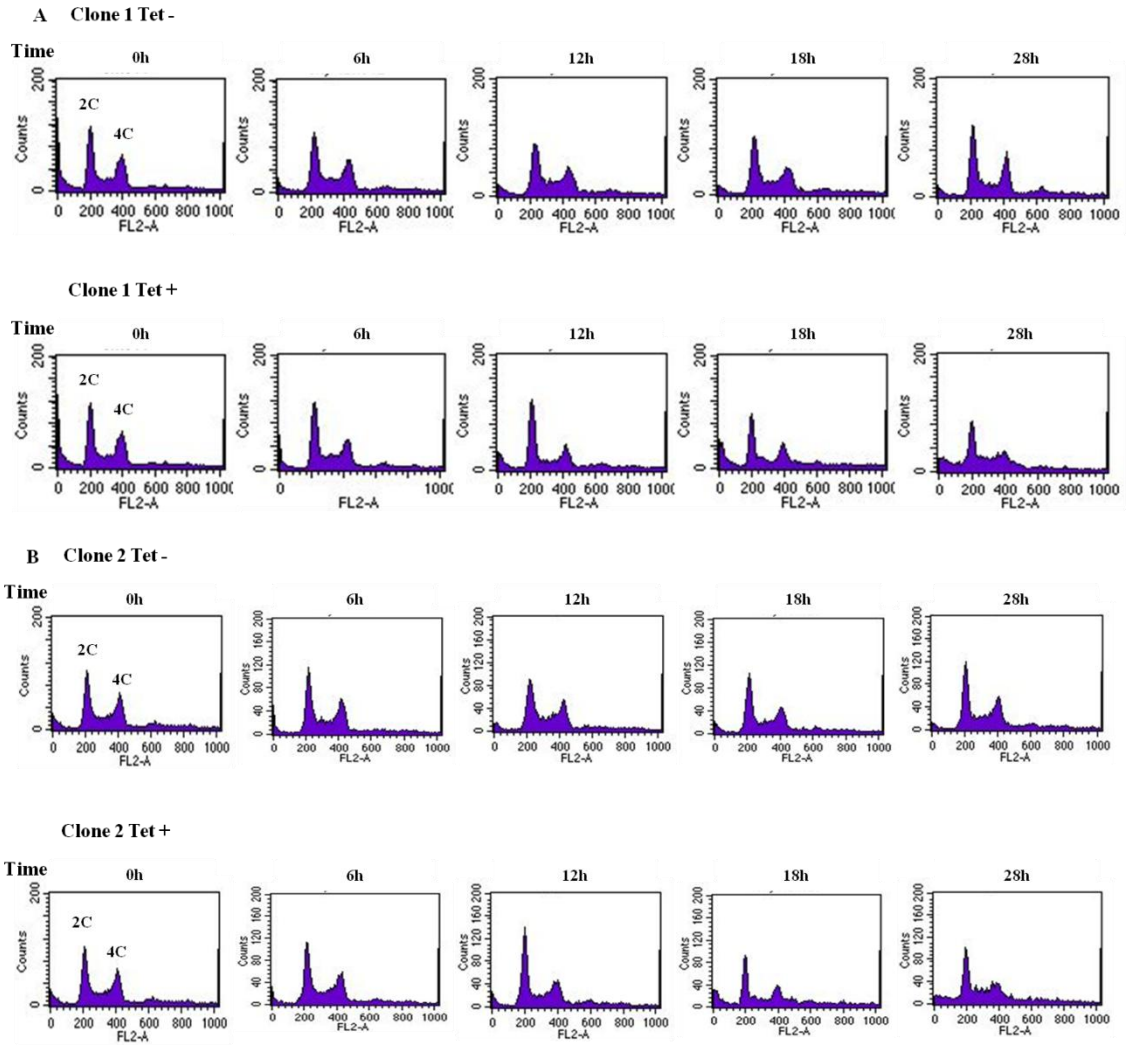

Figure 3. 24 - Flow cytometry profiles of BSF *CRK12* RNAi cell line. Two independent clones (Clone 1 - A and Clone 2 - B) were grown in the absence (Tet-) or presence (Tet+) of tet and analysed for DNA content by flow cytometry. The histograms represent the total cell counts (y-axis) plotted against fluorescence (FL2A; x-axis).

Although CRK12 depletion does not cause any apparent effect on cell cycle progression (Figure 3. 24), the contrary is observed for *CYC9* RNAi (Figure 3. 25). The data obtained are consistent between the two clones (Figure 3. 25); and cell cycle alterations are apparent after 12 hours of induction. At this time point, an abnormal peak with fluorescence higher than 4C arises, which implies that cells have undergone a second round of DNA replication without dividing (Figure 3. 25 "8C" peak in "Tet+" panels), generating a polyploid population. This peak increases over time, accompanied by a reduction of the 2C peak, and although oscillations in the 2C and 4C peaks were observed for uninduced cells (Figure 3. 25 "Tet-" panels), no peak corresponding to

polyploid cells emerged. These results suggest that CYC9 depletion causes a defect in cytokinesis, and further experiments were performed to confirm this (section 3.2.5).

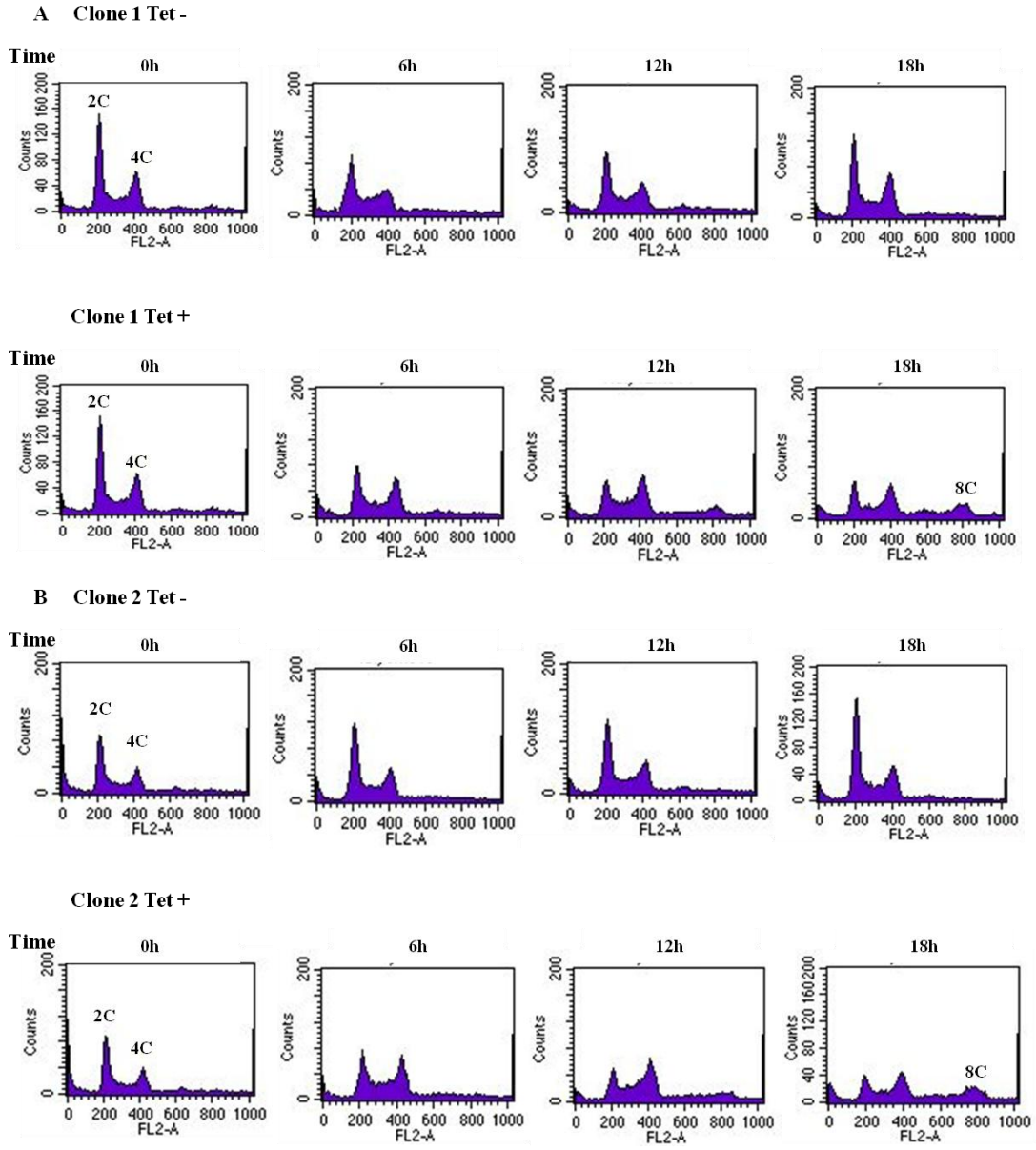

Figure 3. 25 - Flow cytometry profiles of BSF *CYC9* RNAi cell line. Two independent clones (Clone 1 - A and Clone 2 - B) were grown in the absence (Tet-) or presence (Tet+) of tet and analysed for DNA content by flow cytometry. The histograms represent the total cell counts (y-axis) plotted against fluorescence (FL2A; x-axis).

3.2.5. **CYC9 knockdown causes defects in cytokinesis**

Analysis of the nuclear and kinetoplast content of each cell (Nucleus (N)/Kinetoplast (K) configuration) allows the classification of trypanosomes as to their cell cycle stage. Cells start the cycle with one nuclear and one kinetoplast (1N1K), corresponding to G1 phase. Kinetoplast division starts prior to nuclear division and takes less time to conclude, which means that cells in G2 phase present a 1N2K configuration. 2N2K cells appear upon mitosis, and cytokinesis gives rise to two daughter 1N1K cells.

To further investigate the effects of CYC9 depletion on cell cycle progression, cells were classified according to their nucleus/kinetoplast (N/K) configuration by staining them with DAPI (section 2.6.1), and cell cycle progression was analysed over time for two independent clones. Approximately 200 cells were categorized for each time point (Figure 3. 26).

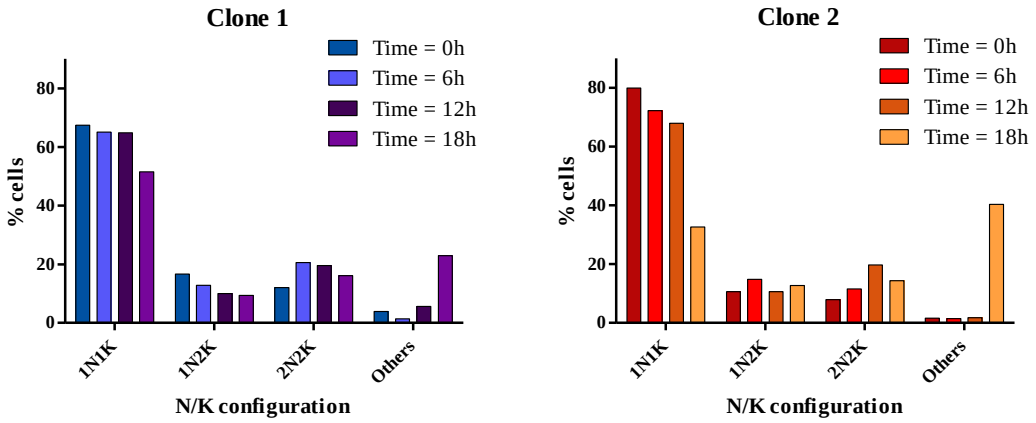

Figure 3. 26 – DAPI staining of BSF *CYC9* RNAi cell lines. Two independent clones (Clone 1 and Clone 2) were grown in tet, and at regular intervals, samples were taken and cells stained with DAPI. The nucleus (N) and kinetoplast (K) configurations of approximately 200 cells were determined for each time point.

CYC9 knockdown primarily affects the proportion of 2N2K cells in the overall population, which doubles in number after 12 hours of tet induction (Figure 3. 26). The 2N2K cell increase is accompanied by a decrease in 1N1K cells, consistent with what was observed by flow cytometry (Figure 3. 25). At later time points the number of cells

with multiple N/K (others) increases, indicating that 2N2K cells are not undergoing cytokinesis correctly. When classifying the cytokinesis stage of these 2N2K cells (Figure 3. 27), results reveal a noticeable increase in cells that have already started cytokinesis and are undergoing furrow ingression (Figure 3. 28 middle panel), from 4% to 40% and 8% to 22%, at 18 hours post-induction, for clone 1 and clone 2, respectively (Figure 3. 27 "Furrow ingression" data). In parallel, cells that have actually reached abscission (Figure 3. 28 bottom panel) decrease to approximately half of that observed for uninduced cells, while the majority of cells have not yet started cell division (Figure 3. 27). DAPI data are in accordance with what was seen by flow cytometry (Figure 3. 25), as depletion of CYC9 seems to inhibit cytokinesis.

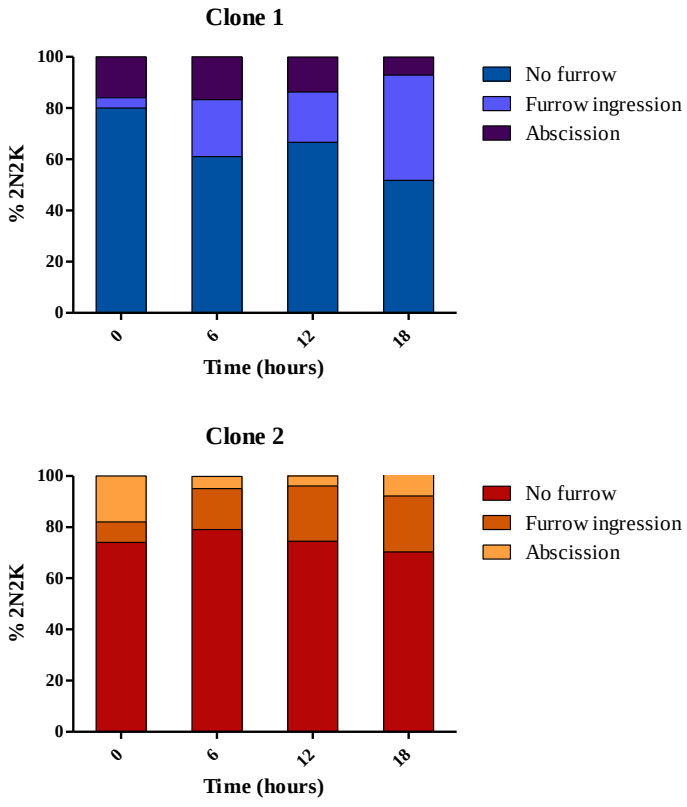

Figure 3. 27 - Analysis of the cytokinesis stage of 2N2K cells following depletion of CYC9 in BSF *T. brucei*. Approximately 50 cells were classified according to the absence (no furrow) or presence of a cleavage furrow (furrow ingression), or if they were undergoing abscission.

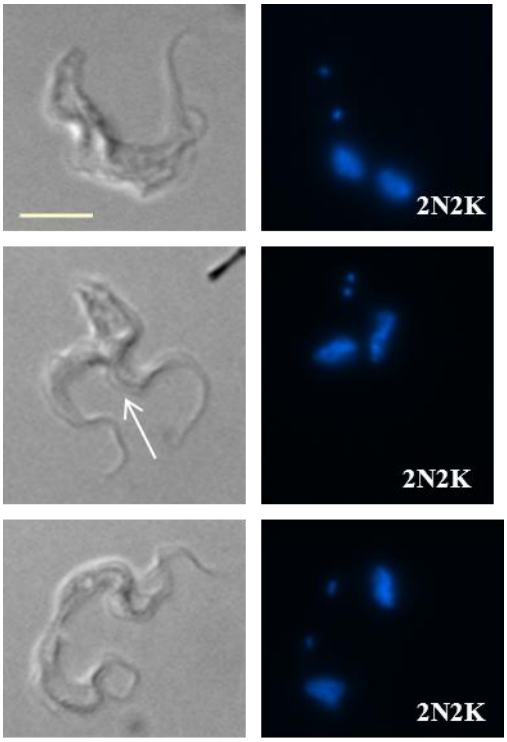

Figure 3. 28 - DAPI staining of typical 2N2K cells at different cytokinesis stages. Top panel – 2N2K cell with no furrow; middle panel – cell undergoing furrow ingression; bottom panel – cell in abscission. Left panels – DIC. Right panels – DAPI staining with nucleus (N)/kinetoplast (K) configuration indicated The arrow indicates the cleavage furrow. Scale bar – 5 µm.

Microscope analyses of induced cells reveal the appearance of a population with abnormal N/K configurations, termed "others" (Figure 3. 26), many of which correspond to cells with multiple nuclei and kinetoplasts (Figure 3. 29). This increase in ploidy mirrors the results obtained by DAPI staining (Figure 3. 26) and flow cytometry (Figure 3. 25), and such cells constitute about 23% and 40% of the total population at 18 hours post-induction, for clone 1 and clone 2, respectively. Inside this polyploid population, some cells present an invagination at their anterior end (Figure 3. 29, white arrows), indicating the beginning of the ingression of the cleavage furrow, while others seemed to attempt abscission (Figure 3. 29 right bottom panel). However, these cells are probably unable to complete cytokinesis, explaining the accumulation of cells with abnormal configurations.

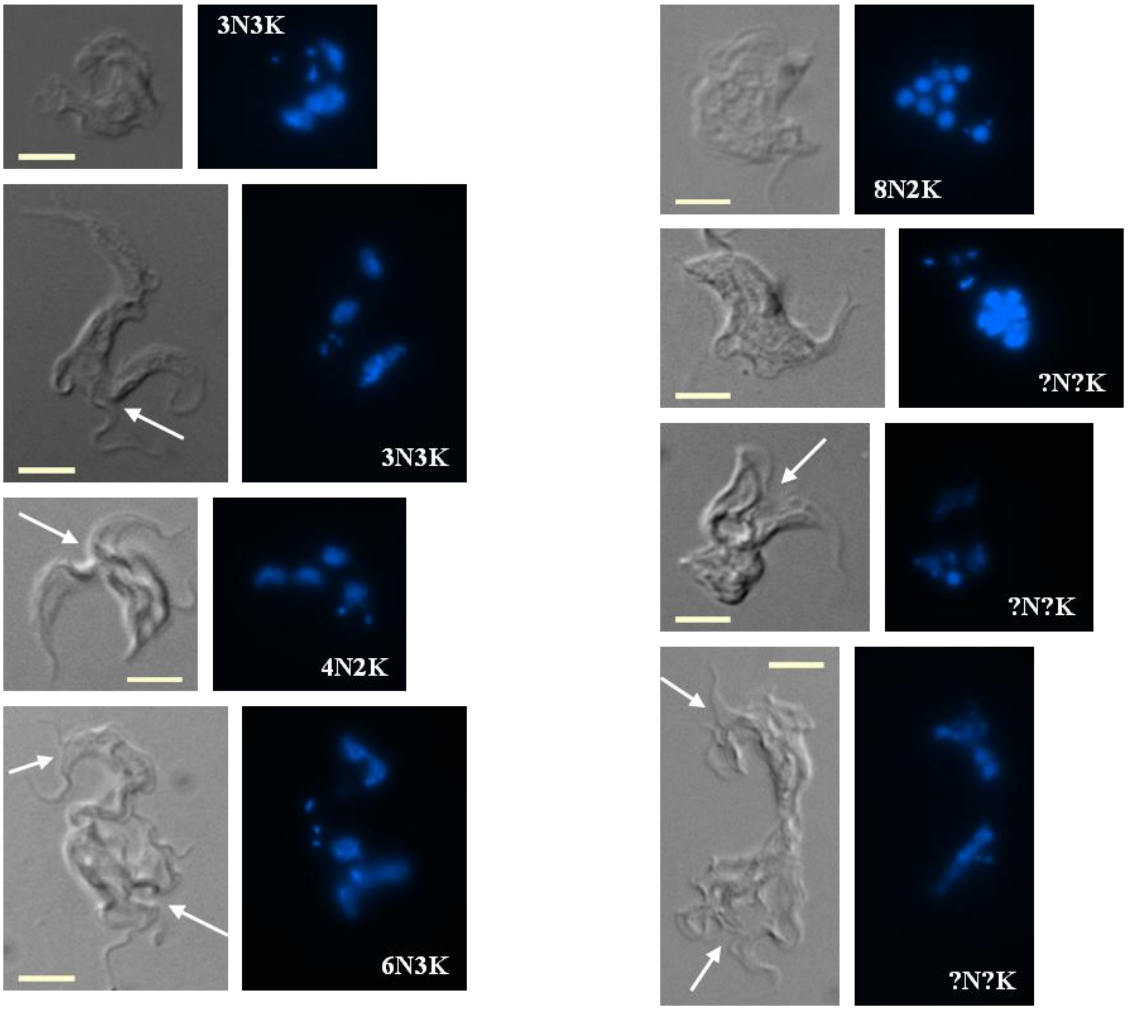

Figure 3. 29 – DAPI staining of multinucleate/kinetoplast cells visible at 18 hours post *CYC9* RNAi induction in the BSF. Left panels – DIC. Right panels – DAPI staining with nucleus (N)/kinetoplast (K) configuration indicated. Arrows point to cleavage furrows. Scale bars – 5 µm.

Results from this study prove that CYC9 acts as a cytokinesis regulator, inhibiting this cell cycle phase once depleted, causing a stall during furrow ingression and leading to accumulation of "monster" cells with multiple nuclei and kinetoplast. Its nuclear localisation suggests that CYC9's function as a cytokinesis regulator might come from controlling expression of genes involved in cytokinesis, rather than acting directly in cytokinesis control.

Although genomic analysis has allowed the identification of 10 CYCs in *T. brucei* (CYC2-11), functional investigations have only been achieved for a few of them, as RNA interference studies have not generated any noticeable phenotype for some regulators. In 2003, knockdown studies revealed the role of CYC2 and CYC6 in PCF

trypanosomes (Li and Wang, 2003), demonstrating that these two CYCs are essential for correct cell cycle progression in this life cycle stage. Such results arose from RNAi studies of 7 different CYCs in PCF trypanosomes, and only CYC2 and CYC6 caused growth arrest and detectable phenotypes. Flow cytometry and N/K configuration analyses demonstrated that CYC2 regulates the G1/S transition (Li and Wang, 2003). On the contrary, CYC6 seems to control the G2/M transition, and CYC6 depletion leads to a mitotic block in 90% of the cell population, after only 24 hours of tet induction (Li and Wang, 2003). CYC6's role as a mitotic regulator was further confirmed in BSF trypanosomes (Hammarton *et al.*, 2003a), although differences in cell cycle control between the two life cycle stages leads to different phenotypes, namely the existence of a mitosis/cytokinesis checkpoint in BSF trypanosomes (Ploubidou *et al.*, 1999, Hammarton *et al.*, 2003b). CYC2 was further investigated and in 2004 it was shown that it exhibited a similar function in progression through G1 phase in BSF (Hammarton *et al.*, 2004), although in this stage depletion of CYC2 did not influence cell morphology.

CYC9 is the first CYC to be demonstrated to have a role in cytokinesis. Although being grouped into different CYC classes (CYC2 and CYC6 are PHO80-like and mitotic-like CYCs, respectively, while CYC9 has been characterised as a transcriptional CYC) all these proteins seem to have roles as regulators of cell cycle progression, controlling different phases of cell division.

How CYC9's interacting kinase influences cell cycle progression was further investigated.

3.2.6. **CRK12 knockdown causes defects in endocytosis**

BSF *CRK12* RNAi cell lines were also analysed as to the effects of this knockdown on the cell cycle, by staining cells with DAPI (section 2.6.1) and analysing their N/K configuration and cytokinesis stage. In accordance with what was observed by flow cytometry, CRK12 depletion does not cause any cell cycle defect (Figure 3. 30), as N/K configurations remain more or less constant over the 18 hours of tet induction.

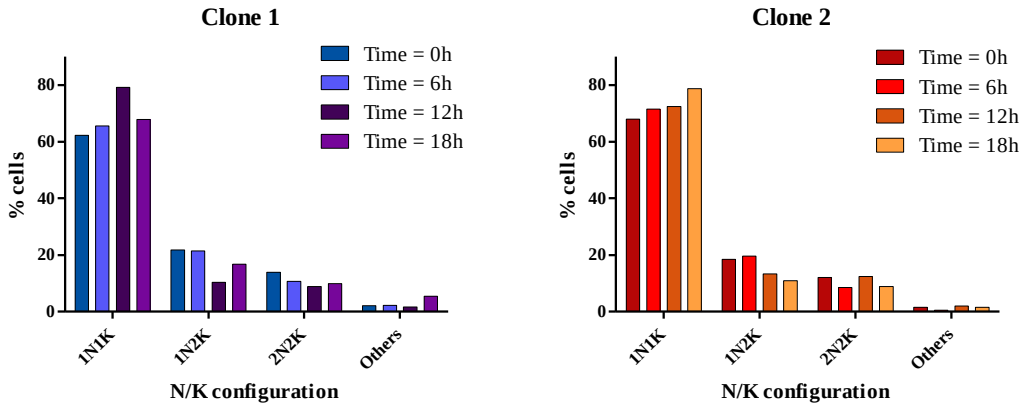

Figure 3. 30 - DAPI staining of BSF *CRK12* RNAi cell lines. Two independent clones (Clone 1 and Clone 2) were grown in tet, and at regular intervals, samples were taken and cells stained with DAPI. The nucleus (N) and kinetoplast (K) configurations of approximately 200 cells were determined for each time point.

A close analysis of 2N2K cells after 12 hours of CRK12 depletion revealed an intense shift in cytokinesis stage (Figure 3. 31). Cells that are stalled during abscission increase from 18% to approximately 57 % and from 16% to 60% for clone 1 and clone 2, respectively (Figure 3. 31 abscission). Such increase reflects the decrease in cells that have not yet started cell division (Figure 3. 31 no furrow), while the proportion of cells undergoing furrow ingression remains constant throughout the RNAi induction (Figure 3. 31 furrow ingression). Despite this, cells continue to divide normally as no abnormal N/K configurations appear and 1N1K cells continue to arise (Figure 3. 30), which allows us to conclude that CRK12 does not exhibit a major role as a cell cycle regulator. In fact, as BSF trypanosomes often start a new cycle before completing abscission, CRK12 depletion might lead to an increase in the proportion of these cells without subsequently preventing cell cycle progression.

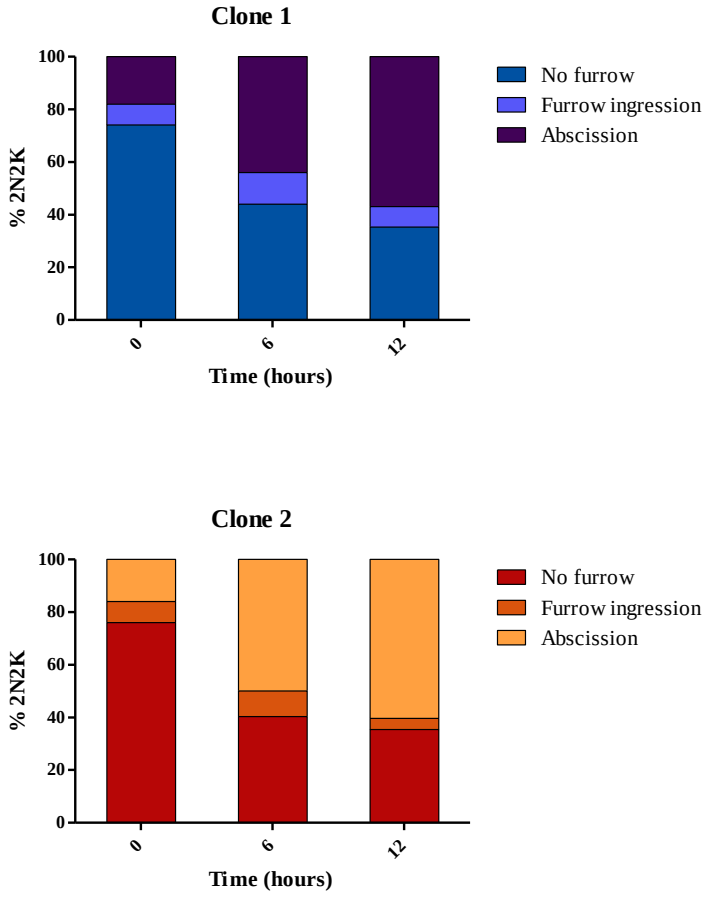

Figure 3. 31 - Analysis of the cytokinesis stage of 2N2K cells following depletion of CRK12 in BSF *T. brucei*. Approximately 50 cells were classified according to the absence (no furrow) or presence of a cleavage furrow (furrow ingression), or if they were undergoing abscission.

On the other hand, a thorough examination of DAPI stained cells disclosed a peculiar phenotype caused by CRK12 knockdown. Induced cells present defects in kinetoplast positioning in 1N2K (Figure 3. 32 panel A) and 2N2K (Figure 3. 32 panel B) cells, with the number of abnormal cells increasing over time (Figure 3. 33), being absent at time 0. Uninduced cells display a longitudinal arrangement of the two kinetoplasts along the axis of the cell (Figure 3. 32 – tet), while in abnormal cells, the kinetoplasts are positioned laterally (Figure 3. 32 + tet), and in some cells, concentrated at the tip of the cell (Figure 3. 32, cells marked with asterisks).

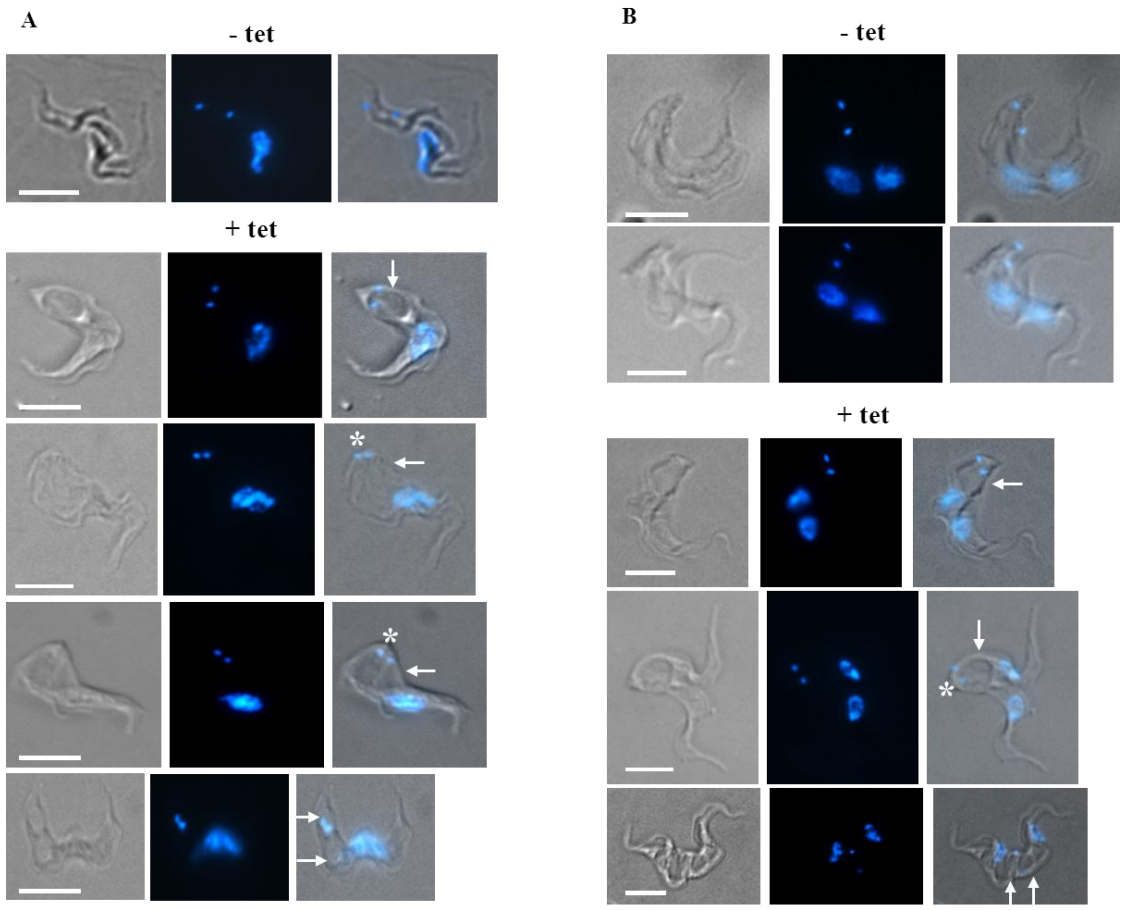

Figure 3. 32 - DAPI staining of BSF cells with enlarged FPs following CRK12 RNAi induction. For each clone, 50 1N2K (A) and 50 2N2K (B) cells from uninduced (- tet) and induced for 18 hours (+ tet) cultures were examined for the presence of enlarged FPs (indicated by arrows). Left panels – DIC; middle panels – DAPI; right panels – DIC/DAPI merge. Asterisks indicate cells where kinetoplasts are concentrated at the tip of the cell. N: nucleus; K: kinetoplast. Scale bars – 5 µm.

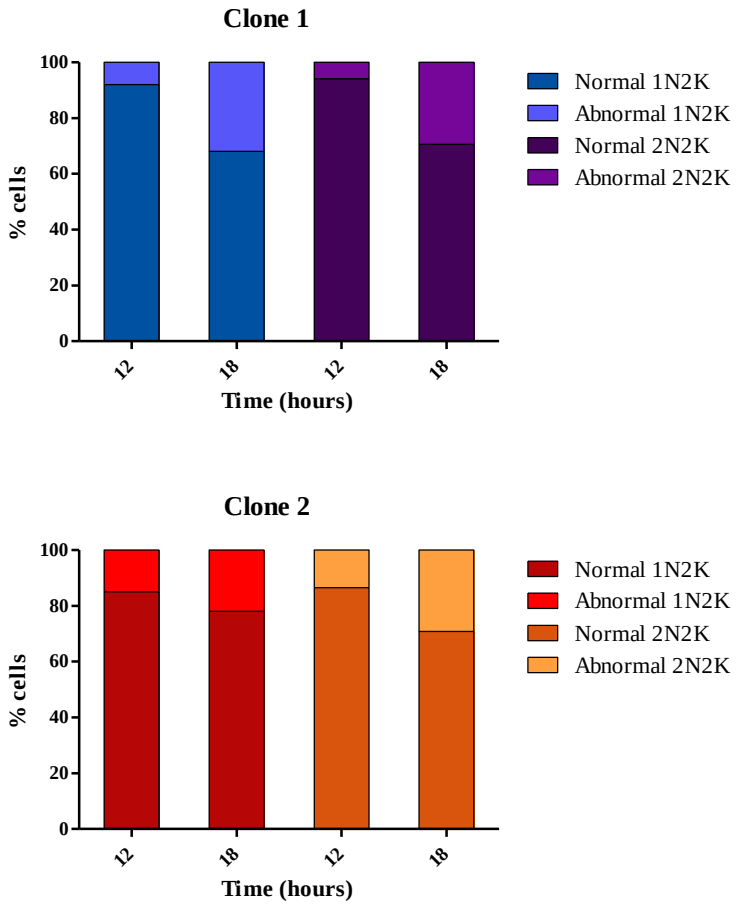

Figure 3. 33 – Quantification of abnormal kinetoplast positioning in 1N2K and 2N2K cells following induction of *CRK12* RNAi. Approximately 50 1N2K and 50 2N2K cells from two independent *CRK12* RNAi clones were analysed to determine the position of the kinetoplasts at 12 and 18 hours after tet induction. N: nucleus; K: kinetoplast.

After 18 hours of tet induction, abnormal 1N2K cells comprised an average of 27% of total 1N2K cells, while 30% 2N2K cells have abnormally positioned kinetoplasts (Figure 3. 33). This phenotype seems to result from an abnormally enlarged FP (Figure 3. 32 white arrows) that hinders their normal localisation, either pushing them to the tip of the cell or forcing them to remain laterally around the pocket. The number of cells with enlarged FPs increases over time after induction of RNAi, and although this phenotype is visible in some 1N1K cells, the enlargement is stronger and more frequently present in 1N2K and 2N2K cells. After 18 hours of tet induction, approximately 23% and 17% of 1N2K and 2N2K cells, respectively, possess an enlarged FP. The enlargement of the FP is also observed in electron micrographs

(Figure 3. 34), which correlates well with the presence of the enlarged vacuole located between the kinetoplast and nucleus in the DAPI staining cells observed (Figure 3. 32).

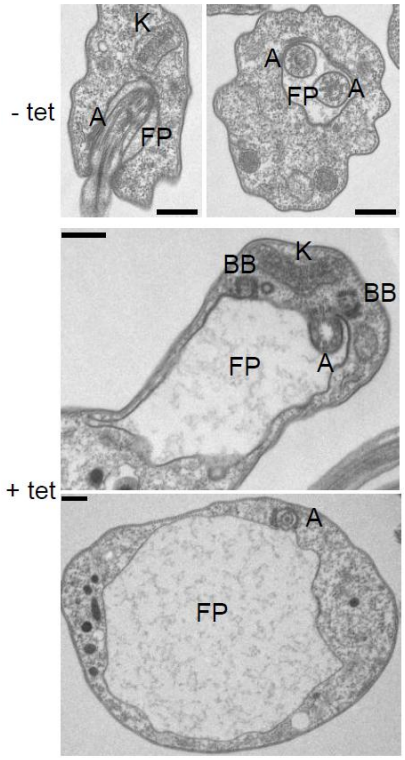

Figure 3. 34 – TEM images of FPs for uninduced (-tet) and induced (+tet) *CRK12* BSF RNAi cells. A – Axoneme; BB – basal body; FP – flagellar pocket; K – Kinetoplast. Scale bars - 500 nm.

Enlargement of the FP (also known as the "Big-eye" phenotype) has been associated with endocytosis defects (Allen *et al.*, 2003), where membrane delivery is not affected but removal is blocked, as the FP is the site of both endocytosis and exocytosis. To investigate if CRK12 depletion causes defects in endocytosis, general membrane uptake was followed by using a fluorescent lipophilic dye - FM4-64 (section 2.5.1), a reversible lipid-binding protein that associates with membranes and is therefore useful to show internalisation from the FP. Both at 4ºC and 37ºC, FM4-64 is taken up by uninduced cells (Figure 3. 35 left panels) and induced cells with no apparent deformation of the FP (Figure 3. 35 middle panels), while cells with enlarged FP present no signal (Figure 3. 35 right panels). In previous uptake assays with FM4-64 at 37ºC to analyse endocytosis defects in different RNAi cell lines (Allen *et al.*, 2003, Hall *et al.*, 2004a), uninduced cells take up the dye while cells with enlarged FP retain the dye in the FP (Allen *et al.*, 2003) or close to it (Hall *et al.*, 2004a), and do not internalise

it. In this study, the abnormal cells show a defect in endocytosis since FM4-64 is not internalised, but the fluorescent dye does not remain in the proximity of the FP (Figure 3. 35 right panels) probably due to diffusion of the compound when the cells are washed.

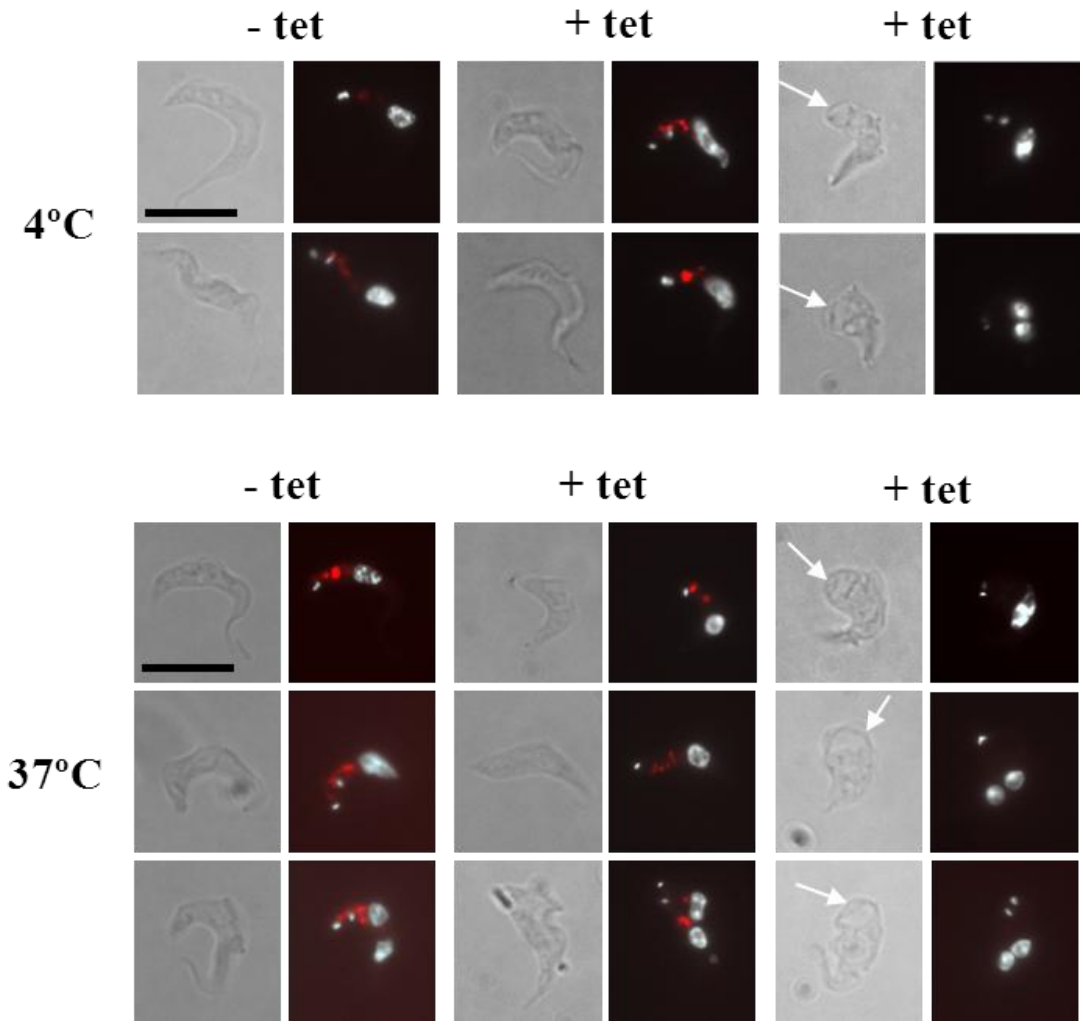

Figure 3. 35 – FM4-64 uptake assay using *CRK12* BSF RNAi cells. Uptake assays were performed at 4°C and 37°C using *CRK12* RNAi cells, which had been induced (+ tet) or not (- tet) with tet for 18 hours. Left panels – DIC; right panels –DAPI (white)/FM4-64 (red) merge. Arrows point to enlarged FPs. Scale bars – 10 µm.

As FM4-64 does not represent a naturally transported ligand for trypanosomes, Tf uptake was also investigated. In contrast to fluid-phase ligands and fluorescent lipid-binding proteins, Tf internalisation is receptor-mediated (Steverding *et al.*, 1995, Steverding, 2000), and use of fluorescently tagged transferrin allows receptor-linked

endocytosis to be followed (section 2.5.2). Uptake of AF594-transferrin at 37ºC is impaired by CRK12 depletion, whether the cell displays an enlarged FP or not (Figure 3. 36). AF594-transferrin remain in the FP, even in cells exhibiting FP enlargement (Figure 3. 36 +tet), which suggests that CRK12 knockdown blocks receptor-linked endocytosis.

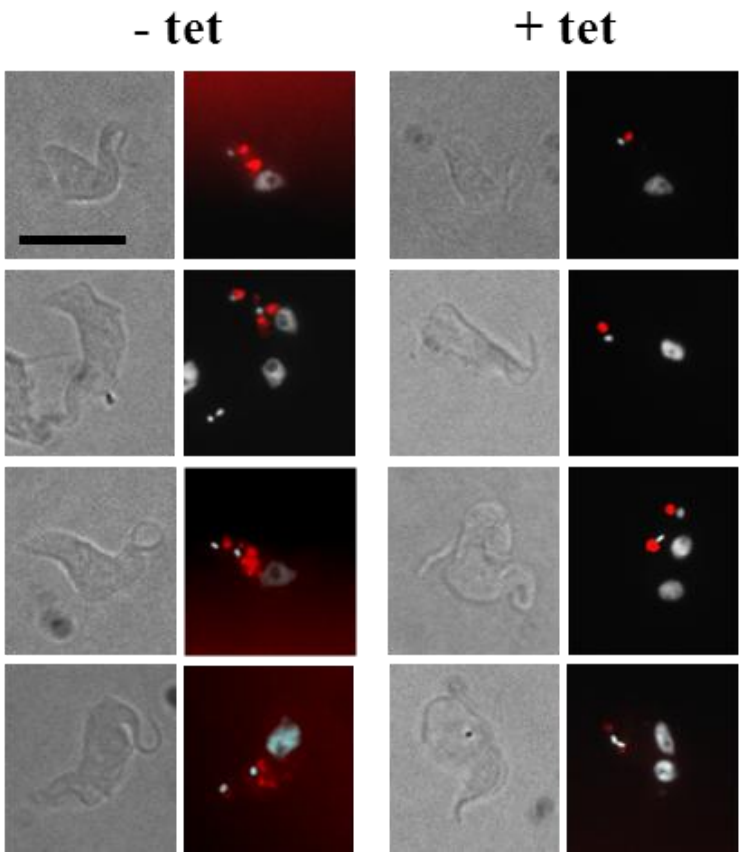

Figure 3. 36 – AF594-transferrin uptake assay using *CRK12* BSF RNAi cells. Uptake assays were performed at 37°C using *CRK12* RNAi cells, which had been induced (+ tet) or not (- tet) with tet for 18 hours. Left panels – DIC; right panels –DAPI (white)/AF594-transferrin (red) merge. Scale bars – 10 µm.

The big-eye phenotype was first observed upon depletion of TbCLH heavy chain (Allen *et al.*, 2003). TbCLH depletion in BSF induces rapid lethality and FP enlargement, and endocytosis is undetectable after 16 hours of RNAi induction, as determined by uptake of FM4-64 (Allen *et al.*, 2003). In contrast with the big-eye phenotype, TbCLH depletion in PCF trypanosomes causes morphological alterations, such as general round up of cells, internal accumulation of vesicles in the cytoplasm observed by EM, and changes in lysosomal trafficking (Allen *et al.*, 2003). A similar

role for CRK12 in PCF was not established, as its depletion did not cause any cell growth defect (Gourguechon and Wang, 2009).

Other proteins have been determined to have a role in endocytosis in trypanosomes (García-Salcedo *et al.*, 2004, Hall *et al.*, 2004a, Hall *et al.*, 2004b). Comparable results to CRK12 were obtained with knockdown of Rab5 proteins (Hall *et al.*, 2004a), where receptor-mediated but also fluid-phase endocytosis are affected by Rab5 depletion in BSF, causing simultaneously mislocalisation of endosomal markers, a decrease in CLH levels and accumulation of the latter around the FP as seen by IFA (Hall *et al.*, 2004a). In contrast, Rab4 depletion inhibits cell growth and causes endocytic defects, blocking liquid-phase transport but not affecting uptake and recycling of transferrin (Hall *et al.*, 2004b). In contrast to CRK12, TbRab4 is involved in regulation of fluid-phase traffic to the lysosome, but not receptor-mediated endocytosis.

Our results suggest that CRK12 depletion prevents receptor-linked endocytosis but also internalisation of lipophilic dyes in cells with abnormally enlarged FPs. It is the first time that a CRK has been associated with regulation of endocytosis. CRK12 might regulate gene expression of endocytic regulators or phosphorylate directly a protein with functions in the endocytic pathway, and thus affect indirectly the uptake and recycling through the FP. As mentioned in section 1.3.2, endocytosis is related to host immune evasion (Barry, 1979, Field and Carrington, 2009, Natesan *et al.*, 2011). As such, the disruption of the endocytic apparatus might affect the ability of *T. brucei* to sustain an infection in the mammalian host. The lower ability of induced *CRK12* RNAi cell lines to sustain an infection in a mouse model demonstrates that CRK12 is essential for cell proliferation *in vivo* (Monnerat *et al.*, 2012). Such data could be related to the direct endocytic defect caused by CRK12 depletion.

In contrast with CRK12's function in endocytosis, its CYC partner, CYC9, has a role in regulating the *T. brucei* cell cycle. A possible explanation, which might also explain why CYC9 presents different functions in the two life cycle stages, is the fact that both proteins might interact with additional partners. Such additional partners might have different functions and their dominant roles could mask CYC9 or CRK12's role in endocytosis or cell cycle regulation, respectively, which would be affected distinctly by the individual RNAi knockdowns. On the other hand, their roles might be compensated

by other proteins upon their absence. This would mean that CYC9 could indeed function as an endocytic regulator and CRK12 might act in cell cycle control, but when depleted these functional roles would be replaced by other proteins and only the phenotype which does not show functional redundancy is visible. Alternatively, and considering that both proteins might regulate both pathways, the protein level necessary to perturb the different functions for each protein might be distinctive and knockdown might reveal only the function which requires a lower protein threshold level.

During this study a novel CRK:CYC complex was identified and RNAi individual knockdown studies have proved each protein to be essential for cellular proliferation *in vitro*. New information was provided on cell cycle regulation, while for the first time a CRK was proved to be involved in regulation of a biological pathway, in this case endocytosis.

3.3. MITOSIS AND CYTOKINESIS ANTIBODIES: PROJECT AIMS

Regulation of cell cycle in *T. brucei* is known to be dependent on many different proteins; however most regulators remain unidentified. In an attempt to identify new mitosis and cytokinesis regulators, parasite populations were synchronized in each of these cycle phases, and antibodies were generated against cytoskeleton proteins expressed in these two phases. Generation of MAbs was performed not by using recombinant proteins, but instead by immunising mice with samples containing unknown antigens from the cytoskeleton fraction of BSF cells. Similar techniques were used in 2008, where authors used flagellar extracts of PCF cells to generate a library of MAbs recognising different elements within the flagellum (Bonhivers *et al.*, 2008a). In this study, cytoskeleton samples of BSF cells were used to immunise mice, similarly to what was done previously in 1989 (Woods *et al.*, 1989), where authors discovered novel probes for different structures within the cytoskeleton. This report will focus on:

- Analysis of cell cycle synchronization
- Production of MAbs against potential proteins upregulated during mitosis and/or cytokinesis

3.3.1. **Cell cycle synchronization**

New methods for *T. brucei* synchronization have been developed recently (Chowdhury *et al.*, 2008, Forsythe *et al.*, 2009), using HU to block dNTP synthesis by inhibiting the enzyme ribonucleotide reductase, and thus stall DNA replication. Such a method allows synchronization of cells during S-phase, and removal of HU induces cells to continue division in a synchronous way for one population doubling time. In theory, parasite populations could be enriched at different cell cycle stages to enable regulatory analyses. This comprises the basis of this project, where pure parasite populations synchronized at mitosis or cytokinesis were used to develop MAbs against cytoskeleton proteins expressed in each cell cycle phase.

Before *T. brucei* synchronization, a growth curve was performed for each life cycle stage to guarantee they were growing at the correct doubling time: 12 hours for PCF (Chowdhury *et al.*, 2008) and 6 hours for BSF (Forsythe *et al.*, 2009). Cells of each life cycle stage were then grown in the presence of HU and cell cycle progression was analysed every two hours by flow cytometry (section 2.2.6) and DAPI staining (section 2.6.1). When needed, intermediate samples were taken. Initial tests were performed with PCF trypanosomes (Figure 3. 37 and Figure 3. 38).

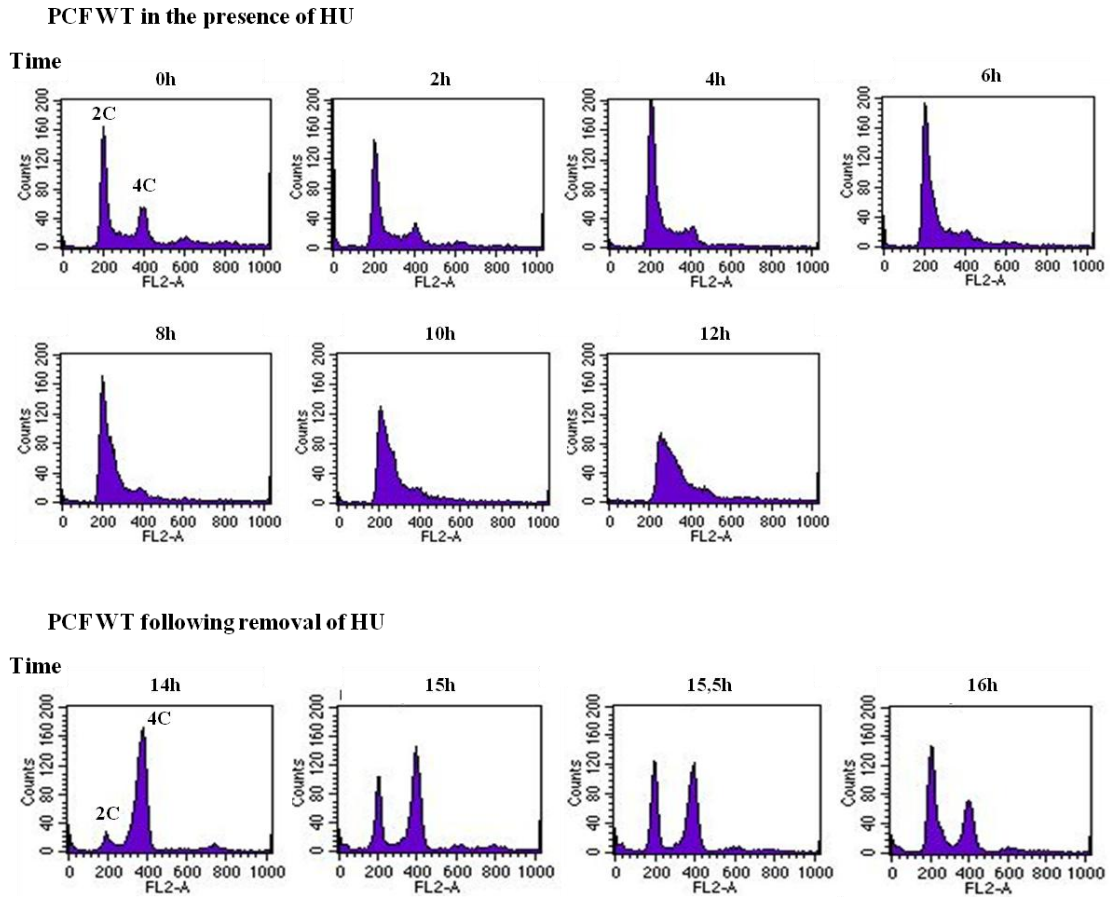

Figure 3. 37 - Flow cytometry profiles of PCF WT cell line, grown in the presence of HU for 12 hours. Cells were grown in medium containing 0.2 mM HU for their doubling time (12 hours), after which cells were allowed to grow in fresh media without HU. Samples were taken for analysis of DNA content; flow cytometry histograms represent cell counts (y-axis) versus fluorescence (FL2A; x-axis).

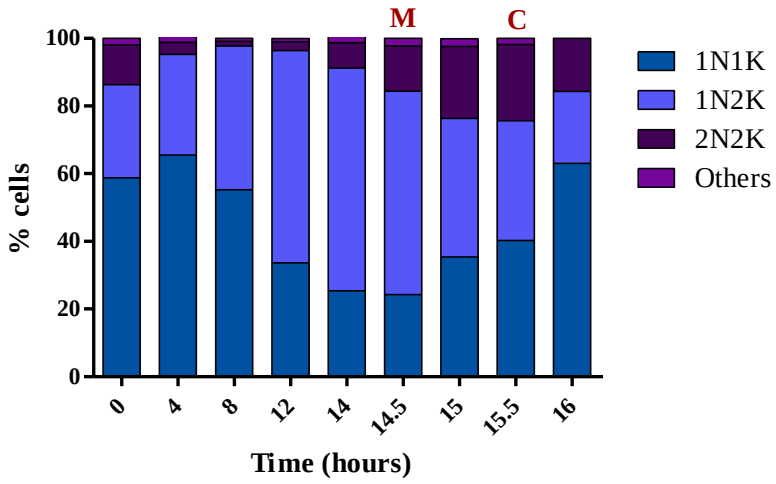

Figure 3. 38 - N/K configuration analysis of PCF WT cells treated with HU. PCF WT cells were grown in the presence of HU for 12 hours, after which HU was removed by centrifugation and cells allowed to grow in fresh medium. Samples were taken and stained with DAPI at the time points indicated, and the nucleus (N)/kinetoplast (K) configurations of ~ 200 cells per timepoint were determined. Others refers to cells with abnormal N/K configuration, while M and C refer to the optimal timepoint to obtain populations enriched for cells in mitosis and cytokinesis, respectively.

Before the addition of HU, a typical flow cytometry profile is observed (Figure 3. 37 time 0 h). This is also consistent with the N/K configuration data (Figure 3. 38), where approximately 60% of cells have one nucleus and one kinetoplast, and 20% have undergone kinetoplast but not nucleus segregation. During synchronization with HU (the first 12 hours), the 2C and 4C peaks decrease gradually, correlating with a clear decrease of 2N2K and 1N1K cells as observed by DAPI staining. The 2C peak shifts gradually to the right until it assumes a central position, consistent with a block in S-phase. Nuclear segregation does not occur and thus virtually no 2N2K cells are present after 12 hours (Figure 3. 38), and consequently no cellular division occurs, thus explaining the decrease in 1N1K cells (Figure 3. 38). Optimal synchronization is obtained after 12 hours of incubation with HU, as described previously (Chowdhury *et al.*, 2008), as previous time points contained mixed populations of cells in G1 and S-phase. At this time point, most of the cells contain an intermediate DNA content (Figure 3. 37), and an average of 60% of the population is 1N2K cells (Figure 3. 38).

After HU removal, there is a progressive appearance of other forms and cells divide in a more or less synchronous manner (Chowdhury *et al.*, 2008, Forsythe *et al.*, 2009). In general, removal of the HU allows the accumulated 1N2K cells to proceed to nuclear division, causing the appearance of 2N2K cells/increase in the 4C peak (Figure 3. 37 and Figure 3. 38), which later on divide generating new 1N1K cells/increase in the 2C peak (Figure 3. 37 and Figure 3. 38).

Between hours 14 and 15 of HU addition, 2N2K cells more than double in number (Figure 3. 38), which means that the population began to undergo mitosis between these time points. Additionally, 1N1K cells increase drastically between hours 15 and 16 of HU addition (Figure 3. 38), indicating that the cells have divided and re-entered G1-phase. For optimization of the time point at which we could find enriched populations for cells undergoing mitosis and cytokinesis, intermediate samples were analysed. Taking into consideration the flow cytometry profiles following HU removal and the N/K configurations, the optimal time point to obtain populations enriched in cells undergoing mitosis and cytokinesis is judged to be 14 ½ hours (Figure 3. 38 "M") and 15 ½ hours (Figure 3. 38 "C") after HU addition, with removal at 12 hours, respectively.

Synchronization at S-phase for BSF trypanosomes occurs when cells are grown for 6 hours in the presence of HU (Forsythe *et al.*, 2009). Similarly, results were obtained for synchronization of BSF trypanosomes (Figure 3. 39 and Figure 3. 40).

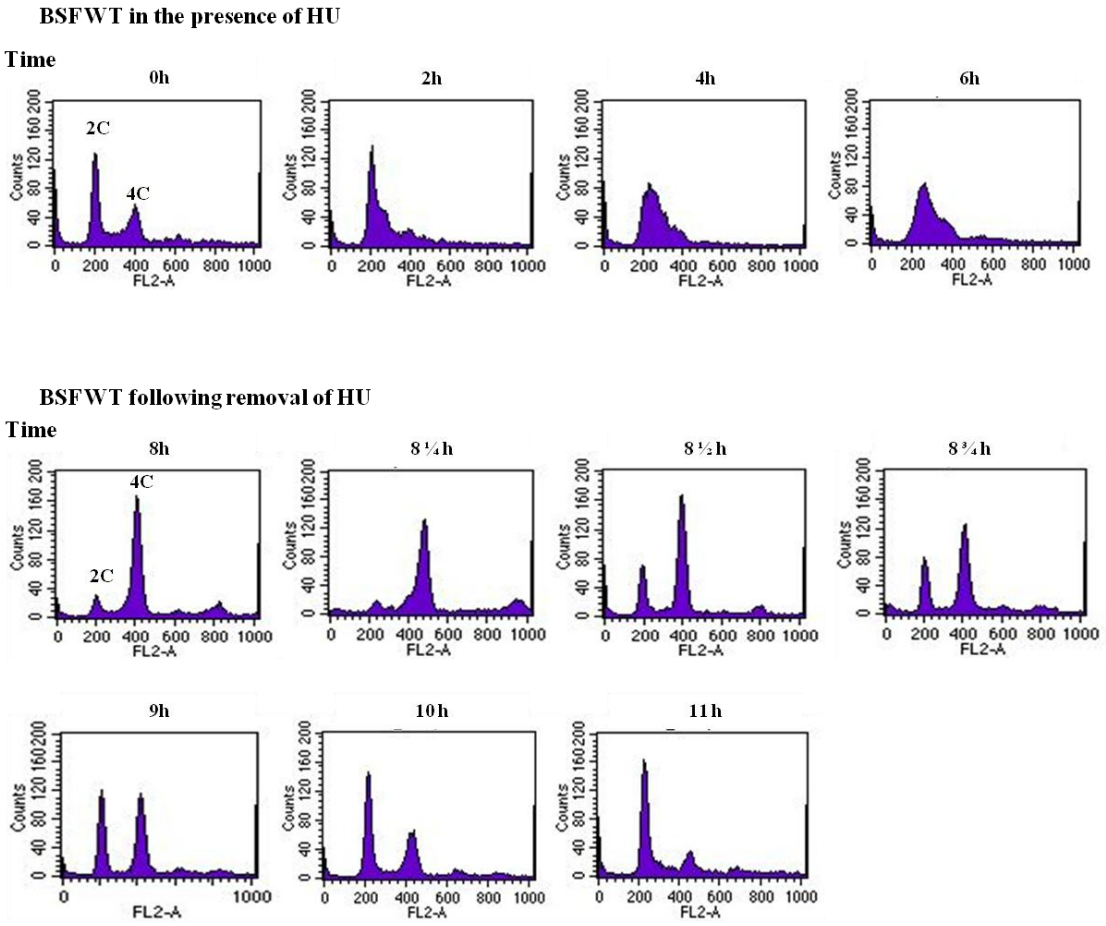

Figure 3. 39 - Flow cytometry profiles of BSF WT cell line, grown in the presence of HU for 6 hours. Cells were grown in medium containing 0,2 mM HU for their doubling time (6 hours), after which cells were allowed to grow in fresh media without HU. Samples were taken for analysis of DNA content; flow cytometry histograms represent cell counts (y-axis) versus fluorescence (FL2A; x-axis).

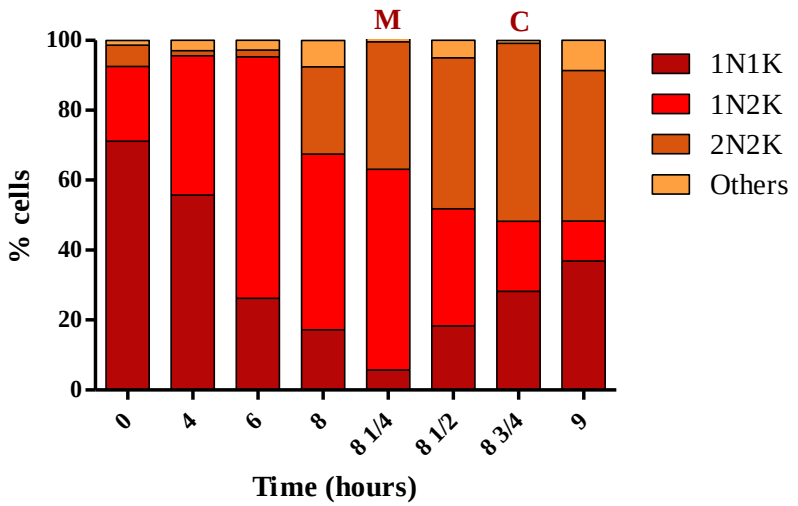

Figure 3. 40 - N/K configuration analysis of BSF WT cells treated with HU. BSF WT cells were grown in the presence of HU for 6 hours, after which HU was removed by centrifugation and cells allowed to grow in fresh medium. Samples were taken and stained with DAPI at the time points indicated, and the nucleus (N)/kinetoplast (K) configurations of ~ 200 cells per timepoint were determined. Others refers to cells with abnormal N/K configuration, while M and C refer to the optimal timepoint to obtain populations enriched for cells in mitosis and cytokinesis, respectively.

Similarly to PCF, removal of HU forces cells to progress through the cell cycle in a synchronous way, as cell growth in fresh medium allows the cells stalled in S-phase to replicate, and later on to undergo cytokinesis. Data analysis of flow cytometry profiles (Figure 3. 39) in conjunction with what is observed by DAPI staining (Figure 3. 40) allowed the identification of mitosis and cytokinesis time points: hour 8 ¼ (Figure 3. 40 "M") and 8 ¾ (Figure 3. 40 "C"), respectively, after the addition of HU at time 0 h and removal at time 6 h.

3.3.2. **Production of MAbs against cytoskeleton proteins expressed during mitosis and cytokinesis in BSF trypanosomes**

With the aim of producing MAbs against cytoskeleton proteins expressed during each phase, $1x10^9$ BSF cells were grown in 0.2 mM HU for 6 hours, and cytoskeleton fractions of populations synchronized in mitosis and cytokinesis were purified (section

2.2.8). Considering that many proteins are expressed during these phases and that antibody production could be directed to the more immunogenic ones, a more thorough analysis would be possible if proteins were separated by size. Consequently, samples were electrophoresed through a 10% polyacrylamide gel (section 2.4.5 and 2.4.6) and analysed for differences between the cytoskeleton of an asynchronous population (Figure 3. 41 lane 1) and those of populations synchronized in mitosis (Figure 3. 41 lane 2) and cytokinesis (Figure 3. 41 lane 3). Although only one distinctive band appeared to show a stronger signal in the mitosis synchronized cytoskeleton (Figure 3. 41 lane 2, indicated in purple), the remaining cytoskeleton preparations were electrophoresed through different polyacrylamide gels (section 2.4.5) and slices cut according to the molecular weight (Table 2. 4). A total of 9 slices were cut for each synchronized cytoskeleton preparation, but only 3 were analysed due to time limitations (Figure 3. 41). The section of the gel containing proteins of 40-60 kDa was neglected (Figure 3. 41) which contains α–tubulin (~ 50 kDa) and as such could interfere with antibody production.

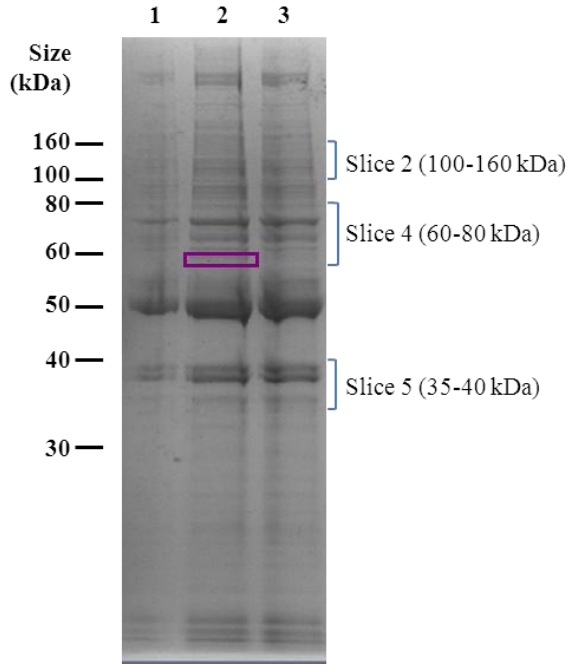

Figure 3. 41 – Cytoskeleton protein samples of BSF WT. Samples obtained after cytoskeleton purification of an asynchronized population (lane 1) and synchronized in mitosis (lane 2) and cytokinesis (lane 3) were separated on a 10% polyacrylamide gel. Slices containing the cytoskeletons of mitosis and cytokinesis populations were cut according to their size and some were used for antibody production (indicated in blue). Purple box – band at approximately 60 kDa with stronger signal in mitosis. Ladder – BenchMark protein ladder.

The insolubility of cytoskeleton proteins makes them impossible to produce as recombinant samples for injection or even to use for screening by ELISA. As an alternative, the gel slices were frozen in liquid nitrogen and ground up (section 2.7.1), and injected directly into the mice with the help of PBS. An average of 3 to 4 injections were given of each sample per mouse before the mice were sacrificed and hybridomas were produced (section 2.7.3). Five mice were sacrificed, each injected with a different polyacrylamide gel slice (Table 3. 4).

Table 3. 4 – Identification of the different fusions performed during this study, using mitosis and cytokinesis cytoskeleton samples for immunisation of Balb/c mice.

Fusion ID	Synchronized culture used for injection	Protein weight interval (kDa)
M5	Mitosis	35 to 40
C5	Cytokinesis	35 to 40
M4	Mitosis	60 to 80
C4	Cytokinesis	60 to 80
M2	Mitosis	100 to 160

As no screening was possible using the supernatants from 96 well plates, the hybridomas were transferred to 24 well plates (section 2.7.4) to allow the production of enough supernatant and consequently screen by WB (section 2.7.7). Supernatants were screened against cytoskeleton preparations of cultures synchronized in the respective cell cycle phase (Figure 3. 42) and considered positive when recognising proteins within the expected molecular weight or outside the expected range but with a distinct or specific signal.

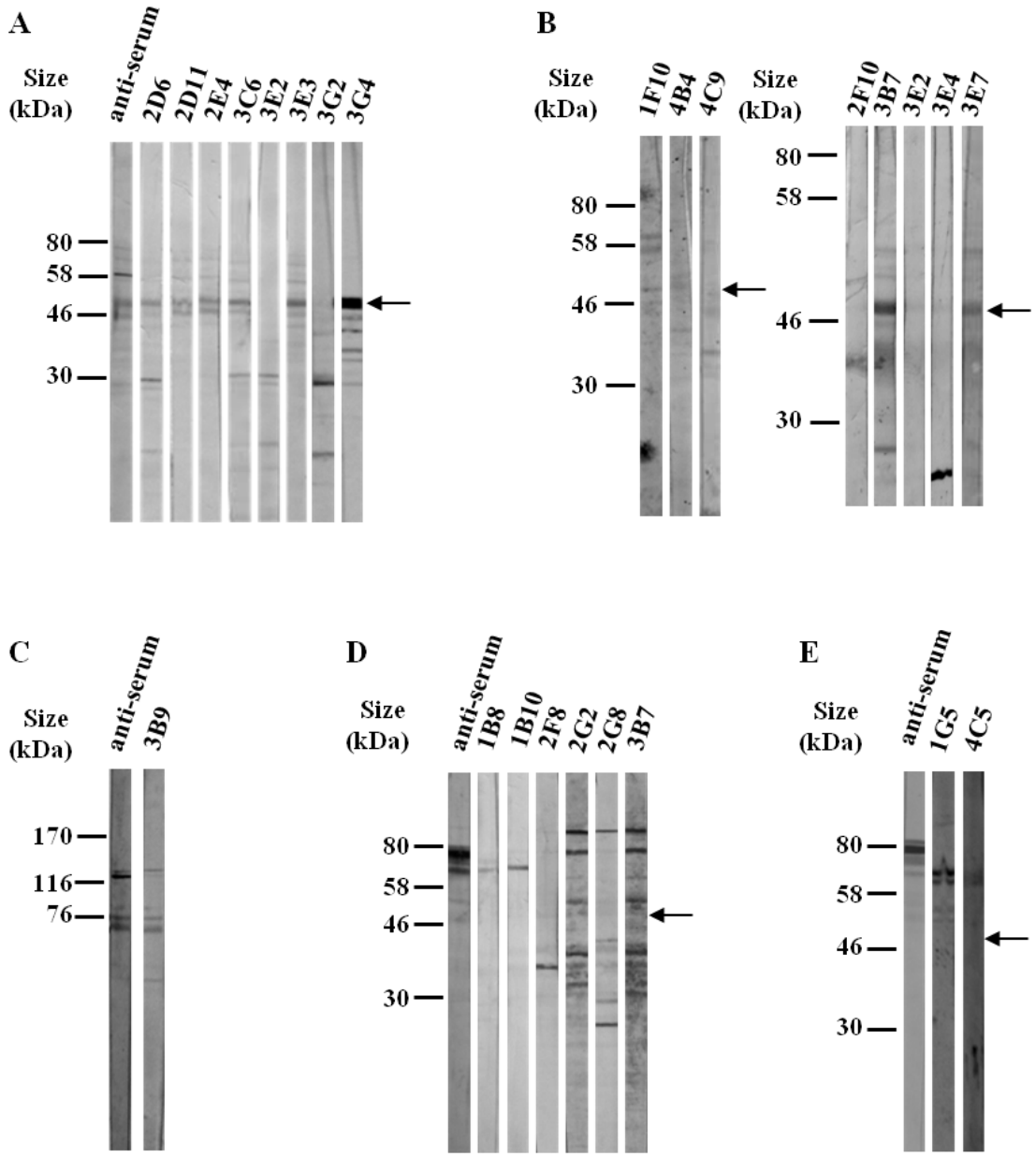

Figure 3. 42 - WB analysis of antibodies generated against proteins expressed during mitosis and cytokinesis. Cytoskeleton samples of asynchronous and synchronized cultures ($2x10^6$ cells/lane) in mitosis or cytokinesis were used for screening of MAbs, according to the cell cycle phase the antibodies were directed against. A – M5 fusion (35-40 kDa); B – C5 fusion (35-40 kDa); C – M2 fusion (100-160 kDa); D – M4 fusion (60-80 kDa); E – C4 fusion (60-80 kDa). The identity of each antibody is indicated at the top of each lane. For all screening, the antibodies were used neat and the antiserum obtained from the sacrificed mouse's blood was diluted 1:10,000. The secondary antibody used was an AP-conjugated anti-mouse polyvalent IgG+IgM+IgA antibody, and a broad range pre-stained protein marker (7 – 175 kDa, NEB) was used to check protein size, except in C where the Amersham HMW calibration kit (Invitrogen) was used. Arrows point to possible α-tubulin bands.

The fusion efficiencies ranged from 5% to 19% (Table 3. 5), within the range of what was calculated for α-CRK12 antibodies when considering the 96 well plates

results (Table 3. 3 – 17% efficiency). It is necessary to take into account that development of these WBs was performed with an alkaline-phosphatase kit, and thus appearance of bands for supernatants containing low amounts and/or low affinity antibody, could have been interrupted by blocking the reaction too soon. The presence of highly immunogenic proteins besides tubulin affects antibody production, as different antibodies from distinct hybridoma cultures recognise bands with the same size (Figure 3. 42).

Table 3. 5 – Results from WB screening of mitosis and cytokinesis antibodies against cytoskeleton extracts. Cytoskeleton extracts of BSF WT cell lines synchronized in either mitosis or cytokinesis were used to screen hybridoma supernatants from 24 well plates by WB. Supernatants were deemed to be positive if recognising proteins within the expected molecular weight or outside the expected range but with a distinct or specific signal. The efficiency of antibody production is presented as a ratio of the positive results to the total number of supernatants tested.

Fusion ID	No. supernatants tested from 24 well plates	No. positive supernatants by WB
M5	198	10
Efficiency*		5%
C5	156	12
Efficiency*		8%
M4	175	23
Efficiency*		19%
C4	206	25
Efficiency*		12%
M2	139	11
Efficiency*		8%

*- calculated as Efficiency= $\frac{\text{Positive sup.}}{\text{Sup. tested}} \times 100$.

The data presented consists of a representation of all the 81 antibodies tested and considered positive. One fact to take into account is that some MAbs and antiserum recognise a band at approximately 50 kDa, which could correspond to the parasite's tubulin (Figure 3. 42 - arrow). Although the polyacrylamide slice containing this protein was rejected, the above and below slices (number 4 and 5 respectively) might have included a small amount of tubulin and thus could have interfered with antibody production against cell cycle regulated proteins due to tubulin's high immunogenicity.

The mitosis 5 (35-40 kDa) fusion generated 10 positive hybridomas (Table 3. 5), some of which are quite distinct (3E2 and 3G2) as they show more specificity towards a

band of the expected size and less cross-reaction (Figure 3. 42 panel A). On the contrary, the antibody identified as 3G4 recognises a particular pattern of proteins with different sizes, ranging from 30 to 60 kDa, but has a strong signal just below 58 kDa which could correspond to *T. brucei* tubulin (Figure 3. 42 panel A). Antibodies directed towards cytokinesis proteins within the same range of sizes (Cytokinesis 5) show similar signals towards proteins around 50 kDa, while some like 4C9 seem to recognise specifically a 35 kDa protein (Figure 3. 42 panel B).

One fusion was performed using proteins with sizes between 100 and 160 kDa, from a mitotic synchronized population (M2), yielding 11 positive hybridomas (Table 3. 5). The most interesting supernatant (3B9) shows a pattern similar to the antiserum (Figure 3. 42 panel B), recognising two proteins with ≈ 116 kDa, cross-reacting however with smaller proteins of ≈ 70 kDa. As opposed to 3B9, the antiserum recognises the lower 116 kDa band with higher intensity.

The final hybridomas were produced with cytoskeleton proteins ranging from 60 to 80 kDa, from both mitosis (M4) and cytokinesis (C4) synchronized parasite populations. The M4 and C4 anti-sera recognise bands with different intensities within the desired molecular weight range (Figure 3. 42 panel D and E), while some generated antibodies from C4 recognise proteins with ≈ 60 kDa and once more show cross-reaction with other proteins (Figure 3. 42 panel E). The M4 antibodies give peculiar signals (Figure 3. 42 panel D), as some supernatants like 2G2, 2G8 and 3B7 show very heterogeneous patterns when comparing with others; and for example 2F8 presents what looks like a single band at approximately 35 kDa.

Hybridoma cell stocks (section 2.7.4) were prepared for all positive hybridomas prior to further screening.

3.3.3. **Classification of the cell cycle specificity of the generated antibodies**

Considering that the aim of this project was to analyse mitosis and cytokinesis regulators, further classification of the generated antibodies consisted of examining their specificity towards each cell cycle phase. As a total of 81 supernatants remained after

the initial screen, a more adequate approach was to categorize them first by dot-blotting and analyse the more promising ones by IFA and WB. One important feature to take into consideration is that some supernatants seem to have a mix of different isotypes/antibodies, sometimes displaying distinct results. In these cases, the antibodies are not monoclonal, although all supernatants during this project are referred to as MAbs.

Dot-blot analysis simplifies classification of antibodies, as fewer cells are used ($4x10^5$ cells as opposed to $2x10^6$ for WB; section 2.4.8), samples are applied directly to a nitrocellulose membrane without needing electrophoresis or transfer systems, and results allow a fast classification of antibodies according to the samples they recognise more strongly. For each antibody, cytoskeleton preparations from asynchronous, synchronized in mitosis and synchronized in cytokinesis cultures were allowed to dry onto the membrane, and MAbs were incubated with the three samples simultaneously. Results for the supernatants with more promising features are represented in Figure 3. 43.

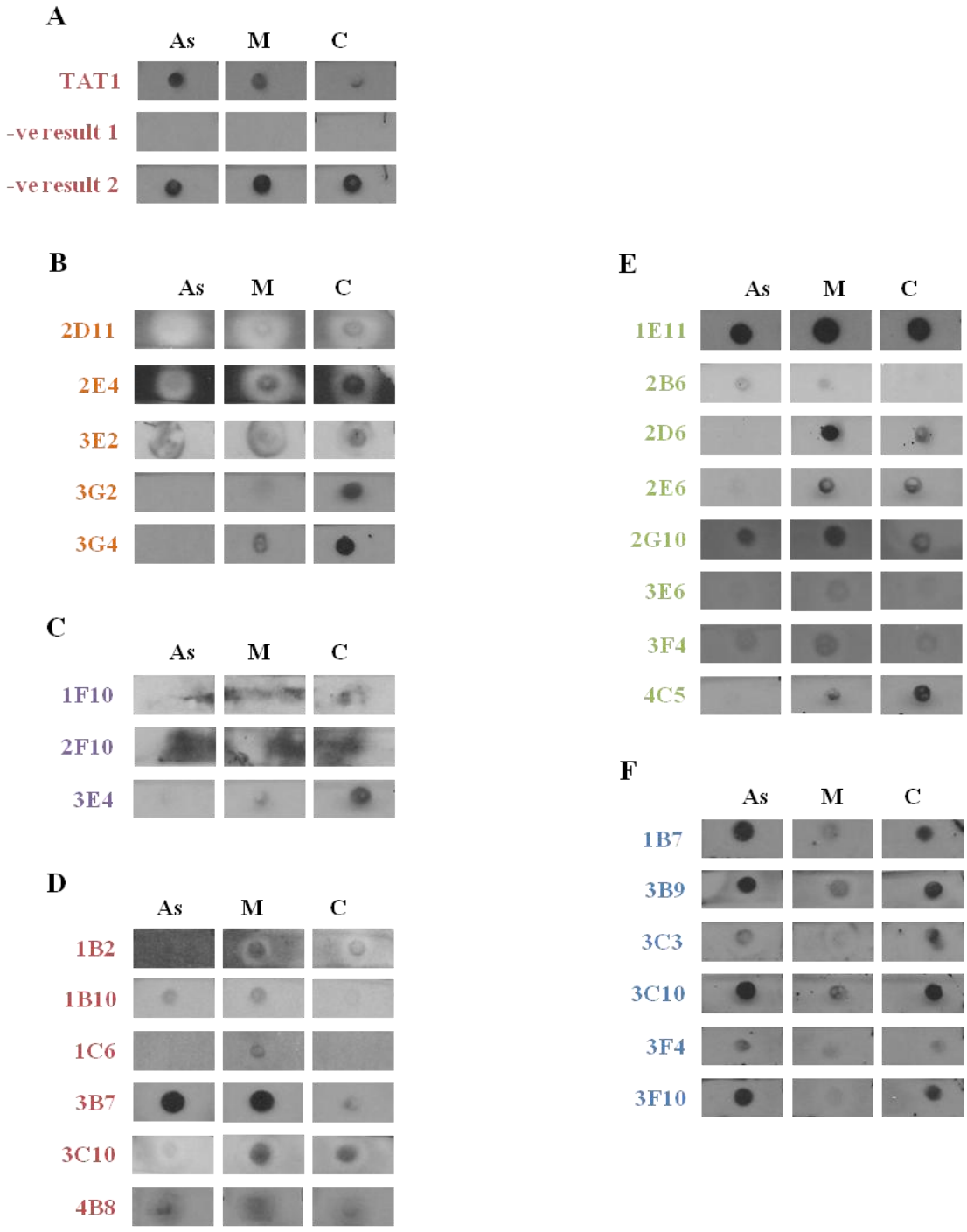

Figure 3. 43 - Characterisation of the generated antibodies using mitotic and cytokinetic synchronized populations. Supernatants were screened by dot-blot against cytoskeleton preparations from *T. brucei* BSF cells ($4x10^5$ cells per dot) from asynchronous (As), synchronized in mitosis (M) and synchronized in cytokinesis (C) populations. Primary antibodies were used neat (except for TAT1) and an anti-mouse IgG+IgM HRP conjugated secondary antibody was used. A –Positive control using TAT1 antibody (against α-tubulin) and two examples of typical negative results; B-F: dot-blots of antibodies showing differential signals for the different cytoskeleton populations. B: –antibodies directed against mitotic proteins with 35 to 40 kDa (M5); C: antibodies directed against cytokinetic proteins with 35 to 40 kDa (C5); D –antibodies directed against mitotic proteins with 60 to 80 kDa (M4); E –antibodies directed against cytokinetic proteins with 60 to 80 kDa (C4); F –antibodies directed against mitotic proteins with 100 to 160 kDa (M2).

Categorization of antibodies was performed considering the intensity of the signal Supernatants without any signal, those recognising all samples with similar intensity and those recognising the asynchronous sample with higher affinity (Figure 3. 43 panel A) were rejected. As a positive control, anti α–tubulin antibody (TAT1, (Woods *et al.*, 1989)) was used (Figure 3. 43 panel A). Results for all individual supernatants are summarized in Figure 3. 43 and Table 3. 6.

Table 3. 6 – Classification of distinct MAbs according to the cell cycle phase specificity. Antibodies were classified by dot-blotting according to the cytoskeleton sample recognised most strongly (As – asynchronous; M – Mitosis; C – Cytokinesis).

MAb ID	Dot-blot results	MAb ID	Dot-blot results
M5-2D11	C	M4-1B2	M
M5-2E4	C	M4-1B10	As / M
M5-3E2	C	M4-1C6	M
M5-3G2	C	M4-3B7	M
M5-3G4	C	M4-3C10	M / C
C5-1F10	C	M4-4B8	As / M
C5-2F10	C	C4-1E11	M / C
C5-3E4	C	C4-2B6	As / M
M2-1B7	As / C	C4-2D6	M / C
M2-3B9	As / C	C4-2E6	M / C
M2-3C3	C	C4-2G10	M
M2-3C10	As / C	C4-3E6	M
M2-3F4	As / C	C4-3F4	M
M2-3F10	As / C	C4-4C5	C

The TAT1 MAb (Woods *et al.*, 1989) was similarly generated to the MAbs in this study, using salt extracted cytoskeletons of a *T. brucei* PCF culture. This antibody recognises total α-tubulin, which comprises tyrosinated, detyrosinated and acetylated α –tubulin. Immunolocalisation studies using the TAT1 antibody reveal a similar distribution to acetylated α –tubulin (Woods *et al.*, 1989), which displays an intense fluorescent and homogeneous signal throughout the cell body, remaining constant over the cell cycle (Sasse and Gull, 1988). In contrast, tyrosinated α –tubulin fluorescence is cell cycle dependent (Sherwin *et al.*, 1987), being considered as a marker for newly synthesized microtubules. Cells at the start of the cell cycle display a bright fluorescence at the posterior third of the cell, which later progresses to the newly formed flagellum that remains fluorescent until reaching full length. Once this happens

and the kinetoplasts fully divide, the flagellum and the posterior end no longer display α-tubulin staining. In cells undergoing mitosis, the cell body fluorescence is lost almost completely, and the only organelles still stained are the old and new basal bodies (Sherwin *et al.*, 1987). This contrasts with acetylated α –tubulin which is present in the intranuclear mitotic spindles (Sasse and Gull, 1988).

IFA of acetylated and tyrosinated α-tubulin results in completely different patterns, and this might reflect at the protein expression level. However, no studies have analysed α-tubulin expression during the cell cycle, and as such expression at mitosis and cytokinesis was followed during this study. The TAT1 antibody seems to recognise the asynchronous and mitotic samples more strongly, revealing only a faint signal towards the cytokinesis population (Figure 3. 43 panel A).

All specific antibodies generated against proteins with molecular weights between 35 and 40 kDa (M5 and C5) recognise the cytokinesis fraction more strongly than the asynchronous and synchronized in mitosis lysates (Figure 3. 43 panel B and panel C; Table 3. 6). Some supernatants display a weaker signal towards the mitotic sample, which would suggest that these proteins are expressed more strongly at the late phase of the cell cycle.

MAbs produced from cytoskeleton proteins with sizes ranging from 100 to 160 kDa (M2) display also higher intensity for preparations enriched in cells undergoing cytokinesis (Table 3. 6), despite the fact that some supernatants equally recognise the cytoskeleton of an asynchronous population (Figure 3. 43 panel F). The main fact to consider is their weaker recognition of enriched mitotic samples. An asynchronous population has approximately 7% of 2N2K cells, of which only a few are undergoing cytokinesis. Similar intensities for asynchronous and enriched cytokinesis populations suggests high expression of these proteins in cells undergoing cytokinesis, as well as in cells in G1 and S-phase, which constitute most of the cells in an asynchronous population. On the contrary, cells going through mitosis appear to display a down-regulation of these proteins, suggesting a cell cycle dependent protein expression.

Finally, antibodies from fusions M4 and C4 (proteins ranging from 60 to 80 kDa) show a wide variety of cell cycle recognition profiles. While some supernatants

react strongly with both mitosis and cytokinesis samples, but only weakly with the asynchronous sample, pointing to a concentration of the recognised proteins in late cell cycle phases, some are specific for mitosis (6 in total including 3 from C4 fusion) or cytokinesis (1 from C4 fusion), and 3 show similar signals for both the asynchronous and mitotic populations. The latter might refer again to proteins up-regulated during mitosis but also expressed in G1 and/or S-phase cells, while in cells going through cytokinesis protein expression is down-regulated.

A total of 28 supernatants were selected through this method, rejecting supernatants without any signal, those recognising all samples with similar intensity and those recognising the asynchronous sample with higher affinity, and used for further characterisation (section 3.3.4 to 3.3.8). MAbs were analysed by WB (section 2.4.7) to determine the proteins they recognised, their specificity and expression in different cell cycle phases. Simultaneously, localisation of the target proteins in the cytoskeleton of BSF parasites was determined by IFA (section 2.6.4), using neat supernatants as primary antibodies. For both techniques, a set of two different secondary antibodies were used, directed against IgG and IgM anti-mouse antibodies, to account for the mixture of isotypes present in each supernatant. A lot of antibodies recognise a doublet at around 38 kDa and another around 50 kDa, even if presenting a signal against other proteins, which was considered to be a background signal. MAbs were organized according to their IFA localisation patterns (section 3.3.4. to 3.3.8).

3.3.4. **Characterisation of MAbs recognising proteins with cytoplasmic distribution or with inconclusive results**

Of the 28 selected antibodies, 15 give either inconclusive results or cytoplasmic distribution with no apparent connection with any cytoskeleton structure. These MAbs were organized according to the fusion from which they were generated, and from the lower to the higher MW protein interval used for mice immunisation.

A total of 3 MAbs obtained from fusion M5 (Table 3. 6) were analysed by WB and IFA and display a punctate distribution throughout the cell body (M5-2D11, M5-3E2 and M5-3G4).

The supernatant identified as M5-2D11 displays a background pattern by WB with anti-mouse IgG, but shows an extra band with anti-mouse IgM in between the 2 doublet bands of approximately 38 kDa (Figure 3. 44 A arrow), stronger for mitotic and cytokinetic enriched populations. The data obtained are consistent with previous WB results visualised with this supernatant (Figure 3. 42), and the stronger signal in the cytokinesis synchronized sample with anti-mouse IgM (Figure 3. 44 A anti-mouse IgM) goes in accordance with dot-blot results (Figure 3. 43).

Although WB results discriminates isotypes, this is not the case in the IFA assays (Figure 3. 44 B), as both anti-mouse IgM and IgG display similar distributions. M5-2D11 seems to recognise proteins with a cytoplasmic distribution, being excluded from the nucleus and typical components of the trypanosome's cytoskeleton.

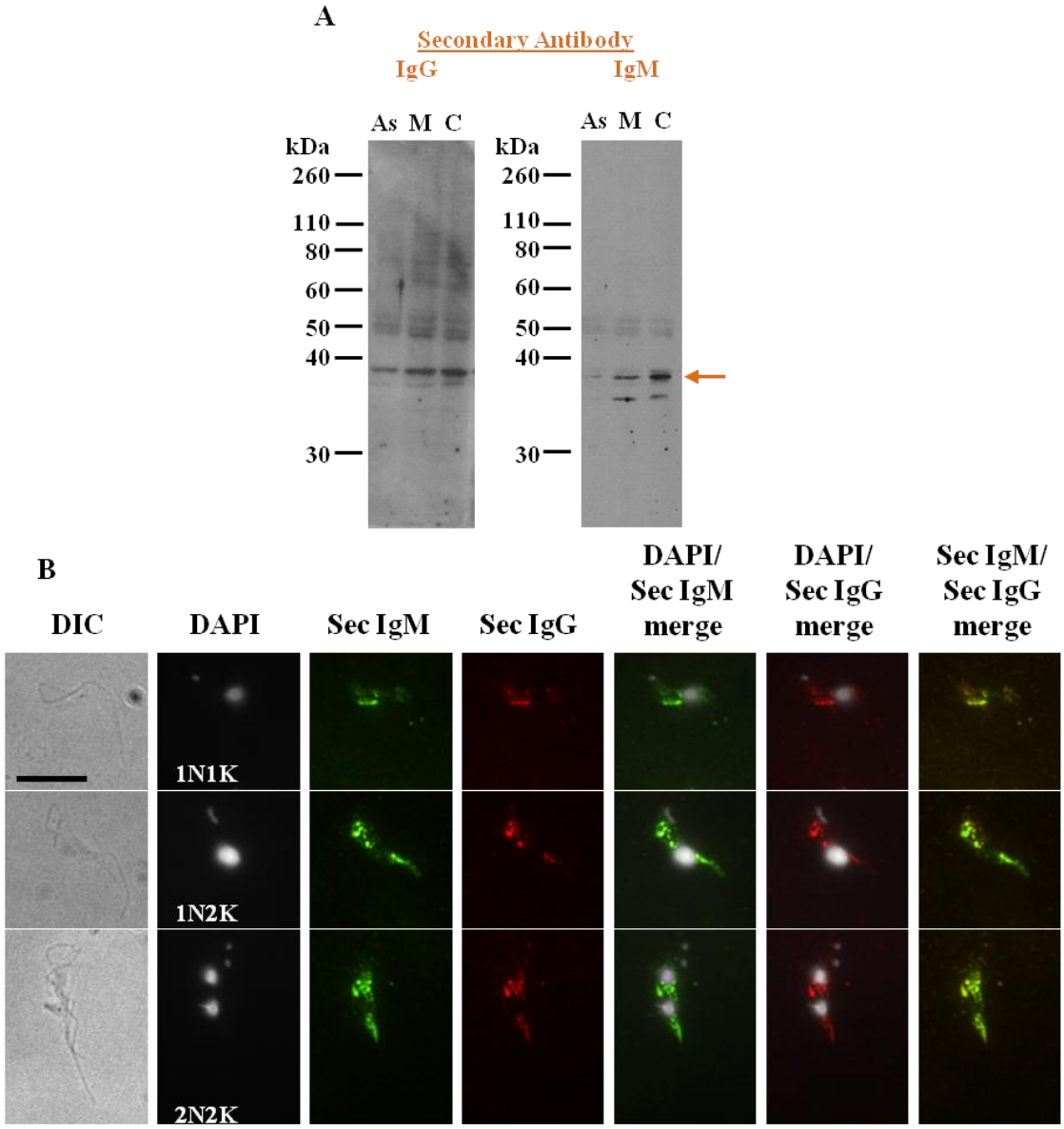

Figure 3. 44 - Characterisation of MAb M5-2D11. A – WB. Cytoskeleton preparations of asynchronous cultures (As) and synchronized cultures in mitosis (M) and cytokinesis (C) were probed with neat M5-2D11 overnight at 4ºC. The blot was initially probed with a secondary anti-mouse IgG antibody (HRP conjugated) and developed, before being stripped, re-incubated with the same primary antibody and a secondary anti-mouse IgM antibody (HRP conjugated). Ladder - Novex Sharp Pre-stained Protein Standard (Invitrogen). The arrow points to a protein band recognised with a stronger signal in the mitotic and cytokinetic enriched populations. B- IFA using BSF WT cells. Cells were incubated with neat M5-2D11 antibody followed by Alexa Fluor 488 (AF488)-conjugated goat anti-mouse IgM (Green) or Alexa Fluor 594 (AF594)-conjugated goat anti-mouse IgG (Red). Panels from left to right: DIC, DAPI staining of nuclei (N) and kinetoplasts (K), AF488 (Sec IgM), AF594 (Sec IgG), DAPI/AF488 merge, DAPI/AF594 merge and AF488/AF594 merge. Scale bar – 10 µm.

Supernatant M5-3E2 presents a stronger signal for proteins in enriched mitotic and cytokinetic cultures by WB, particularly a doublet of approximately 80 kDa (Figure

3. 45 A). In accordance, previous dot-blot results proved that this MAbs reacts strongly with enriched cytokinesis samples (Figure 3. 43), recognising with less affinity the mitosis sample. However, the supernatant cross-reacts with different proteins, particularly of smaller sizes, showing stronger recognition of the lower band of the 50 kDa doublet and the higher band of the 38 kDa doublet (Figure 3. 45 A).

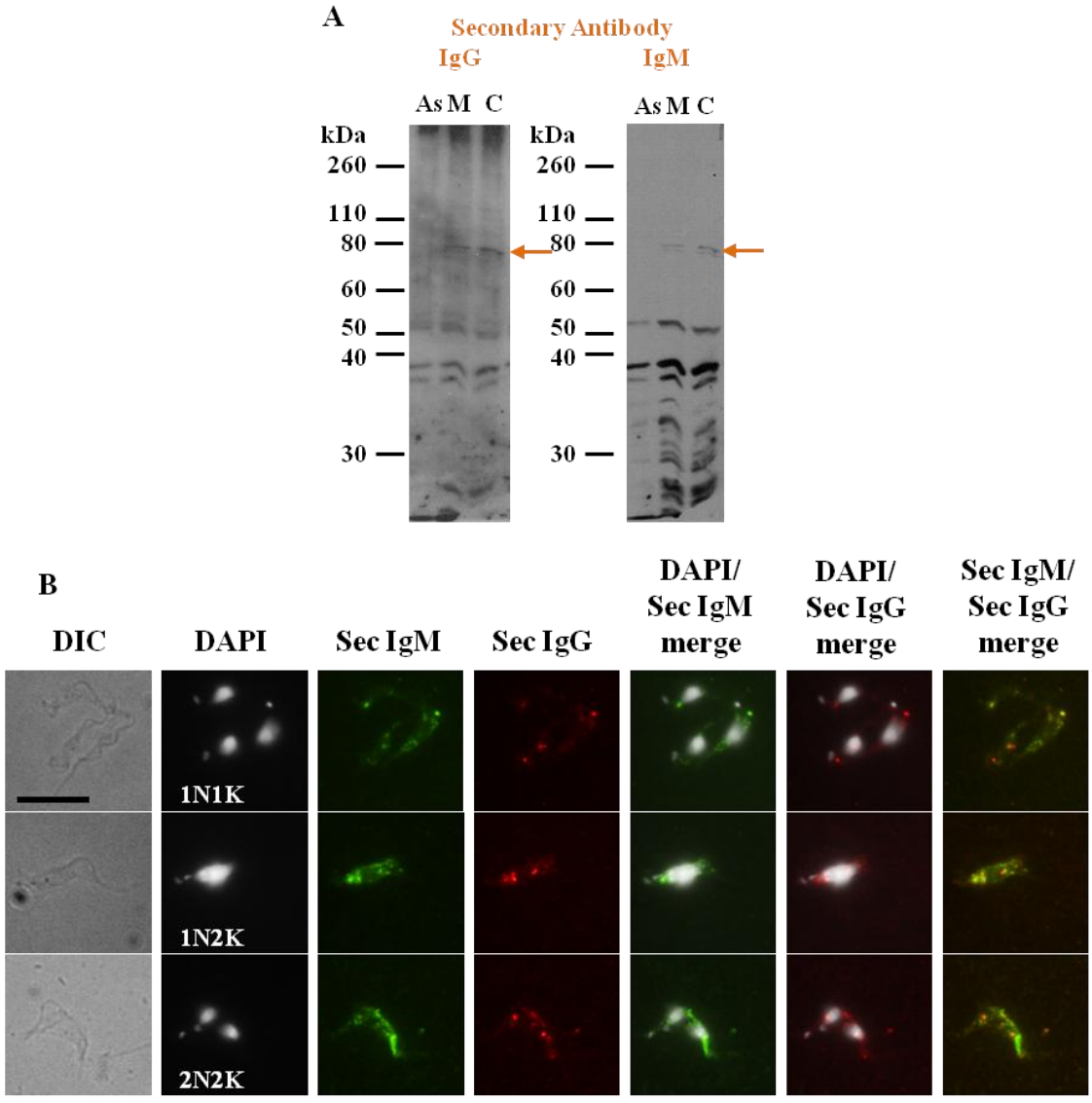

Figure 3. 45 - Characterisation of MAb M5-3E2. A – WB. Cytoskeleton preparations of asynchronous cultures (As) and synchronized cultures in mitosis (M) and cytokinesis (C) were probed with neat M5-3E2 overnight at 4ºC. The blot was initially probed with a secondary anti-mouse IgG antibody (HRP conjugated) and developed, before being stripped, re-incubated with the same primary antibody and a secondary anti-mouse IgM antibody (HRP conjugated). Ladder - Novex Sharp Pre-stained Protein Standard (Invitrogen). The arrow points to a protein band recognised with a stronger signal in the mitotic and cytokinetic enriched populations. B- IFA using BSF WT cells. Cells were incubated with neat M5-3E2 antibody followed by Alexa Fluor 488 (AF488)-conjugated goat anti-mouse IgM (Green) or Alexa Fluor 594 (AF594)-conjugated goat anti-mouse IgG (Red). Panels from left to right: DIC, DAPI staining of nuclei (N) and kinetoplasts (K), AF488 (Sec IgM), AF594 (Sec IgG), DAPI/AF488 merge, DAPI/AF594 merge and AF488/AF594 merge. Scale bar – 10 µm.

In terms of the localisation, M5-3E2 displays a punctate distribution throughout the cell body (Figure 3. 45 B).

The antibody identified as M5-3G4 cross-reacts intensely with different proteins, showing once again bands at ≈ 50 kDa probably corresponding to tubulin, and recognising in parallel heavy proteins between 80 and 110 kDa (Figure 3. 46 A). The proteins recognised by the different secondary antibodies by WB are similar, as a longer exposure of the WB with anti-mouse IgG showed the same pattern as the anti-mouse IgM WB. However, the intensity at which they were recognised seems to differ as different secondary antibodies react more strongly with different proteins. For example, anti-IgG recognises the 110 kDa protein stronger than the anti-IgM, while the latter reacts stronger with the 50 kDa doublet (Figure 3. 46 A). No specific signal is seen for the cytokinesis sample by WB, as opposed to the results obtained by dot-blot (Figure 3. 43), although it is necessary to take into account that polyvalent secondary antibodies were used for the latter. Interestingly, the recognition pattern obtained by WB is quite different from the one observed in previous assays (Figure 3. 42), which might suggest loss of some MAb producing cells during hybridoma maintenance.

Immunolocalisation is similar for both anti-IgG and anti-IgM antibodies (Figure 3. 46 B), with a signal distributed through the cell body, being excluded from the flagellum.

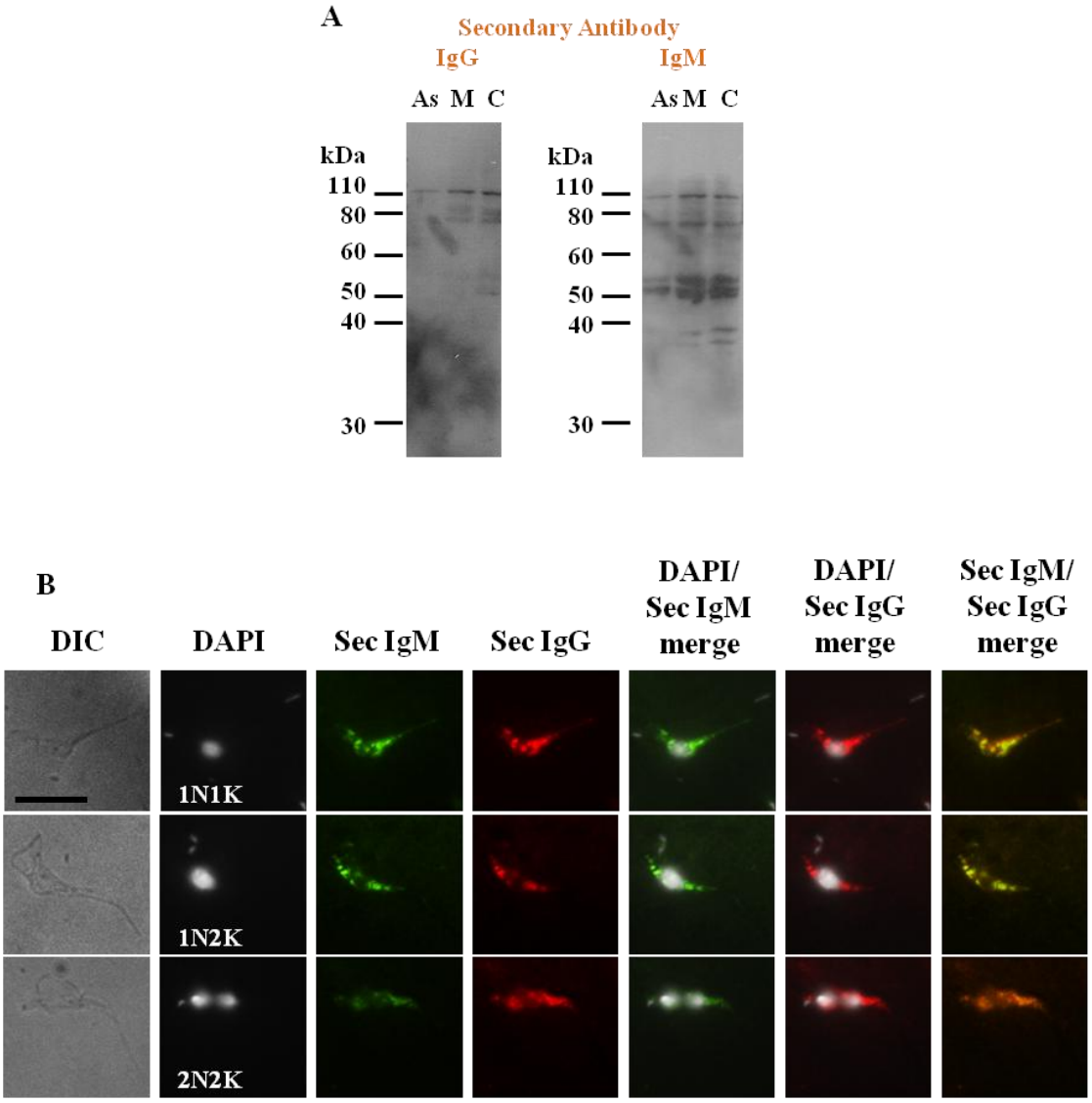

Figure 3. 46 - Characterisation of MAb M5-3G4. A – WB. Cytoskeleton preparations of asynchronous cultures (As) and synchronized cultures in mitosis (M) and cytokinesis (C) were probed with neat M5-3G4 overnight at 4ºC. The blot was initially probed with a secondary anti-mouse IgG antibody (HRP conjugated) and developed, before being stripped, re-incubated with the same primary antibody and a secondary anti-mouse IgM antibody (HRP conjugated). Ladder - Novex Sharp Pre-stained Protein Standard (Invitrogen). B- IFA using BSF WT cells. Cells were incubated with neat M5-3G4 antibody followed by Alexa Fluor 488 (AF488)-conjugated goat anti-mouse IgM (Green) or Alexa Fluor 594 (AF594)-conjugated goat anti-mouse IgG (Red). Panels from left to right: DIC, DAPI staining of nuclei (N) and kinetoplasts (K), AF488 (Sec IgM), AF594 (Sec IgG), DAPI/AF488 merge, DAPI/AF594 merge and AF488/AF594 merge. Scale bar – 10 µm.

From fusion C5, three MAbs were selected by dot-blot, all demonstrating stronger signals towards cytokinesis protein samples (Table 3. 6) than to mitosis or asynchronous protein lysates. WB attempts to further classify these antibodies were unsuccessful, as neither anti-IgM or IgG secondary antibodies showed any signal

towards cytoskeleton samples of BSF parasites. As such only data obtained for the polyvalent mix could be considered (Figure 3. 42), which besides not allowing differentiation between different antibody classes, is not as sensitive as ECL due to the developing method used (AP).

Among the three C5 selected supernatants, C5-2F10 does not show recognition of any particular cytoskeleton organelle, although showing some brighter staining in some areas (Figure 3. 47), similar for anti-IgM and IgG secondary antibodies. Once again, the fact that the WB result did not allow any conclusion made it impossible during this study to analyse which proteins were recognised by this supernatant.

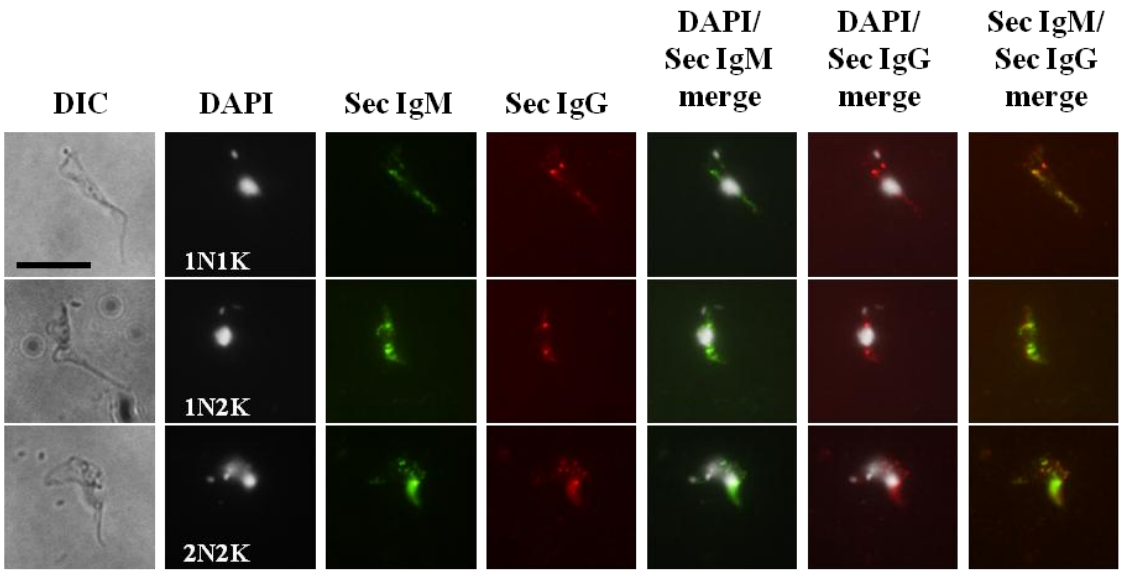

Figure 3. 47 - Characterisation of MAb C5-2F10 by IFA using BSF WT cells. Cells were incubated with neat C5-2F10 antibody followed by Alexa Fluor 488 (AF488)-conjugated goat anti-mouse IgM (Green) or Alexa Fluor 594 (AF594)-conjugated goat anti-mouse IgG (Red). Panels from left to right: DIC, DAPI staining of nuclei (N) and kinetoplasts (K), AF488 (Sec IgM), AF594 (Sec IgG), DAPI/AF488 merge, DAPI/AF594 merge and AF488/AF594 merge. Scale bar – 10 µm.

The M4 antibodies were generated using proteins ranging from 60 to 80 kDa (Table 3. 4). Among the ones classified by dot-blot, M4-1B2 and M4-4B8 were rejected as they do not show any particular band by WB (only the background doublets with equal intensities), and IFA using these antibodies gives very weak signals and no particular localisation (results not shown). Antibody concentration in these supernatants might not be sufficient to recognise the target proteins.

From this fusion, supernatant M4-1B10 shows inconclusive results by IFA. This MAb recognises a band of approximately 65 kDa with an anti-IgG secondary antibody by WB (Figure 3. 48 A), in accordance with the results obtained previously using a polyvalent secondary antibody (Figure 3. 42). However, by IFA using an anti-IgG antibody, no structure in the cytoskeleton samples is recognised (Figure 3. 48 B), while using an anti-IgM secondary antibody, which recognises only background bands by WB (results not shown), shows background staining of the cell body (Figure 3. 48 B). In this case, a low antibody concentration of the IgG isotype could have hindered IFA, or this MAb might not be useful for immunolocalisation assays. Although showing by dot-blot a slightly stronger signal towards mitosis (Figure 3. 43), such results are not seen by WB, nor by IFA.

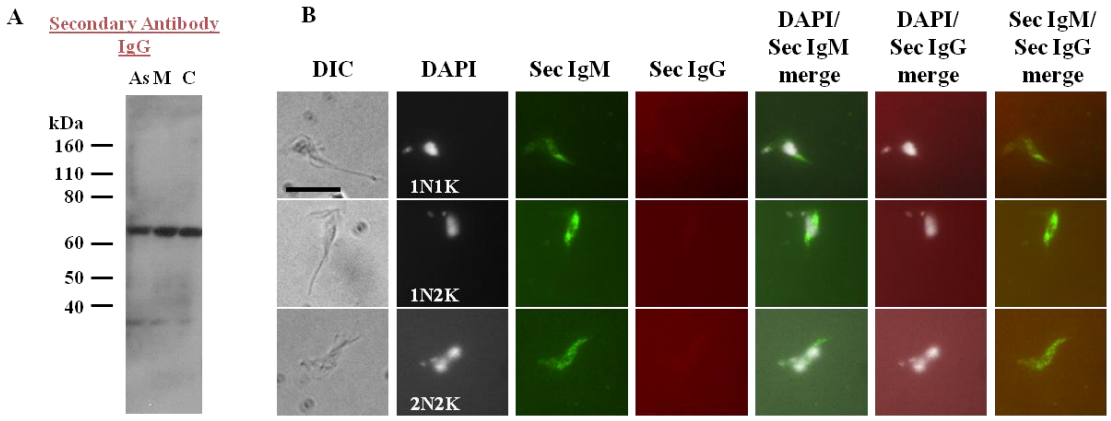

Figure 3. 48 - Characterisation of MAb M4-1B10. A – WB. Cytoskeleton preparations of asynchronous cultures (As) and synchronized cultures in mitosis (M) and cytokinesis (C) were probed with neat M4-1B10 overnight at 4ºC. The blot was initially probed with a secondary anti-mouse IgG antibody (HRP conjugated) and developed, before being stripped, re-incubated with the same primary antibody and a secondary anti-mouse IgM antibody (HRP conjugated). Only results for the anti-mouse IgG antibody are presented here. Ladder - Novex Sharp Pre-stained Protein Standard (Invitrogen). B- IFA using BSF WT cells. Cells were incubated with neat M4-1B10 antibody followed by Alexa Fluor 488 (AF488)-conjugated goat anti-mouse IgM (Green) or Alexa Fluor 594 (AF594)-conjugated goat anti-mouse IgG (Red). Panels from left to right: DIC, DAPI staining of nuclei (N) and kinetoplasts (K), AF488 (Sec IgM), AF594 (Sec IgG), DAPI/AF488 merge, DAPI/AF594 merge and AF488/AF594 merge. Scale bar – 10 µm.

The antibody identified as M4-1C6 appears once again to recognise the 38 kDa doublet as a background signal, but also recognises a ≈ 75 kDa protein when anti-IgG is used (Figure 3. 49 A). This protein is only recognised in the asynchronous sample, contrasting with the dot-blot results that suggest the antibody gave a stronger signal for proteins involved in mitosis (Figure 3. 43). The signal obtained by IFA, although

showing some brighter staining in some areas, is present throughout much of the cell body and does not seem to focus on any particular cytoskeleton component (Figure 3. 49 B).

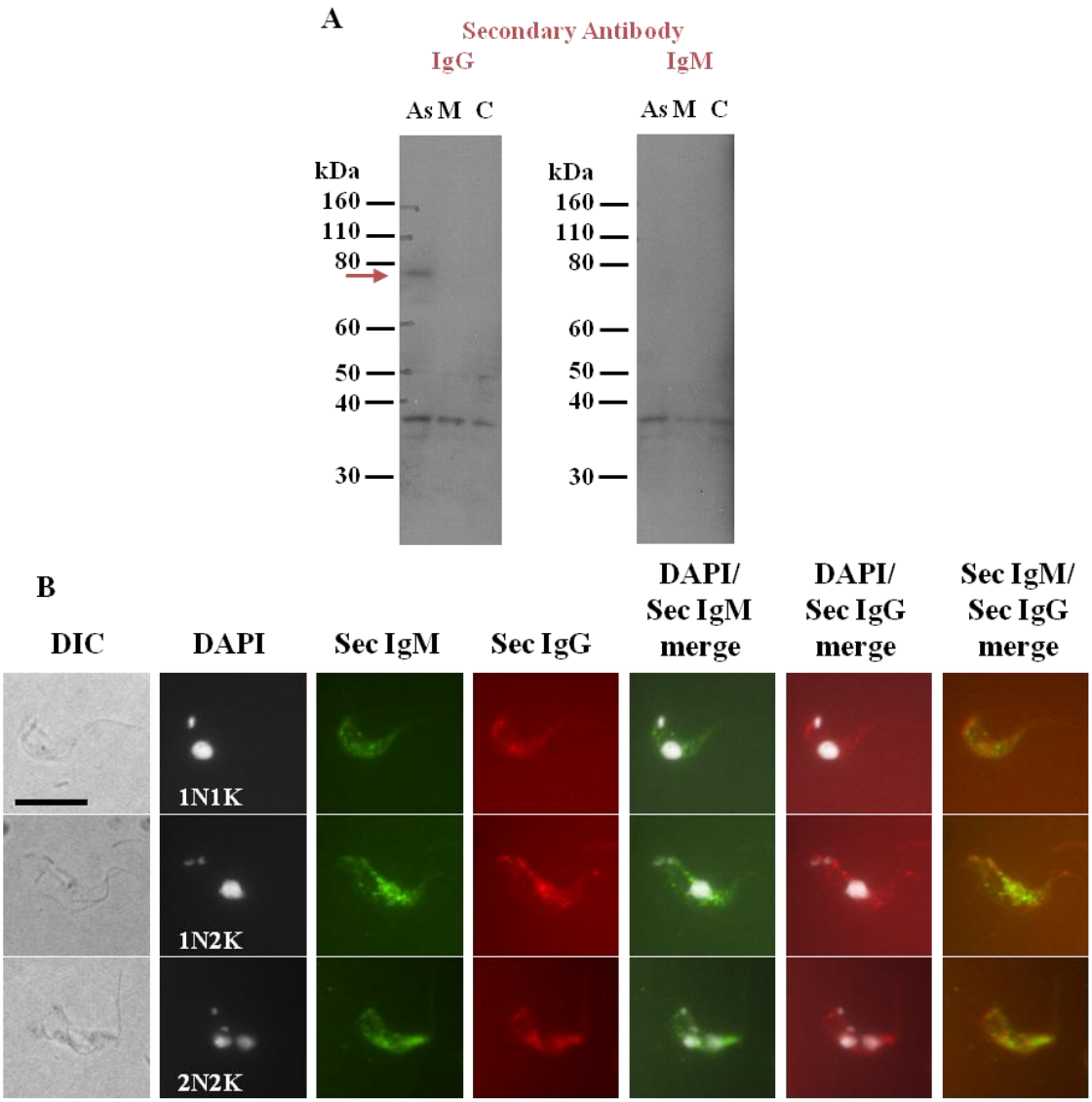

Figure 3. 49 - Characterisation of MAb M4-1C6. A – WB. Cytoskeleton preparations of asynchronous cultures (As) and synchronized cultures in mitosis (M) and cytokinesis (C) were probed with neat M4-1C6 overnight at 4ºC. The blot was initially probed with a secondary anti-mouse IgG antibody (HRP conjugated) and developed, before being stripped, re-incubated with the same primary antibody and a secondary anti-mouse IgM antibody (HRP conjugated). Ladder - Novex Sharp Pre-stained Protein Standard (Invitrogen). The arrow points to a protein band recognised with a stronger signal in the asynchronous populations.B- IFA using BSF WT cells. Cells were incubated with neat M4-1C6 antibody followed by Alexa Fluor 488 (AF488)-conjugated goat anti-mouse IgM (Green) or Alexa Fluor 594 (AF594)-conjugated goat anti-mouse IgG (Red). Panels from left to right: DIC, DAPI staining of nuclei (N) and kinetoplasts (K), AF488 (Sec IgM), AF594 (Sec IgG), DAPI/AF488 merge, DAPI/AF594 merge and AF488/AF594 merge. Scale bar – 10 µm.

Supernatant M4-3B7 had shown with mixed secondary antibodies a recognition pattern of several proteins, including two stronger bands around 80 kDa, and another around 40 kDa (Figure 3. 42). To confirm these WB results and to screen for localisation by IFA, a fresh supernatant sample was obtained from the same hybridoma cell line, as was done for all the other supernatants. However, contamination of this supernatant prevented its use. The only results for this antibody were thus obtained using the initial supernatant sample used in primary WB screenings (Figure 3. 42), which was tested only by WB with an anti-IgG secondary antibody (Figure 3. 50).

WB screening against different synchronized samples shows M4-3B7 antibody to recognise a 110 kDa protein exclusively expressed in mitosis (Figure 3. 50). In accordance, previous dot-blot results had proved that this MAb reacts strongly with enriched mitosis samples (Figure 3. 43). However, these results do not coincide with previous WB results (Figure 3. 42), which could be related to the different secondary antibodies used or loss of hybridoma producing cells. Such results would need further confirmation with new supernatant sample.

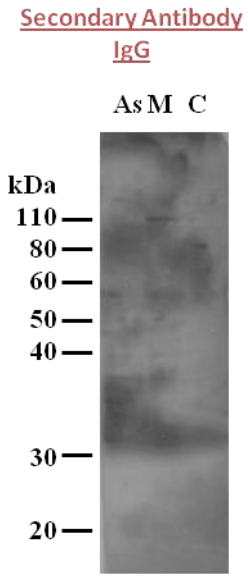

Figure 3. 50 - Characterisation of MAb M4-3B7 by WB. Cytoskeleton preparations of asynchronous cultures (As) and synchronized cultures in mitosis (M) and cytokinesis (C) were probed with neat M4-3B7 overnight at 4ºC. The blot was probed with a secondary anti-mouse IgG antibody (HRP conjugated) developed. Ladder - Novex Sharp Pre-stained Protein Standard (Invitrogen).

Antibodies obtained using 60-80 kDa proteins from the cytoskeleton of a cytokinesis synchronized BSF culture (C4) do not show particularly interesting results by WB, but their IFA localisations are quite distinctive. Among them, supernatant C4-2E6 seems to recognise proteins with a cytoplasmic distribution, with no apparent concentration at any cytoskeleton component, while WB studies were unsuccessful (results not shown). On the other hand, while WB results for C4-2G10 were also inconclusive, the IFA studies shows some brighter fluorescent points for both isotypes (Figure 3. 51), although the signal is too faint and with no particular localisation to analyse. Similar indeterminate data was obtained for C4-3E6 (Figure 3. 52), showing no specific signal by WB and or by IFA.

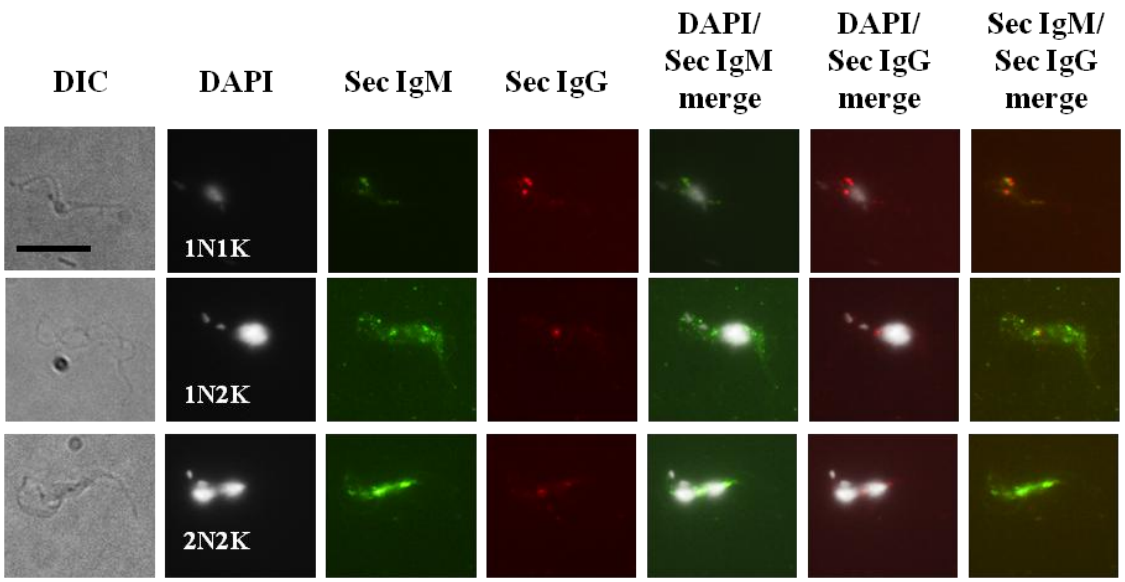

Figure 3. 51 - Characterisation of MAb C4-2G10 by IFA using BSF WT cells. Cells were incubated with neat C4-2G10 antibody followed by Alexa Fluor 488 (AF488)-conjugated goat anti-mouse IgM (Green) or Alexa Fluor 594 (AF594)-conjugated goat anti-mouse IgG (Red). Panels from left to right: DIC, DAPI staining of nuclei (N) and kinetoplasts (K), AF488 (Sec IgM), AF594 (Sec IgG), DAPI/AF488 merge, DAPI/AF594 merge and AF488/AF594 merge. Scale bar – 10 µm.

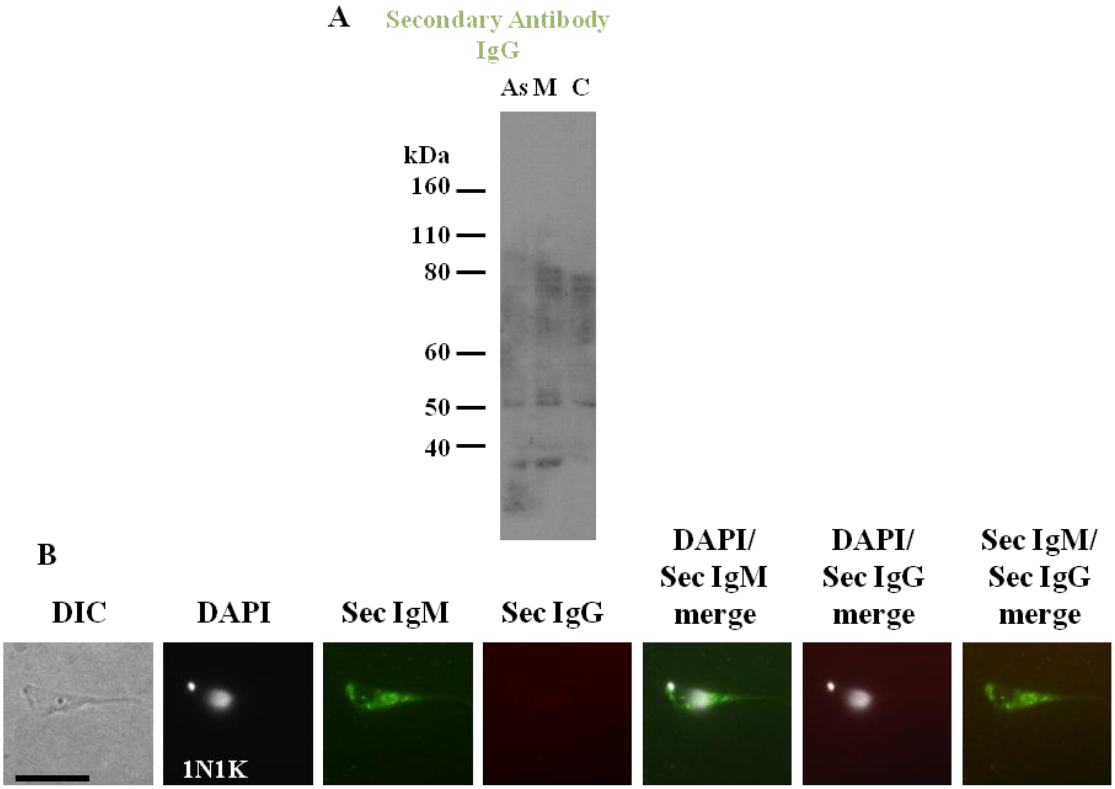

Figure 3. 52 - Characterisation of MAb C4-3E6. A – WB. Cytoskeleton preparations of asynchronous cultures (As) and synchronized cultures in mitosis (M) and cytokinesis (C) were probed with neat C4-3E6 overnight at 4ºC. The blot was initially probed with a secondary anti-mouse IgG antibody (HRP conjugated) and developed, before being stripped, re-incubated with the same primary antibody and a secondary anti-mouse IgM antibody (HRP conjugated). Only results for the anti-mouse IgG antibody are presented here. Ladder - Novex Sharp Pre-stained Protein Standard (Invitrogen). B- IFA using BSF WT cells. Cells were incubated with neat C4-3E6 antibody followed by Alexa Fluor 488 (AF488)-conjugated goat anti-mouse IgM (Green) or Alexa Fluor 594 (AF594)-conjugated goat anti-mouse IgG (Red). Panels from left to right: DIC, DAPI staining of nuclei (N) and kinetoplasts (K), AF488 (Sec IgM), AF594 (Sec IgG), DAPI/AF488 merge, DAPI/AF594 merge and AF488/AF594 merge. Scale bar – 10 µm.

Antibody C4-3F4 does not detect any specific protein by WB (results not shown). Its IFA pattern does not appear to co-localise with any specific cytoskeleton structure (Figure 3. 53), staining mainly the cytoplasm and being excluded from the nucleus, flagellum and kinetoplast. Some cells present brighter staining at the posterior tip of the cell, and also sometimes brighter dots appear close to the kinetoplasts (Figure 3. 53 1N2K arrows). For some cells, the cell body seems to be completely stained but in a more punctate pattern than seen for α–tubulin (Figure 3. 53 1N1K). The data obtained did not allow any specific conclusion to be drawn about the cellular distribution of its target.

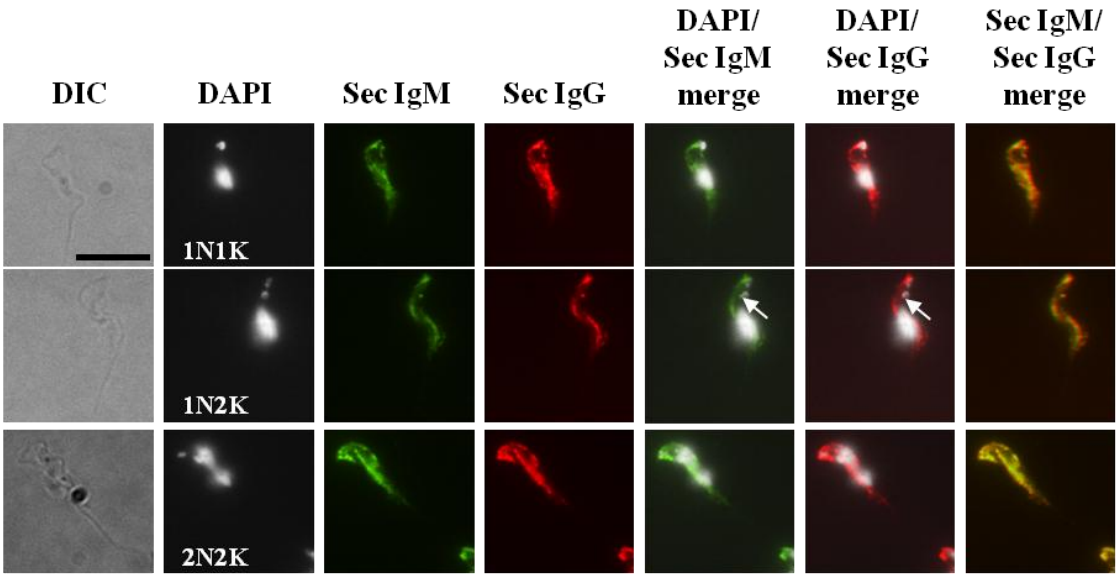

Figure 3. 53 - Characterisation of MAb C4-3F4 by IFA using BSF WT cells. Cells were incubated with neat C4-3F4 antibody followed by Alexa Fluor 488 (AF488)-conjugated goat anti-mouse IgM (Green) or Alexa Fluor 594 (AF594)-conjugated goat anti-mouse IgG (Red). Panels from left to right: DIC, DAPI staining of nuclei (N) and kinetoplasts (K), AF488 (Sec IgM), AF594 (Sec IgG), DAPI/AF488 merge, DAPI/AF594 merge and AF488/AF594 merge. The arrows point to the brighter dots located close to the kinetoplasts. Scale bar – 10 µm.

The last fusion analysed was generated against proteins ranging from 100 to 160 kDa, only from the mitotic sample (M2), resulting in 6 supernatants selected by dot-blotting (Table 3. 6). Due to the high molecular weight of the sample, initial WB experiments were performed with 8% gels (Table 2. 9) and later repeated with 14% gels, and the best results are presented.

Despite the fact that several attempts were made for immunolocalisation of M2-3C3, microscopic images do not show any signal for any of the isotypes (results not shown). Similarly, M2-3F4 does not show any fluorescence with either of the secondary antibodies (results not shown). As for WB results, both supernatants recognise one of the bands in the 38 kDa and 50 kDa doublets, although such signals might just be background bands and not correspond to any specific interaction (Figure 3. 54). Antibody concentration in these supernatants might not be sufficient to recognise the target proteins, or they can also be expressed in low abundance in *T. brucei* BSF cells.

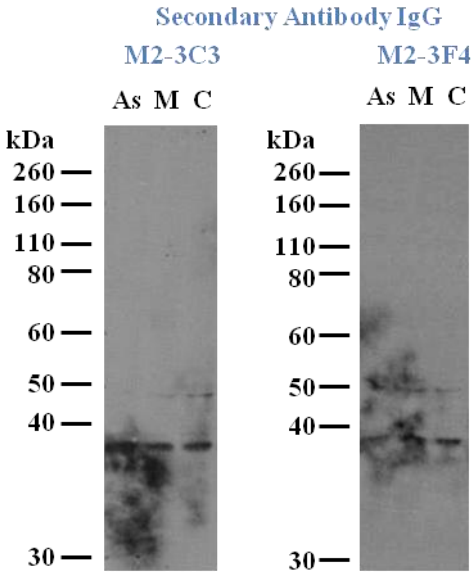

Figure 3. 54 - Characterisation of MAbs M2-3C3 and M2-3F4 by WB. Cytoskeleton preparations of asynchronous cultures (As) and synchronized cultures in mitosis (M) and cytokinesis (C) were electrophoresed in 14% gels, transferred to a nitrocellulose membrane and probed with neat M2-3C3 (left panel) or neat M2-3F4 (right panel) overnight at 4ºC. The blot was initially probed with a secondary anti-mouse IgG antibody (HRP conjugated) and developed, before being stripped, re-incubated with the same primary antibody and a secondary anti-mouse IgM antibody (HRP conjugated). Only results for the anti-mouse IgG antibody are presented here. Ladder - Novex Sharp Pre-stained Protein Standard (Invitrogen).

3.3.5. **Characterisation of MAbs recognising the cell body and the flagellum**

Two distinct antibodies from C4 fusion recognise the whole cell body and the flagellum – C4-2B6 (Figure 3. 56) and C4-4C5 (Figure 3. 57). Such staining is similar to what has been seen for anti-tubulin antibodies (Woods *et al.*, 1989). During this study, the anti-tubulin control was performed using TAT1 antibody. Although no localisation experiments were performed with it, WB results show that it recognises the 50 kDa doublet, as was expected (Figure 3. 55). As opposed to previous dot-blot results (Figure 3. 43), TAT1 recognises the asynchronous and synchronized cytoskeleton samples with the same intensity by WB.

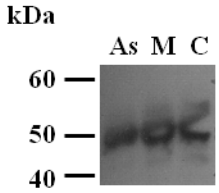

Figure 3. 55 - Characterisation of anti-tubulin antibody (TAT1) antibody by WB. Cytoskeleton preparations of asynchronous cultures (As) and synchronized cultures in mitosis (M) and cytokinesis (C) were probed with neat TAT1 overnight at 4°C and a secondary anti-mouse IgG antibody (HRP conjugated), before being developed. Ladder - Novex Sharp Pre-stained Protein Standard (Invitrogen).

WB results for C4-2B6 show that both secondary antibody isotypes recognise a doublet around 50 kDa (Figure 3. 56 A), which could correspond to α and β-tubulin. However, such results were not confirmed using antibodies giving identical IFA localisation, like C4-4C5 (Figure 3. 57), as WB results were inconclusive due to supernatant contamination (results not shown). On the other hand, this doublet has been seen as a background staining for a lot of the antibodies generated during this study, although the intensity of the signal by WB for C4-2B6 might be stronger than for the others. It is also necessary to take into consideration that there could be many protein doublets around 50 kDa, and further work would be needed for better characterisation of these antibodies.

To allow confirmation of tubulin recognition and identify which isotype of α-tubulin is recognised, competition experiments with synthetic peptides could be used. This technique has been used previously by authors that also generated MAbs from cytoskeleton preparations containing unknown antigens (Woods *et al.*, 1989). The idea would be to produce different α-tubulin peptides, with distinct post-translational modifications, incubate each isotype with the antibody supernatants (C4-2B6 and C4-4C5) and use these solutions as primary antibodies for WB against *T. brucei* proteins. Results would indicate if the synthetic peptide could compete out the binding of the generated MAb to *T. brucei* tubulin and which post-translational modification could cause such competition, concluding in parallel if C4-2B6 and C4-4C5 were in fact interacting with tubulin.

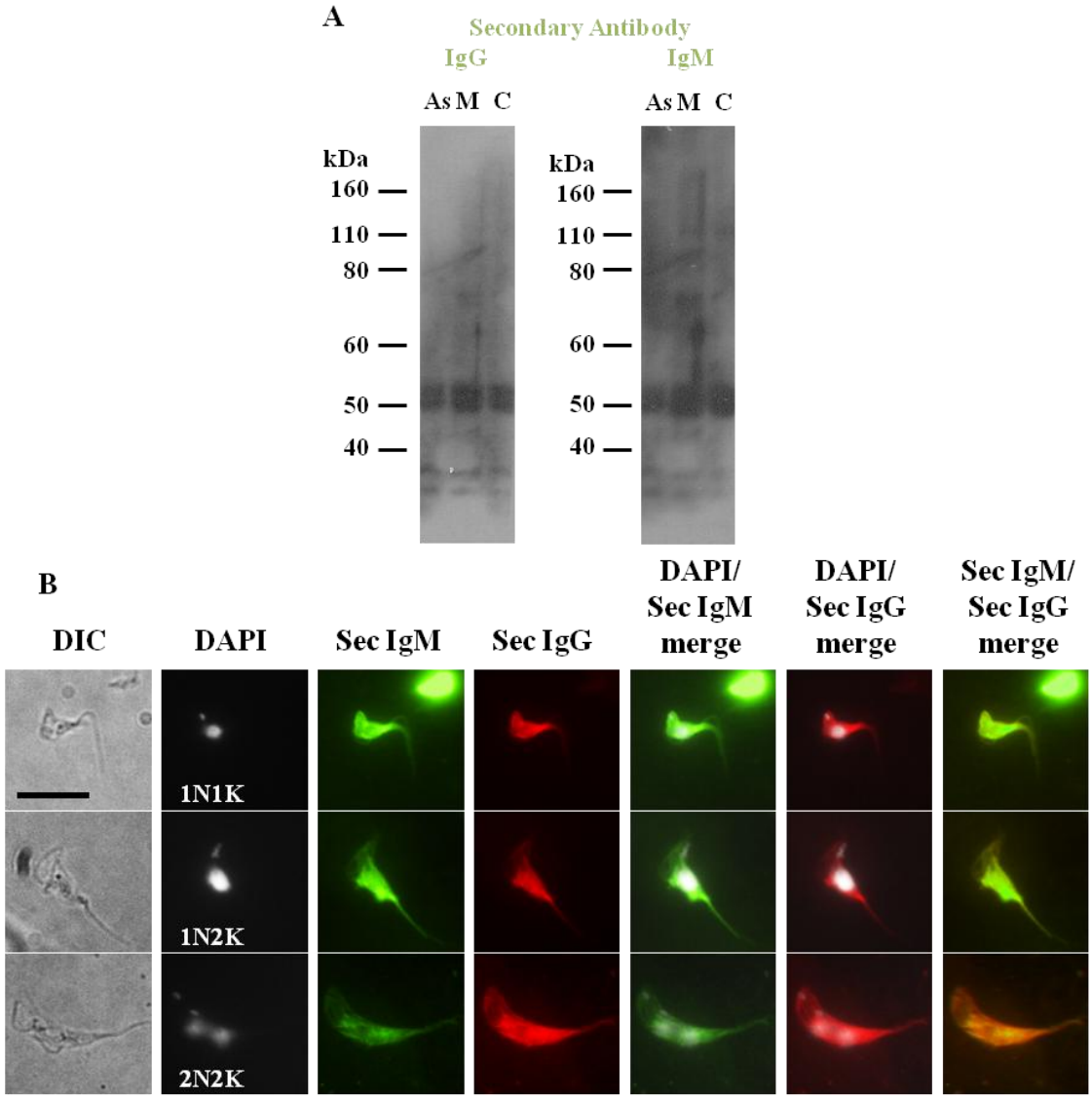

Figure 3. 56 - Characterisation of MAb C4-2B6. A – WB. Cytoskeleton preparations of asynchronous cultures (As) and synchronized cultures in mitosis (M) and cytokinesis (C) were probed with neat C4-2B6 overnight at 4ºC. The blot was initially probed with a secondary anti-mouse IgG antibody (HRP conjugated) and developed, before being stripped, re-incubated with the same primary antibody and a secondary anti-mouse IgM antibody (HRP conjugated). Ladder - Novex Sharp Pre-stained Protein Standard (Invitrogen). B- IFA using BSF WT cells. Cells were incubated with neat C4-2B6 antibody followed by Alexa Fluor 488 (AF488)-conjugated goat anti-mouse IgM (Green) or Alexa Fluor 594 (AF594)-conjugated goat anti-mouse IgG (Red).Panels from left to right: DIC, DAPI staining of nuclei (N) and kinetoplasts (K), AF488 (Sec IgM), AF594 (Sec IgG), DAPI/AF488 merge, DAPI/AF594 merge and AF488/AF594 merge. Scale bar – 10 µm.

Both C4-2B6 and C4-4C5 reveal similar staining patterns by IFA (Figure 3. 56 and Figure 3. 57), although their dot-blot results towards different cell cycle phases present differences between the two antibodies: while the latter shows a more intensive

signal towards the cytokinesis sample, C4-2B6 recognises the mitotic samples more strongly (Figure 3. 43 E). These differences between cell cycle phases are not visualised in WB or IFA results. When taking into consideration C4-2B6, the higher expression of the recognised protein in mitotic cell cycle phase might indicate recognition of mitotic spindles. The images analysed during this study do not allow any conclusion as to spindle staining, but co-localisation assays with KMX antibody would allow a more thorough analysis (Birkett *et al.*, 1985). As for C4-4C5, which shows a very clear signal against enriched cytokinesis cytoskeleton samples by dot-blot, it does not show any brighter signal for cells in this cell cycle phase by IFA (Figure 3. 57).

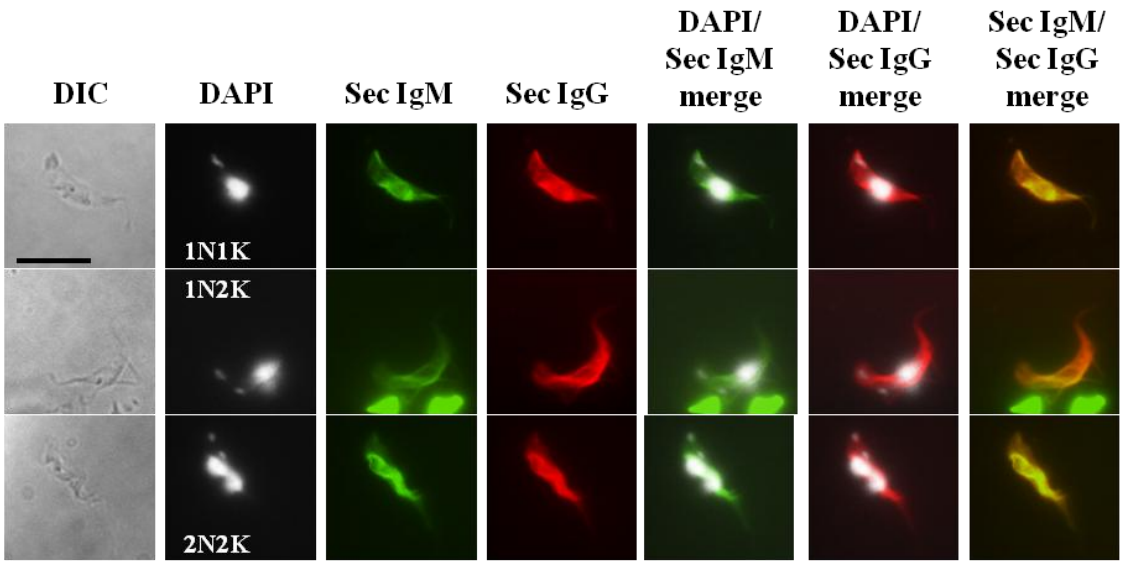

Figure 3. 57 - Characterisation of MAb C4-4C5 by IFA using BSF WT cells. Cells were incubated with neat C4-4C5 antibody followed by Alexa Fluor 488 (AF488)-conjugated goat anti-mouse IgM (Green) or Alexa Fluor 594 (AF594)-conjugated goat anti-mouse IgG (Red). Panels from left to right: DIC, DAPI staining of nuclei (N) and kinetoplasts (K), AF488 (Sec IgM), AF594 (Sec IgG), DAPI/AF488 merge, DAPI/AF594 merge and AF488/AF594 merge. Scale bar – 10 µm.

Comparable immunolocalisation has been seen for other proteins, like the microtubule binding protein (MAP) known as WCB. This high molecular mass protein (~ 138 kDa) has been determined to localise across the whole cell body (Woods *et al.*, 1992, Baines and Gull, 2008). In contrast to C4-2B6 and C4-4C5, WCB remains excluded from the flagellum.

One interesting feature of both C4-2B6 and C4-4C5 is the weaker staining of the posterior end of some 1N2K and 2N2K cells (Figure 3. 56 B and Figure 3. 57). This has been seen previously for CAP15 protein (Vedrenne *et al.*, 2002), although in this case failure to stain the posterior end is visible for all cells and once again there is no visible staining of the flagellum.

The data obtained suggest that the proteins recognised by MAbs C4-2B6 and C4-4C5 could be functionally related. Their corset-like localisation is identical to tubulin, the major protein found in the subpellicular microtubules, meaning that the recognised proteins might be associated with the subpellicular cytoskeleton. This structure is the basic scaffold that determines cell shape and is responsible for mitosis and flagellar movements (section 1.4.2). WB and IFA assays using tubulin from different species as performed in similar published works (Woods *et al.*, 1989) would allow analyses as to the specificity of the generated MAb against *T. brucei* tubulin, while immunogold EM would show if these supernatants recognise both the pellicular and axonemal microtubules. For such experiments, purification and concentration of the generated MAbs would be necessary to increase specificity and reduce background cross-reactions, allowing a better understanding of the proteins with which the generated MAbs interact with. In order to conclude whether the antibody recognises the mitotic spindle staining, as suggested by the stronger signal by dot-blot against cells in late cell cycle phases, co-staining with KMX antibody (Birkett *et al.*, 1985) and higher resolution microscopy would be necessary.

The brighter staining of the anterior and less dynamic end visible in some cells with the generated MAbs has been previously observed for two different MAPs – WCB and CAP15, although these do not co-localise to the flagellum. These proteins are responsible for maintaining the connections between the individual microtubules and the cross-bridges to the plasma membrane (Robinson *et al.*, 1991, Kohl and Gull, 1998) (section 1.4.8). Co-localisation experiments with known antibodies recognising the subpellicular cytoskeleton, MAPs and anti-tubulin antibodies could lead to a better characterisation of the generated MAbs.

In parallel, pull-down assays would allow purification of the interacting proteins from the cell extract and mass spectrometry experiments would permit further

characterisation. Finally, the use of phage-display libraries would help identify the target proteins, and their role in stability of the microtubule corset could be assessed by knockdown or knockout strategies, if not known already.

3.3.6. **Characterisation of MAbs recognising the BB/FP region**

Immunolocalisation studies showed that C5-3E4 antibody detects two very small structures towards the posterior end of the *T. brucei* cell (Figure 3. 58). This supernatant gave inconclusive results by WB using different secondary antibody isotypes (results not shown), but previous results with polyvalent secondary antibodies has detected a small molecular weight protein, at approximately 25 kDa (Figure 3. 42).

Although dot-blot analysis show a stronger recognition of proteins from enriched cytokinetic cultures (Figure 3. 43), this does not translate at the IFA level. Cells undergoing cytokinesis or in the last phase of the cell cycle present the same fluorescence intensity as cells in G_1 or G_2 phase. IFA images suggest that both isotypes recognise the BBs, although the signal from using an anti-IgM secondary antibody also displays a cytoplasmic distribution (Figure 3. 58).

Staining with C5-3E4 is similar to the one found with BBA4 antibody (Woods *et al.*, 1989), for which the proteins detected have not been identified. However, no co-localisation was performed with these 2 antibodies and at this resolution differences between the two would be difficult to distinguish. The staining remains excluded from the flagellum, as opposed to, for example, staining for KMP-11 (Li and Wang, 2008) and kinesin9B (Demonchy *et al.*, 2009), which are BB and flagellar proteins. Although some staining occurred for some areas of the cell body, it does not seem to coincide with the nucleus or the bilobe, as observed for example in localisation of TBBC (Dilbeck *et al.*, 1999) or Centrin1 (Selvapandiyan *et al.*, 2007), respectively, which are also BB associated proteins. Tyrosinated α–tubulin (Sherwin *et al.*, 1987) and γ–tubulin (Scott *et al.*, 1997) have been proved to be BB proteins, but their localisation displays a dynamic profile over the cell cycle, which does not happen with C5-3E4.

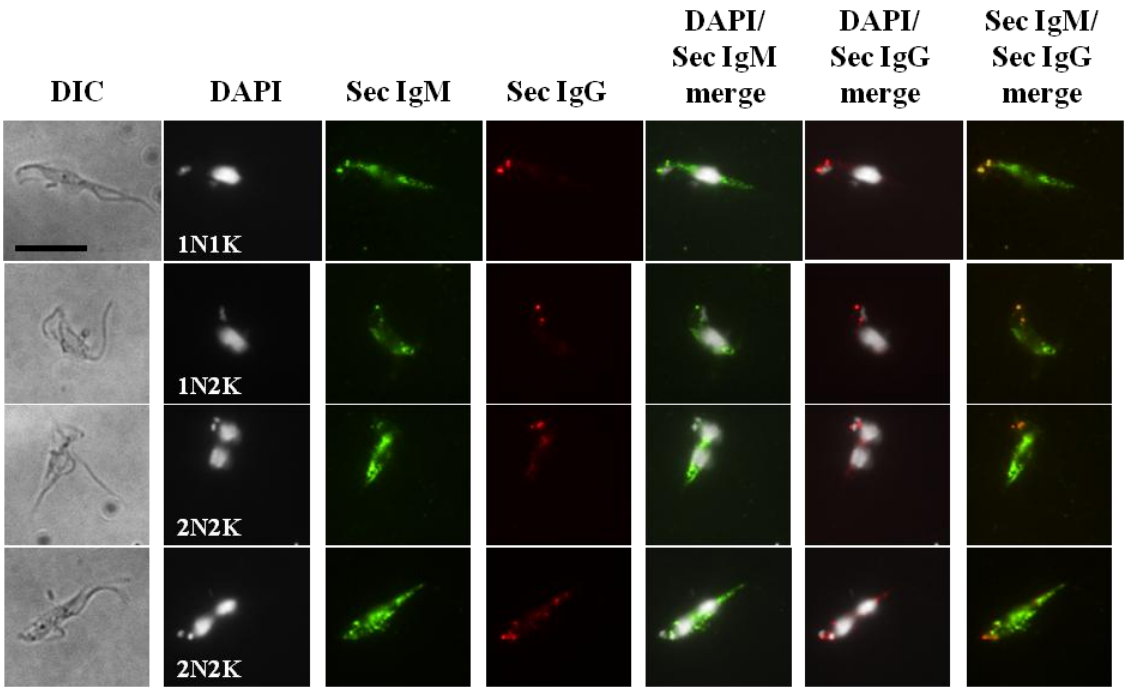

Figure 3. 58 - Characterisation of MAb C5-3E4 by IFA using BSF WT cells. Cells were incubated with neat C5-3E4 antibody followed by Alexa Fluor 488 (AF488)-conjugated goat anti-mouse IgM (Green) or Alexa Fluor 594 (AF594)-conjugated goat anti-mouse IgG (Red). Panels from left to right: DIC, DAPI staining of nuclei (N) and kinetoplasts (K), AF488 (Sec IgM), AF594 (Sec IgG), DAPI/AF488 merge, DAPI/AF594 merge and AF488/AF594 merge. Scale bar – 10 µm.

Although microscopic analysis appears to suggest BB staining, it is also possible that C5-3E4 could overlap with the FP. Performing co-staining with an anti-CRAM antibody, which is known to concentrate in the FP (Lee *et al.*, 1990), would help to eliminate this possibility. On the other hand, immunogold EM with a pure and specific antibody could help understand if the recognised antigen localises to the FPC, like BILBO1 (Bonhivers *et al.*, 2008b).

A study published in 2000 revealed a trypanosomal protein that is localised to the proximal region of the axoneme, being called the flagellum transition zone component (FTZC) (Bringaud *et al.*, 2000). Antibodies raised against FTZC recognise different proteins with MW ranging from 145 to 270 kDa, and although RNAi studies were performed to study the effects of FTZC ablation in *T. brucei*, no obvious phenotype is observed (Bringaud *et al.*, 2000). The flagellum transition zone (FTZ) seems to demarcate the beginning of the flagellar axoneme, where filaments connect microtubule doublets to the flagellar membrane (Briggs *et al.*, 2004, Bonhivers *et al.*,

2008b, Ralston *et al.*, 2009). In 2007 authors postulated that this zone functions as a quality control checkpoint for proteins entering the flagellum (Stephan *et al.*, 2007). If further work confirmed that C5-3E4 recognises components of this transition zone, the antigen it interacted with might also function as a filter in this selective protein entry to the flagellum.

Further work would thus be needed to confirm the structure recognised by this supernatant and, if recognising the BB, distinguish between pro and mature BB staining. Initial analysis to identify the recognised antigen could be performed by co-staining with BBA4 (Woods *et al.*, 1989), CRAM (Lee *et al.*, 1990), anti-BILBO1 (Bonhivers *et al.*, 2008b), MAb22 (Pradel *et al.*, 2006, Absalon *et al.*, 2007), anti-FPZC (Bringaud *et al.*, 2000) among others. On the other hand, repeating WB experiments with more concentrated and pure antibodies could allow a better knowledge of the identified antigen, as some known BB/FP/FTZC proteins have very different MW. Also, the use of a purer supernatant would help eliminate background staining by IFA, and check for co-staining of other organelles, such as the flagellum or the bilobe.

In later years, the use of MAb production to study proteins in *T. brucei* cell biology has increased. For example, the immunisation of mice with flagellar extracts from PCF *T. brucei* cells allowed the production of several MAbs, including MAb22, which recognises an unidentified antigen found in both the pro and mature basal bodies (Pradel *et al.*, 2006, Absalon *et al.*, 2007). Later on, the authors developed a novel EM technique, which used limited detergent extraction of cells without extracting the mitochondrial double membrane, thus maintaining the kinetoplast, mitochondrion and the TAC intact (Bonhivers *et al.*, 2008a). This novel EM labelling assay illustrated the binding of MAb22 to the BB-mitochondrial linker proteins, providing for the first time the identification of a TAC component (Bonhivers *et al.*, 2008a). Similar experiments could be performed in the future, to better identify the structure to which C5-3E4 binds to.

Only after a thorough characterisation of this antibody can conclusions be made about the functional role of the identified proteins in *T. brucei* cell biology or cell cycle. On the one hand, if the protein is associated with the FP it could be involved in the endo-exocytic pathway of the parasite (section 1.3.2), possibly assuming an important

role in host immune evasion; or act in FP biogenesis and consequently on cellular viability as BILBO1 does (Bonhivers *et al.*, 2008b). On the other hand, association with the BB, considered as the MTOC in *T. brucei* (section 1.4.6), could suggest a role in cell morphogenesis and correct organelle division (Ploubidou *et al.*, 1999, Pradel *et al.*, 2006, Lacomble *et al.*, 2010, Gluenz *et al.*, 2011). The recognised antigen could have a role in BB replication or function, and subsequently cause a block in cell cycle progression once depleted. Either way, C5-3E4 could be important in characterising BB/FP/FTZC biogenesis, or even provide a new tool for the characterisation of cytoskeleton mediated kinetoplast segregation.

3.3.7. **Characterisation of MAbs with flagellar distribution**

Nine antibodies generated during this study present IFA signals with flagellar distribution, five of which stain the whole flagellum (C5-1F10, M4-3C10, C4-2D6, M2-3B9, M2-3C10) while the remaining ones seem to identify proteins in this organelle at specific points (M5-2E4, C4-1E11, M2-1B7, M2-3F10).

3.3.7.1. Characterisation of MAbs recognising the whole flagellar structure

The five MAbs staining the whole flagellar structure could be interacting with proteins of the PFR, the FAZ or the flagellar axoneme (section 1.4). During this study it was impossible to conclude about the recognised structure, but analysis of the DIC/IFA merge images could help to narrow down the hypothesis. In fact, for two of these MAbs - C5-1F10 (Figure 3. 59 and Figure 3. 60) and M4-3C10 (Figure 3. 61 and Figure 3. 62) – the staining terminates at the end of the cell, not recognising the whole flagellum, and could as such correspond to recognition of a FAZ protein. On the contrary, for M2-3B9 the staining covers the full length of the flagellum, excluding interaction with a FAZ protein (Figure 3. 63 and Figure 3. 64).

The antibody identified as C5-1F10 displays quite different localisations according to the isotype of the secondary antibody used for IFA (Figure 3. 59). While

IFA using an anti-IgM secondary antibody reveals a cytoplasmic signal with no particular concentration at any cytoskeleton component, IFA using an anti-IgG secondary antibody seems to highlight the flagellum (Figure 3. 59).

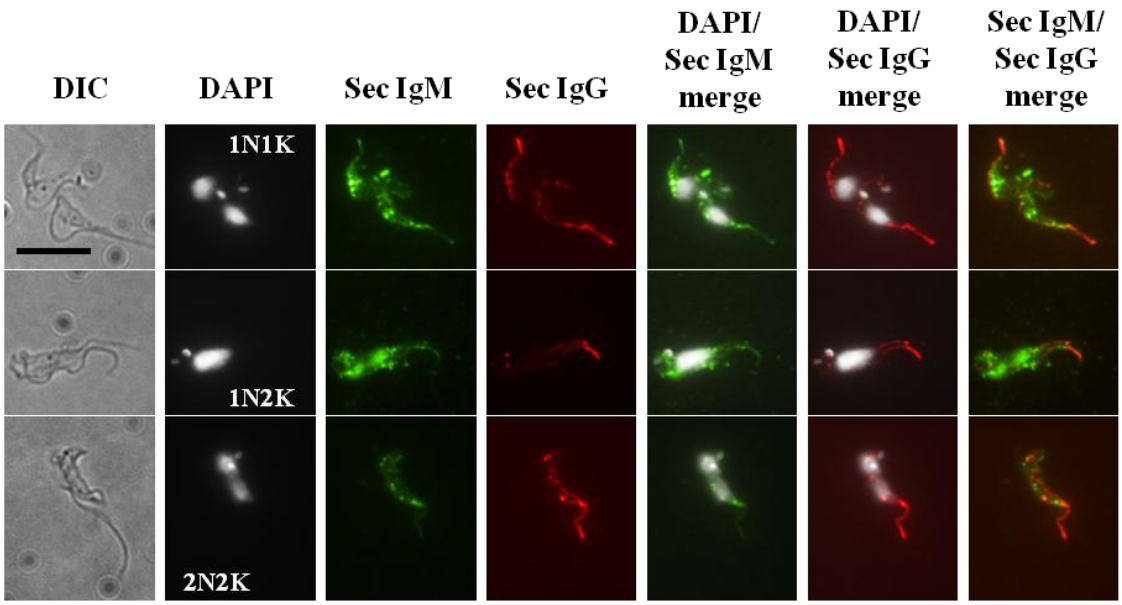

Figure 3. 59 - Characterisation of MAb C5-1F10 by IFA using BSF WT cells. Cells were incubated with neat C5-1F10 antibody followed by Alexa Fluor 488 (AF488)-conjugated goat anti-mouse IgM (Green) or Alexa Fluor 594 (AF594)-conjugated goat anti-mouse IgG (Red). Panels from left to right: DIC, DAPI staining of nuclei (N) and kinetoplasts (K), AF488 (Sec IgM), AF594 (Sec IgG), DAPI/AF488 merge, DAPI/AF594 merge and AF488/AF594 merge. Scale bar – 10 µm.

To confirm whether the antibody recognises the FAZ, the flagellar axoneme or the PFR would involve further work, including co-staining with known antibodies that recognise components of the structures mentioned and a high resolution microscope, or even immunogold labelling to allow a better contrast and higher sensitivity. Nevertheless, the results obtained during this study when considering the IFA/DIC merge images (Figure 3. 60), suggest recognition of a FAZ protein (section 1.4.4), as the staining does not include the full length of the flagellum. In fact, in the regions where the flagellum is detached (Figure 3. 60 bottom cell), the fluorescent signal remains in the cell body and excludes axonemal staining. Such IFA pattern was similar to the one obtained in previous published results (Woods *et al.*, 1989), which also used cytoskeleton samples to immunise mice and produce MAbs. Two FAZ staining MAbs

were characterised: CD10 (Woods *et al.*, 1989), which recognised a >300 kDa protein and detects an intermittently punctate line along the FAZ; and DOT1 (Woods *et al.*, 1989), which gives a more punctate pattern and also detects material at the distal tip of the flagellum. The more punctate pattern visualised for C5-1F10 with anti-IgG antibodies, when compared to other generated MAbs (see Figure 3. 61), resembles the one obtained with DOT1 IFA (Woods *et al.*, 1989), although no staining of the distal tip of the flagellum is visible. This lack of staining could be due to low antibody concentration instead of an actual antigen effect.

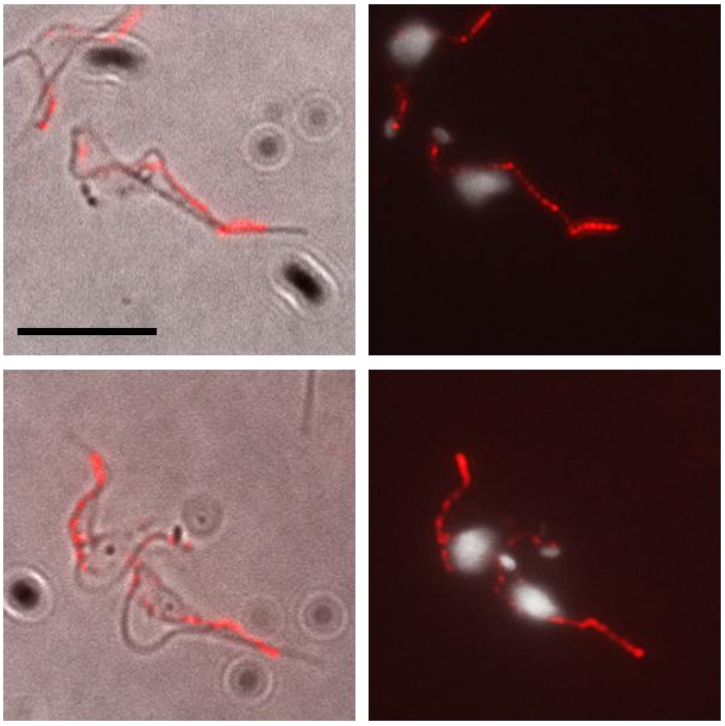

Figure 3. 60 - Characterisation of the MAb C5-1F10 as to its flagellar localisation. IFA images were obtained as previously and panels show the DIC/AF594 merge (left) and DAPI/AF594 (right) for different cells. Scale bar – 10 µm.

Although IFA with C5-1F10 displays a bright staining close to the kinetoplasts, it is not possible to conclude if antibodies are recognising BBs, as the signal is quite weak and such staining is not clearly visible for all cells (Figure 3. 59). Co-staining with YL1/2 (Kilmartin *et al.*, 1982) or BBA4 (Woods *et al.*, 1989) antibodies would allow proper co-localisation.

Dot-blot classification of C5-1F10 (Figure 3. 43 panel B) suggests it preferentially recognises cytokinesis samples, although such results could be unreliable if the antibody has a considerable background signal. Immunolocalisation data indicates that the recognised protein is expressed in all cell cycle phases, although a more thorough analysis of possible up-regulation during cytokinesis could have been performed by WB analyses.

As WB data for C5-1F10 was inconclusive and as seen for other antibodies in this study they can recognise (or show cross-reaction with) proteins outside the molecular weight interval used for injection, multiple proteins could have been recognised by this supernatant. Increasing the specificity and strength of the generated antibody by purification and concentration experiments would allow a better classification of the recognised antigens, and permit further functional studies. Because anti-IgM secondary antibodies reveal only background cell staining, it would be interesting to purify anti-IgG antibodies by affinity chromatography using a protein G HP purification column, and screen the resulting purified MAb.

The other antibody indicating FAZ staining – M4-3C10 - displays background bands by WB, although the intensity of the upper band of the 38 kDa doublet is stronger with an anti-IgG secondary antibody (Figure 3. 61 A). In terms of localisation, both secondary antibody isotypes display a bright signal for the trypanosome flagellum, despite the fact that anti-IgM secondary antibodies seem once more to co-stain the cytoplasm (Figure 3. 61 B).

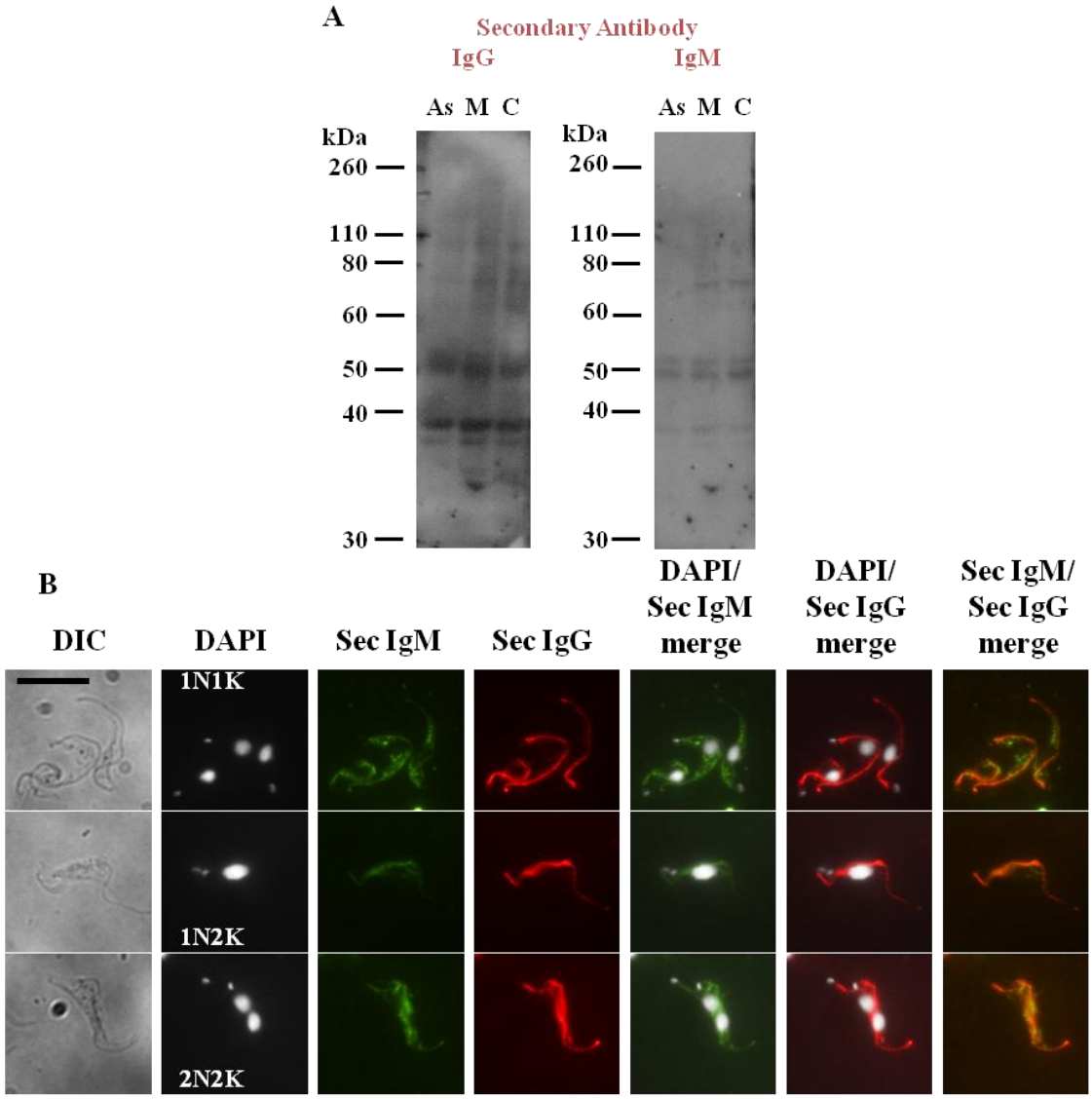

Figure 3. 61 - Characterisation of MAb M4-3C10. A – WB. Cytoskeleton preparations of asynchronous cultures (As) and synchronized cultures in mitosis (M) and cytokinesis (C) were probed with neat M4-3C10 overnight at 4ºC. The blot was initially probed with a secondary anti-mouse IgG antibody (HRP conjugated) and developed, before being stripped, re-incubated with the same primary antibody and a secondary anti-mouse IgM antibody (HRP conjugated). Ladder - Novex Sharp Pre-stained Protein Standard (Invitrogen). B- IFA using BSF WT cells. Cells were incubated with neat M4-3C10 antibody followed by Alexa Fluor 488 (AF488)-conjugated goat anti-mouse IgM (Green) or Alexa Fluor 594 (AF594)-conjugated goat anti-mouse IgG (Red). Panels from left to right: DIC, DAPI staining of nuclei (N) and kinetoplasts (K), AF488 (Sec IgM), AF594 (Sec IgG), DAPI/AF488 merge, DAPI/AF594 merge and AF488/AF594 merge. Scale bar – 10 µm.

Conclusion as to whether the antibody recognises the PFR, FAZ or the axoneme itself is impossible with these results, although once again lack of staining of the full length flagellum seems to indicate FAZ recognition (Figure 3. 62). Although this localisation is similar to that observed for C5-1F10 (Figure 3. 60), staining for this

antibody is not as punctate as for the previous one, and a faint signal is clearly observed close to each kinetoplast, which could indicate BB/FP recognition (Figure 3. 62 arrow). Co-staining with antibodies recognising the axoneme, PFR, FAZ and the BB would allow a more accurate conclusion to be drawn. Additionally, a bright staining is visible at the distal end of the part of the flagellum that is stained (Figure 3. 62).

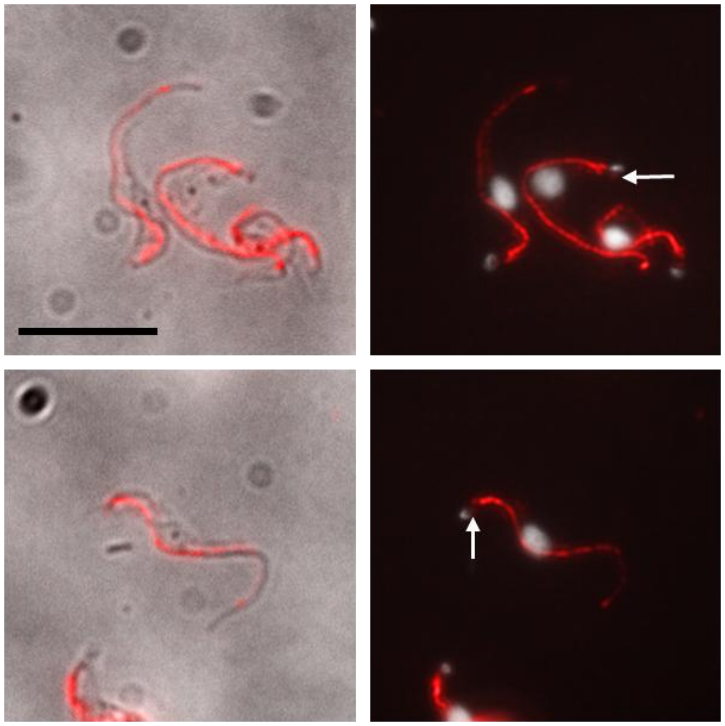

Figure 3. 62 - Characterisation of the MAb M4-3C10 as to its flagellar localisation. IFA images were obtained as previously and panels show the DIC/AF594 merge (left) and DAPI/AF594 (right) for different cells. The arrows indicate the points adjacent to the kinetoplasts that might indicate BB staining. Scale bar – 10 µm.

In *T. brucei*, two FAZ components have been characterised so far: FLA1, identified as a homologue of a *T. cruzi* protein involved in flagellum adhesion (Nozaki *et al.*, 1996), which seems to be necessary for flagellum attachment and cytokinesis (LaCount *et al.*, 2002), and FAZ1, also identified using generated MAbs (Kohl *et al.*, 1999) and shown to be involved in flagellum attachment (Vaughan *et al.*, 2008). If a similar protein is in fact the antigen to which C5-1F10 and M4-3C10 antibodies bind to, these proteins could be functionally related, and as such this antibody could be a valuable tool for studying flagellum attachment.

The punctate pattern observed for C5-1F10 is also similar to that observed in 2002 for trypanin localisation assays (Hutchings *et al.*, 2002). This protein seems to localise to the flagellum/FAZ, exhibiting a well-defined punctate distribution along one side of the PFR (Hutchings *et al.*, 2002). When performing knockdown studies, trypanin (-) mutants, although possessing an active flagellum, are unable to coordinate flagellar beat and EM analysis reveal a destabilization of the connections between the flagellar apparatus and the subpellicular cytoskeleton (Hutchings *et al.*, 2002). Later on, this role as a cytoskeletal linker protein and its function in flagellum-based cell motility were proven to be essential for cell viability in BSF trypanosomes (Ralston and Hill, 2006). During this study, authors proved that BSF cells without trypanin failed to undergo cytokinesis, accumulating cells with multiple flagella, nuclei, kinetoplasts, mitochondria, and FAZ structures (Ralston and Hill, 2006).

Although needing confirmation, the parallel binding of anti-IgG antibodies from M4-3C10 to the BB resembles that seen for CC2D (Zhou *et al.*, 2011). Recently, this 100 kDa protein has been localised to the FAZ and BB, with IFA presenting simultaneous staining of FAZ-associated ER (Zhou *et al.*, 2011). Depletion of CC2D blocks the assembly of a new FAZ, influencing directly the daughter cell length by controlling subpellicular microtubules synthesis. Immunolocalisation similarities between CC2D and M4-3C10 might suggest identical roles in cellular morphogenesis, as the unknown antigen of M4-3C10 might also influence the formation of the new FAZ filament. Identification of the recognised antigen is thus vital for future work.

As opposed to the previous MAbs with flagellar distribution, supernatant M2-3B9 recognises the full length of the flagellum (Figure 3. 63 B). M2-3B9 presents similar results for both isotypes, whether by WB or by IFA (Figure 3. 63), although once again anti-IgG secondary antibodies seem to be less reactive with background bands and show less cytoplasmic staining.

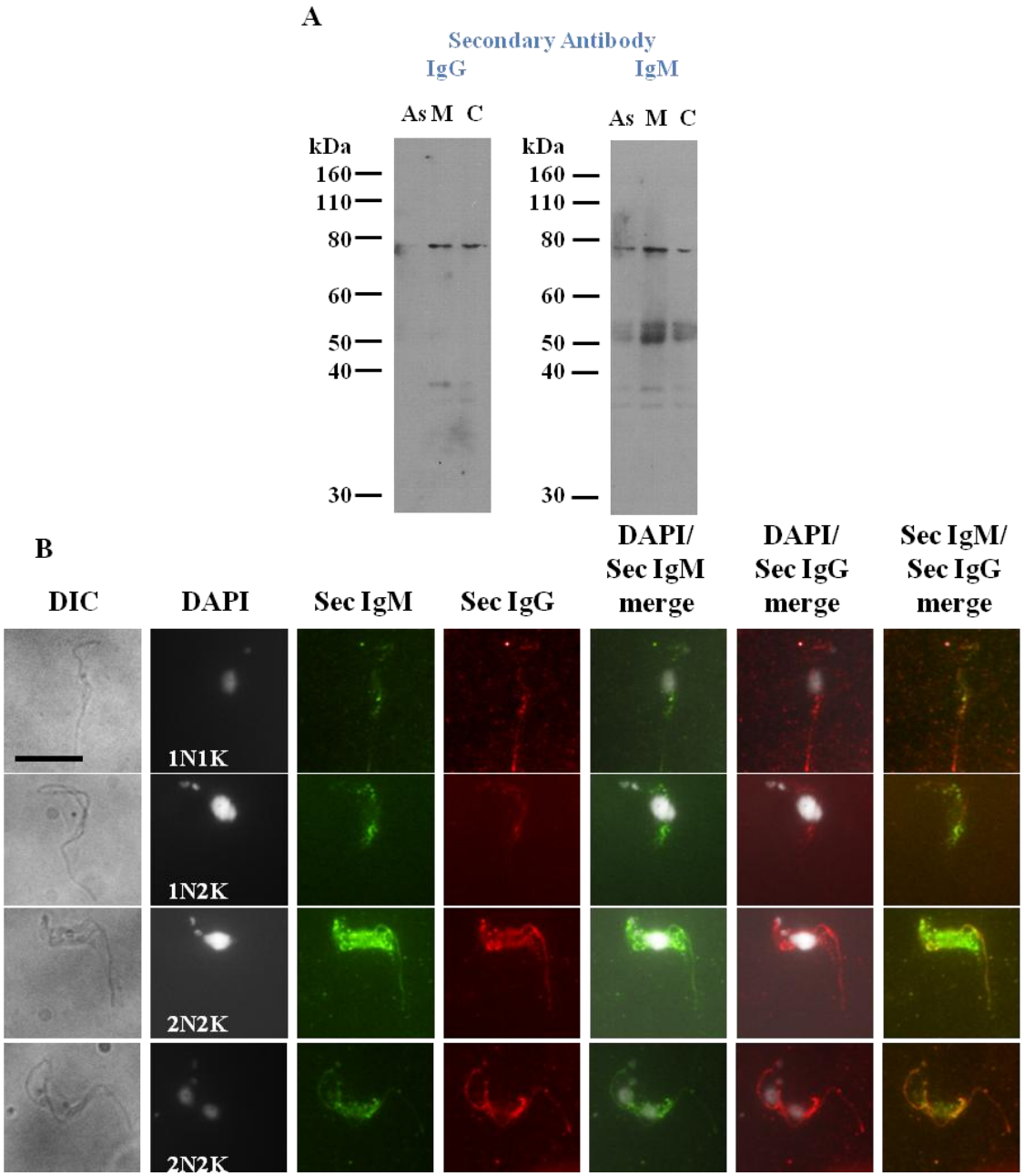

Figure 3. 63 - Characterisation of MAb M2-3B9. A – WB. Cytoskeleton preparations of asynchronous cultures (As) and synchronized cultures in mitosis (M) and cytokinesis (C) were probed with neat M2-3B9 overnight at 4ºC. The blot was initially probed with a secondary anti-mouse IgG antibody (HRP conjugated) and developed, before being stripped, re-incubated with the same primary antibody and a secondary anti-mouse IgM antibody (HRP conjugated). Ladder - Novex Sharp Pre-stained Protein Standard (Invitrogen). B- IFA using BSF WT cells. Cells were incubated with neat M2-3B9 antibody followed by Alexa Fluor 488 (AF488)-conjugated goat anti-mouse IgM (Green) or Alexa Fluor 594 (AF594)-conjugated goat anti-mouse IgG (Red). Panels from left to right: DIC, DAPI staining of nuclei (N) and kinetoplasts (K), AF488 (Sec IgM), AF594 (Sec IgG), DAPI/AF488 merge, DAPI/AF594 merge and AF488/AF594 merge. Scale bar – 10 µm.

The WB results show a band of approximately 80 kDa for both isotypes (Figure 3. 63 A), particularly stronger for cytoskeletons from mitosis and cytokinesis synchronized cultures. Such a band was seen for other antibodies, such as M4-3C10 (Figure 3. 61) and M5-3G2 (Figure 3. 74), which also recognise flagellar structures. However, antibodies with weak cytoplasmic patterns like M5-3G4 (Figure 3. 46) and M5-3E2 (Figure 3. 45) also display a weak signal at approximately this MW. Further purification and isotype separation of all these supernatants would allow a better comparison.

When analysing the DIC/IFA merge images (Figure 3. 64), supernatant M2-3B9 stains the full length of the flagellum, which suggests it does not interact with FAZ components. M2-3B9 could be interacting instead with PFR or axonemal proteins, and further work would thus be needed to distinguish which structure is recognised.

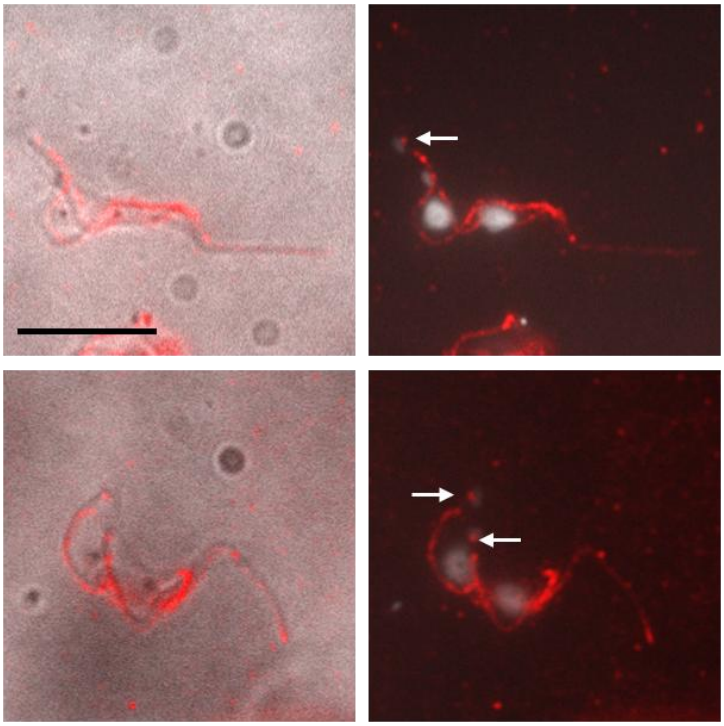

Figure 3. 64 - Characterisation of the MAb M2-3B9 as to its flagellar localisation. IFA images were obtained as previously and panels show the AF594 (red)/DIC merge (left) and the AF594 (red)/DAPI merge (right) for different cells. The arrows indicate the points adjacent to the kinetoplasts that might indicate BB staining. Scale bar – 10 µm.

Early analyses showed that the PFR consisted of two similar proteins (PFR1 and PFR2) (section 1.4.5). Later studies combining RNAi experiments and comparative proteomics allowed the identification of 20 novel components of the PFR, and so far a total of 40 proteins have been associated with the PFR (section 1.4.5). If in fact M2-3B9 supernatant recognises the PFR, it could be interacting with one of these already identified antigens, and assume a role in cellular motility, which has been proved to be essential for viability of BSF trypanosomes (Bastin *et al.*, 1998, Broadhead *et al.*, 2006).

Over the years, different proteins have been associated with the PFR, assuming similar staining patterns as visualised for M2-3B9, like Rab23 (Lumb and Field, 2011), Kif13-4 (Chan and Ersfeld, 2010) or PDEB1 (phosphodiesterase-1) (Oberholzer *et al.*, 2007). However, not all of them have been related directly with flagellum construction and maintenance. Recent studies involving *Rab23* RNAi cell lines proved that its expression is nonessential for proliferation of BSF and PCF cells, causing no defects in cell cycle progression (Lumb and Field, 2011). Analysis of PDEB1 function was performed in parallel with the other cAMP phosphodiesterase – PDEB2. Five genes that code for class 1 PDEs have been identified in *T. brucei* and their nomenclature has been established (Beavo, 1995, Kunz *et al.*, 2006). TbPDEB1 and TbPDEB2 are tandemly arranged on chromosome 9 and code for similar PDEs. Although their localisation is quite distinct, with PDEB1 being localised exclusively in the PFR on the flagellum and PFR2 being mostly cytoplasmic, RNAi against the two mRNAs has revealed they complement each other (Oberholzer *et al.*, 2007). On the contrary, double ablation strategies lead to cell death in BSF trypanosomes and completely prevents and eliminates trypanosome infection in the mouse model (Oberholzer *et al.*, 2007). These two proteins are thus essential for virulence, and have consequently been considered as good targets for antitrypanosomal drug therapy (Laxman and Beavo, 2007, Bland *et al.*, 2011). If specificity and sensitivity of M2-3B9 would be increased, in order to identify which antigen(s) it binds too, it would be interesting in the future to use this MAb to better understand the importance of PFR proteins in flagellum maintenance or/and trypanosome virulence.

On the other hand, M2-3B9 could be recognising axonemal proteins (section 1.4.7). Among these, 25.5 kDa TAX2 (trypanosome axonemal protein) and 21 kDa

SAXO (stop axonemal protein) have been localised to the flagellar axoneme and proven to have specific functions in linking the outer doublet microtubules and the central pair (Farr and Gull, 2009) or assume a role in flagellum motility (Dacheux *et al.*, 2012), respectively. If in fact recognising the axoneme, M2-3B9 could be used to understand the stability of the flagellar axoneme and its role in controlling flagellar beat. As flagellum stability is directly linked with an accurate cell division, M2-3B9 could be a serious candidate for cell cycle defect studies.

One interesting aspect about this MAb is that it shows parallel staining close to the kinetoplasts, which could correspond to BB/FP staining (Figure 3. 64), as seen for other flagellar-associated MAbs generated during this study. As WB results do not present a specific band (Figure 3. 63 A), no conclusion is possible as to if this pattern is due to recognition of one antigen or to several. In fact, M2-3B9 might be interacting with different proteins, one of them assuming a BB (or FP) location while the other protein(s) present a flagellar distribution. Besides co-staining with commercial BB-staining antibodies like BBA4 (Woods *et al.*, 1989), co-localisation with the MAb C5-3E4 generated during this project could also be performed. This would depend on a prior separation of the different antibody isotypes and purification to increase specificity of each antibody, in order to perform co-staining assays with distinct secondary antibodies to distinguish the IFA signal of the two MAbs.

If in fact the IFA pattern observed for M2-3B9 corresponds to a single protein, the antigen distribution resembles that observed for KMP-11 (Li and Wang, 2008) and kinesin9B (KIF9B) (Demonchy *et al.*, 2009). KMP-11 distribution was visualised using an HA tagged cell line, while KIF9B IFA was performed using an anti-KIF9B antibody. As opposed to KIF9B, the KIF9A protein localises only to the flagellum, visible by IFA with anti-KIF9A antibody (Demonchy *et al.*, 2009). To confirm the recognised structure, KMP-11 localisation was compared with that of YL1/2 and α-CRAM antibody, to reject FP staining, while double staining with L8C4 (PFR marker, (Kohl *et al.*, 1999)) or MAb25 (axoneme marker, (Dacheux *et al.*, 2012)) showed KIF9B associated with the axoneme together with the BB-associated fluorescence. Although the data obtained by WB does not allow any conclusion to be taken about KMP-11 (11

kDa) or KIF9B (115 kDa) being the recognised protein, the existence of tagged cell lines and specific antibodies against each protein could lead to more accurate analyses.

The interaction of M2-3B9 supernatant with either one of these proteins could provide a tool to study BB segregation and PFR assembly. In fact, *KMP-11* RNAi studies revealed inhibition of BB segregation and cytokinesis in induced cells in both *T. brucei* forms, causing in parallel FAZ construction defects and consequently flagellar detachment only for PCF cells (Li and Wang, 2008). On the contrary, KIF9B affects the assembly of the PFR, although being present in the axoneme and BB (Demonchy *et al.*, 2009). Ablation of KIF9B leads to appearance of cells with abnormal flagella and large blocks of PFR-like material alternating with regions where no PFR is present.

For the remaining flagellum-associating MAbs, IFA results are not as clear. One example is M2-3C10 (Figure 3. 65).

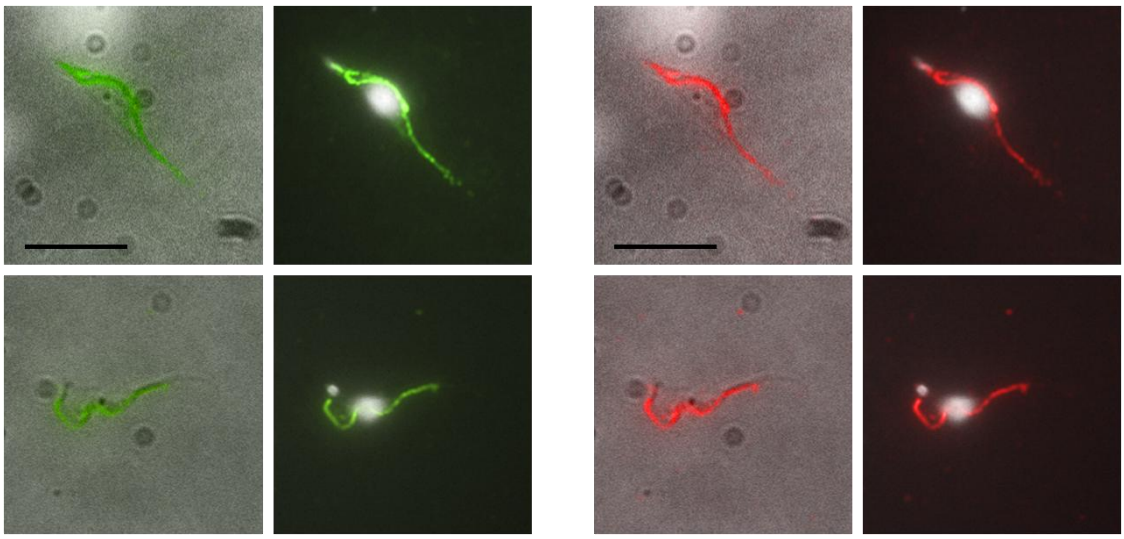

Figure 3. 65 - Characterisation of the MAb M2-3C10 as to its flagellar localisation. IFA images were obtained as previously. Panels from left to right: DIC/Af488 merge, DAPI/AF488, DIC/Af594 merge and DAPI/AF594 merge for different cells. Scale bar – 10 µm.

The antibody seems to recognise the BB/FP for cells in all cell cycle stages (Figure 3. 66 arrows), although some doubts remain when considering the flagellar staining. For some cells, the staining does not seem to extend to the full length of the flagellum (Figure 3. 65 bottom 1N1K cell), suggesting that the protein would be located

to the FAZ, as seen for C5-1F10 (Figure 3. 59). On the other hand, the top cell presented in Figure 3. 65 displays what looks like a flagellar location, where staining covers the full length of the flagellum, corresponding possibly to an axonemal or PFR antigen.

The ≈ 38 kDa band is once again detected by WB (Figure 3. 66 A), as seen for other antibodies that detect FAZ components, as M4-3C10 (Figure 3. 61). This could suggest it belongs to a component of one of these cytoskeleton structures and, similarly to what has been done previously (Woodward *et al.*, 1995), re-injection of this slice in mice and production of new MAbs against that unique antigen could indicate if in fact it corresponds to this localisation.

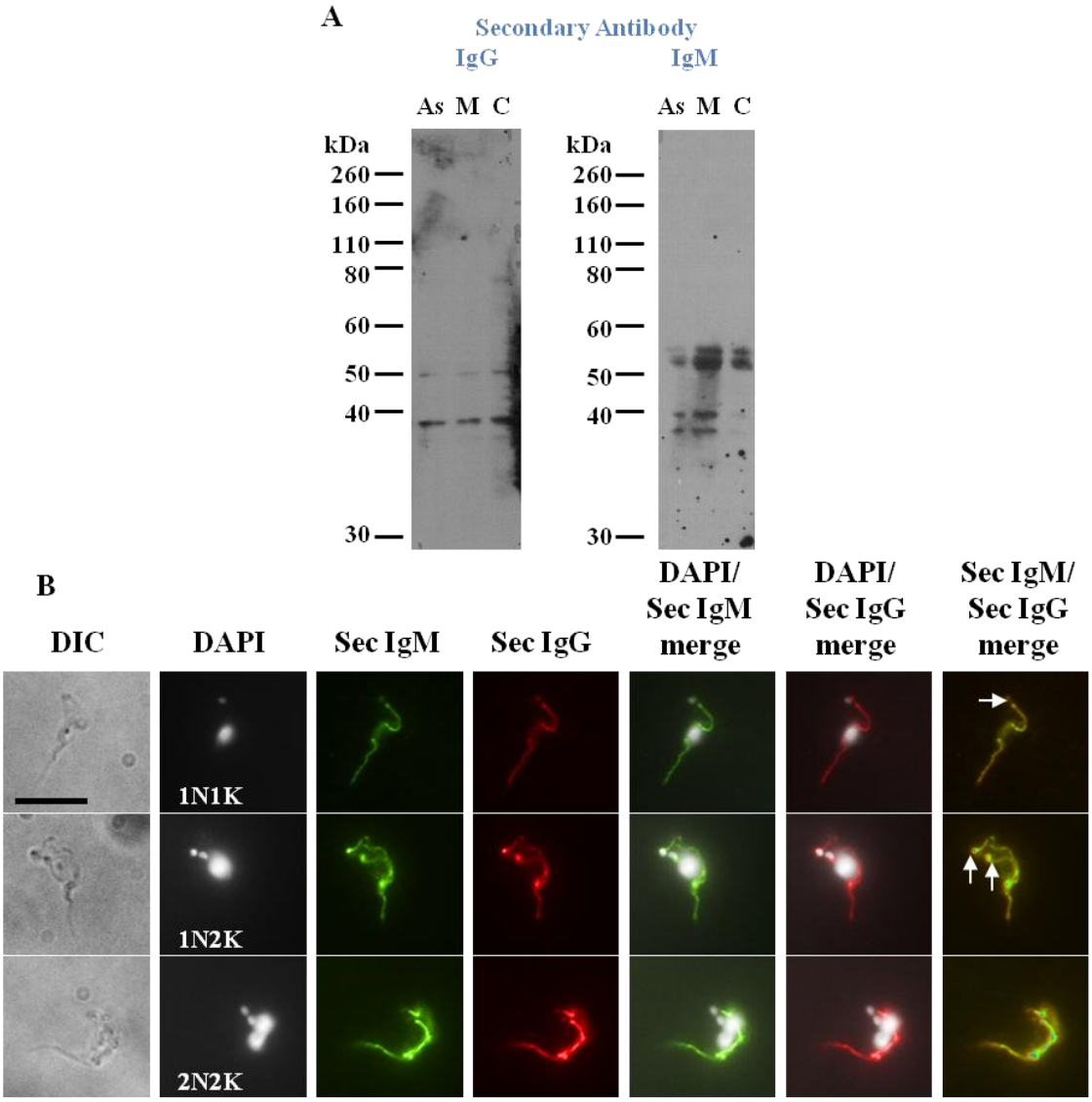

Figure 3. 66 - Characterisation of MAb M2-3C10. A – WB. Cytoskeleton preparations of asynchronous cultures (As) and synchronized cultures in mitosis (M) and cytokinesis (C) were probed with neat M2-3C10 overnight at 4ºC. The blot was initially probed with a secondary anti-mouse IgG antibody (HRP conjugated) and developed, before being stripped, re-incubated with the same primary antibody and a secondary anti-mouse IgM antibody (HRP conjugated). Ladder - Novex Sharp Pre-stained Protein Standard (Invitrogen). B- IFA using BSF WT cells. Cells were incubated with neat M2-3C10 antibody followed by Alexa Fluor 488 (AF488)-conjugated goat anti-mouse IgM (Green) or Alexa Fluor 594 (AF594)-conjugated goat anti-mouse IgG (Red). Panels from left to right: DIC, DAPI staining of nuclei (N) and kinetoplasts (K), AF488 (Sec IgM), AF594 (Sec IgG), DAPI/AF488 merge, DAPI/AF594 merge and AF488/AF594 merge. The arrows indicate the points adjacent to the kinetoplasts that might indicate BB staining. Scale bar – 10 µm.

Another flagellar recognising MAb that gives insufficient IFA results, in order to hypothesize about the flagellar structure it recognises, is C4-2D6 (Figure 3. 67 and Figure 3. 68). Although initial IFA analyses point also to FAZ recognition, the existence

of a very faint signal towards the end of the flagellum makes it resemble PFR or axonemal staining (Figure 3. 67 brackets).

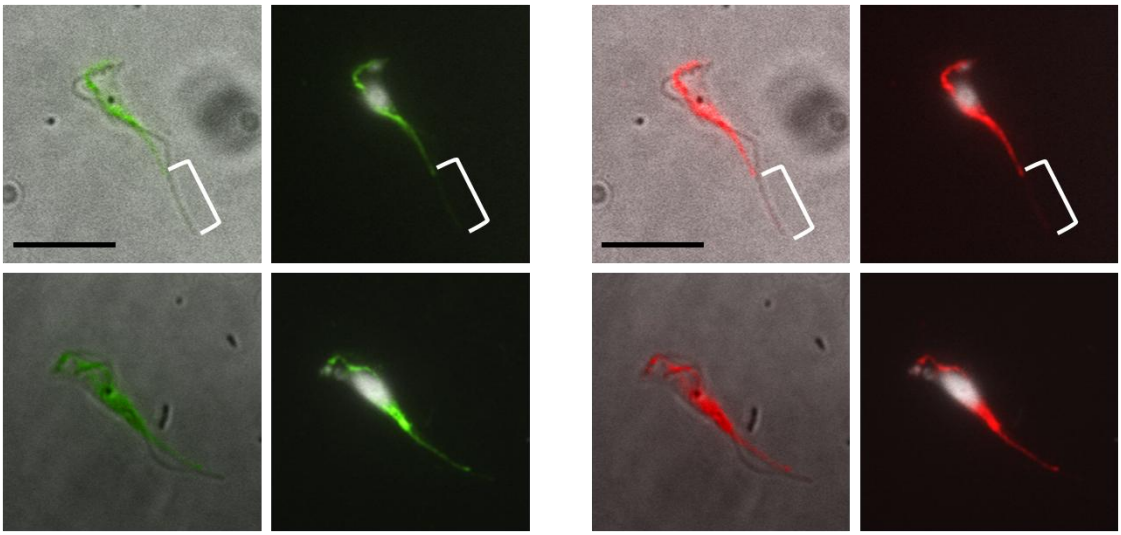

Figure 3. 67 - Characterisation of the MAb C4-2D6 as to its flagellar localisation. IFA images were obtained as previously. Panels from left to right: DIC/Af488 merge, DAPI/AF488, DIC/Af594 merge and DAPI/AF594 merge for different cells. The brackets point to the faint staining of the posterior end of the flagellum. Scale bar – 10 µm.

This supernatant is stronger by dot-blot against mitosis and cytokinesis proteins (Figure 3. 43 E); however, the WB results are inconclusive (Figure 3. 68 A). When used for IFA studies, C4-2D6 recognises both the old and new flagellum when either anti-IgG or anti-IgM secondary antibodies are used (Figure 3. 67 and Figure 3. 68 B). Additionally, two points at the posterior end of the cell, adjacent to the kinetoplasts, are also detected, corresponding to the BB/FP region (Figure 3. 68 arrows).

The IFA signal appears to extend further along the proximal end of the flagellum than the PFR does, suggesting recognition of an axonemal protein, as the PFR consists of an extra-axonemal structure present only in the flagellum from the point of exit from the cell. Once again, such conclusion could only be confirmed using higher sensitivity EM. Another alternative for confirmation of a flagellum recognised antigen, thus ruling out the possibility that C4-2D6 interacted with a FAZ protein, would be to repeat IFA analyses with detergent-insoluble cytoskeletons and removing cell body microtubules with high salt, as used by other authors (Woodward *et al.*, 1995). The results would show if the generated MAb detects intimate components of the flagellum cytoskeleton, and conclude as to its integrity even under high salt conditions.

As WB results are inconclusive, the specificity of the generated antibody could not be assessed, and staining of the different structures could not be determined to correspond to different proteins, or belong to the same protein.

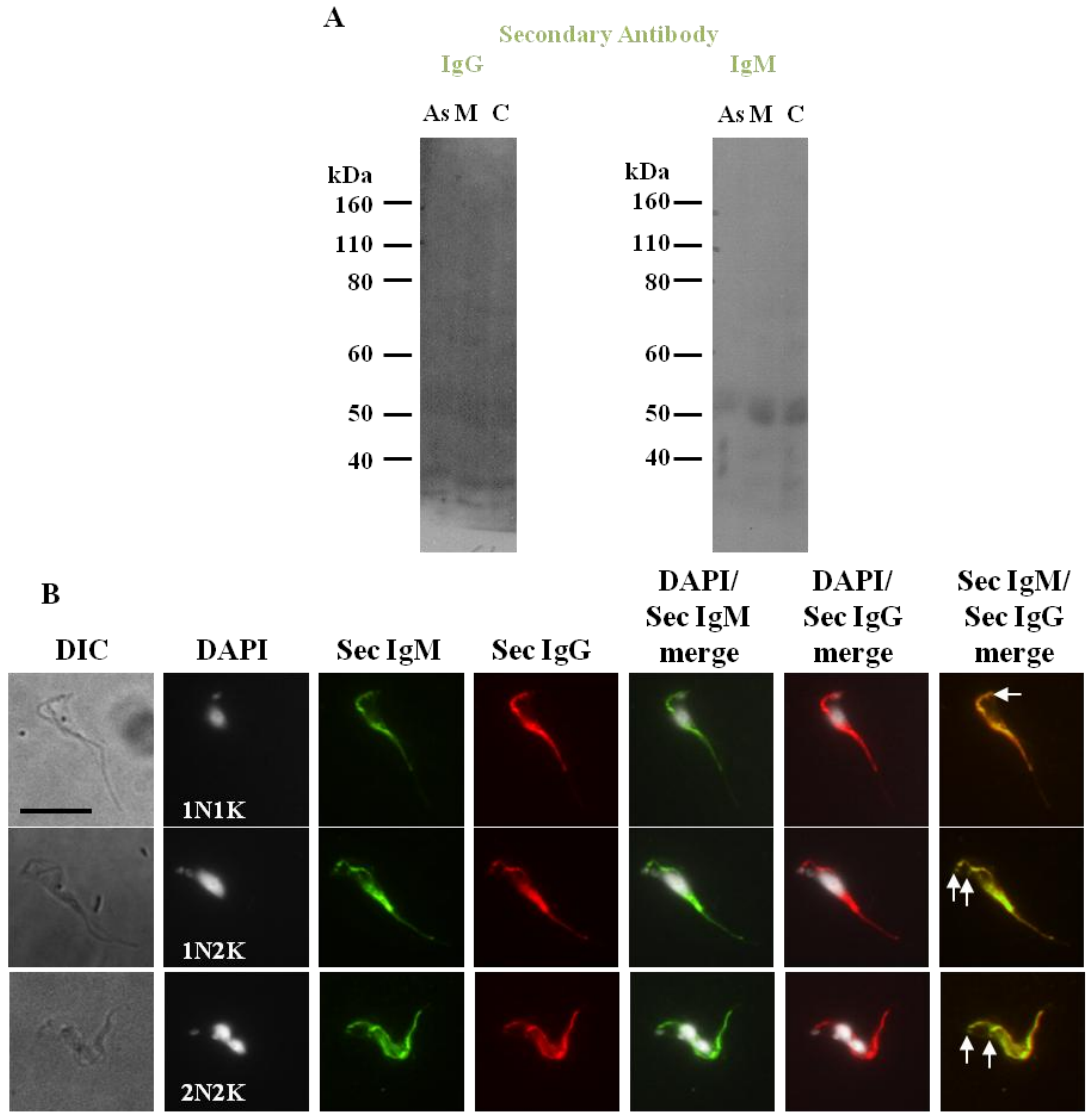

Figure 3. 68 - Characterisation of MAb C4-2D6. A – WB. Cytoskeleton preparations of asynchronous cultures (As) and synchronized cultures in mitosis (M) and cytokinesis (C) were probed with neat C4-2D6 overnight at 4ºC. The blot was initially probed with a secondary anti-mouse IgG antibody (HRP conjugated) and developed, before being stripped, re-incubated with the same primary antibody and a secondary anti-mouse IgM antibody (HRP conjugated). Ladder - Novex Sharp Pre-stained Protein Standard (Invitrogen). B- IFA using BSF WT cells. Cells were incubated with neat C4-2D6 antibody followed by Alexa Fluor 488 (AF488)-conjugated goat anti-mouse IgM (Green) or Alexa Fluor 594 (AF594)-conjugated goat anti-mouse IgG (Red). The arrows indicate the two points adjacent to the kinetoplasts that might indicate BB/FP staining. Panels from left to right: DIC, DAPI staining of nuclei (N) and kinetoplasts (K), AF488 (Sec IgM), AF594 (Sec IgG), DAPI/AF488 merge, DAPI/AF594 merge and AF488/AF594 merge. Scale bar – 10 µm.

3.3.7.2. Characterisation of MAbs recognising specific points in the flagellum

Four antibodies from different fusions recognise points along the flagellum without displaying a continuous pattern. One MAb was generated from a cytokinesis sample containing 80-100 kDa proteins (C4-1E11), while the remaining ones originated from mitotic synchronized samples with 35-40 kDa proteins (M5-2E4) and 100-160 kDa proteins (M2-1B7 and M2-3F10).

Of all these MAbs recognising points along the flagellar structure, supernatant C4-1E11 can be considered the least specific one, as in some cells the full length of the flagellum is also stained (Figure 3. 69 B marked with "stars"). The existence of brighter points along the flagellum could be due to possible damaging of this structure during cytoskeleton extraction, rather than these actually corresponding to the location of a specific antigen. Further work would be necessary to address this hypothesis. On the other hand, WB results with anti-IgG secondary antibodies show that this supernatant also recognises strongly the upper band of the 38 kDa doublet (Figure 3. 69 A), as was the case for other generated antibodies displaying flagellar localisation (M5-2E4 (Figure 3. 70) and M4-3C10 (Figure 3. 61)).

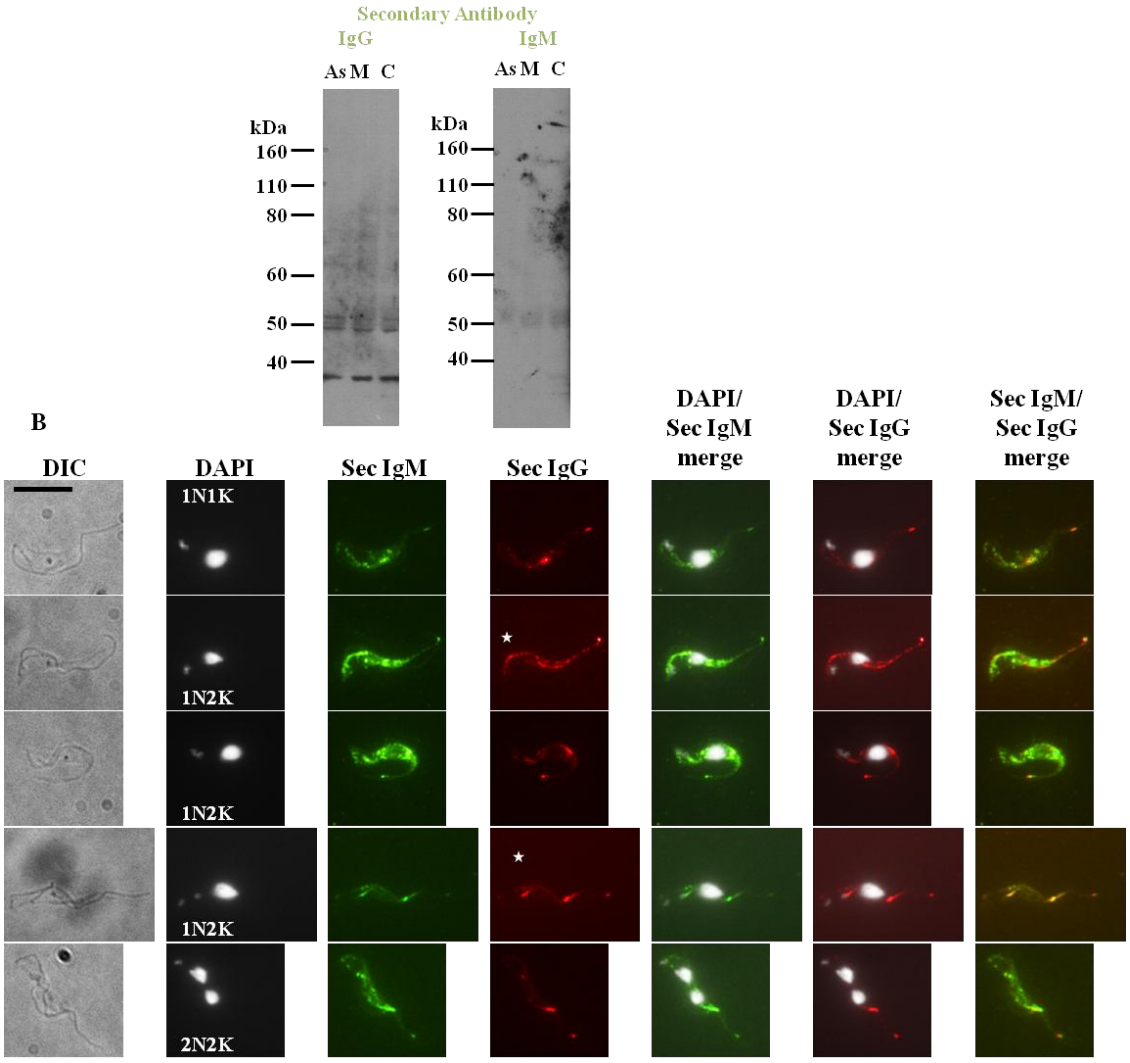

Figure 3. 69 - Characterisation of MAb C4-1E11. A – WB. Cytoskeleton preparations of asynchronous cultures (As) and synchronized cultures in mitosis (M) and cytokinesis (C) were probed with neat C4-1E11 overnight at 4ºC. The blot was initially probed with a secondary anti-mouse IgG antibody (HRP conjugated) and developed, before being stripped, re-incubated with the same primary antibody and a secondary anti-mouse IgM antibody (HRP conjugated). Ladder - Novex Sharp Pre-stained Protein Standard (Invitrogen). B- IFA using BSF WT cells. Cells were incubated with neat C4-1E11 antibody followed by Alexa Fluor 488 (AF488)-conjugated goat anti-mouse IgM (Green) or Alexa Fluor 594 (AF594)-conjugated goat anti-mouse IgG (Red). Star indicates cells were the full flagellum is stained. Panels from left to right: DIC, DAPI staining of nuclei (N) and kinetoplasts (K), AF488 (Sec IgM), AF594 (Sec IgG), DAPI/AF488 merge, DAPI/AF594 merge and AF488/AF594 merge. Scale bar – 10 µm.

The supernatant M5-2E4 does not display any specific signal by WB but recognises proteins with distinct localisations by IFA (Figure 3. 70 B). Most importantly, anti-IgG and IgM secondary antibodies recognise proteins that seem to localise quite differently (Figure 3. 70 B), although displaying some cross-localisation.

Both anti-IgG and IgM secondary antibodies recognise specific points in the flagellum, but anti-IgM IFA also shows distribution throughout the cell body. Interestingly, the anti-IgM distribution does not show exclusion from the nucleus as observed for other antibodies. As for anti-IgG secondary antibodies, they recognise a point at the end of the flagellum in all 1N1K cells (Figure 3. 70 B "1N1K" cell) and two specific points for other cell cycle phases (Figure 3. 70 B "1N2K" and "2N2K" cells).

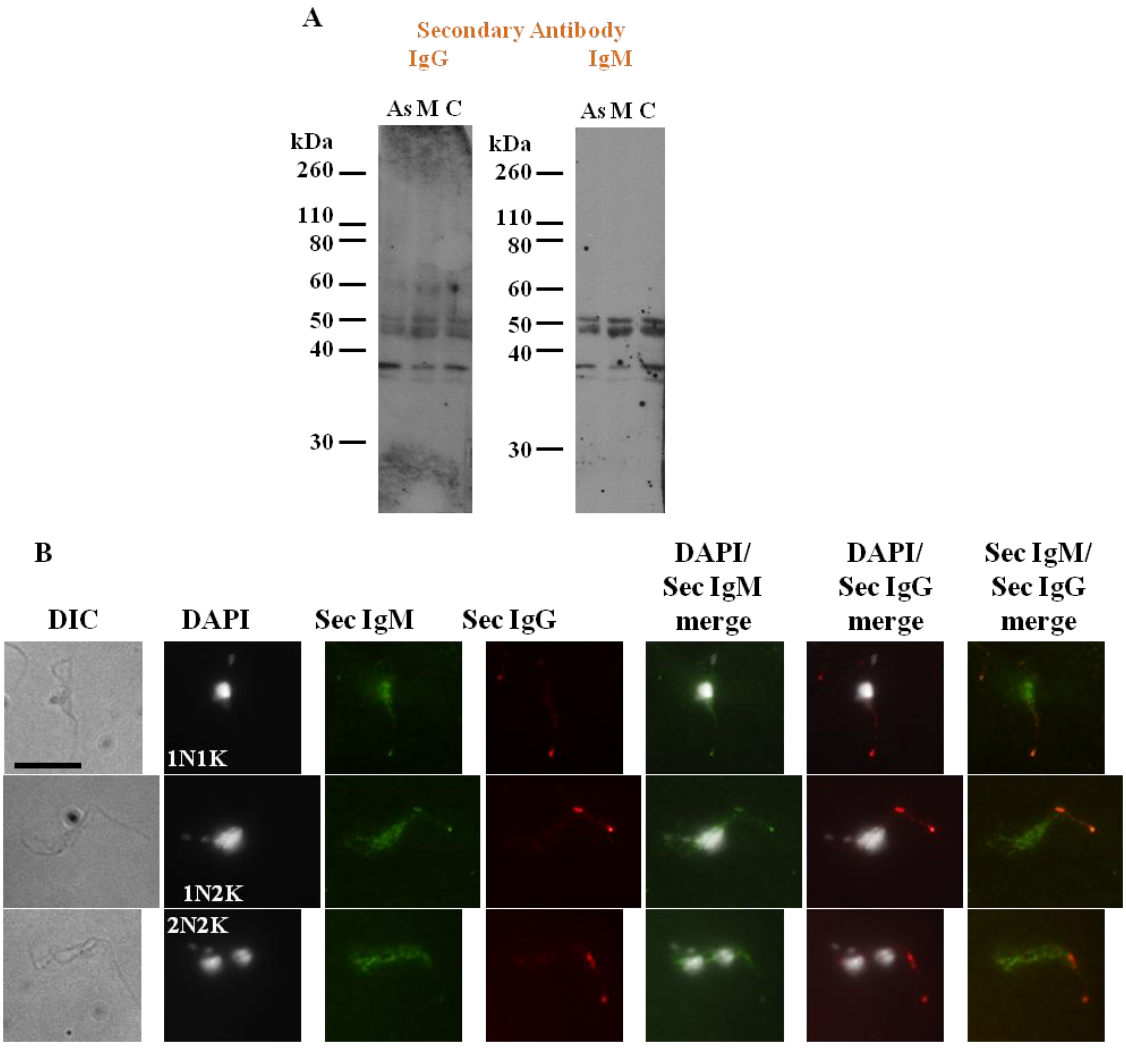

Figure 3. 70 - Characterisation of MAb M5-2E4. A – WB. Cytoskeleton preparations of asynchronous cultures (As) and synchronized cultures in mitosis (M) and cytokinesis (C) were probed with neat M5-2E4 overnight at 4ºC. The blot was initially probed with a secondary anti-mouse IgG antibody (HRP conjugated) and developed, before being stripped, re-incubated with the same primary antibody and a secondary anti-mouse IgM antibody (HRP conjugated). Ladder - Novex Sharp Pre-stained Protein Standard (Invitrogen). B- IFA using BSF WT cells. Cells were incubated with neat M5-2E4 antibody followed by Alexa Fluor 488 (AF488)-conjugated goat anti-mouse IgM (Green) or Alexa Fluor 594 (AF594)-conjugated goat anti-mouse IgG (Red). Panels from left to right: DIC, DAPI staining of nuclei (N) and kinetoplasts (K), AF488 (Sec IgM), AF594 (Sec IgG), DAPI/AF488 merge, DAPI/AF594 merge and AF488/AF594 merge. Scale bar – 10 µm.

For M2-1B7, WB results are not very successful and only anti-IgG secondary antibodies recognise a 260 kDa protein from an 8% gel, present only in the mitosis and cytokinesis samples (Figure 3. 71 A). While anti-IgM secondary antibodies recognise proteins located throughout the cytoplasm, with no specific localisation, anti-IgG antibodies display a similar localisation to previous antibodies. A bright fluorescent signal is seen at the end of the flagellum (Figure 3. 71 B) and for some cells in the middle, as seen for M5-2E4 (Figure 3. 70). Other supernatants during this study revealed similar localisations (for example C4-1E11 and M2-3F10), all recognising by WB a ≈ 38 kDa protein (Figure 3. 69 and Figure 3. 73). Two dots are seen near the kinetoplasts, although for some 2N2K cells they seem to be located close to only one of the kinetoplasts and not both (Figure 3. 71 B "2N2K" cell). As the signal is quite weak, probably due to a low antibody concentration, no conclusions could be taken for this supernatant as to its recognition of specific cytoskeleton organelles.

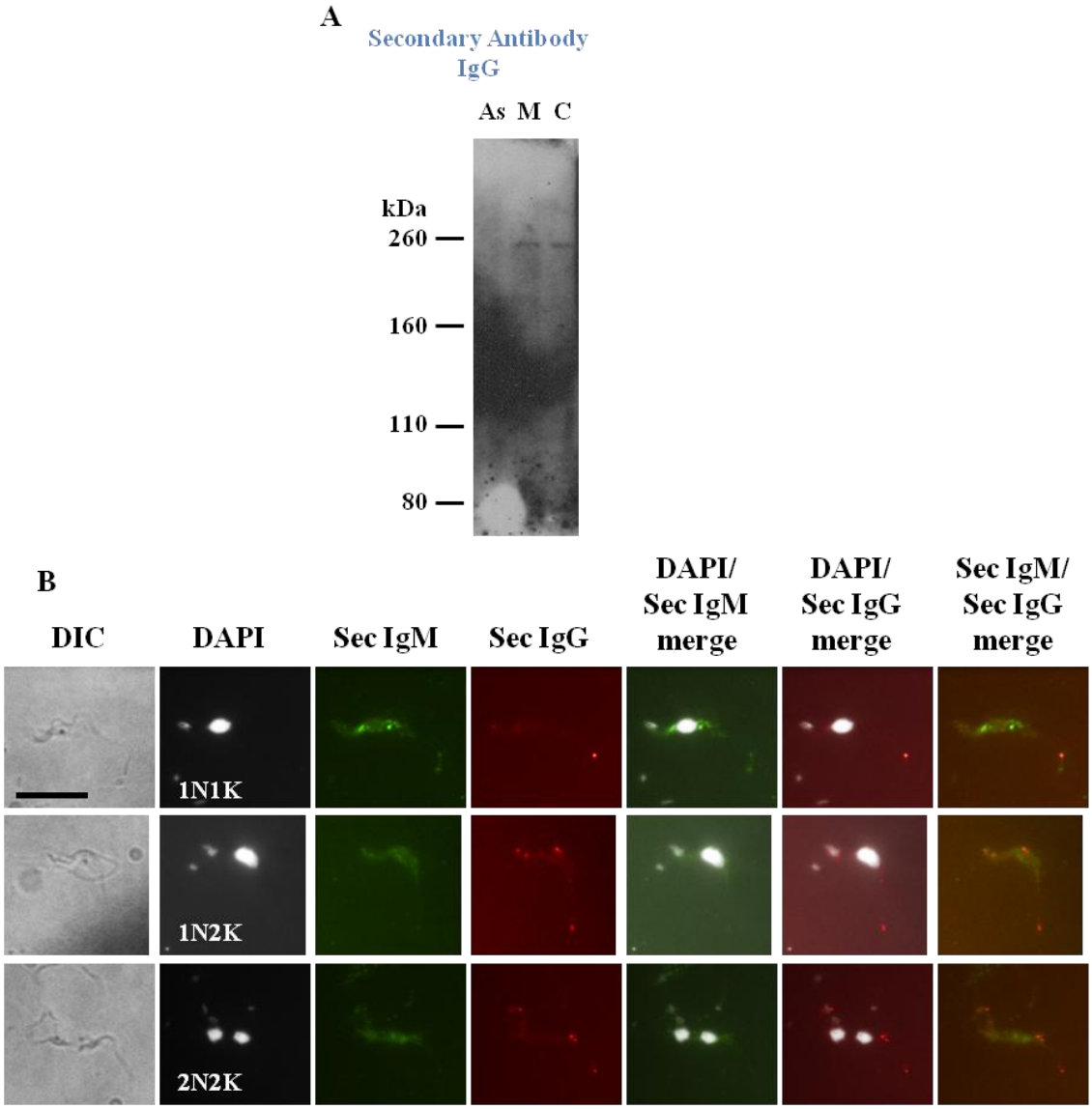

Figure 3. 71 - Characterisation of MAb M2-1B7. A – WB. Cytoskeleton preparations of asynchronous cultures (As) and synchronized cultures in mitosis (M) and cytokinesis (C) were probed with neat M2-1B7 overnight at 4ºC. The blot was initially probed with a secondary anti-mouse IgG antibody (HRP conjugated) and developed, before being stripped, re-incubated with the same primary antibody and a secondary anti-mouse IgM antibody (HRP conjugated). Only results for the anti-mouse IgG antibody are presented here. Ladder - Novex Sharp Pre-stained Protein Standard (Invitrogen). B- IFA using BSF WT cells. Cells were incubated with neat M2-1B7 antibody followed by Alexa Fluor 488 (AF488)-conjugated goat anti-mouse IgM (Green) or Alexa Fluor 594 (AF594)-conjugated goat anti-mouse IgG (Red). Panels from left to right: DIC, DAPI staining of nuclei (N) and kinetoplasts (K), AF488 (Sec IgM), AF594 (Sec IgG), DAPI/AF488 merge, DAPI/AF594 merge and AF488/AF594 merge. Scale bar – 10 µm.

Initial conclusions could indicate that the protein recognised by M5-2E4 and M2-1B7 localise to both the mature and developing flagellum during the cell cycle, as seen previously for kinesin 13-2 (Chan *et al.*, 2010, Chan and Ersfeld, 2010). However,

this protein has been localised to the distal tip of the flagellum in interphase cells and at the tip of both mature and developing flagellum during the cell cycle, which was not observed for M5-2E4 and M2-1B7, nor for C4-1E11 (Figure 3. 72 arrows). As opposed to KIF13-2, the IFA signal for the generated MAbs is located at the end of the flagellum but not at the tip (Figure 3. 72 arrows).

If in fact these antibodies are interacting with proteins localised to the end of the old and new flagellum, they could become highly valuable tools for following up flagella development. A more thorough analysis would be necessary to understand if such staining reveals a dynamic pattern, as would be expected for antibodies recognising the tip of the growing flagellum. If on the other hand the IFA signal remains in the same location during cell cycle, it could mean recognition of a possible furrow ingression protein.

A more accurate analysis of the exact localisation of the recognised proteins would be possible with purification of the IgG antibodies from the M5-2E4 supernatant, confirming subcellular localisation by cell fractionation and co-staining with antibodies that recognise flagellar proteins and specifically the new/old flagellum.

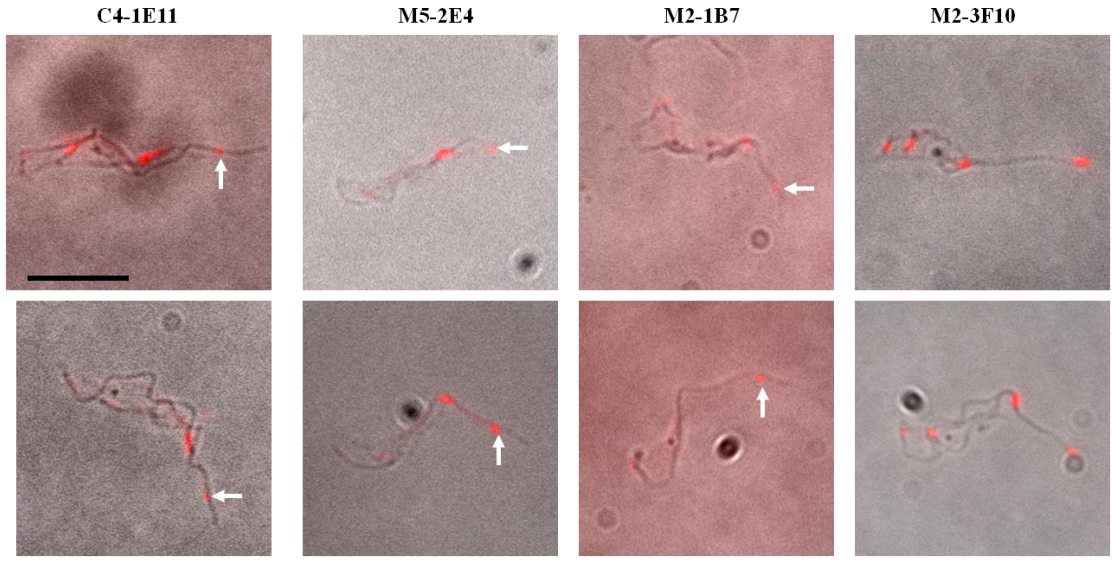

Figure 3. 72 - Characterisation of the MAbs C4-1E11, M5-2E4, M2-1B7 and M2-3F10 as to their flagellar localisation. IFA images were obtained as previously and panels show the AF594 (red)/DIC merge (left) for different cells. The arrows indicate the IFA signal at the end of old the flagellum but not exactly at the tip. Scale bar – 10 µm.

The final antibody – M2-3F10 - recognises by WB a 38 kDa protein with secondary anti-IgG antibodies, demonstrating a stronger signal for the asynchronous cytoskeleton sample (Figure 3. 73 A). Attempts to screen this supernatant by WB using an anti-mouse IgM secondary antibody were unsuccessful. Further, the IFA pattern is quite distinct (Figure 3. 73 B). Two dots are observed at the posterior end close to the kinetoplast, suggesting BB/FP staining, and the tip of the flagellum is stained for cells in all cell cycle phases. For 1N2K and 2N2K cells, another specific signal appears in a flagellar location (Figure 3. 73 B), which could correspond once again to the tip of the developing flagellum.

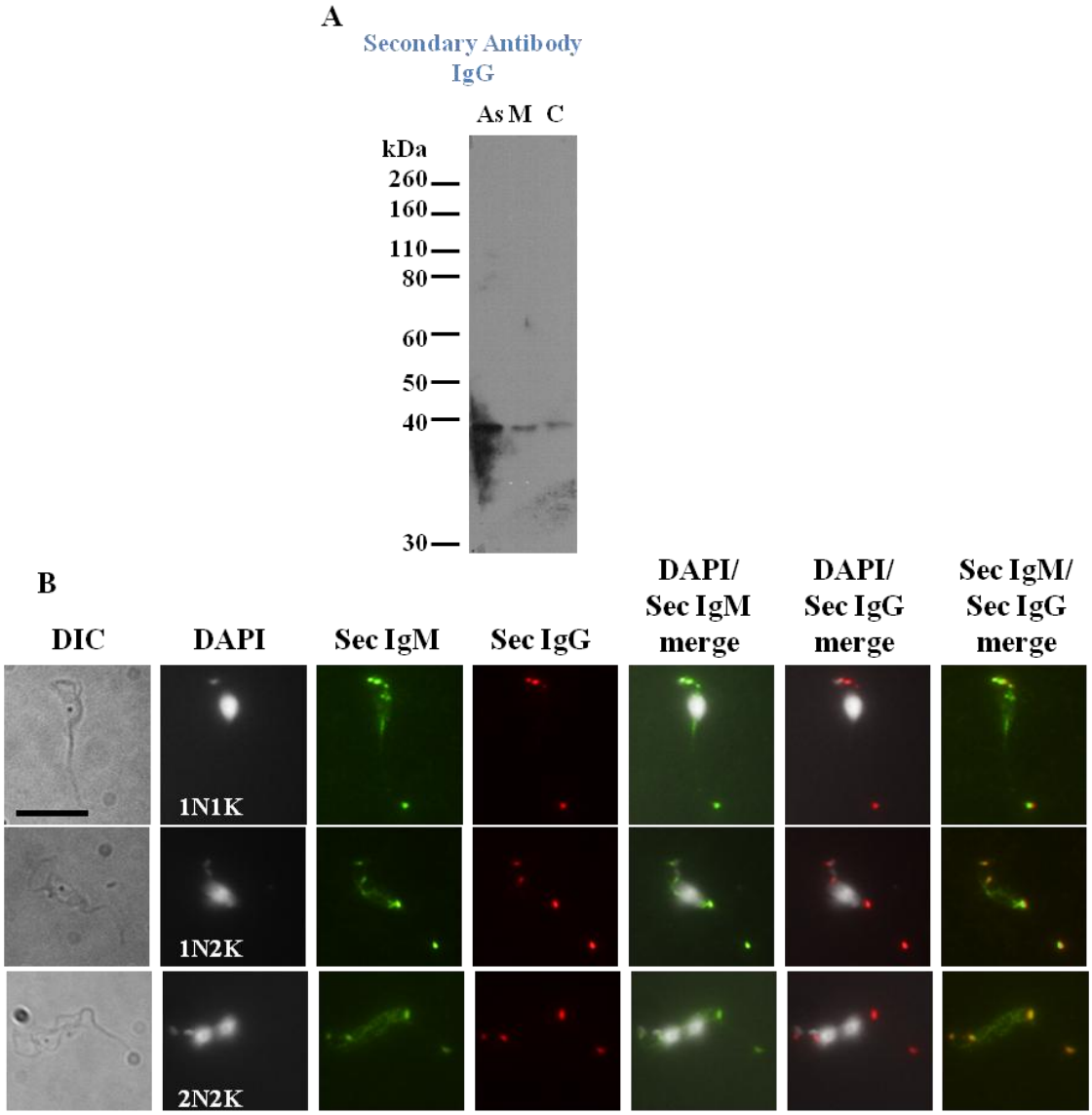

Figure 3. 73 - Characterisation of MAb M2-3F10. A – WB. Cytoskeleton preparations of asynchronous cultures (As) and synchronized cultures in mitosis (M) and cytokinesis (C) were probed with neat M2-3F10 overnight at 4ºC. The blot was initially probed with a secondary anti-mouse IgG antibody (HRP conjugated) and developed, before being stripped, re-incubated with the same primary antibody and a secondary anti-mouse IgM antibody (HRP conjugated). Only results for the anti-mouse IgG antibody are presented here. Ladder - Novex Sharp Pre-stained Protein Standard (Invitrogen). B- IFA using BSF WT cells. Cells were incubated with neat M2-3F10 antibody followed by Alexa Fluor 488 (AF488)-conjugated goat anti-mouse IgM (Green) or Alexa Fluor 594 (AF594)-conjugated goat anti-mouse IgG (Red). Panels from left to right: DIC, DAPI staining of nuclei (N) and kinetoplasts (K), AF488 (Sec IgM), AF594 (Sec IgG), DAPI/AF488 merge, DAPI/AF594 merge and AF488/AF594 merge. Scale bar – 10 µm.

As opposed to previous described antibodies with similar IFA distribution, the bright point at the posterior end of the cell does coincide with the flagellum tip (Figure 3. 72). In general, M2-3F10 recognises the BB, the tip of the old flagellum and a third

point which is absent from 1N1K cells. The lack of such staining in these cells might indicate that it corresponds to the tip of the new flagellum, resembling the localisation of Kif13-2 (Chan and Ersfeld, 2010). To better understand if this staining corresponds to the flagellar tip of both old and new flagellum, it would be interesting to analyse cells undergoing furrow ingression or during abscission and confirm if the IFA signal is still present at the tip of both flagella. This MAb could provide a novel mean of following the dynamic pattern under flagellar division.

In 1995 a MAb previously raised against bovine sperm flagellum cytoskeletal antigens is reported to detect flagellum associated structures in *T. brucei* (Woodward *et al.*, 1995). Its IFA localisation is quite similar to M2-3F10, as both BS7 and M2-3F10 stain the distal tip of both the old and new flagella, and BS7 also presents a fluorescent dot close to the kinetoplast, quite visible for cytoskeleton samples prepared using high salt extraction techniques. When characterised by WB using total *T. brucei* cell extracts, BS7 co-interacts with a lot of polypeptides, leading authors to believe that it might recognise an aminoacid sequence or a post-translational modification common to several *T. brucei* proteins. Separation of these polypeptides and further use as antigens for generation of polyclonal antisera lead to the production of two monospecific antisera, both recognising BB proteins by IFA, one with 43 kDa and the other with 47 kDa (Woodward *et al.*, 1995). The smaller protein is also recognised by the anti-BB antibody BBA4. The supernatant M2-3F10 recognises by WB a protein with approximately 38 kDa, but it would be interesting to compare this MAb with BBA4, BS7 and BS7 specific antisera against the 43 kDa protein, by WB and IFA.

3.3.8. **Characterisation of MAbs with unique localisation**

Supernatant M5-3G2 shows very similar WB results to M5-3E2 (Figure 3. 45 A), recognising more strongly samples from cultures synchronized in mitosis and cytokinesis, particularly two doublets of 80 and 50 kDa (Figure 3. 74 A arrow). WB results are in accordance with previous dot-blot results, which had shown that this MAb reacts strongly with cytoskeleton samples of cells late in the cell cycle, especially against enriched cytokinetic cultures (Figure 3. 43). However, the cross-reaction with

proteins with smaller molecular weights is quite strong, making it difficult to distinguish between specifically recognised proteins and background cross-reaction (Figure 3. 74 A).

Although presenting similar WB data, M5-3E2 displays a punctate distribution throughout the cell body (Figure 3. 45 B), while M5-3G2 presents a novel distribution, recognising the nucleus, the kinetoplasts and the flagellum (Figure 3. 74 B). Such a localisation pattern has not been identified yet in *T. brucei*. However, WB results do not show specificity of either anti-IgG or anti-IgM antibodies, making it impossible to analyse which protein(s) are responsible for this distribution pattern. On the other hand, a ≈ 25 kDa protein is recognised quite strongly, meaning that smaller proteins could be the target of this antibody, while the higher bands represent just a background signal, but new WB analyses would be needed to confirm this.

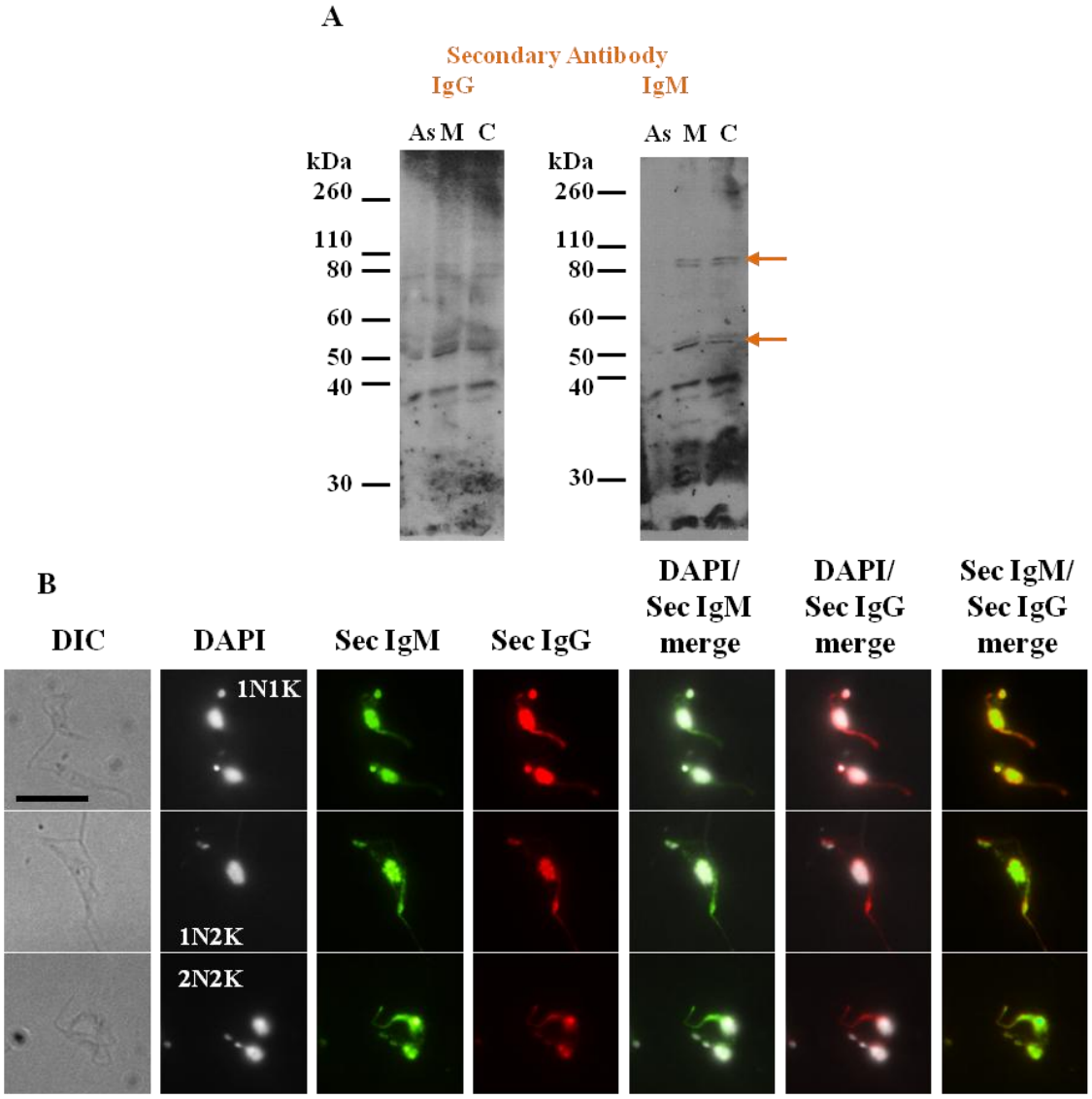

Figure 3. 74 - Characterisation of MAb M5-3G2. A – WB. Cytoskeleton preparations of asynchronous cultures (As) and synchronized cultures in mitosis (M) and cytokinesis (C) were probed with neat M5-3G2 overnight at 4ºC. The blot was initially probed with a secondary anti-mouse IgG antibody (HRP conjugated) and developed, before being stripped, re-incubated with the same primary antibody and a secondary anti-mouse IgM antibody (HRP conjugated). Ladder - Novex Sharp Pre-stained Protein Standard (Invitrogen). The arrows point to the protein band recognised with stronger signals in the mitotic and cytokinetic enriched populations. B- IFA using BSF WT cells. Cells were incubated with neat M5-3G2 antibody followed by Alexa Fluor 488 (AF488)-conjugated goat anti-mouse IgM (Green) or Alexa Fluor 594 (AF594)-conjugated goat anti-mouse IgG (Red). Panels from left to right: DIC, DAPI staining of nuclei (N) and kinetoplasts (K), AF488 (Sec IgM), AF594 (Sec IgG), DAPI/AF488 merge, DAPI/AF594 merge and AF488/AF594 merge. Scale bar – 10 µm.

Once again, the IFA results do not correlate with previous assays that suggest higher expression of the recognised proteins in late cell cycle phases. A bright staining is visible for cells in all cell cycle phases, with both anti-IgG and IgM antibodies.

This MAb is quite interesting as to the localisation of the target protein, presenting a distinct immunolocalisation pattern. The reduction of background cross-reactions and increase in antibody specificity would allow more thorough conclusions as to the protein (s) identified by this supernatant. Once again pull-down assays, mass spectrometry experiments and the use of phage-display libraries could be used for additional characterisation of the target protein. Being the first time a protein localises to such distinct organelles as the kinetoplast, nucleus and flagellum, its functional role in cell biology/cell cycle would be quite interesting to follow. If in fact the protein is highly expressed in cells undergoing cytokinesis, even if by IFA the antibody seems to stain cells in different cell cycle phases equally, it might be involved in regulation of cellular division.

This project has allowed the generation and classification of different MAbs by using protein samples containing unknown antigens. Although much work remains to be done, a lot of experiments would need further work to allow better classification of antibodies, and no antibody revealed a valid recognition of a protein with possible function in cell cycle regulation, very interesting MAbs have been produced. They could function as tools for understanding *T. brucei* cell biology, and also to follow different cellular processes.

4. CONCLUSIONS

There is a direct link between the life cycle of *T. brucei* and cell cycle regulation (Matthews, 1999, Hammarton *et al.*, 2003b). Significant advances in our understanding of cell cycle control in *T. brucei* has made it clear that regulation of cell cycle progression in *T. brucei* is quite unique and distinct from that in mammals, and this lead several authors to believe that regulatory proteins could present good drug targets (Hammarton *et al.*, 2003b, Naula *et al.*, 2005).

Over the years, considerable progress has been made in identifying molecular regulators, elucidating their functions and understanding the role of cell cycle markers/checkpoints (Sherwin and Gull, 1989a, Woodward and Gull, 1990, Ploubidou *et al.*, 1999). This was made possible by the sequencing of *T. brucei* genome in 2005 (Berriman *et al.*, 2005), together with transcriptome analyses and RNAi screens (Tu and Wang, 2005a, Tu and Wang, 2005b, Monnerat *et al.*, 2009, Mackey *et al.*, 2011, Alsford *et al.*, 2011, Archer *et al.*, 2011). However, many regulatory proteins remain unidentified and the pathways they control are still unknown.

Many functional studies of regulatory proteins have only been possible due to the help of antibodies specifically recognising them (Kohl *et al.*, 1999, Bonhivers *et al.*, 2008a, Li and Wang, 2008, Dacheux *et al.*, 2012). On the other hand, characterisation of cellular components has been made feasible by the generation of MAbs against cellular preparations purified from *T. brucei* cells (Woods *et al.*, 1989, Woodward *et al.*, 1995, Pradel *et al.*, 2006).

MAb production has been extensively used for the study of different diseases caused by parasitic protozoa. For example in Leishmaniasis, MAbs have been analysed as possible markers for visceral leishmaniasis diagnosis (Santarém *et al.*, 2005), for treatment follow-up (Qu *et al.*, 1991, Todolí *et al.*, 2010), and even to distinguish between different species and subspecies (McMahon-Pratt *et al.*, 1982, Chaves *et al.*, 2003), transforming MAb techniques into a novel typing and diagnosis method. Similarly, production of MAbs has long been used for detection of *T. evansi* (Nantulya *et al.*, 1989, Diall *et al.*, 1992) and *T. brucei* species (Kanwe *et al.*, 1992, Olaho-Mukani *et al.*, 1992), and in 1987 a MAb-based laboratory technique was also developed to distinguish different *Trypanosoma* species (Nantulya *et al.*, 1987), proving that MAb-

based techniques could become useful techniques for immunodiagnosis of African trypanosomiasis.

Besides the primary use of MAb production in detection and typing methods against several pathogenic species, several studies have been performed to investigate the use of MAbs or immunisation strategies as therapeutic techniques. For example, several studies about MAb effect on parasite survival have been performed in *T. cruzi* (Luhrs *et al.*, 2003, Cortés-Figueroa *et al.*, 2008), with a paper published in 2003 demonstrating that injection with recombinant PFR proteins conferred protection against *T. cruzi* infection (Luhrs *et al.*, 2003). Over the years, several studies have been performed in *T. brucei* on the lytic activity of generated MAbs against Metacyclic Variable Antigen Types (M-VATs) (Crowe *et al.*, 1984), ganglioside antigen (Tsujimura *et al.*, 2005) and tubulin (Lubega *et al.*, 2002, Kateete *et al.*, 2012). Also, recent work has used *T. brucei* as an epitope-display platform, as an alternative approach for antibody production (Stavropoulos and Papavasiliou, 2010).

However, the need to build more sensitive and specific tests and the need for a more efficient therapeutic strategies calls for the generation of new and more specific MAbs (Desquesnes, 1996). This project appeared as a result of these needs and was developed in two directions. The first one was to produce MAbs against recombinant proteins involved in cell cycle regulation, like PLK (results not shown), MOB1 (results not shown) and CRK12, and study their use in antibody based therapies. In parallel emerged the interaction study of CRK12 and CYC9 and their function in *T. brucei* biological processes. The second project had the aim of identifying new proteins as cell cycle regulators, involving production of MAbs against protein samples containing unknown antigens.

4.1. CRK12 AND CYC9 FUNCTION IN DISTINCT BIOLOGICAL PROCESSES BUT COMPRISE A NOVEL CRK:CYC COMPLEX IN *T. BRUCEI*

Among the different cell cycle regulators that are vital for assuring an accurate progression through the cell cycle and generating viable progeny are the CRKs and their CYC partners (Mottram, 1994, Nigg, 1995, Satyanarayana and Kaldis, 2009). So far, eleven CRKs and ten CYCs have been identified in *T. brucei*, although a role in cell cycle regulation has not been established for all of them and only two active CRK:CYC complexes have been identified *in vivo* (Van Hellemond *et al.*, 2000, Hammarton *et al.*, 2003a, Gourguechon *et al.*, 2007). Although some CRKs have been proved to interact with certain CYCs *in vitro* (Gourguechon *et al.*, 2007, Gourguechon and Wang, 2009), this has not been confirmed using *T. brucei* cells.

Previous work performed by members of the Hammarton lab suggested that CRK12 and CYC9 are interacting partners. These results were quite interesting as not much is known about CYC9 and the only data published so far for CRK12 indicates that, although not being an essential protein for PCF cells (Gourguechon and Wang, 2009), CRK12 is vital for BSF proliferation (Mackey *et al.*, 2011).

As previous attempts to produce CYC9 as a soluble recombinant protein were unsuccessful, antibodies were produced against the kinase CRK12. Anti-CRK12 MAbs were generated by immunisation of Balb/c mice with recombinant 6xHis:CRK12 (84.6 kDa), previously cloned, expressed and purified. Purification efficiency was quite low (approximately 1 mg per 200 ml of *E.coli* culture) due to the low solubility of 6xHis:CRK12, degradation problems, weak interactions between the desired protein and the purification column and weak stability of the purified protein. The two mice injected intraperitoneally with 6xHis:CRK12 gave high antibody titres (higher than 1:6400), although only the one with higher titre was sacrificed and used for production of hybridoma cell lines.

The calculated fusion efficiency when considering the 199 tested supernatants was 4%, with 8 final positive hybridomas, screened by ELISA and WB using different

recombinant proteins and *T. brucei* cell lysates. One supernatant (4D7), which recognised the desired protein in PCF cell lines was selected for further work. MAb 4D7 displayed specific signals against CRK12 in *T. brucei* BSF WT and PCF WT cell extracts, and showed a clear decrease in CRK12 expression in BSF RNAi cell lines from 12 hours post-induction. When tested against ty:CRK12 over-expression cell lines, 4D7 recognised more strongly CRK12 in the induced BSF and PCF cell lysates than in uninduced lysates, although interacting also with possible degradation products. Interestingly, the induced band corresponded to a protein doublet, which suggests interaction of 4D7 with the native protein and the induced tagged version. Attempts were made to confirm this, using an anti-TY antibody (BB2), but results were inconclusive (results not shown). In conclusion, 4D7 MAb recognises CRK12 in distinct *T. brucei* cell extracts in a specific way, presenting a novel antibody with potential use in different studies.

Anti-CRK12 MAb 4D7 was also analysed as to its ability to pull-down CRK12 from a BSF cell lysate and for immunolocalisation studies. When used in IP assays, 4D7 is capable of pulling CRK12 down from the cell lysate, although with low efficiency. An antibody concentration issue or low binding between the antibody and the beads might have interfered with this experiment. Also, the lack of a cross-linking step between the beads and the antibody might have influenced the purification efficiency.

Localisation studies were performed using the hybridoma supernatant as a primary antibody, as the purification of MAb 4D7 was unsuccessful. The fact that this supernatant might not have been concentrated or pure enough might have hindered this assay, or MAb 4D7 might just not be suitable for IFA studies. Nevertheless, a punctate distribution was visible for both BSF and PCF cells, with no clear concentration at any cellular component. Because IFA with 4D7 did not show any decrease in fluorescence signal when using *CRK12* RNAi cell lines, this MAb might not be specific in immunolocalisation studies.

Although antibody production was quite efficient, relative to the fact that 4D7 recognises CRK12 specifically by WB, the lack of a successful purification of this supernatant prevented further work. On the other hand, time constraints did not allow a

second attempt on MAb purification, meaning that *in vitro* and *in vivo* analyses on the lytic activity of MAb 4D7 and protection studies with recombinant CRK12 were not performed. As further studies revealed that CRK12 is essential for proliferation of *T. brucei in vitro* and *in vivo*, it would have been interesting to check if 4D7 lead to clearance and neutralization of *T. brucei* in both models.

Furthermore, it would be interesting to analyse CRK12 expression in different cell cycle phases. An attempt to check this at the protein level was performed, using synchronized protein samples generated during this project, but results were not very clean and as such no conclusions were made (results not shown).

The idea that CRK12 and CYC9 form a complex originated from a yeast-two hybrid assay with all the CRKs and CYCs identified in *T. brucei*. Further work by previous lab members involving IP studies indicated that these proteins interacted *in vivo* in PCF trypanosomes. As such, confirmation of the interaction in BSF cell lines was needed.

During these studies, different tagged cell lines were generated or used, which allow detection of the desired proteins, given the lack of specific and high affinity antibodies. For co-purification studies, a BSF cell line with ty:CRK12 expression under inducible control was used, while CYC9:TAP was co-expressed from the endogenous locus. CRK12 was pulled-down with an anti-TY antibody (BB2), and co-purification was analysed by WB using a PAP antibody against the TAP tag fused to CYC9. Although once again the pull-down of ty:CRK12 was not very efficient, it was sufficient to lead to co-purification of CYC9. In conclusion, CRK12:CYC9 constitutes a novel CRK:CYC complex identified in both life cycle stages.

With this novel result came the idea to check for co-localisation by IFA. In fact, if these proteins interact, their localisation at a certain time should coincide. Once again tagged cell lines were used with commercial antibodies recognising the tags. An anti-protein A antibody was used in PCF and BSF CYC9:TAP cell lines, due to its higher specificity for IFA when compared to the PAP antibody, while for the BSF ty:CRK12 over-expression cell line, an anti-TY antibody was used. Co-localisation studies with

CYC9:TAP and ty:CRK12 using the same cell line were not feasible as the anti-protein A antibody interacts strongly with other IgGs, interfering with TY fluorescence.

Although presenting distinct distributions, CRK12 and CYC9 exhibit potentially overlapping localisations. While CYC9 is located in the nucleus of both PCF and BSF cells in all cell cycle stages, CRK12 exhibits a cytoplasmic distribution in BSF trypanosomes, with possible enrichment between the nucleus and the kinetoplast(s). A possible concentration of CRK12 is visible at the nucleus periphery, which could mean that this kinase and CYC9 interact at this zone. As CYC concentration varies in a cyclical fashion, CRK12 and CYC9 might interact at those points during specific stages. For example, the phosphorylation status of CRK12/CYC9 could mean that only a part of CRK12 would be concentrated at the nucleus periphery, in order to interact with CYC9 . In fact, their localisation might only coincide when CYC9 is activating CRK12, which could mean on the other hand that the endogenous CYC would move to the nucleus periphery at certain time points in the cell cycle, in order to interact with CRK12.

The fact that they regulate different biological processes in *T. brucei* and might be interacting with additional partners might reflect on their localisation. On the other hand, as activation of the kinase depends on CYC activity, the presence of CRK12 over-expressed might affect its localisation at the subcellular level.

Further studies should aim at confirming this. The initial step should be to co-localise both proteins, by using different sets of antibodies or different cell lines. Additionally, both proteins should be analysed when expressed at endogenous levels, although attempts to do this by *in situ* fluorescent microscopy of ty:GFP:CRK12 were unsuccessful, probably due to the low level of the kinase expression.

As IFA studies were performed using tagged cell lines, one should take into consideration that presence of such tag might affect the natural protein localisation. The ideal localisation studies should be performed in WT cell lines, with anti-CYC9 and anti-CRK12 antibodies.

As CRK12 and CYC9 present a novel complex in *T. brucei*, that display different but possibly overlapping localisations, it was interesting to analyse their

function in the parasite. This was done by studying BSF RNAi cell lines, and results show that CRK12 and CYC9 are essential for cell proliferation *in vitro*, as silencing of either of them caused a clear growth arrest.

As CRKs and CYCs are among the regulatory proteins that are fundamental for cell cycle control and their depletion leads normally to cell cycle defects, flow cytometry and DAPI analyses were performed to assess RNAi effects on cell cycle progression. If on the one hand, CRK12 depletion does not cause any obvious cell cycle defect, the opposite is true for CYC9 depletion. Both flow cytometry and DAPI studies revealed that *CYC9* RNAi causes most 2N2K cells to be stalled during furrow ingression, leading to an evident decrease in the number of cells that actually reach the final stage of cytokinesis, abscission. Consequently, this leads to the appearance of a population with abnormal N/K configurations, many of which corresponded to cells with multiple nuclei and kinetoplasts ("monster" cells). After 18 hours of RNAi induction, such cells constitute of approximately 30% of the total population. In conclusion, CYC9 depletion inhibits cytokinesis.

CYC9 is the first CYC proved to function as a cytokinesis regulator. Its functional role differs from other CYCs, as CYC2 and CYC6 regulate G_1/S transition and mitosis, respectively (Li and Wang, 2003, Hammarton *et al.*, 2004). However, all these proteins share a role in controlling cell cycle progression. Taking into consideration its nuclear localisation, CYC9 might function in controlling expression of genes involved in cytokinesis. Future work would be needed to confirm this and to analyse the effect of depletion of CYC9 on other genes. As these studies suggest that CYC9 could be interacting with other proteins besides CRK12, the first step would be to try and identify those proteins by using pull-down assays. If in fact those proteins showed function in cytokinesis control, it would be interesting to analyse their level of gene expression before and after *CYC9* RNAi induction and also their localisation in subcellular compartments.

As for CRK12, no accumulation of abnormal cells is visible after RNAi induction, meaning that CRK12 does not assume a major role as a cell cycle regulator.

An interesting phenotype is however visible after a careful microscope analysis of induced cells. After 18 hours post-induction, an average of 27% and 30% of 1N2K and 2N2K cells, respectively, present abnormally positioned kinetoplasts. This was not considered to be as a direct result from kinetoplast movement, but more likely to reflect an abnormally enlarged FP, that either pushes both kinetoplasts to the tip of the cell or forces them to assume a lateral position around the FP. In fact, approximately 23% and 17% of 1N2K and 2N2K cells respectively, possess an enlarged FP after 18 hours of CRK12 depletion.

Confirmation of this phenotype was performed by TEM, where electron micrographs clearly show an enlarged vacuole while the remaining organelles remain normal. This phenotype, first described in *CLH* RNAi BSF cell lines as the "Big-Eye" phenotype (Allen *et al.*, 2003), has been associated with endocytosis defects. In such cells, the FP, site of both endocytosis and exocytosis, becomes massively enlarged due to a blockage in membrane removal while delivery remains normal.

To examine the effect of CRK12 depletion in endocytosis, cells were induced for 18 hours and uptake of FM4-64 was followed. This fluorescent lipid-binding probe associates with membranes and is taken up into cells via the endocytic pathway and removed by recycling, providing a useful tool to follow internalisation from the FP (Field and Carrington, 2004, Field *et al.*, 2004). FM4-64 is visible in the FP at 4ºC and after 30 seconds internalised material can already be seen. Intracellular staining increases with time reaching a maximum at about 5 minutes (Field *et al.*, 2004), which is the time used during this study. Results show that FM4-64 is efficiently taken up by uninduced cells and induced normal cells, both at 4ºC and 37ºC. On the contrary, for induced cells presenting an enlarged FP, no internalisation is visible. As opposed to assays from other authors (Allen *et al.*, 2003, Hall *et al.*, 2004a), the dye does not stay in the FP or close to it, and probably diffuses out the FP when the cells are washed.

In contrast to fluid-phase ligands and fluorescent lipid-binding proteins, Tf internalisation is receptor-mediated (Steverding *et al.*, 1995, Steverding, 2000). As Tf represents a naturally transported ligand for trypanosomes, fluorescently tagged Tf (AF594- transferrin) was used to follow receptor-linked endocytosis. A block in Tf uptake is observed at 37ºC, for both cells with and without an enlarged FP. This

fluorescent ligand remains in the FP, proving that CRK12 knockdown blocks receptor-linked endocytosis.

This study is the first time a CRK is connected with regulation of endocytosis, and demonstrated to have a critical role in this pathway. CRK12 seems to prevent receptor-linked endocytosis but also causes a defect in internalisation of lipophilic dyes in cells with abnormally enlarged FP. The way this kinase regulates this biological pathway is not yet understood, but might involve phosphorylation of a protein involved in the endocytic machinery. Although no phosphorylation of common generic CDK substrates is visible, CRK12 is an active kinase *in vivo* as it undergoes autophosphorylation (Monnerat *et al.*, 2012). This could indicate a high specificity of CRK12 activity and, together with its enrichment between the kinetoplast (s) and nucleus where the endosomal markers are concentrated, creates the idea that CRK12 interacts with a component of the endocytic pathway. However, one cannot rule out that CRK12 might control gene expression of endocytic regulators, and thus indirectly affect this process. CRK12 could provide a useful tool to increase the understanding of the endocytic machinery of *T. brucei*, a process so divergent from that of other eukaryotes (Adung'a *et al.*, 2013).

TbRAB5 knockdown also blocks receptor-mediated endocytosis (Hall *et al.*, 2004a), as opposed to TbRab4 that affects regulation of fluid-phase but not receptor mediated trafficking (Hall *et al.*, 2004b). Although the role of CRK12 in fluid-phase endocytosis was not analysed during this study, it could be examined with the use of fluorescent dextran as a marker. On the other hand, attempts were made to monitor endosomal compartments with Concanavalin A, but results were not very clear and optimization is required (results not shown). Besides TbRab5 depletion leading to receptor-linked endocytosis defects, it also caused the mislocalisation of endosomal markers, a decrease in CLH levels and accumulation of this protein around the FP (Hall *et al.*, 2004a). Although endosomal markers were not analysed for *CRK12* RNAi cells nor the level of CLH expression, CLH localisation was followed. Results show that, instead of localising to tubule-vesicular structures in the cytoplasm (Morgan *et al.*, 2001), CLH remained at the periphery of the FP in cells with an enlarged FP (Monnerat *et al.*, 2012).

Previous published results for CRK12 show that this kinase is not essential for PCF proliferation *in vitro*, although a significant reduction in the mRNA levels was verified (Gourguechon and Wang, 2009). No further work was performed in this life cycle stage, although it would have been interesting to analyse if CRK12 depletion in PCF trypanosomes causes morphological alterations, as TbCLH does (Allen *et al.*, 2003). In fact, TbCLH knockdown only causes endocytosis defects in the BSF trypanosomes, while in PCF cells leads to a general round up of cells, internal accumulation of vesicles in the cytoplasm observed by EM, and changes in lysosomal trafficking (Allen *et al.*, 2003). One major difference is that this leads to rapid lethality of PCF cultures, which is not observed for *CRK12* RNAi induction in the insect form (Gourguechon and Wang, 2009). Also, the fact that endocytosis rate is 10 fold higher in the mammalian form, due to its dual role in removal of surface-bound antibodies and in nutrient acquisition, could explain the strong effect of CRK12 depletion in BSF but not in PCF trypanosomes.

It is quite intriguing that, although CRK12 and CYC9 form an active complex in *T. brucei*, they regulate different biological processes in BSF trypanosomes. This might indicate that CRK12 and/or CYC9 interact with additional proteins to control the different processes.

On the other hand, it is possible some kinases/CYCs functionally replace others. In fact, CYC9 might have a potential role in endocytosis control while CRK12 might indeed act as a cell cycle regulator, but once depleted this function is provided by another CYC or CRK, respectively. Finally, if both proteins do indeed regulate both pathways, the threshold level required to affect both processes could be very high, meaning that knockdown of CRK12 or CYC9 affects either endocytosis or cytokinesis, but not both.

Confirmation of either one of these hypothesis would involve further work. Mass spectrometry analyses of the protein sample co-purified with either CRK12 or CYC9 could shed light onto which protein (s) they also interact with. Comparative proteomic studies could also be performed using knockdown cell lines, in order to help identify proteins associated with CRK12/CYC9 function in endocytosis/cytokinesis. Additionally, several authors have studied different proteins involved in these

processes. For example, it would be interesting to analyse CRK12 presence or influence in other RNAi cell lines for early or late endosomal proteins, and check for possible co-interactions or functional redundancy.

During this project, the function of CRK12 and CYC9 was examined thoroughly, and for the first time a trypanosomatid CRK is shown to have a role outside cell cycle regulation. Also, because depletion of CRK12 or CYC9 is lethal in BSF stage *T. brucei*, this novel complex could function as a potential drug target.

4.2. MITOSIS AND CYTOKINESIS ANTIBODIES

The second project developed during this study aimed at identifying proteins with novel functions in cell cycle regulation, namely during mitosis and cytokinesis. This idea appeared from the fact that several authors have been able to identify proteins in *T. brucei* cytoskeleton by first producing antibodies against specific cell lysates (Woods *et al.*, 1989, Bonhivers *et al.*, 2008a). In this project, by using cytoskeleton samples of cultures synchronized in mitosis and cytokinesis, the aim would be to find possible regulators of each phase. On the other hand, as *T. brucei* cell cycle has shown to be dependent on several microtubule events (Robinson *et al.*, 1995, Ploubidou *et al.*, 1999, Kohl *et al.*, 2003, Broadhead *et al.*, 2006, Pradel *et al.*, 2006, Gluenz *et al.*, 2011), instead of using the total cell extract, cytoskeleton purified samples were used instead. Also, structures of the cytoskeleton have been proved to be essential during mammalian infection (Griffiths *et al.*, 2007).

In order to obtain enriched *T. brucei* cultures in mitosis and cytokinesis, parasites were first synchronized in mitosis, by using HU to stall DNA replication (Chowdhury *et al.*, 2008, Forsythe *et al.*, 2009). Cells were grown in HU for one doubling time, 6 hours for BSF and 12 hours for PCF trypanosomes, after which cells were washed and allowed to progress through the cell cycle in a synchronous way, by growing in fresh medium without HU. For the first time, an optimal time point for which to obtain cellular populations in mitosis and cytokinesis was determined. The optimal time point to obtain populations enriched in mitotic cells is 14 ½ hours and 8 ¼

hours, after HU addition with removal at the doubling time, for PCF and BSF trypanosomes, respectively. Similarly, cytokinesis synchronized time points were determined to be hour 15 ½ for PCF and 8 ¾ for BSF, considering once again HU addition at time 0 and removal at the respective doubling time.

Due to time limit constraints, work was performed using the BSF synchronized samples. As cytoskeleton samples are insoluble and contain highly immunogenic proteins like tubulin which might interfere with antibody production, synchronized cytoskeleton preparations were electrophoresed in polyacrylamide gels, cut into slices of different MWt, ground up and injected directly in the mice. A total of 9 slices were cut for each preparation, rejecting the 40 to 60 kDa slice which contains tubulin, but only 5 slices were used: M5 (Mitosis 35-40 kDa); C5 (Cytokinesis 35-40 kDa); M4 (Mitosis 60-80 kDa); C4 (Cytokinesis 60-80 kDa); M2 (Mitosis 100-160 kDa).

Supernatants were screened directly from 24 well plates by WB. The fusion efficiencies ranged from 5% to 19%, resulting in a total of 81 positive hybridomas for all fusions. Some of these supernatants give quite unique patterns, and while some recognise a single protein others seem to recognise a large range of MW antigens but with distinct intensities. It is necessary to take into consideration that the lack of a screening method for 96 well plates might have led to the loss of a lot of positive hybridomas, and the use of an alkaline-phosphatase developing method could have prevented a proper identification of weaker but positive supernatants.

The initial strategy for classification of these 81 antibodies and rejection of the less interesting ones was based on their localisation patterns identified by IFA. Prior to that, some antibodies were classified as to their isotype, and interestingly all of the 10 tested antibodies (from C4 and M4 fusion) are of the IgM class (results not shown). This contrasts with the results obtained for antibodies generated against recombinant proteins, like α-CRK12 and α-PLK MAbs (results not shown), which were all revealed to be of the IgG isotype.

During an immune response, IgM antibodies are the first to appear and eliminate pathogens. They constitute the early stage of B cell mediated immunity before there are sufficient IgG antibodies. An immature B cell has surface bound IgM, and a mature B

cell can express more than one cell surface antibody (IgM/IgD). On antigen stimulation, the B cell proliferates and develops into a plasma cell containing surface bound IgM or a memory B cell expressing IgG or IgA. Thus, the IgG antibodies provide the majority of antibody-based immunity and are formed after class switching and maturation of the antibody response, participating on the secondary immune response.

Normally, generated MAbs should be of the IgG class, as the IgM isotype usually shows less specificity and affinity for the antigen molecule.

Results from this project suggest that when using protein samples containing polyacrylamide and other SDS-PAGE components for the production of MAbs, no antigen switching is visible and the immune response mainly comprises the production of IgM antibodies. On the contrary, when mice are immunised with recombinant antigens, secondary immune responses are activated and IgG antibodies are the most abundant ones. It would seem that the use of recombinant protein for immunisation strategies is better for the production of MAbs.

However, when considering the use of antibodies to induce lysis and agglutination of trypanosomes, IgM antibodies appear to be more potent than IgG in potentiating these effects (Takayanagi and Enriquez, 1973, Musoke *et al.*, 1981). In fact, one of the primary studies on the use of MAbs as therapeutic agents was based on the use of IgM generated MAbs (Crowe *et al.*, 1984).

On the other hand, upon trypanosome infection, the mammalian host mounts an immune response, and several authors over the years have studied these mechanisms (Sternberg, 2004) and how immunoglobulin changes affects *T. brucei* (Takayanagi and Enriquez, 1973, Musoke *et al.*, 1981, Pinder *et al.*, 1984, Taylor and Mertens, 1999) or even *T. cruzi* (Pereira *et al.*, 2003) infection. For example, in neutralization infectivity tests using infected bovines, the trypanolytic efficiency of the first peak in the immune response is mainly due to IgM antibodies rather than IgG1 (Musoke *et al.*, 1981). The opposite is true for the second peak (Musoke *et al.*, 1981). Although B cells are crucial for periodic peak parasitaemia clearance (Magez *et al.*, 2008), trypanosomes induce B cell apoptosis, preventing the induction of protective memory responses and making it difficult for the infected host to mount a proper antibody immune response (Radwanska

et al., 2008, Magez *et al.*, 2010). In fact, it has been suggested that protection from infection in immunisation models is attributed to IgM or the initial host response, rather than the immunological memory (Radwanska *et al.*, 2008, Magez *et al.*, 2010).

It seems that, although common strategies for MAb production suggest IgG antibodies as better for therapeutic studies, the importance of the early IgM response in African Trypanosomiasis infections makes the fact that all the tested antibodies produced with cytoskeleton samples containing SDS-PAGE components are of the IgM class quite interesting.

The initial strategy to classify MAbs as to their IFA localisation was set aside, as it would be impossible to perform WB and IFA analyses on 81 supernatants, and as such a primary selection step was needed. Consequently, all 81 supernatants were screened by dot-blot against cytoskeleton samples from *T. brucei* BSF asynchronous cultures, synchronized in mitosis or cytokinesis. A total of 28 supernatants were selected for further work. MAbs from the same fusion do not show the same results, and MAbs from a mitotic sample, for example, do not all recognise more strongly the mitosis synchronized sample. This is the case of the M5 supernatants, as they all recognise the cytokinesis sample more strongly.

The selected 28 MAbs were screened by WB to examine which proteins they recognise and to analyse their specificity towards cell cycle phases. In parallel, supernatants were tested by IFA to check the immunolocalisation of the recognised antigens and to follow it through the cell cycle. For each experiment, separate assays were performed with anti-IgG and anti-IgM secondary antibodies, although we cannot rule out that the secondary antibodies cross react with primary antibodies of the other isotype.

First of all, results show that anti-IgM secondary antibodies seem to be less specific, presenting more cross-reacting bands by WB and more background staining by IFA. Secondly, although MAbs were generated that recognised proteins of different MW, most of them recognise proteins outside the MW interval of the gel slice used for mice immunisation and most of them seem to cross-react with a 38 kDa and a 50 kDa doublet. This could mean that the MAbs might be recognising an amino acid sequence

or a post-translational modification common to several *T. brucei* proteins, as was mentioned for other studies that used similar MAb approaches (Woodward *et al.*, 1995).

Although initial WB results performed during the screening of hybridoma cells looked promising, with some MAbs recognising specific bands or several ones but with distinct intensities, WB screening with different secondary antibodies presents a lot of background bands. These results might indicate loss of hybridoma producing cells during scale-up, maintenance or stock production, or even that the recognised protein is present in low abundance. Similarly, some MAbs present no signal by WB and/or by IFA, which could relate to a low antibody concentration in these samples.

One important fact to take into consideration during this study is the fact that initial dot-blot results do not always correspond with WB or IFA results. In fact, while supernatants like M5-3E2 (Figure 3. 43 and Figure 3. 45) present comparable results by dot-blotting and WB, others like M5-3G4 (Figure 3. 43 and Figure 3. 46), or C4-2B6 (Figure 3. 43 and Figure 3. 56) do not. For example supernatant M5-2D11 (Figure 3. 43 and Figure 3. 44) recognises the cytokinesis cytoskeleton more strongly by dot-blotting, by WB interacts strongly with both the mitosis and the cytokinesis samples, but by IFA does not show any differences between the different cell cycle phases. The synchronized cytokinesis sample contains approximately 50% 2N2K cells that will/are undergoing cytokinesis, as opposed to the 6% present in the asynchronous population. As such, it would be expected that a supernatant reacting strongly with the cytokinesis sample would show a brighter fluorescence in cells at this phase. However, it is necessary to take into consideration that sometimes the signal might have been saturated in WB and/or IFA assays, and the differences in intensity might have become hard to distinguish. On the other hand, these results could indicate that dot-blotting might not be an accurate method to distinguish MAbs according to the cell cycle phase, or maybe separate assays should have been performed with separate secondary antibody isotypes. Still, it allowed us to reject supernatants that did not recognise any of the samples.

While some antibodies revealed distinct patterns by WB with different secondary isotypes, their immunolocalisation by IFA was similar for both anti-IgG and anti-IgM secondary antibodies. This suggests that some antibody isotypes might be more sensitive for one screening assay.

In general, the WB results obtained during this study were not very accurate and future work should involve repeating these assays with more concentrated and purified MAbs. This would allow a better identification of the antigens recognised and also decrease the intensity of background bands. In parallel, it would allow a more accurate understanding of the two protein doublets commonly identified by different MAbs. In fact, although the 50 kDa and 38 kDa protein doublets were recognised by most MAbs, they were stronger for some particular ones, and work should be performed to conclude if this is only background cross reaction or if in fact that doublet is linked to a certain distribution pattern. For example, the 50 kDa doublet was stronger for one MAb with cytoplasmic distribution, one recognising the cell body and the flagellum, and three interacting with proteins in the flagellum and the BB. On the other hand, the 38 kDa doublet was stronger for some inconclusive MAbs, but also for three MAbs with flagellar localisation, even if only at specific points like M2-3F10 (Figure 3. 73) and C4-1E11 (Figure 3. 69). It is possible that proteins with these MW might correspond to the flagellar distributions seen for some of these MAbs.

Similar to the protein doublets frequently recognised, an 80 kDa band often appeared in some WB experiments. Once again, three out of the five MAbs interacting with this band recognised the flagellum, among other organelles. As mentioned above, confirmation of any relationship would involve further work.

The only antibody demonstrating specific WB results was M4-1B10 (Figure 3. 48), which recognises a 65 kDa protein when using anti-IgG secondary antibodies. Because IFA results do not show any particular concentration at a specific cytoskeleton organelle, more work would be necessary, including purification of the IgG fraction of the supernatant by affinity chromatography using a protein G HP column.

The 28 generated MAbs during this study were classified according to their localisation patterns, giving a total of: 5 inconclusive MAbs; 10 with cytoplasmic distribution; 2 recognising cell body and flagellum; 1 recognising the nucleus, kinetoplast and flagellum; 1 recognising BB/FP; 5 with flagellar distribution; and 4 recognising specific points along the flagellum.

Among the most interesting results is M5-3G2, the MAb interacting with the nucleus, kinetoplast and flagellum (Figure 3. 74). As the WB is not very specific, no conclusions can be taken as to if this pattern corresponds to a single antigen being recognised or to several proteins. If indeed this localisation corresponds to a single protein, it would be interesting to try and identify which one, as no similar localisation has been yet described in *T. brucei*.

In terms of immunolocalisation studies, MAbs generated during this project were efficient in recognising different cytoskeleton components. However, some distributions could potentially be attributed to different organelles, e.g BB/FP staining, and as such some localisation patterns need to be further analysed. One of the first steps to better classify the generated MAbs would be to purify them and obtain them at higher concentrations, so that co-localisation studies with commercial antibodies could be performed.

On the other hand, a high resolution microscopy would be necessary to distinguish between PFR/axoneme/FAZ staining. In fact, several studies have used immunoEM labeling to help localise antigens in these structures (Woods *et al.*, 1989, Woodward *et al.*, 1995, Kohl *et al.*, 1999).

For some MAbs, the lack of a clear IFA staining could have been due to the method itself. In fact, all IFA staining was performed using methanol fixation and a comparison should be performed using PFA fixation. This could have a major influence on IFA signal distribution, as seen for example for the cytoskeleton protein VAMP-associated protein VAP (Lacomble *et al.*, 2012), which locates to the BB, flagellum and ER in PFA fixed cells but looses ER staining when using methanol.

A very useful technique developed by Woodward and colleagues in 1995 (Woodward *et al.*, 1995) is to remove the bands recognized by WB and inject each one in different mice, allowing them to overcome the fact that the generated MAbs recognised different bands in the total cell extract. As in this project the generated MAbs interacted with different proteins, it would be interesting in the future to understand if a particular protein band corresponds to a particular location.

Future work would be needed to better characterise the proteins recognised. If WB results are unsuccessful, an alternative approach could be to use phage display to try and identify the protein target. Alternatively, IP experiments would allow purification of the antigens each MAb binds to, and mass-spectrometry would permit identification of the co-purified proteins.

Only after a better understanding of the antigens recognised and establishment of a correspondence between a WB band and an IFA localisation, could a functional role be inferred for the recognised proteins. Additionally, it would allow a proper establishment of the future use of the generated MAbs, either as possible therapeutic agents or as important tools to study biological mechanisms in *T. brucei*.

4.3. FINAL CONCLUSIONS

During this project, generation of MAbs has been proven to be a useful tool to increase our knowledge on *T. brucei* parasites. In parallel, a novel CRK:CYC complex has been identified, that could be used for future therapeutic strategies. For the first time, a link was found between regulation of endocytosis and a CRK, while its interacting CYC partner presents a role in cytokinesis control.

Major work was performed to produce and characterise MAbs against cytoskeleton components that could function as cell cycle regulators, although many protein samples remained to be injected and many characterisation experiments were not performed due to the limited amount of time. Even though no new proteins were found to act as cell cycle regulators, this technique provides a good alternative for the production of MAbs.

Although time limitations did not allow studies on the trypanolytic activity of the generated MAbs, their possible use as therapeutic agents or even a more accurate characterisation of some of the generated MAbs, this study provides a first step in that direction.

REFERENCES

ABSALON, S., BLISNICK, T., BONHIVERS, M., KOHL, L., CAYET, N., TOUTIRAIS, G., BUISSON, J., ROBINSON, D. & BASTIN, P. 2008a. Flagellum elongation is required for correct structure, orientation and function of the flagellar pocket in *Trypanosoma brucei*. *J Cell Sci,* 121**,** 3704-16.

ABSALON, S., BLISNICK, T., KOHL, L., TOUTIRAIS, G., DORÉ, G., JULKOWSKA, D., TAVENET, A. & BASTIN, P. 2008b. Intraflagellar transport and functional analysis of genes required for flagellum formation in trypanosomes. *Mol Biol Cell,* 19**,** 929-44.

ABSALON, S., KOHL, L., BRANCHE, C., BLISNICK, T., TOUTIRAIS, G., RUSCONI, F., COSSON, J., BONHIVERS, M., ROBINSON, D. & BASTIN, P. 2007. Basal body positioning is controlled by flagellum formation in *Trypanosoma brucei*. *PLoS One,* 2**,** e437.

ACOSTA-SERRANO, A., COLE, R. N., MEHLERT, A., LEE, M. G., FERGUSON, M. A. & ENGLUND, P. T. 1999. The procyclin repertoire of *Trypanosoma brucei*. Identification and structural characterization of the Glu-Pro-rich polypeptides. *J Biol Chem,* 274**,** 29763-71.

ADUNG'A, V. O., GADELHA, C. & FIELD, M. C. 2013. Proteomic analysis of clathrin interactions in trypanosomes reveals dynamic evolution of endocytosis. *Traffic*.

AFFOLTER, M., HEMPHILL, A., RODITI, I., MÜLLER, N. & SEEBECK, T. 1994. The repetitive microtubule-associated proteins MARP-1 and MARP-2 of *Trypanosoma brucei*. *J Struct Biol,* 112**,** 241-51.

AGBO, E. C., MAJIWA, P. A., CLAASSEN, E. J. & ROOS, M. H. 2001. Measure of molecular diversity within the *Trypanosoma brucei* subspecies *Trypanosoma brucei brucei* and *Trypanosoma brucei gambiense* as revealed by genotypic characterization. *Exp Parasitol,* 99**,** 123-31.

ALLEN, C. L., GOULDING, D. & FIELD, M. C. 2003. Clathrin-mediated endocytosis is essential in *Trypanosoma brucei*. *EMBO J,* 22**,** 4991-5002.

ALSFORD, S., ECKERT, S., BAKER, N., GLOVER, L., SANCHEZ-FLORES, A., LEUNG, K. F., TURNER, D. J., FIELD, M. C., BERRIMAN, M. & HORN, D. 2012. High-throughput decoding of antitrypanosomal drug efficacy and resistance. *Nature,* 482**,** 232-6.

ALSFORD, S. & HORN, D. 2008. Single-locus targeting constructs for reliable regulated RNAi and transgene expression in *Trypanosoma brucei*. *Mol Biochem Parasitol,* 161**,** 76-9.

ALSFORD, S., TURNER, D. J., OBADO, S. O., SANCHEZ-FLORES, A., GLOVER, L., BERRIMAN, M., HERTZ-FOWLER, C. & HORN, D. 2011. High-throughput phenotyping using parallel sequencing of RNA interference targets in the African trypanosome. *Genome Res,* 21**,** 915-24.

APTED, F. I. 1980. Present status of chemotherapy and chemopropylaxis of human trypanosomiasis in the Eastern Hemisphere. *Pharmacol Ther,* 11**,** 391-413.

ARCHER, S. K., INCHAUSTEGUI, D., QUEIROZ, R. & CLAYTON, C. 2011. The cell cycle regulated transcriptome of *Trypanosoma brucei*. *PLoS One,* 6**,** e18425.

BAINES, A. & GULL, K. 2008. WCB is a C2 domain protein defining the plasma membrane - sub-pellicular microtubule corset of kinetoplastid parasites. *Protist,* 159**,** 115-25.

BAKKER, B. M., WESTERHOFF, H. V. & MICHELS, P. A. 1995. Regulation and control of compartmentalized glycolysis in bloodstream form *Trypanosoma brucei*. *J Bioenerg Biomembr,* 27**,** 513-25.

BANERJEE, S., SEN, A., DAS, P. & SAHA, P. 2006. *Leishmania donovani* cyclin 1 (LdCyc1) forms a complex with cell cycle kinase subunit CRK3 (LdCRK3) and is possibly involved in S-phase-related activities. *FEMS Microbiol Lett,* 256**,** 75-82.

BANGS, J. D., UYETAKE, L., BRICKMAN, M. J., BALBER, A. E. & BOOTHROYD, J. C. 1993. Molecular cloning and cellular localization of a BiP homologue in *Trypanosoma brucei*. Divergent ER retention signals in a lower eukaryote. *J Cell Sci,* 105 (Pt 4)**,** 1101-13.

BARKER, C., BARBOUR, K. W., BERGER, F. G. & HAJDUK, S. L. 2001. Activity of human trypanosome lytic factor in mice. *Mol Biochem Parasitol,* 117**,** 129-36.

BARON, D. M., KABUTUTU, Z. P. & HILL, K. L. 2007a. Stuck in reverse: loss of LC1 in *Trypanosoma brucei* disrupts outer dynein arms and leads to reverse flagellar beat and backward movement. *J Cell Sci,* 120**,** 1513-20.

BARON, D. M., RALSTON, K. S., KABUTUTU, Z. P. & HILL, K. L. 2007b. Functional genomics in *Trypanosoma brucei* identifies evolutionarily conserved components of motile flagella. *J Cell Sci,* 120**,** 478-91.

BARQUILLA, A., CRESPO, J. L. & NAVARRO, M. 2008. Rapamycin inhibits trypanosome cell growth by preventing TOR complex 2 formation. *Proc Natl Acad Sci U S A,* 105**,** 14579-84.

BARRETT, M. P. 2006. The rise and fall of sleeping sickness. *The Lancet,* 367**,** 1377-1378.

BARRETT, M. P., BURCHMORE, R. J. S., STICH, A., LAZZARI, J. O., FRASCH, A. C., CAZZULO, J. J. & KRISHNA, S. 2003. The trypanosomiasis. *The Lancet,* 362**,** 1469-1480.

BARRETT, M. P., MOTTRAM, J. C. & COOMBS, G. H. 1999. Recent advances in identifying and validating drug targets in trypanosomes and leishmanias. *Trends in Microbiology,* 7**,** 82-88.

BARRY, J. D. 1979. Capping of variable antigen on *Trypanosoma brucei,* and its immunological and biological significance. *J Cell Sci,* 37**,** 287-302.

BASTIN, P., BAGHERZADEH, Z., MATTHEWS, K. R. & GULL, K. 1996a. A novel epitope tag system to study protein targeting and organelle biogenesis in *Trypanosoma brucei*. *Mol Biochem Parasitol,* 77**,** 235-9.

BASTIN, P., MACRAE, T. H., FRANCIS, S. B., MATTHEWS, K. R. & GULL, K. 1999a. Flagellar morphogenesis: protein targeting and assembly in the paraflagellar rod of trypanosomes. *Mol Cell Biol,* 19**,** 8191-200.

BASTIN, P., MATTHEWS, K. R. & GULL, K. 1996b. The paraflagellar rod of kinetoplastida: solved and unsolved questions. *Parasitol Today,* 12**,** 302-7.

BASTIN, P., PULLEN, T. J., MOREIRA-LEITE, F. F. & GULL, K. 2000. Inside and outside of the trypanosome flagellum:a multifunctional organelle. *Microbes Infect,* 2**,** 1865-74.

BASTIN, P., PULLEN, T. J., SHERWIN, T. & GULL, K. 1999b. Protein transport and flagellum assembly dynamics revealed by analysis of the paralysed trypanosome mutant snl-1. *J Cell Sci,* 112 (Pt 21)**,** 3769-77.

BASTIN, P., SHERWIN, T. & GULL, K. 1998. Paraflagellar rod is vital for trypanosome motility. *Nature,* 391**,** 548.

BAUM, S. G., WITTNER, M., NADLER, J. P., HORWITZ, S. B., DENNIS, J. E., SCHIFF, P. B. & TANOWITZ, H. B. 1981. Taxol, a microtubule stabilizing agent, blocks the replication of *Trypanosoma cruzi*. *Proc Natl Acad Sci U S A,* 78**,** 4571-5.

BEAVO, J. A. 1995. Cyclic nucleotide phosphodiesterases: functional implications of multiple isoforms. *Physiol Rev,* 75**,** 725-48.

BENZ, C., CLUCAS, C., MOTTRAM, J. C. & HAMMARTON, T. C. 2012. Cytokinesis in bloodstream stage *Trypanosoma brucei* requires a family of katanins and spastin. *PLoS One,* 7**,** e30367.

BERRIMAN, M., GHEDIN, E., HERTZ-FOWLER, C., BLANDIN, G., RENAULD, H., BARTHOLOMEU, D. C., LENNARD, N. J., CALER, E., HAMLIN, N. E., HAAS, B., BOHME, U., HANNICK, L., ASLETT, M. A., SHALLOM, J., MARCELLO, L., HOU, L., WICKSTEAD, B., ALSMARK, U. C. M., ARROWSMITH, C., ATKIN, R. J., BARRON, A. J., BRINGAUD, F., BROOKS, K., CARRINGTON, M., CHEREVACH, I., CHILLINGWORTH, T., CHURCHER, C., CLARK, L. N., CORTON, C. H., CRONIN, A., DAVIES, R. M., DOGGETT, J., DJIKENG, A., FELDBLYUM, T., FIELD, M. C., FRASER, A., GOODHEAD, I., HANCE, Z., HARPER, D., HARRIS, B. R., HAUSER, H., HOSTETLER, J., IVENS, A., JAGELS, K., JOHNSON, D., JOHNSON, J., JONES, K., KERHOR, A. X., KOO, H., LARKE, N., LANDFEAR, S., LARKIN, C., LEECH, V., LINE, A., LORD, A., MACLEOD, A., MOONEY, P. J., MOULE, S., MARTIN, D. M. A., MORGAN, G. W., MUNGALL, K., NORBERTCZAK, H., ORMOND, D., PAI, G., PEACOCK, C. S., PETERSON, J., QUAIL, M. A., RABBINOWITSCH, E., RAJANDREAM, A., REITTER, C., SALZBERG, S. L., SANDERS, M., SCHOBEL, S., SHARP, S., SIMMONDS, M., SIMPSON, A. J., TALLON, L., TURNER, C. M. R., TAIT, A., TIVEY, A. R., VAN AKEN, S., WALKER, D., WANLESS, D., WANG, S., WHITE, B., WHITE, O., WHITEHEAD, S., WOODWARD, J., WORTMAN, J., ADAMS, M. D., EMBLEY, T. M., GULL, K., ULLU, E., BARRY, J. D., FAIRLAMB, A.

H., OPPERDOES, F., BARRELL, B. G., DONELSON, J. E., HALL, N., FRASER, C. M., *et al.* 2005. The Genome of the African Trypanosome *Trypanosoma brucei*. *Science,* 309**,** 416-422.

BIEBINGER, S., WIRTZ, L. E., LORENZ, P. & CLAYTON, C. 1997. Vectors for inducible expression of toxic gene products in bloodstream and procyclic *Trypanosoma brucei*. *Mol Biochem Parasitol,* 85**,** 99-112.

BIRKETT, C. R., FOSTER, K. E., JOHNSON, L. & GULL, K. 1985. Use of monoclonal antibodies to analyse the expression of a multi-tubulin family. *FEBS Lett,* 187**,** 211-8.

BITTER, W., GERRITS, H., KIEFT, R. & BORST, P. 1998. The role of transferrin-receptor variation in the host range of *Trypanosoma brucei*. *Nature,* 391**,** 499-502.

BLAND, N. D., WANG, C., TALLMAN, C., GUSTAFSON, A. E., WANG, Z., ASHTON, T. D., OCHIANA, S. O., MCALLISTER, G., COTTER, K., FANG, A. P., GECHIJIAN, L., GARCEAU, N., GANGURDE, R., ORTENBERG, R., ONDRECHEN, M. J., CAMPBELL, R. K. & POLLASTRI, M. P. 2011. Pharmacological validation of *Trypanosoma brucei* phosphodiesterases B1 and B2 as druggable targets for African sleeping sickness. *J Med Chem,* 54**,** 8188-94.

BLOOM, J. & CROSS, F. R. 2007. Multiple levels of cyclin specificity in cell-cycle control. *Nat Rev Mol Cell Biol,* 8**,** 149-60.

BOCHUD-ALLEMANN, N. & SCHNEIDER, A. 2002. Mitochondrial substrate level phosphorylation is essential for growth of procyclic *Trypanosoma brucei*. *J Biol Chem,* 277**,** 32849-54.

BONHIVERS, M., LANDREIN, N., DECOSSAS, M. & ROBINSON, D. R. 2008a. A monoclonal antibody marker for the exclusion-zone filaments of *Trypanosoma brucei*. *Parasit Vectors,* 1**,** 21.

BONHIVERS, M., NOWACKI, S., LANDREIN, N. & ROBINSON, D. R. 2008b. Biogenesis of the trypanosome endo-exocytotic organelle is cytoskeleton mediated. *PLoS Biol,* 6**,** e105.

BRANCHE, C., KOHL, L., TOUTIRAIS, G., BUISSON, J., COSSON, J. & BASTIN, P. 2006. Conserved and specific functions of axoneme components in trypanosome motility. *J Cell Sci,* 119**,** 3443-55.

BRIGGS, L. J., MCKEAN, P. G., BAINES, A., MOREIRA-LEITE, F., DAVIDGE, J., VAUGHAN, S. & GULL, K. 2004. The flagella connector of *Trypanosoma brucei*: an unusual mobile transmembrane junction. *J Cell Sci,* 117**,** 1641-51.

BRINGAUD, F., ROBINSON, D. R., BARRADEAU, S., BITEAU, N., BALTZ, D. & BALTZ, T. 2000. Characterization and disruption of a new *Trypanosoma brucei* repetitive flagellum protein, using double-stranded RNA inhibition. *Mol Biochem Parasitol,* 111**,** 283-97.

BROADHEAD, R., DAWE, H. R., FARR, H., GRIFFITHS, S., HART, S. R., PORTMAN, N., SHAW, M. K., GINGER, M. L., GASKELL, S. J., MCKEAN,

P. G. & GULL, K. 2006. Flagellar motility is required for the viability of the bloodstream trypanosome. *Nature,* 440**,** 224-7.

BRUN, R., BLUM, J., CHAPPUIS, F. & BURRI, C. 2010. Human African Trypanosomiasis. *The Lancet,* 375**,** 148-159.

BRUN, R. & SCHÖNENBERGER 1979. Cultivation and *in vitro* cloning or procyclic culture forms of *Trypanosoma brucei* in a semi-defined medium. Short communication. *Acta Trop,* 36**,** 289-92.

BUGUET, A., BISSER, S., JOSENANDO, T., CHAPOTOT, F. & CESPUGLIO, R. 2005. Sleep structure: a new diagnostic tool for stage determination in sleeping sickness. *Acta tropica,* 93**,** 107-117.

BULLARD, W., KIEFT, R., CAPEWELL, P., VEITCH, N. J., MACLEOD, A. & HAJDUK, S. L. 2012. Haptoglobin-hemoglobin receptor independent killing of African trypanosomes by human serum and trypanosome lytic factors. *Virulence,* 3**,** 72-6.

BURCHMORE, R. J. S., OGBUNUDE, P. O. J., ENANGA, B. & BARRETT, M. P. 2002. Chemotherapy of human african trypanosomiasis. *Current pharmaceutical design,* 8**,** 257-267.

BURKARD, G., FRAGOSO, C. M. & RODITI, I. 2007. Highly efficient stable transformation of bloodstream forms of *Trypanosoma brucei*. *Mol Biochem Parasitol,* 153**,** 220-3.

BURRI, C. & BRUN, R. 2003. Eflornithine for the treatment of human African trypanosomiasis. *Parasitol Res,* 90 Supp 1**,** S49-52.

BURRI, C. & KEISER, J. 2001. Pharmacokinetic investigations in patients from northern Angola refractory to melarsoprol treatment. *Trop Med Int Health,* 6**,** 412-20.

BÜSCHER, P., LEJON, V., MAGNUS, E. & VAN MEIRVENNE, N. 1999. Improved latex agglutination test for detection of antibodies in serum and cerebrospinal fluid of *Trypanosoma brucei gambiense* infected patients. *Acta Trop,* 73**,** 11-20.

CAPEWELL, P., VEITCH, N. J., TURNER, C. M., RAPER, J., BERRIMAN, M., HAJDUK, S. L. & MACLEOD, A. 2011. Differences between *Trypanosoma brucei gambiense* groups 1 and 2 in their resistance to killing by trypanolytic factor 1. *PLoS Negl Trop Dis,* 5**,** e1287.

CATTAND, P., MIEZAN, B. T. & DE RAADT, P. 1988. Human African trypanosomiasis: use of double centrifugation of cerebrospinal fluid to detect trypanosomes. *Bull World Health Organ,* 66**,** 83-6.

CAVALIER-SMITH, T. 1993. Kingdom Protozoa and Its 18 Phyla. *Microbiological Reviews,* 57**,** 953-994.

CHAN, K. Y. & ERSFELD, K. 2010. The role of the Kinesin-13 family protein TbKif13-2 in flagellar length control of *Trypanosoma brucei*. *Mol Biochem Parasitol,* 174**,** 137-40.

CHAN, K. Y., MATTHEWS, K. R. & ERSFELD, K. 2010. Functional characterisation and drug target validation of a mitotic kinesin-13 in *Trypanosoma brucei*. *PLoS Pathog,* 6**,** e1001050.

CHAN, M. M. & FONG, D. 1994. Plant microtubule inhibitors against trypanosomatids. *Parasitol Today,* 10**,** 448-51.

CHAPPUIS, F., LOUTAN, L., SIMARRO, P., LEJON, V. & BUSCHER, P. 2005. Options for Field Diagnosis of Human African Trypanosomiasis. *Clinical Microbiology Reviews,* 18**,** 133-146.

CHAVES, C. S., SOARES, D. C., DA SILVA, R. P. & SARAIVA, E. M. 2003. Characterization of the species- and stage-specificity of two monoclonal antibodies against *Leishmania amazonensis*. *Exp Parasitol,* 103**,** 152-9.

CHOWDHURY, A. R., ZHAO, Z. & ENGLUND, P. T. 2008. Effect of hydroxyurea on procyclic *Trypanosoma brucei*: an unconventional mechanism for achieving synchronous growth. *Eukaryot Cell,* 7**,** 425-8.

COOPER, R., DE JESUS, A. R. & CROSS, G. A. 1993. Deletion of an immunodominant *Trypanosoma cruzi* surface glycoprotein disrupts flagellum-cell adhesion. *J Cell Biol,* 122**,** 149-56.

CORTÉS-FIGUEROA, A. A., PÉREZ-TORRES, A., SALAIZA, N., CABRERA, N., ESCALONA-MONTAÑO, A., RONDÁN, A., AGUIRRE-GARCÍA, M., GÓMEZ-PUYOU, A., PÉREZ-MONTFORT, R. & BECKER, I. 2008. A monoclonal antibody that inhibits *Trypanosoma cruzi* growth *in vitro* and its reaction with intracellular triosephosphate isomerase. *Parasitol Res,* 102**,** 635-43.

COX, F. E. G. 2004. History of sleeping sickness (African trypanosomiasis). *Infectious disease clinics in north america,* 18**,** 231-245.

CROWE, J. S., LAMONT, A. G., BARRY, J. D. & VICKERMAN, K. 1984. Cytotoxicity of monoclonal antibodies to *Trypanosoma brucei*. *Trans R Soc Trop Med Hyg,* 78**,** 508-13.

DACHEUX, D., LANDREIN, N., THONNUS, M., GILBERT, G., SAHIN, A., WODRICH, H., ROBINSON, D. R. & BONHIVERS, M. 2012. A MAP6-related protein is present in protozoa and is involved in flagellum motility. *PLoS One,* 7**,** e31344.

DAUTRY-VARSAT, A., CIECHANOVER, A. & LODISH, H. F. 1983. pH and the recycling of transferrin during receptor-mediated endocytosis. *Proc Natl Acad Sci U S A,* 80**,** 2258-62.

DE GRAFFENRIED, C. L., HO, H. H. & WARREN, G. 2008. Polo-like kinase is required for Golgi and bilobe biogenesis in *Trypanosoma brucei*. *J Cell Biol,* 181**,** 431-8.

DE GREEF, C., IMBERECHTS, H., MATTHYSSENS, G., VAN MEIRVENNE, N. & HAMERS, R. 1989. A gene expressed only in serum-resistant variants of *Trypanosoma brucei rhodesiense*. *Mol Biochem Parasitol,* 36**,** 169-76.

DEMONCHY, R., BLISNICK, T., DEPREZ, C., TOUTIRAIS, G., LOUSSERT, C., MARANDE, W., GRELLIER, P., BASTIN, P. & KOHL, L. 2009. Kinesin 9 family members perform separate functions in the trypanosome flagellum. *J Cell Biol,* 187**,** 615-22.

DESQUESNES, M. 1996. Evaluation of three antigen detection tests (monoclonal trapping ELISA) for African trypanosomes, with an isolate of *Trypanosoma vivax* from French Guyana. *Ann N Y Acad Sci,* 791**,** 172-84.

DIALL, O., NANTULYA, V. M., LUCKINS, A. G., DIARRA, B. & KOUYATE, B. 1992. Evaluation of mono- and polyclonal antibody-based antigen detection immunoassays for diagnosis of *Trypanosoma evansi* infection in the dromedary camel. *Rev Elev Med Vet Pays Trop,* 45**,** 149-53.

DILBECK, V., BERBEROF, M., VAN CAUWENBERGE, A., ALEXANDRE, H. & PAYS, E. 1999. Characterization of a coiled coil protein present in the basal body of *Trypanosoma brucei*. *J Cell Sci,* 112 (Pt 24)**,** 4687-94.

ENGSTLER, M., PFOHL, T., HERMINGHAUS, S., BOSHART, M., WIEGERTJES, G., HEDDERGOTT, N. & OVERATH, P. 2007. Hydrodynamic flow-mediated protein sorting on the cell surface of trypanosomes. *Cell,* 131**,** 505-15.

FAGOONEE, S., GBUREK, J., HIRSCH, E., MARRO, S., MOESTRUP, S. K., LAURBERG, J. M., CHRISTENSEN, E. I., SILENGO, L., ALTRUDA, F. & TOLOSANO, E. 2005. Plasma protein haptoglobin modulates renal iron loading. *Am J Pathol,* 166**,** 973-83.

FARR, H. & GULL, K. 2009. Functional studies of an evolutionarily conserved, cytochrome b5 domain protein reveal a specific role in axonemal organisation and the general phenomenon of post-division axonemal growth in trypanosomes. *Cell Motil Cytoskeleton,* 66**,** 24-35.

FERNANDES, A. P., NELSON, K. & BEVERLEY, S. M. 1993. Evolution of nuclear ribosomal RNAs in kinetoplastid protozoa: Perspectives on the age and origins of parasitism. *Proceedings of National Academy of Sciences,* 90**,** 11608-11612.

FEVRE, E. M., PICOZZI, K., JANNIN, J., WELBURN, S. C. & MAUDLIN, I. 2006. Human African Trypanosomiasis: Epidemiology and Control. *Advances in Parasitology,* 61**,** 167-202.

FIELD, H., FARJAH, M., PAL, A., GULL, K. & FIELD, M. C. 1998. Complexity of trypanosomatid endocytosis pathways revealed by Rab4 and Rab5 isoforms in *Trypanosoma brucei*. *J Biol Chem,* 273**,** 32102-10.

FIELD, H., SHERWIN, T., SMITH, A. C., GULL, K. & FIELD, M. C. 2000. Cell-cycle and developmental regulation of TbRAB31 localisation, a GTP-locked Rab protein from *Trypanosoma brucei*. *Mol Biochem Parasitol,* 106**,** 21-35.

FIELD, M. C., ALLEN, C. L., DHIR, V., GOULDING, D., HALL, B. S., MORGAN, G. W., VEAZEY, P. & ENGSTLER, M. 2004. New approaches to the microscopic imaging of *Trypanosoma brucei*. *Microsc Microanal,* 10**,** 621-36.

FIELD, M. C. & CARRINGTON, M. 2004. Intracellular membrane transport systems in *Trypanosoma brucei*. *Traffic,* 5**,** 905-13.

FIELD, M. C. & CARRINGTON, M. 2009. The trypanosome flagellar pocket. *Nature Reviews Microbiology,* 7**,** 775-786.

FILHO, S. A., PEREIRA DE ALMEIDA, E. R. & GANDER, E. S. 1978. The influence of hydroxyurea and colchicine on growth and morphology of *Trypanosoma cruzi*. *Acta Trop,* 35**,** 229-37.

FORDE, R. M. 1902. The discovery of the human *Trypanosoma*. *British Medical Journal,* 2**,** 1741.

FORSYTHE, G. R., MCCULLOCH, R. & HAMMARTON, T. C. 2009. Hydroxyurea-induced synchronisation of bloodstream stage *Trypanosoma brucei*. *Mol Biochem Parasitol,* 164**,** 131-6.

GALLO, J. M. & PRECIGOUT, E. 1988. Tubulin expression in trypanosomes. *Biol Cell,* 64**,** 137-43.

GARCÍA-SALCEDO, J. A., PÉREZ-MORGA, D., GIJÓN, P., DILBECK, V., PAYS, E. & NOLAN, D. P. 2004. A differential role for actin during the life cycle of *Trypanosoma brucei*. *EMBO J,* 23**,** 780-9.

GEERTS, S., HOLMES, P. H., EISLER, M. C. & DIALL, O. 2001. African bovine trypanosomiasis: the problem of drug resistance. *Trends Parasitol,* 17**,** 25-8.

GENOVESE, G., FRIEDMAN, D. J., ROSS, M. D., LECORDIER, L., UZUREAU, P., FREEDMAN, B. I., BOWDEN, D. W., LANGEFELD, C. D., OLEKSYK, T. K., USCINSKI KNOB, A. L., BERNHARDY, A. J., HICKS, P. J., NELSON, G. W., VANHOLLEBEKE, B., WINKLER, C. A., KOPP, J. B., PAYS, E. & POLLAK, M. R. 2010. Association of trypanolytic ApoL1 variants with kidney disease in African Americans. *Science,* 329**,** 841-5.

GIBSON, W. & BAILEY, M. 1994. Genetic exchange in *Trypanosoma brucei*: evidence for meiosis from analysis of a cross between drug-resistant transformants. *Mol Biochem Parasitol,* 64**,** 241-52.

GIBSON, W. & BAILEY, M. 2003. The development of *Trypanosoma brucei* within the tsetse fly midgut observed using green fluorescent trypanosomes. *Kinetoplastid Biol Dis,* 2**,** 1.

GIBSON, W., PEACOCK, L., FERRIS, V., WILLIAMS, K. & BAILEY, M. 2008. The use of yellow fluorescent hybrids to indicate mating in *Trypanosoma brucei*. *Parasit Vectors,* 1**,** 4.

GIBSON, W. & STEVENS, J. 1999. Genetic exchange in Trypanosomatidae. *Advances in parasitology,* 43.

GLUENZ, E., POVELONES, M. L., ENGLUND, P. T. & GULL, K. 2011. The kinetoplast duplication cycle in *Trypanosoma brucei* is orchestrated by cytoskeleton-mediated cell morphogenesis. *Mol Cell Biol,* 31**,** 1012-21.

GOTTESDIENER, K., GARCIÁ-ANOVEROS, J., LEE, M. G. & VAN DER PLOEG, L. H. 1990. Chromosome organization of the protozoan *Trypanosoma brucei*. *Mol Cell Biol,* 10**,** 6079-83.

GOURGUECHON, S., SAVICH, J. M. & WANG, C. C. 2007. The multiple roles of cyclin E1 in controlling cell cycle progression and cellular morphology of *Trypanosoma brucei*. *J Mol Biol,* 368**,** 939-50.

GOURGUECHON, S. & WANG, C. C. 2009. CRK9 contributes to regulation of mitosis and cytokinesis in the procyclic form of *Trypanosoma brucei*. *BMC Cell Biol,* 10**,** 68.

GRAB, D. J., WELLS, C. W., SHAW, M. K., WEBSTER, P. & RUSSO, D. C. 1992. Endocytosed transferrin in African trypanosomes is delivered to lysosomes and may not be recycled. *Eur J Cell Biol,* 59**,** 398-404.

GRIFFITHS, S., PORTMAN, N., TAYLOR, P. R., GORDON, S., GINGER, M. L. & GULL, K. 2007. RNA interference mutant induction *in vivo* demonstrates the essential nature of trypanosome flagellar function during mammalian infection. *Eukaryot Cell,* 6**,** 1248-50.

GULL, K. 1999. The cytoskeleton of trypanosomatid parasites. *Annu Rev Microbiol,* 53**,** 629-55.

GULL, K. 2003. Host-parasite interactions and trypanosome morphogenesis: a flagellar pocketful of goodies. *Curr Opin Microbiol,* 6**,** 365-70.

GÓMEZ, E. B., SANTORI, M. I., LARÍA, S., ENGEL, J. C., SWINDLE, J., EISEN, H., SZANKASI, P. & TÉLLEZ-IÑÓN, M. T. 2001. Characterization of the *Trypanosoma cruzi* Cdc2p-related protein kinase 1 and identification of three novel associating cyclins. *Mol Biochem Parasitol,* 113**,** 97-108.

HAGER, K. M. & HAJDUK, S. L. 1997. Mechanism of resistance of African trypanosomes to cytotoxic human HDL. *Nature,* 385**,** 823-6.

HAJDUK, S. L., MOORE, D. R., VASUDEVACHARYA, J., SIQUEIRA, H., TORRI, A. F., TYTLER, E. M. & ESKO, J. D. 1989. Lysis of *Trypanosoma brucei* by a toxic subspecies of human high density lipoprotein. *J Biol Chem,* 264**,** 5210-7.

HALL, B., ALLEN, C. L., GOULDING, D. & FIELD, M. C. 2004a. Both of the Rab5 subfamily small GTPases of *Trypanosoma brucei* are essential and required for endocytosis. *Mol Biochem Parasitol,* 138**,** 67-77.

HALL, B. S., PAL, A., GOULDING, D. & FIELD, M. C. 2004b. Rab4 is an essential regulator of lysosomal trafficking in trypanosomes. *J Biol Chem,* 279**,** 45047-56.

HALLER, L., ADAMS, H., MEROUZE, F. & DAGO, A. 1986. Clinical and pathological aspects of human African trypanosomiasis (*T. b. gambiense*) with particular reference to reactive arsenical encephalopathy. *Am J Trop Med Hyg,* 35**,** 94-9.

HAMMARTON, T. C. 2007. Cell cycle regulation in *Trypanosoma brucei*. *Mol Biochem Parasitol,* 153**,** 1-8.

HAMMARTON, T. C., CLARK, J., DOUGLAS, F., BOSHART, M. & MOTTRAM, J. C. 2003a. Stage-specific differences in cell cycle control in *Trypanosoma brucei* revealed by RNA interference of a mitotic cyclin. *J Biol Chem,* 278**,** 22877-86.

HAMMARTON, T. C., ENGSTLER, M. & MOTTRAM, J. C. 2004. The *Trypanosoma brucei* cyclin, CYC2, is required for cell cycle progression through G1 phase

and for maintenance of procyclic form cell morphology. *J Biol Chem,* 279**,** 24757-64.

HAMMARTON, T. C., KRAMER, S., TETLEY, L., BOSHART, M. & MOTTRAM, J. C. 2007a. *Trypanosoma brucei* Polo-like kinase is essential for basal body duplication, kDNA segregation and cytokinesis. *Mol Microbiol,* 65**,** 1229-48.

HAMMARTON, T. C., LILLICO, S. G., WELBURN, S. C. & MOTTRAM, J. C. 2005. *Trypanosoma brucei* MOB1 is required for accurate and efficient cytokinesis but not for exit from mitosis. *Mol Microbiol,* 56**,** 104-16.

HAMMARTON, T. C., MONNERAT, S. & MOTTRAM, J. C. 2007b. Cytokinesis in trypanosomatids. *Curr Opin Microbiol,* 10**,** 520-7.

HAMMARTON, T. C., MOTTRAM, J. C. & DOERIG, C. 2003b. The cell cycle of parasitic protozoa: potential for chemotherapeutic exploitation. *Prog Cell Cycle Res,* 5**,** 91-101.

HART, S. R., LAU, K. W., HAO, Z., BROADHEAD, R., PORTMAN, N., HÜHMER, A., GULL, K., MCKEAN, P. G., HUBBARD, S. J. & GASKELL, S. J. 2009. Analysis of the trypanosome flagellar proteome using a combined electron transfer/collisionally activated dissociation strategy. *J Am Soc Mass Spectrom,* 20**,** 167-75.

HEMPHILL, A., AFFOLTER, M. & SEEBECK, T. 1992. A novel microtubule-binding motif identified in a high molecular weight microtubule-associated protein from *Trypanosoma brucei*. *J Cell Biol,* 117**,** 95-103.

HIDE, G. & TAIT, A. 2009. Molecular epidemiology of African sleeping sickness. *Parasitology,* 136**,** 1491-1500.

HIGGINS, M. K., TKACHENKO, O., BROWN, A., REED, J., RAPER, J. & CARRINGTON, M. 2013. Structure of the trypanosome haptoglobin-hemoglobin receptor and implications for nutrient uptake and innate immunity. *Proc Natl Acad Sci U S A.*

HIRUMI, H. & HIRUMI, K. 1989. Continuous cultivation of *Trypanosoma brucei* blood stream forms in a medium containing a low concentration of serum protein without feeder cell layers. *J Parasitol,* 75**,** 985-9.

HUA, S. B., MUTOMBA, M. C. & WANG, C. C. 1997. Regulated expression of cyclin-1 during differentiation of *Trypanosoma brucei* from bloodstream form to procyclic form. *Mol Biochem Parasitol,* 84**,** 255-8.

HUGHES, L. C., RALSTON, K. S., HILL, K. L. & ZHOU, Z. H. 2012. Three-dimensional structure of the Trypanosome flagellum suggests that the paraflagellar rod functions as a biomechanical spring. *PLoS One,* 7**,** e25700.

HUNGER-GLASER, I. & SEEBECK, T. 1997. Deletion of the genes for the paraflagellar rod protein PFR-A in *Trypanosoma brucei* is probably lethal. *Mol Biochem Parasitol,* 90**,** 347-51.

HUTCHINGS, N. R., DONELSON, J. E. & HILL, K. L. 2002. Trypanin is a cytoskeletal linker protein and is required for cell motility in African trypanosomes. *J Cell Biol,* 156**,** 867-77.

IKEDA, K. N. & DE GRAFFENRIED, C. L. 2012. Polo-like kinase is necessary for flagellum inheritance in *Trypanosoma brucei*. *J Cell Sci*.

ILBOUDO, H., BERTHIER, D., CAMARA, M., CAMARA, O., KABORE, J., LENO, M., KELETIGUI, S., CHANTAL, I., JAMONNEAU, V., BELEM, A. M., CUNY, G. & BUCHETON, B. 2012. APOL1 expression is induced by *Trypanosoma brucei gambiense* infection but is not associated with differential susceptibility to sleeping sickness. *Infect Genet Evol,* 12**,** 1519-1523.

IMBODEN, M., MÜLLER, N., HEMPHILL, A., MATTIOLI, R. & SEEBECK, T. 1995. Repetitive proteins from the flagellar cytoskeleton of African trypanosomes are diagnostically useful antigens. *Parasitology,* 110 (Pt 3)**,** 249-58.

ITEN, M., MATOVU, E., BRUN, R. & KAMINSKY, R. 1995. Innate lack of susceptibility of Ugandan *Trypanosoma brucei rhodesiense* to DL-alpha-difluoromethylornithine (DFMO). *Trop Med Parasitol,* 46**,** 190-4.

JAMONNEAU, V., ILBOUDO, H., KABORÉ, J., KABA, D., KOFFI, M., SOLANO, P., GARCIA, A., COURTIN, D., LAVEISSIÈRE, C., LINGUE, K., BÜSCHER, P. & BUCHETON, B. 2012. Untreated human infections by *Trypanosoma brucei gambiense* are not 100% fatal. *PLoS Negl Trop Dis,* 6**,** e1691.

JAMONNEAU, V., TRUC, P., GARCIA, A., MAGNUS, E. & BÜSCHER, P. 2000. Preliminary evaluation of LATEX/*T. b. gambiense* and alternative versions of CATT/*T. b. gambiense* for the serodiagnosis of human african trypanosomiasis of a population at risk in Côte d'Ivoire: considerations for mass-screening. *Acta Trop,* 76**,** 175-83.

JEFFRIES, T. R., MORGAN, G. W. & FIELD, M. C. 2001. A developmentally regulated rab11 homologue in *Trypanosoma brucei* is involved in recycling processes. *J Cell Sci,* 114**,** 2617-26.

JOHNSON, J. G. & CROSS, G. A. 1977. Carbohydrate composition of variant-specific surface antigen glycoproteins from *Trypanosoma brucei*. *J Protozool,* 24**,** 587-91.

JOSHI, P. P., SHEGOKAR, V. R., POWAR, R. M., HERDER, S., KATTI, R., SALKAR, H. R., DANI, V. S., BHARGAVA, A., JANNIN, J. & TRUC, P. 2005. Human trypanosomiasis caused by *Trypanosoma evansi* in India: the first case report. *The American Journal of Tropical Medicine and Hygiene,* 73**,** 491-495.

KABIRI, M., FRANCO, J. R., SIMARRO, P. P., RUIZ, J. A., SARSA, M. & STEVERDING, D. 1999. Detection of *Trypanosoma brucei gambiense* in sleeping sickness suspects by PCR amplification of expression-site-associated genes 6 and 7. *Trop Med Int Health,* 4**,** 658-61.

KANMOGNE, G. D., ASONGANYI, T. & GIBSON, W. C. 1996. Detection of *Trypanosoma brucei gambiense,* in serologically positive but aparasitaemic sleeping-sickness suspects in Cameroon, by PCR. *Ann Trop Med Parasitol,* 90**,** 475-83.

KANWE, A. B., BENGALY, Z., SAULNIER, D. & DUVALLET, G. 1992. [Evaluation of the test for detecting trypanosoma circulating antigens using monoclonal antibodies. Experimental and natural infections]. *Rev Elev Med Vet Pays Trop,* 45**,** 265-71.

KATEETE, D., ALEZUYO, C., NANTEZA, A., ASIIMWE, C. & LUBEGA, G. 2012. In Vitro Trypanocidal Activity of Antibodies to Bacterially Expressed *Trypanosoma brucei* Tubulin. *Iran J Parasitol,* 7**,** 54-63.

KIEFT, R., CAPEWELL, P., TURNER, C. M., VEITCH, N. J., MACLEOD, A. & HAJDUK, S. 2010. Mechanism of *Trypanosoma brucei gambiense* (group 1) resistance to human trypanosome lytic factor. *Proc Natl Acad Sci U S A,* 107**,** 16137-41.

KILMARTIN, J. V., WRIGHT, B. & MILSTEIN, C. 1982. Rat monoclonal antitubulin antibodies derived by using a new nonsecreting rat cell line. *J Cell Biol,* 93**,** 576-82.

KLINGBEIL, M. M. & ENGLUND, P. T. 2004. Closing the gaps in kinetoplast DNA network replication. *Proc Natl Acad Sci U S A,* 101**,** 4333-4.

KOHL, L. & GULL, K. 1998. Molecular architecture of the trypanosome cytoskeleton. *Mol Biochem Parasitol,* 93**,** 1-9.

KOHL, L., ROBINSON, D. & BASTIN, P. 2003. Novel roles for the flagellum in cell morphogenesis and cytokinesis of trypanosomes. *EMBO J,* 22**,** 5336-46.

KOHL, L., SHERWIN, T. & GULL, K. 1999. Assembly of the paraflagellar rod and the flagellum attachment zone complex during the *Trypanosoma brucei* cell cycle. *J Eukaryot Microbiol,* 46**,** 105-9.

KOYFMAN, A. Y., SCHMID, M. F., GHEIRATMAND, L., FU, C. J., KHANT, H. A., HUANG, D., HE, C. Y. & CHIU, W. 2011. Structure of *Trypanosoma brucei* flagellum accounts for its bihelical motion. *Proc Natl Acad Sci U S A,* 108**,** 11105-8.

KOZMINSKI, K. G., BEECH, P. L. & ROSENBAUM, J. L. 1995. The *Chlamydomonas* kinesin-like protein FLA10 is involved in motility associated with the flagellar membrane. *J Cell Biol,* 131**,** 1517-27.

KUMAR, P. & WANG, C. C. 2006. Dissociation of cytokinesis initiation from mitotic control in a eukaryote. *Eukaryot Cell,* 5**,** 92-102.

KUNZ, S., BEAVO, J. A., D'ANGELO, M. A., FLAWIA, M. M., FRANCIS, S. H., JOHNER, A., LAXMAN, S., OBERHOLZER, M., RASCON, A., SHAKUR, Y., WENTZINGER, L., ZORAGHI, R. & SEEBECK, T. 2006. Cyclic nucleotide specific phosphodiesterases of the kinetoplastida: a unified nomenclature. *Mol Biochem Parasitol,* 145**,** 133-5.

KYAMBADDE, J. W., ENYARU, J. C., MATOVU, E., ODIIT, M. & CARASCO, J. F. 2000. Detection of trypanosomes in suspected sleeping sickness patients in Uganda using the polymerase chain reaction. *Bull World Health Organ,* 78**,** 119-24.

KÖHLER, G. & MILSTEIN, C. 1975. Continuous cultures of fused cells secreting antibody of predefined specificity. *Nature,* 256**,** 495-7.

LACOMBLE, S., VAUGHAN, S., DEGHELT, M., MOREIRA-LEITE, F. F. & GULL, K. 2012. A *Trypanosoma brucei* protein required for maintenance of the flagellum attachment zone and flagellar pocket ER domains. *Protist,* 163**,** 602-15.

LACOMBLE, S., VAUGHAN, S., GADELHA, C., MORPHEW, M. K., SHAW, M. K., MCINTOSH, J. R. & GULL, K. 2009. Three-dimensional cellular architecture of the flagellar pocket and associated cytoskeleton in trypanosomes revealed by electron microscope tomography. *J Cell Sci,* 122**,** 1081-90.

LACOMBLE, S., VAUGHAN, S., GADELHA, C., MORPHEW, M. K., SHAW, M. K., MCINTOSH, J. R. & GULL, K. 2010. Basal body movements orchestrate membrane organelle division and cell morphogenesis in *Trypanosoma brucei*. *J Cell Sci,* 123**,** 2884-91.

LACOUNT, D. J., BARRETT, B. & DONELSON, J. E. 2002. *Trypanosoma brucei* FLA1 is required for flagellum attachment and cytokinesis. *J Biol Chem,* 277**,** 17580-8.

LAI, D., HASHIMI, H., LUN, Z., AYALA, F. J. & LUKES, J. 2008. Adaptations of *Trypanosoma brucei* to gradual loss of kinetoplast DNA: *Trypanosoma equiperdum* and *Trypanosoma evansi* are petite mutants of *T. brucei*. *Proceedings of the National Academy of Sciences,* 105**,** 1999-2004.

LANDFEAR, S. M. & IGNATUSHCHENKO, M. 2001. The flagellum and flagellar pocket of trypanosomatids. *Mol Biochem Parasitol,* 115**,** 1-17.

LAVERAN, A. 1902. De l'action du sérum humain sur le trypanosome de Nagana (*Tr. brucei*). *C R Acad Sci,* 134**,** 735-739.

LAXMAN, S. & BEAVO, J. A. 2007. Cyclic nucleotide signaling mechanisms in trypanosomes: possible targets for therapeutic agents. *Mol Interv,* 7**,** 203-15.

LEE, M. G., BIHAIN, B. E., RUSSELL, D. G., DECKELBAUM, R. J. & VAN DER PLOEG, L. H. 1990. Characterization of a cDNA encoding a cysteine-rich cell surface protein located in the flagellar pocket of the protozoan *Trypanosoma brucei*. *Mol Cell Biol,* 10**,** 4506-17.

LEJON, V., BÜSCHER, P., MAGNUS, E., MOONS, A., WOUTERS, I. & VAN MEIRVENNE, N. 1998. A semi-quantitative ELISA for detection of *Trypanosoma brucei gambiense* specific antibodies in serum and cerebrospinal fluid of sleeping sickness patients. *Acta Trop,* 69**,** 151-64.

LEJON, V., KWETE, J. & BUSCHER, P. 2003. Towards saliva-based screening for sleeping sickness? *Tropical Medicine and International Health,* 8**,** 585-588.

LEWIS, E. A. & LANGRIDGE, W. P. 1947. Developmental forms of *Trypanosoma brucei* in the saliva of *Glossina pallidipes* and *Glossina austeni*. *Ann Trop Med Parasitol,* 41**,** 6-13.

LI, Z., LEE, J. H., CHU, F., BURLINGAME, A. L., GÜNZL, A. & WANG, C. C. 2008. Identification of a novel chromosomal passenger complex and its unique localization during cytokinesis in *Trypanosoma brucei*. *PLoS One,* 3**,** e2354.

LI, Z., UMEYAMA, T. & WANG, C. C. 2009. The Aurora Kinase in *Trypanosoma brucei* plays distinctive roles in metaphase-anaphase transition and cytokinetic initiation. *PLoS Pathog,* 5**,** e1000575.

LI, Z., UMEYAMA, T. & WANG, C. C. 2010. Polo-like kinase guides cytokinesis in *Trypanosoma brucei* through an indirect means. *Eukaryot Cell,* 9**,** 705-16.

LI, Z. & WANG, C. C. 2003. A PHO80-like cyclin and a B-type cyclin control the cell cycle of the procyclic form of *Trypanosoma brucei*. *J Biol Chem,* 278**,** 20652-8.

LI, Z. & WANG, C. C. 2008. KMP-11, a basal body and flagellar protein, is required for cell division in *Trypanosoma brucei*. *Eukaryot Cell,* 7**,** 1941-50.

LIGTENBERG, M. J., BITTER, W., KIEFT, R., STEVERDING, D., JANSSEN, H., CALAFAT, J. & BORST, P. 1994. Reconstitution of a surface transferrin binding complex in insect form *Trypanosoma brucei*. *EMBO J,* 13**,** 2565-73.

LINDEMANN, C. B. & KANOUS, K. S. 1997. A model for flagellar motility. *Int Rev Cytol,* 173**,** 1-72.

LUBEGA, G. W., BYARUGABA, D. K. & PRICHARD, R. K. 2002. Immunization with a tubulin-rich preparation from *Trypanosoma brucei* confers broad protection against African trypanosomosis. *Exp Parasitol,* 102**,** 9-22.

LUHRS, K. A., FOUTS, D. L. & MANNING, J. E. 2003. Immunization with recombinant paraflagellar rod protein induces protective immunity against *Trypanosoma cruzi* infection. *Vaccine,* 21**,** 3058-69.

LUMB, J. H. & FIELD, M. C. 2011. Rab23 is a flagellar protein in *Trypanosoma brucei*. *BMC Res Notes,* 4**,** 190.

MACGREGOR, P., SZÖŐR, B., SAVILL, N. J. & MATTHEWS, K. R. 2012. Trypanosomal immune evasion, chronicity and transmission: an elegant balancing act. *Nat Rev Microbiol,* 10**,** 431-8.

MACKEY, Z. B., KOUPPARIS, K., NISHINO, M. & MCKERROW, J. H. 2011. High-throughput analysis of an RNAi library identifies novel kinase targets in *Trypanosoma brucei*. *Chem Biol Drug Des,* 78**,** 454-63.

MACLEOD, A., TAIT, A. & TURNER, C. M. R. 2001a. The population genetics of *Trypanosoma brucei* and the orgin of human infectivity. *Philosophical Transaction of the royal society London,* 356**,** 1035-1044.

MACLEOD, A., WELBURN, S., MAUDLIN, I., TURNER, C. M. R. & TAIT, A. 2001b. Evidence for Multiple Origins of Human Infectivity in *Trypanosoma brucei* Revealed by Minisatellite Variant Repeat Mapping. *Journal of molecular evolution,* 52**,** 290-301.

MACLEOD, E. T., DARBY, A. C., MAUDLIN, I. & WELBURN, S. C. 2007. Factors affecting trypanosome maturation in tsetse flies. *PLoS One,* 2**,** e239.

MACRAE, T. H. & GULL, K. 1990. Purification and assembly in vitro of tubulin from *Trypanosoma brucei brucei*. *Biochem J,* 265**,** 87-93.

MADISON-ANTENUCCI, S., GRAMS, J. & HAJDUK, S. L. 2002. Editing machines: the complexities of trypanosome RNA editing. *Cell,* 108**,** 435-8.

MAGEZ, S., CALJON, G., TRAN, T., STIJLEMANS, B. & RADWANSKA, M. 2010. Current status of vaccination against African trypanosomiasis. *Parasitology,* 137**,** 2017-27.

MAGEZ, S., SCHWEGMANN, A., ATKINSON, R., CLAES, F., DRENNAN, M., DE BAETSELIER, P. & BROMBACHER, F. 2008. The role of B-cells and IgM antibodies in parasitemia, anemia, and VSG switching in *Trypanosoma brucei*-infected mice. *PLoS Pathog,* 4**,** e1000122.

MAGNUS, E., VERVOORT, T. & VAN MEIRVENNE, N. 1978. A card-agglutination test with stained trypanosomes (C.A.T.T.) for the serological diagnosis of *T. b. gambiense* trypanosomiasis. *Ann Soc Belg Med Trop,* 58**,** 169-76.

MAIER, A. & STEVERDING, D. 1996. Low affinity of *Trypanosoma brucei* transferrin receptor to apotransferrin at pH 5 explains the fate of the ligand during endocytosis. *FEBS Lett,* 396**,** 87-9.

MATOVU, E., ENYARU, J. C., LEGROS, D., SCHMID, C., SEEBECK, T. & KAMINSKY, R. 2001a. Melarsoprol refractory *T. b. gambiense* from Omugo, north-western Uganda. *Trop Med Int Health,* 6**,** 407-11.

MATOVU, E., SEEBECK, T., ENYARU, J. C. K. & KAMINSKY, R. 2001b. Drug resistance in *Trypanosoma brucei spp*., the causative agent of sleeping sickness in man and nagana in cattle. *Microbes and infection,* 3**,** 763-770.

MATTHEWS, K. R. 1999. Developments in the differentiation of *Trypanosoma brucei*. *Parasitol Today,* 15**,** 76-80.

MATTHEWS, K. R. 2005. The developmental cell biology of *Trypanosoma brucei*. *J Cell Sci,* 118**,** 283-90.

MATTHEWS, K. R., ELLIS, J. R. & PATEROU, A. 2004. Molecular regulation of the life cycle of African trypanosomes. *Trends Parasitol,* 20**,** 40-7.

MATTHEWS, K. R. & GULL, K. 1994. Evidence for an interplay between cell cycle progression and the initiation of differentiation between life cycle forms of African trypanosomes. *J Cell Biol,* 125**,** 1147-56.

MATTHEWS, K. R., SHERWIN, T. & GULL, K. 1995. Mitochondrial genome repositioning during the differentiation of the African trypanosome between life cycle forms is microtubule mediated. *J Cell Sci,* 108 (Pt 6)**,** 2231-9.

MAY, E. & ALLOLIO, B. 1991. Fatal toxic epidermal necrolysis during suramin therapy. *Eur J Cancer,* 27**,** 1338.

MCCULLOCH, R. 2004. Antigenic variation in African trypanosomes: monitoring progress. *Trends Parasitol,* 20**,** 117-21.

MCKEAN , P. & GULL, K. 2010. The flagellar pocket of Trypanosomatids: a critical feature for cell morphogenesis and pathogenicity. *Microbiology Monographs,* 17**,** 87-113.

MCKEAN, P. G. 2003. Coordination of cell cycle and cytokinesis in *Trypanosoma brucei*. *Curr Opin Microbiol,* 6**,** 600-7.

MCMAHON-PRATT, D., BENNETT, E. & DAVID, J. R. 1982. Monoclonal antibodies that distinguish subspecies of *Leishmania braziliensis. J Immunol,* 129**,** 926-7.

MCPHERSON, P. S. 2002. The endocytic machinery at an interface with the actin cytoskeleton: a dynamic, hip intersection. *Trends Cell Biol,* 12**,** 312-5.

MEHLERT, A. & FERGUSON, M. A. 2007. Structure of the glycosylphosphatidylinositol anchor of the *Trypanosoma brucei* transferrin receptor. *Mol Biochem Parasitol,* 151**,** 220-3.

MEHLERT, A., WORMALD, M. R. & FERGUSON, M. A. 2012. Modeling of the N-glycosylated transferrin receptor suggests how transferrin binding can occur within the surface coat of *Trypanosoma brucei*. *PLoS Pathog,* 8**,** e1002618.

MEHLITZ, D., ZILLMANN, U., SCOTT, C. M. & GODFREY, D. G. 1982. Epidemiological studies on the animal reservoir of Gambiense sleeping sickness. Part III. Characterization of trypanozoon stocks by isoenzymes and sensitivity to human serum. *Tropenmed Parasitol,* 33**,** 113-8.

MELVILLE, S. E., LEECH, V., GERRARD, C. S., TAIT, A. & BLACKWELL, J. M. 1998. The molecular karyotype of the megabase chromosomes of *Trypanosoma brucei* and the assignment of chromosome markers. *Mol Biochem Parasitol,* 94**,** 155-73.

MILLER, J. H. 1972. Experiments in molecular genetics.

MILLER, M. J., WRIGHTSMAN, R. A. & MANNING, J. E. 1996. *Trypanosoma cruzi*: protective immunity in mice immunized with paraflagellar rod proteins is associated with a T-helper type 1 response. *Exp Parasitol,* 84**,** 156-67.

MILNER, J. D. & HAJDUK, S. L. 1999. Expression and localization of serum resistance associated protein in *Trypanosoma brucei rhodesiense*. *Mol Biochem Parasitol,* 104**,** 271-83.

MOLINA-PORTELA, M. E. P., LUGLI, E. B., RECIO-PINTO, E. & RAPER, J. 2005. Trypanosome lytic factor, a subclass of high-density lipoprotein, forms cation-selective pores in membranes. *Mol Biochem Parasitol,* 144**,** 218-26.

MOLINA-PORTELA, M. P., SAMANOVIC, M. & RAPER, J. 2008. Distinct roles of apolipoprotein components within the trypanosome lytic factor complex revealed in a novel transgenic mouse model. *J Exp Med,* 205**,** 1721-8.

MONNERAT, S., ALMEIDA COSTA, C. I., FORKERT, A., BENZ, C., HAMILTON, A., TETLEY, L., BURCHMORE, R., NOVO, C., MOTTRAM, J. C. & HAMMARTON, T. C. 2012. Identification and Functional Characterisation of CRK12:CYC9, a Novel Cyclin Dependent Kinase (CDK)-Cyclin Complex in *Trypanosoma brucei*. (*submitted*)

MONNERAT, S., CLUCAS, C., BROWN, E., MOTTRAM, J. C. & HAMMARTON, T. C. 2009. Searching for novel cell cycle regulators in *Trypanosoma brucei* with an RNA interference screen. *BMC Res Notes,* 2**,** 46.

MOREIRA-LEITE, F. F., SHERWIN, T., KOHL, L. & GULL, K. 2001. A trypanosome structure involved in transmitting cytoplasmic information during cell division. *Science,* 294**,** 610-2.

MORGAN, D. O. 1995. Principles of CDK regulation. *Nature,* 374**,** 131-4.

MORGAN, G. W., ALLEN, C. L., JEFFRIES, T. R., HOLLINSHEAD, M. & FIELD, M. C. 2001. Developmental and morphological regulation of clathrin-mediated endocytosis in *Trypanosoma brucei*. *J Cell Sci,* 114**,** 2605-15.

MORGAN, G. W., HALL, B. S., DENNY, P. W., CARRINGTON, M. & FIELD, M. C. 2002a. The kinetoplastida endocytic apparatus. Part I: a dynamic system for nutrition and evasion of host defences. *Trends Parasitol,* 18**,** 491-6.

MORGAN, G. W., HALL, B. S., DENNY, P. W., FIELD, M. C. & CARRINGTON, M. 2002b. The endocytic apparatus of the kinetoplastida. Part II: machinery and components of the system. *Trends Parasitol,* 18**,** 540-6.

MORRIS, J. C., WANG, Z., DREW, M. E., PAUL, K. S. & ENGLUND, P. T. 2001. Inhibition of bloodstream form *Trypanosoma brucei* gene expression by RNA interference using the pZJM dual T7 vector. *Mol Biochem Parasitol,* 117**,** 111-3.

MOTTRAM, J. C. 1994. cdc2-related protein kinases and cell cycle control in trypanosomatids. *Parasitol Today,* 10**,** 253-7.

MUSOKE, A. J., NANTULYA, V. M., BARBET, A. F., KIRONDE, F. & MCGUIRE, T. C. 1981. Bovine immune response to African ;trypanosomes: specific antibodies to variable surface glycoproteins of *Trypanosoma brucei*. *Parasite Immunol,* 3**,** 97-106.

NANTULYA, V. M., BAJYANA SONGA, E. & HAMERS, R. 1989. Detection of circulating trypanosomal antigens in *Trypanosoma evansi*-infected animals using a *T. brucei* group-specific monoclonal antibody. *Trop Med Parasitol,* 40**,** 263-6.

NANTULYA, V. M., MUSOKE, A. J., RURANGIRWA, F. R., SAIGAR, N. & MINJA, S. H. 1987. Monoclonal antibodies that distinguish *Trypanosoma congolense, T. vivax and T. brucei*. *Parasite Immunol,* 9**,** 421-31.

NATESAN, S. K., BLACK, A., MATTHEWS, K. R., MOTTRAM, J. C. & FIELD, M. C. 2011. *Trypanosoma brucei brucei*: endocytic recycling is important for mouse infectivity. *Exp Parasitol,* 127**,** 777-83.

NATESAN, S. K., PEACOCK, L., MATTHEWS, K., GIBSON, W. & FIELD, M. C. 2007. Activation of endocytosis as an adaptation to the mammalian host by trypanosomes. *Eukaryot Cell,* 6**,** 2029-37.

NAULA, C., PARSONS, M. & MOTTRAM, J. C. 2005. Protein kinases as drug targets in trypanosomes and *Leishmania*. *Biochim Biophys Acta,* 1754**,** 151-9.

NAVARRO, M. & GULL, K. 2001. A pol I transcriptional body associated with VSG mono-allelic expression in *Trypanosoma brucei*. *Nature,* 414**,** 759-63.

NGÔ, H., TSCHUDI, C., GULL, K. & ULLU, E. 1998. Double-stranded RNA induces mRNA degradation in *Trypanosoma brucei*. *Proc Natl Acad Sci U S A,* 95**,** 14687-92.

NIGG, E. A. 1995. Cyclin-dependent protein kinases: key regulators of the eukaryotic cell cycle. *Bioessays,* 17**,** 471-80.

NOZAKI, T., HAYNES, P. A. & CROSS, G. A. 1996. Characterization of the *Trypanosoma brucei* homologue of a *Trypanosoma cruzi* flagellum-adhesion glycoprotein. *Mol Biochem Parasitol,* 82**,** 245-55.

OBERHOLZER, M., MARTI, G., BARESIC, M., KUNZ, S., HEMPHILL, A. & SEEBECK, T. 2007. The *Trypanosoma brucei* cAMP phosphodiesterases TbrPDEB1 and TbrPDEB2: flagellar enzymes that are essential for parasite virulence. *FASEB J,* 21**,** 720-31.

OGBADOYI, E., ERSFELD, K., ROBINSON, D., SHERWIN, T. & GULL, K. 2000. Architecture of the *Trypanosoma brucei* nucleus during interphase and mitosis. *Chromosoma,* 108**,** 501-13.

OGBADOYI, E. O., ROBINSON, D. R. & GULL, K. 2003. A high-order trans-membrane structural linkage is responsible for mitochondrial genome positioning and segregation by flagellar basal bodies in trypanosomes. *Mol Biol Cell,* 14**,** 1769-79.

OLAHO-MUKANI, W., MUNYUA, W. K. & NJOGU, A. R. 1992. An enzyme-linked immunosorbent assay (ELISA) for the detection of trypanosomal antigens in goat serum using a monoclonal antibody. *J Immunoassay,* 13**,** 217-29.

OLAHO-MUKANI, W., NYANG'AO, J. M., NGAIRA, J. M., OMUSE, J. K., MBWABI, D., TENGEKYON, K. M., NJENGA, J. N. & IGWEH, A. C. 1994. Immunoassay of circulating trypanosomal antigens in sleeping sickness patients undergoing treatment. *J Immunoassay,* 15**,** 69-77.

OLI, M. W., COTLIN, L. F., SHIFLETT, A. M. & HAJDUK, S. L. 2006. Serum resistance-associated protein blocks lysosomal targeting of trypanosome lytic factor in *Trypanosoma brucei*. *Eukaryot Cell,* 5**,** 132-9.

OVERATH, P., CZICHOS, J., STOCK, U. & NONNENGAESSER, C. 1983. Repression of glycoprotein synthesis and release of surface coat during transformation of *Trypanosoma brucei*. *EMBO J,* 2**,** 1721-8.

OVERATH, P. & ENGSTLER, M. 2004. Endocytosis, membrane recycling and sorting of GPI-anchored proteins: *Trypanosoma brucei* as a model system. *Mol Microbiol,* 53**,** 735-44.

PAL, A., HALL, B. S., NESBETH, D. N., FIELD, H. I. & FIELD, M. C. 2002. Differential endocytic functions of *Trypanosoma brucei* Rab5 isoforms reveal a glycosylphosphatidylinositol-specific endosomal pathway. *J Biol Chem,* 277**,** 9529-39.

PAPADOPOULOS, M. C., ABEL, P. M., AGRANOFF, D., STICH, A., TARELLI, E., BELL, B. A., PLANCHE, T., LOOSEMORE, A., SAADOUN, S., WILKINS, P. & KRISHNA, S. 2004. A novel and accurate diagnostic test for human African trypanosomiasis. *The lancet,* 363**,** 1358-1363.

PARSONS, M. 2004. Glycosomes: parasites and the divergence of peroxisomal purpose. *Mol Microbiol,* 53**,** 717-24.

PAYS, E., VANHAMME, L. & PÉREZ-MORGA, D. 2004. Antigenic variation in *Trypanosoma brucei*: facts, challenges and mysteries. *Curr Opin Microbiol,* 7**,** 369-74.

PAYS, E., VANHOLLEBEKE, B., VANHAMME, L., PATURIAUX-HANOCQ, F., NOLAN, D. P. & PÉREZ-MORGA, D. 2006. The trypanolytic factor of human serum. *Nat Rev Microbiol,* 4**,** 477-86.

PAZOUR, G. J., DICKERT, B. L. & WITMAN, G. B. 1999. The DHC1b (DHC2) isoform of cytoplasmic dynein is required for flagellar assembly. *J Cell Biol,* 144**,** 473-81.

PEACOCK, L., FERRIS, V., SHARMA, R., SUNTER, J., BAILEY, M., CARRINGTON, M. & GIBSON, W. 2011. Identification of the meiotic life cycle stage of *Trypanosoma brucei* in the tsetse fly. *Proc Natl Acad Sci U S A,* 108**,** 3671-6.

PEREIRA, V. R., LORENA, V. M., VERÇOSA, A. F., SILVA, E. D., FERREIRA, A. G., MONTARROYOS, U. R., SILVA, A. P. & GOMES, Y. M. 2003. Antibody isotype responses in Balb/c mice immunized with the cytoplasmic repetitive antigen and flagellar repetitive antigen of *Trypanosoma cruzi*. *Mem Inst Oswaldo Cruz,* 98**,** 823-5.

PINDER, M., LIBEAU, G., HIRSCH, W., TAMBOURA, I., HAUCK-BAUER, R. & ROELANTS, G. E. 1984. Anti-trypanosome specific immune responses in bovids of differing susceptibility to African trypanosomiasis. *Immunology,* 51**,** 247-58.

PLOUBIDOU, A., ROBINSON, D. R., DOCHERTY, R. C., OGBADOYI, E. O. & GULL, K. 1999. Evidence for novel cell cycle checkpoints in trypanosomes: kinetoplast segregation and cytokinesis in the absence of mitosis. *J Cell Sci,* 112 (Pt 24)**,** 4641-50.

PORTMAN, N. & GULL, K. 2010. The paraflagellar rod of kinetoplastid parasites: from structure to components and function. *Int J Parasitol,* 40**,** 135-48.

PORTMAN, N., LACOMBLE, S., THOMAS, B., MCKEAN, P. G. & GULL, K. 2009. Combining RNA interference mutants and comparative proteomics to identify protein components and dependences in a eukaryotic flagellum. *J Biol Chem,* 284**,** 5610-9.

PRADEL, L. C., BONHIVERS, M., LANDREIN, N. & ROBINSON, D. R. 2006. NIMA-related kinase TbNRKC is involved in basal body separation in *Trypanosoma brucei*. *J Cell Sci,* 119**,** 1852-63.

PRICE, H. P., GÜTHER, M. L., FERGUSON, M. A. & SMITH, D. F. 2010. Myristoyl-CoA:protein N-myristoyltransferase depletion in trypanosomes causes avirulence and endocytic defects. *Mol Biochem Parasitol,* 169**,** 55-8.

PRIOTTO, G., FOGG, C., BALASEGARAM, M., ERPHAS, O., LOUGA, A., CHECCHI, F., GHABRI, S. & PIOLA, P. 2006. Three drug combinations for late-stage *Trypanosoma brucei gambiense* sleeping sickness: a randomized clinical trial in Uganda. *PLoS Clin Trials,* 1**,** e39.

PRIOTTO, G., KASPARIAN, S., MUTOMBO, W., NGOUAMA, D., GHORASHIAN, S., ARNOLD, U., GHABRI, S., BAUDIN, E., BUARD, V., KAZADI-KYANZA, S., ILUNGA, M., MUTANGALA, W., POHLIG, G., SCHMID, C., KARUNAKARA, U., TORREELE, E. & KANDE, V. 2009. Nifurtimox-eflornithine combination therapy for second-stage African *Trypanosoma brucei gambiense* trypanosomiasis: a multicentre, randomised, phase III, non-inferiority trial. *Lancet,* 374**,** 56-64.

PRIOTTO, G., KASPARIAN, S., NGOUAMA, D., GHORASHIAN, S., ARNOLD, U., GHABRI, S. & KARUNAKARA, U. 2007. Nifurtimox-eflornithine combination therapy for second-stage *Trypanosoma brucei gambiense* sleeping sickness: a randomized clinical trial in Congo. *Clin Infect Dis,* 45**,** 1435-42.

PÉPIN, J. & MILORD, F. 1994. The treatment of human African trypanosomiasis. *Adv Parasitol,* 33**,** 1-47.

PÉPIN, J., MILORD, F., KHONDE, A., NIYONSENGA, T., LOKO, L. & MPIA, B. 1994. Gambiense trypanosomiasis: frequency of, and risk factors for, failure of melarsoprol therapy. *Trans R Soc Trop Med Hyg,* 88**,** 447-52.

PÉPIN, J., MILORD, F., KHONDE, A. N., NIYONSENGA, T., LOKO, L., MPIA, B. & DE WALS, P. 1995. Risk factors for encephalopathy and mortality during melarsoprol treatment of *Trypanosoma brucei gambiense* sleeping sickness. *Trans R Soc Trop Med Hyg,* 89**,** 92-7.

PÉREZ-MORGA, D., VANHOLLEBEKE, B., PATURIAUX-HANOCQ, F., NOLAN, D. P., LINS, L., HOMBLÉ, F., VANHAMME, L., TEBABI, P., PAYS, A., POELVOORDE, P., JACQUET, A., BRASSEUR, R. & PAYS, E. 2005. Apolipoprotein L-I promotes trypanosome lysis by forming pores in lysosomal membranes. *Science,* 309**,** 469-72.

QU, J. Q., XU, Y. X., BAO, Y. F., YANG, Y. T. & WANG, J. Y. 1991. [Application of monoclonal antibodies against *Leishmania donovani,* II. Detection of circulating antigen in sera of visceral leishmaniasis before and after treatment]. *Zhongguo Ji Sheng Chong Xue Yu Ji Sheng Chong Bing Za Zhi,* 9**,** 21-3.

RADWANSKA, M., GUIRNALDA, P., DE TREZ, C., RYFFEL, B., BLACK, S. & MAGEZ, S. 2008. Trypanosomiasis-induced B cell apoptosis results in loss of protective anti-parasite antibody responses and abolishment of vaccine-induced memory responses. *PLoS Pathog,* 4**,** e1000078.

RALSTON, K. S. & HILL, K. L. 2006. Trypanin, a component of the flagellar Dynein regulatory complex, is essential in bloodstream form African trypanosomes. *PLoS Pathog,* 2**,** e101.

RALSTON, K. S., KABUTUTU, Z. P., MELEHANI, J. H., OBERHOLZER, M. & HILL, K. L. 2009. The *Trypanosoma brucei* flagellum: moving parasites in new directions. *Annu Rev Microbiol,* 63**,** 335-62.

RALSTON, K. S., LERNER, A. G., DIENER, D. R. & HILL, K. L. 2006. Flagellar motility contributes to cytokinesis in *Trypanosoma brucei* and is modulated by

an evolutionarily conserved dynein regulatory system. *Eukaryot Cell,* 5**,** 696-711.

RAPER, J., FUNG, R., GHISO, J., NUSSENZWEIG, V. & TOMLINSON, S. 1999. Characterization of a novel trypanosome lytic factor from human serum. *Infect Immun,* 67**,** 1910-6.

RAPER, J., PORTELA, M. P., LUGLI, E., FREVERT, U. & TOMLINSON, S. 2001. Trypanosome lytic factors: novel mediators of human innate immunity. *Curr Opin Microbiol,* 4**,** 402-8.

RIFKIN, M. R. 1978. Identification of the trypanocidal factor in normal human serum: high density lipoprotein. *Proc Natl Acad Sci U S A,* 75**,** 3450-4.

RINDISBACHER, L., HEMPHILL, A. & SEEBECK, T. 1993. A repetitive protein from *Trypanosoma brucei* which caps the microtubules at the posterior end of the cytoskeleton. *Mol Biochem Parasitol,* 58**,** 83-96.

ROBERTSON, M. 1913. Notes on the life-history of *Trypanosoma gambiense,* with a brief reference to the cycles of *Trypanosoma nanum* and *Trypanosoma pecorum* in *Glossina palpalis*. 203**,** 161-184.

ROBINSON, D., BEATTIE, P., SHERWIN, T. & GULL, K. 1991. Microtubules, tubulin, and microtubule-associated proteins of trypanosomes. *Methods Enzymol,* 196**,** 285-99.

ROBINSON, D. R. & GULL, K. 1991. Basal body movements as a mechanism for mitochondrial genome segregation in the trypanosome cell cycle. *Nature,* 352**,** 731-3.

ROBINSON, D. R., SHERWIN, T., PLOUBIDOU, A., BYARD, E. H. & GULL, K. 1995. Microtubule polarity and dynamics in the control of organelle positioning, segregation, and cytokinesis in the trypanosome cell cycle. *J Cell Biol,* 128**,** 1163-72.

RODITI, I., SCHWARZ, H., PEARSON, T. W., BEECROFT, R. P., LIU, M. K., RICHARDSON, J. P., BÜHRING, H. J., PLEISS, J., BÜLOW, R. & WILLIAMS, R. O. 1989. Procyclin gene expression and loss of the variant surface glycoprotein during differentiation of *Trypanosoma brucei*. *J Cell Biol,* 108**,** 737-46.

ROSENBAUM, J. L., COLE, D. G. & DIENER, D. R. 1999. Intraflagellar transport: the eyes have it. *J Cell Biol,* 144**,** 385-8.

ROTUREAU, B., SUBOTA, I. & BASTIN, P. 2011. Molecular bases of cytoskeleton plasticity during the *Trypanosoma brucei* parasite cycle. *Cell Microbiol,* 13**,** 705-16.

RUSSELL, D. G., NEWSAM, R. J., PALMER, G. C. & GULL, K. 1983. Structural and biochemical characterisation of the paraflagellar rod of *Crithidia fasciculata*. *Eur J Cell Biol,* 30**,** 137-43.

SANTARÉM, N., TOMÁS, A., OUAISSI, A., TAVARES, J., FERREIRA, N., MANSO, A., CAMPINO, L., CORREIA, J. M. & CORDEIRO-DA-SILVA, A. 2005. Antibodies against a *Leishmania infantum* peroxiredoxin as a possible

marker for diagnosis of visceral leishmaniasis and for monitoring the efficacy of treatment. *Immunol Lett,* 101**,** 18-23.

SASSE, R. & GULL, K. 1988. Tubulin post-translational modifications and the construction of microtubular organelles in *Trypanosoma brucei*. *J Cell Sci,* 90 (Pt 4)**,** 577-89.

SATYANARAYANA, A. & KALDIS, P. 2009. Mammalian cell-cycle regulation: several Cdks, numerous cyclins and diverse compensatory mechanisms. *Oncogene,* 28**,** 2925-39.

SCHELL, D., BOROWY, N. K. & OVERATH, P. 1991. Transferrin is a growth factor for the bloodstream form of *Trypanosoma brucei*. *Parasitol Res,* 77**,** 558-60.

SCHLAEPPI, K., DEFLORIN, J. & SEEBECK, T. 1989. The major component of the paraflagellar rod of *Trypanosoma brucei* is a helical protein that is encoded by two identical, tandemly linked genes. *J Cell Biol,* 109**,** 1695-709.

SCHNAUFER, A., PANIGRAHI, A. K., PANICUCCI, B., IGO, R. P., WIRTZ, E., SALAVATI, R. & STUART, K. 2001. An RNA ligase essential for RNA editing and survival of the bloodstream form of *Trypanosoma brucei*. *Science,* 291**,** 2159-62.

SCHNEIDER, A., PLESSMANN, U. & WEBER, K. 1997. Subpellicular and flagellar microtubules of *Trypanosoma brucei* are extensively glutamylated. *J Cell Sci,* 110 (Pt 4)**,** 431-7.

SCOTT, V., SHERWIN, T. & GULL, K. 1997. gamma-tubulin in trypanosomes: molecular characterisation and localisation to multiple and diverse microtubule organising centres. *J Cell Sci,* 110 (Pt 2)**,** 157-68.

SEEBECK, T., WHITTAKER, P. A., IMBODEN, M. A., HARDMAN, N. & BRAUN, R. 1983. Tubulin genes of *Trypanosoma brucei*: a tightly clustered family of alternating genes. *Proc Natl Acad Sci U S A,* 80**,** 4634-8.

SELVAPANDIYAN, A., KUMAR, P., MORRIS, J. C., SALISBURY, J. L., WANG, C. C. & NAKHASI, H. L. 2007. Centrin1 is required for organelle segregation and cytokinesis in *Trypanosoma brucei*. *Mol Biol Cell,* 18**,** 3290-301.

SHERWIN, T. & GULL, K. 1989a. The cell division cycle of *Trypanosoma brucei brucei*: timing of event markers and cytoskeletal modulations. *Philos Trans R Soc Lond B Biol Sci,* 323**,** 573-88.

SHERWIN, T. & GULL, K. 1989b. Visualization of detyrosination along single microtubules reveals novel mechanisms of assembly during cytoskeletal duplication in trypanosomes. *Cell,* 57**,** 211-21.

SHERWIN, T., SCHNEIDER, A., SASSE, R., SEEBECK, T. & GULL, K. 1987. Distinct localization and cell cycle dependence of COOH terminally tyrosinolated alpha-tubulin in the microtubules of *Trypanosoma brucei brucei*. *J Cell Biol,* 104**,** 439-46.

SILVERMAN, J. S., SCHWARTZ, K. J., HAJDUK, S. L. & BANGS, J. D. 2011. Late endosomal Rab7 regulates lysosomal trafficking of endocytic but not biosynthetic cargo in *Trypanosoma brucei*. *Mol Microbiol,* 82**,** 664-78.

SIMARRO, P. P., JANNIN, J. & CATTAND, P. 2008. Eliminating Human African Trypanosomiasis: Where Do We Stand and What Comes Next? *PLoS Medicine,* 5**,** 174-180.

SIMPSON, A. G. B., STEVENS, J. R. & LUKES, J. 2006. The evolution and diversity of kinetoplastid flagellates. *TRENDS in Parasitology,* 22**,** 168-174.

SMITH, A. B., ESKO, J. D. & HAJDUK, S. L. 1995. Killing of trypanosomes by the human haptoglobin-related protein. *Science,* 268**,** 284-6.

SMITH, D. H., PEPIN, J. & STICH, A. H. R. 1998. Human African trypanosomiasis: an emerging public health crisis. *British medical bulletin,* 54**,** 341-355.

SOUZA, W., SANT'ANNA, C. & CUNHA-E-SILVA, N. 2009. Electron microscopy and cytochemistry analysis of the endocytic pathway of pathogenic protozoa. Progress in Histochemistry and Cytochemistry.

SPITZNAGEL, D., O'ROURKE, J. F., LEDDY, N., HANRAHAN, O. & NOLAN, D. P. 2010. Identification and characterization of an unusual class I myosin involved in vesicle traffic in *Trypanosoma brucei*. *PLoS One,* 5**,** e12282.

STAMNES, M. 2002. Regulating the actin cytoskeleton during vesicular transport. *Curr Opin Cell Biol,* 14**,** 428-33.

STAVROPOULOS, P. & PAPAVASILIOU, F. N. 2010. Using *T. brucei* as a biological epitope-display platform to elicit specific antibody responses. *J Immunol Methods,* 362**,** 190-4.

STEPHAN, A., VAUGHAN, S., SHAW, M. K., GULL, K. & MCKEAN, P. G. 2007. An essential quality control mechanism at the eukaryotic basal body prior to intraflagellar transport. *Traffic,* 8**,** 1323-30.

STEPHENS, J. W. W. & FANTHAM, H. B. 1910. On the peculiar morphology of a trypanosome from a case of sleeping sickness and the possibility of its being a new species (*T.rhodesiense*). *Annals of tropical medicine and parasitology,* 4**,** 343-350.

STEPHENS, N. A. & HAJDUK, S. L. 2011. Endosomal localization of the serum resistance-associated protein in African trypanosomes confers human infectivity. *Eukaryot Cell,* 10**,** 1023-33.

STERNBERG, J. & TAIT, A. 1990. Genetic exchange in african trypanosomes. *Trends in genetics,* 6**,** 317-322.

STERNBERG, J. M. 2004. Human African trypanosomiasis: clinical presentation and immune response. *Parasite Immunol,* 26**,** 469-76.

STEVENS, J. R., NOYES, H. A., SCHOFIELD, C. J. & W, G. 2001. The molecular evolution of trypanosomatidae. *Advances in parasitology,* 48**,** 1-55.

STEVERDING, D. 2000. The transferrin receptor of *Trypanosoma brucei*. *Parasitol Int,* 48**,** 191-8.

STEVERDING, D., SEXTON, D. W., CHRYSOCHOIDI, N. & CAO, F. 2012. *Trypanosoma brucei* transferrin receptor can bind C-lobe and N-lobe fragments of transferrin. *Mol Biochem Parasitol*.

STEVERDING, D., STIERHOF, Y. D., CHAUDHRI, M., LIGTENBERG, M., SCHELL, D., BECK-SICKINGER, A. G. & OVERATH, P. 1994. ESAG 6 and 7 products of *Trypanosoma brucei* form a transferrin binding protein complex. *Eur J Cell Biol,* 64**,** 78-87.

STEVERDING, D., STIERHOF, Y. D., FUCHS, H., TAUBER, R. & OVERATH, P. 1995. Transferrin-binding protein complex is the receptor for transferrin uptake in *Trypanosoma brucei*. *J Cell Biol,* 131**,** 1173-82.

SYMULA, R. E., BEADELL, J. S., SISTROM, M., AGBEBAKUN, K., BALMER, O., GIBSON, W., AKSOY, S. & CACCONE, A. 2012. *Trypanosoma brucei gambiense* Group 1 Is Distinguished by a Unique Amino Acid Substitution in the HpHb Receptor Implicated in Human Serum Resistance. *PLoS Negl Trop Dis,* 6**,** e1728.

TAIT, A., BABIKER, E. A. & LE RAY, D. 1984. Enzyme variation in *Trypanosoma brucei spp*. I. Evidence for the sub-speciation of *Trypanosoma brucei gambiense*. *Parasitology,* 89 (Pt 2)**,** 311-26.

TAIT, A. & TURNER, C. M. R. 1990. Genetic exchange in *Trypanosoma brucei*. *Parasitology today,* 6**,** 70-75.

TAKAYANAGI, T. & ENRIQUEZ, G. L. 1973. Effects of the IgG and IgM immunoglobulins in *Trypanosoma gambiense* infections in mice. *J Parasitol,* 59**,** 644-7.

TAYLOR, K. A. & MERTENS, B. 1999. Immune response of cattle infected with African trypanosomes. *Mem Inst Oswaldo Cruz,* 94**,** 239-44.

TETLEY, L., TURNER, C. M., BARRY, J. D., CROWE, J. S. & VICKERMAN, K. 1987. Onset of expression of the variant surface glycoproteins of *Trypanosoma brucei* in the tsetse fly studied using immunoelectron microscopy. *J Cell Sci,* 87 (Pt 2)**,** 363-72.

TETLEY, L. & VICKERMAN, K. 1985. Differentiation in *Trypanosoma brucei*: host-parasite cell junctions and their persistence during acquisition of the variable antigen coat. *J Cell Sci,* 74**,** 1-19.

TODOLÍ, F., GALINDO, I., GÓMEZ-SEBASTIÁN, S., PÉREZ-FILGUEIRA, M., ESCRIBANO, J. M., ALBEROLA, J. & RODRÍGUEZ-CORTÉS, A. 2010. Dynamics and predictive potential of antibodies against insect-derived recombinant *Leishmania infantum* proteins during chemotherapy of naturally infected dogs. *Am J Trop Med Hyg,* 82**,** 795-800.

TOMLINSON, S., JANSEN, A. M., KOUDINOV, A., GHISO, J. A., CHOI-MIURA, N. H., RIFKIN, M. R., OHTAKI, S. & NUSSENZWEIG, V. 1995. High-density-lipoprotein-independent killing of *Trypanosoma brucei* by human serum. *Mol Biochem Parasitol,* 70**,** 131-8.

TRUC, P., JAMONNEAU, V., CUNY, G. & FRÉZIL, J. L. 1999. Use of polymerase chain reaction in human African trypanosomiasis stage determination and follow-up. *Bull World Health Organ,* 77**,** 745-8.

TRUC, P., LEJON, V., MAGNUS, E., JAMONNEAU, V., NANGOUMA, A., VERLOO, D., PENCHENIER, L. & BÜSCHER, P. 2002. Evaluation of the micro-CATT, CATT/*Trypanosoma brucei gambiense*, and LATEX/*T b gambiense* methods for serodiagnosis and surveillance of human African trypanosomiasis in West and Central Africa. *Bull World Health Organ,* 80**,** 882-6.

TSUJIMURA, Y., WATARAI, S., UEMURA, A., OHNISHI, Y. & KODAMA, H. 2005. Effect of anti-ganglioside antibody in experimental *Trypanosoma brucei* infection in mice. *Res Vet Sci,* 78**,** 245-7.

TU, X., KUMAR, P., LI, Z. & WANG, C. C. 2006. An aurora kinase homologue is involved in regulating both mitosis and cytokinesis in *Trypanosoma brucei*. *J Biol Chem,* 281**,** 9677-87.

TU, X. & WANG, C. C. 2004. The involvement of two cdc2-related kinases (CRKs) in *Trypanosoma brucei* cell cycle regulation and the distinctive stage-specific phenotypes caused by CRK3 depletion. *J Biol Chem,* 279**,** 20519-28.

TU, X. & WANG, C. C. 2005a. Coupling of posterior cytoskeletal morphogenesis to the G1/S transition in the *Trypanosoma brucei* cell cycle. *Mol Biol Cell,* 16**,** 97-105.

TU, X. & WANG, C. C. 2005b. Pairwise knockdowns of cdc2-related kinases (CRKs) in *Trypanosoma brucei* identified the CRKs for G1/S and G2/M transitions and demonstrated distinctive cytokinetic regulations between two developmental stages of the organism. *Eukaryot Cell,* 4**,** 755-64.

TYLER, K. M., MATTHEWS, K. R. & GULL, K. 2001. Anisomorphic cell division by African trypanosomes. *Protist,* 152**,** 367-78.

VAN DEN ABBEELE, J., CALJON, G., DE RIDDER, K., DE BAETSELIER, P. & COOSEMANS, M. 2010. *Trypanosoma brucei* modifies the tsetse salivary composition, altering the fly feeding behavior that favors parasite transmission. *PLoS Pathog,* 6**,** e1000926.

VAN DEN ABBEELE, J., CLAES, Y., VAN BOCKSTAELE, D., LE RAY, D. & COOSEMANS, M. 1999. *Trypanosoma brucei* spp. development in the tsetse fly: characterization of the post-mesocyclic stages in the foregut and proboscis. *Parasitology,* 118 (Pt 5)**,** 469-78.

VAN HELLEMOND, J. J., NEUVILLE, P., SCHWARZ, R. T., MATTHEWS, K. R. & MOTTRAM, J. C. 2000. Isolation of *Trypanosoma brucei* CYC2 and CYC3 cyclin genes by rescue of a yeast G(1) cyclin mutant. Functional characterization of CYC2. *J Biol Chem,* 275**,** 8315-23.

VAN NIEUWENHOVE, S. 1999. Present strategies in the treatment of human African trypanosomiasis *Progress in Human African Trypanosomiasis, Sleeping Sickness***,** 235-280.

VAN WEELDEN, S. W., FAST, B., VOGT, A., VAN DER MEER, P., SAAS, J., VAN HELLEMOND, J. J., TIELENS, A. G. & BOSHART, M. 2003. Procyclic *Trypanosoma brucei* do not use Krebs cycle activity for energy generation. *J Biol Chem,* 278**,** 12854-63.

VANHAMME, L. 2010. The human trypanolytic factor: a drug shaped naturally. *Infect Disord Drug Targets,* 10**,** 266-82.

VANHAMME, L., PATURIAUX-HANOCQ, F., POELVOORDE, P., NOLAN, D. P., LINS, L., VAN DEN ABBEELE, J., PAYS, A., TEBABI, P., VAN XONG, H., JACQUET, A., MOGUILEVSKY, N., DIEU, M., KANE, J. P., DE BAETSELIER, P., BRASSEUR, R. & PAYS, E. 2003. Apolipoprotein L-I is the trypanosome lytic factor of human serum. *Nature,* 422**,** 83-7.

VANHOLLEBEKE, B., DE MUYLDER, G., NIELSEN, M. J., PAYS, A., TEBABI, P., DIEU, M., RAES, M., MOESTRUP, S. K. & PAYS, E. 2008. A haptoglobin-hemoglobin receptor conveys innate immunity to *Trypanosoma brucei* in humans. *Science,* 320**,** 677-81.

VANHOLLEBEKE, B. & PAYS, E. 2010. The trypanolytic factor of human serum: many ways to enter the parasite, a single way to kill. *Mol Microbiol,* 76**,** 806-14.

VANHOLLEBEKE, B., UZUREAU, P., MONTEYNE, D., PÉREZ-MORGA, D. & PAYS, E. 2010. Cellular and molecular remodeling of the endocytic pathway during differentiation of *Trypanosoma brucei* bloodstream forms. *Eukaryot Cell,* 9**,** 1272-82.

VAUGHAN, S. & GULL, K. 2003. The trypanosome flagellum. *J Cell Sci,* 116**,** 757-9.

VAUGHAN, S., KOHL, L., NGAI, I., WHEELER, R. J. & GULL, K. 2008. A repetitive protein essential for the flagellum attachment zone filament structure and function in *Trypanosoma brucei*. *Protist,* 159**,** 127-36.

VEDRENNE, C., GIROUD, C., ROBINSON, D. R., BESTEIRO, S., BOSC, C., BRINGAUD, F. & BALTZ, T. 2002. Two related subpellicular cytoskeleton-associated proteins in *Trypanosoma brucei* stabilize microtubules. *Mol Biol Cell,* 13**,** 1058-70.

VICKERMAN, K. 1985. Developmental cycles and biology of pathogenic trypanosomes. *British medical bulletin,* 41**,** 105-114.

VICKERMAN, K. 1994. The evolutionary expansion of the trypanosomatid flagellates. *International journal for parasitology,* 24**,** 1317-1331.

VICKERMAN, K., TETLEY, L., HENDRY, K. A. & TURNER, C. M. 1988. Biology of African trypanosomes in the tsetse fly. *Biol Cell,* 64**,** 109-19.

WANG, Z., MORRIS, J. C., DREW, M. E. & ENGLUND, P. T. 2000. Inhibition of *Trypanosoma brucei* gene expression by RNA interference using an integratable vector with opposing T7 promoters. *J Biol Chem,* 275**,** 40174-9.

WEBSTER, P. & RUSSELL, D. G. 1993. The flagellar pocket of trypanosomatids. *Parasitol Today,* 9**,** 201-6.

WELBURN, S. C. & MAUDLIN, I. 1999. Tsetse-trypanosome interactions: rites of passage. *Parasitol Today,* 15**,** 399-403.

WELBURN, S. C., PICOZZI, K., FÈVRE, E. M., COLEMAN, P. G., ODIIT, M., CARRINGTON, M. & MAUDLIN, I. 2001. Identification of human-infective trypanosomes in animal reservoir of sleeping sickness in Uganda by means of serum-resistance-associated (SRA) gene. *Lancet,* 358**,** 2017-9.

WIRTZ, E. & CLAYTON, C. 1995. Inducible gene expression in trypanosomes mediated by a prokaryotic repressor. *Science,* 268**,** 1179-83.

WIRTZ, E., LEAL, S., OCHATT, C. & CROSS, G. A. 1999. A tightly regulated inducible expression system for conditional gene knock-outs and dominant-negative genetics in *Trypanosoma brucei. Mol Biochem Parasitol,* 99**,** 89-101.

WOODS, A., BAINES, A. J. & GULL, K. 1992. A high molecular mass phosphoprotein defined by a novel monoclonal antibody is closely associated with the intermicrotubule cross bridges in the *Trypanosoma brucei* cytoskeleton. *J Cell Sci,* 103 (Pt 3)**,** 665-75.

WOODS, A., SHERWIN, T., SASSE, R., MACRAE, T. H., BAINES, A. J. & GULL, K. 1989. Definition of individual components within the cytoskeleton of *Trypanosoma brucei* by a library of monoclonal antibodies. *J Cell Sci,* 93 (Pt 3)**,** 491-500.

WOODWARD, R., CARDEN, M. J. & GULL, K. 1994. Molecular characterisation of a novel, repetitive protein of the paraflagellar rod in *Trypanosoma brucei*. *Mol Biochem Parasitol,* 67**,** 31-9.

WOODWARD, R., CARDEN, M. J. & GULL, K. 1995. Immunological characterization of cytoskeletal proteins associated with the basal body, axoneme and flagellum attachment zone of *Trypanosoma brucei*. *Parasitology,* 111 (Pt 1)**,** 77-85.

WOODWARD, R. & GULL, K. 1990. Timing of nuclear and kinetoplast DNA replication and early morphological events in the cell cycle of *Trypanosoma brucei*. *J Cell Sci,* 95 (Pt 1)**,** 49-57.

XONG, H. V., VANHAMME, L., CHAMEKH, M., CHIMFWEMBE, C. E., VAN DEN ABBEELE, J., PAYS, A., VAN MEIRVENNE, N., HAMERS, R., DE BAETSELIER, P. & PAYS, E. 1998. A VSG expression site-associated gene confers resistance to human serum in *Trypanosoma rhodesiense*. *Cell,* 95**,** 839-46.

ZAHAREVITZ, D. W., ANDERSON, L. W., MALINOWSKI, N. M., HYMAN, R., STRONG, J. M. & CYSYK, R. L. 1992. Contribution of de-novo and salvage synthesis to the uracil nucleotide pool in mouse tissues and tumors *in vivo*. *Eur J Biochem,* 210**,** 293-6.

ZHOU, Q., LIU, B., SUN, Y. & HE, C. Y. 2011. A coiled-coil- and C2-domain-containing protein is required for FAZ assembly and cell morphology in *Trypanosoma brucei*. *J Cell Sci,* 124**,** 3848-58.

ZIEGELBAUER, K. & OVERATH, P. 1990. Surface antigen change during differentiation of *Trypanosoma brucei*. *Biochem Soc Trans,* 18**,** 731-3.

ZIEGELBAUER, K., QUINTEN, M., SCHWARZ, H., PEARSON, T. W. & OVERATH, P. 1990. Synchronous differentiation of *Trypanosoma brucei* from bloodstream to procyclic forms in vitro. *Eur J Biochem,* 192**,** 373-8.

ZILLMANN, U., MEHLITZ, D. & SACHS, R. 1984. Identity of Trypanozoon stocks isolated from man and a domestic dog in Liberia. *Tropenmed Parasitol*, 35**,** 105-8.